Role of the homeobox gene *Hesx1/HESX1* in forebrain and pituitary development in mouse and human

EZAT SAJEDI

A thesis submitted to the University of London in fulfilment of the requirements for the degree of Doctor of Philosophy

January 2008

Neural Development Unit
UCL Institute of Child Health
30 Guilford Street
London WC1N 1EH

ProQuest LLC
789 East Eisenhower Parkway
P.O. Box 1346
Ann Arbor, MI 48106-1346

DECLARATION

I, Ezat Sajedi, confirm that the work presented in this thesis is my own. Where information has been derived from other sources, I confirm that this has been indicated in the thesis.

DEDICATION

To my parents, Mahvash and Mehdi, who have given me endless support and guidance every step of the way. Thank you for your kindness and understanding and for everything you've gone through to make sure we have the best opportunities in life.

ABSTRACT

The homeobox gene *Hesx1* encodes a transcriptional repressor that is required, within the anterior neural plate of the vertebrate embryo, for normal forebrain and pituitary development. *Hesx1*$^{-/-}$ mice display variable defects, affecting midline telencephalic commissural tracts, the eyes and the pituitary gland. In humans, mutations in *HESX1* are associated with hypopituitarism and septo-optic dysplasia (SOD), a condition characterised by pituitary abnormalities in association with midline telencephalic structure and optic nerve defects. In this thesis, a dual approach was used, in order to gain insights into HESX1 function.

Firstly, a yeast two-hybrid screen identified DNMT1, LONP2, SRFBP1, SAFB1 and ZFP592 as protein partners of HESX1. Mapping of the interacting regions indicated that different domains of HESX1 are involved in each of these interactions. The five proteins co-localise with HESX1 in the nucleus and their transcripts are co-expressed with *Hesx1* in mouse embryos. Furthermore, these interactions are disrupted by various *HESX1* mutations. The binding with DNMT1 was characterised in more detail, since this protein has a crucial role in gene silencing through its DNA methylation properties. Thus this interaction suggests a novel mechanism for the repressing activity of HESX1.

Secondly, gene targeting was used to generate two knock-in mouse models, based on two autosomal recessive human *HESX1* mutations, I26T and R160C. I26T has been associated with anterior pituitary hypoplasia in a patient, whilst R160C was identified in two siblings with SOD. *Hesx1*$^{I26T/I26T}$ embryos display fully penetrant pituitary defects with frequent occurrence of eye abnormalities, whereas the telencephalon develops normally. *Hesx1*$^{R160C/R160C}$ embryos display more severe forebrain and pituitary defects that are identical to those observed in *Hesx1*$^{-/-}$ mice. These data indicate that *Hesx1-I26T* is a hypomorphic allele, whereas *Hesx1-R160C* yields a null allele and consequently causes a more severe phenotype in mice and humans.

ACKNOWLEDGEMENTS

Firstly, I would like to thank my supervisor, Dr. J.P. Martinez-Barbera, for giving me this fantastic opportunity. Without his help, support, guidance and motivation I could have never achieved what I have today, I am forever grateful for that. I would like to thank Massimo Signore, his and JP's expertise contributed greatly to my thesis, not only for the generation of the mouse models, but also by teaching me so much during my time at ICH. Thank you, it's been great working with you. My thanks also go to Professor M. Dattani, for his support as my secondary supervisor, as well as his collaboration over the past years.

I would also like to thank all the members of Neural Development and Developmental Biology Units, both past and present, for their help and support at various stages of my time here.

I am grateful to Professor P. Scambler and Dr. P. Alatiotis for advice on the yeast two-hybrid screen, as well as the use of reagents and to many others for donation of probes and reagents.

A massive thank you goes to my friends both inside and outside ICH for making sure I don't stress too much, your kindness and support has pulled me through.

Finally, but most importantly, I want to thank my family, Mum, Dad, Sina, Rana and Zari for putting up with me and keeping me sane. You've been an inspiration throughout and I couldn't have completed this work without you.

This work was supported by CHRAT, UCL and the Wellcome Trust.

ABBREVIATIONS

aa	Amino acid
Ac	Acetate
AD	Activation domain
Ade	Adenine
ADE	Anterior definitive endoderm
AME	Anterior axial mesendoderm
ANE	Anterior neural ectoderm
ANR	Anterior neural ridge
AP	Alkaline phosphatase
A-P	Anterior-posterior
APS	Ammonium persulphate
AVE	Anterior visceral endoderm
BCIP	5-bromo-4-choloro-3-indolyl-phosphate
BD	Binding domain
BLAST	Basic Local Alignment Search Tool
BMP	Bone morphogenetic protein
bp	base pair
BS	Binding site
BSA	Bovine serum albumin
C	Carboxy
°C	Degrees Celcius
cDNA	Complementary deoxyribonucleic acid
CNS	Central nervous system
Conc	Concentration
Da	Dalton
DAB	Diaminobenzidine
ddNTP	Dideoxynucleoside triphosphate
ddH_2O	Deionised distilled water
DEPC	Diethyl pyrocarbonate
DMEM	Dulbecco's Modified Eagle's Medium
DMF	N,N-dimethyl formamide
DMSO	Diethyl sulfoxide

DNA	Deoxyribonucleic acid
DBD	DNA binding domain
dNTP	Deoxynucleoside triphosphate
dpc	days post coitum
dsDNA	Double-stranded deoxyribonucleic acid
DTT	Dithiothreitol
D-V	Dorso-ventral
E	Embryonic day
ECL	Enhanced chemiluminescence
EDTA	Ethylenediaminetetraacetic acid
EGO	Early gastrula organiser
EMSA	Electrophoretic mobility shift assay
ES	Embryonic stem
EST	Expressed sequence tag
FGF	Fibroblast growth factor
FGFR	Fibroblast growth factor receptor
g	Gravity
g	Gram
GSK-3β	Glycogen synthase kinase 3 beta
GST	Glutathione-S-transferase
HDAC	Histone deacetylase
HEPES	N-2-hydroxyethylpiperazine-N'-2-ethanesulfonic acid
hr(s)	Hour(s)
HRP	Horseradish peroxidase
IAP	Intracisternal A particle
IMS	Industrial methylated spirit
IP	Immunoprecipitation
IPTG	Isopropyl-1-thio-β-D-galactoside
k	Kilo
Kb	Kilobase
l	Litre
L-R	Left-right
LB	Luria broth
μ	Micro

m	Milli
M	Molar
MAR	Matrix attachement factor
min	Minutes
mRNA	Messenger ribonucleic acid
MW	Molecular weight
n	Nano
nm	Nano meter
N	Amino
NLS	Nuclear localisation signal
Na	Sodium
NBT	4-nitro blue tetrazolium chloride
NTMT	Sodium chloride/Tris/magnesium chloride/Tween buffer
OD	Optical density
o/n	Overnight
ORF	Open Reading Frame
PAGE	Polyacrylamide gel electrophoresis
PBS	Phosphate-buffered saline
PBT	Phosphate-buffered saline and 0.1% Tween-20
PCR	Polymerase chain reaction
PEG	Polyethylene glycol
PFA	Paraformaldehyde
PK	Proteinase K
PMSF	Phenylmethane sulphonyl fluoride
Pol	Polymerase
RA	Retinoic acid
RAI	Retinoic acid induced
RNA	Ribonucleic acid
RNAse	Ribonuclease
RP	Rathke's pouch
rpm	Rotations/revolutions per minute
rt	Room temperature
RT	Reverse transcription
RT-PCR	Reverse transcriptase polymerase chain reaction

SDS	Sodium dodecyl sulphate
sec	Seconds
SHH	Sonic hedgehog
ssDNA	Salmon sperm deoxyribonucleic acid
SSC	Sodium chloride(salt)/sodium citrate buffer
TAE	Tris/acetate/EDTA buffer
TBST	Tris buffered saline with 0.1% Tween-20
TE	Tris/EDTA buffer
TEMED	N,N,N',N'-tetramethylethyleneamine
Temp	Temperature
Tris	Tris(hydroxymethyl)aminomethane
u	Units
UAS	Upstream activating sequence
UTR	Untranslated region
UV	Ultraviolet
VE	Viseral endoderm
v/v	Volume per volume
WT	Wild type
w/v	Weight per volume
X-α-gal	5-bromo-4-chloro-3-indolyl-α-D-galactopyranoside
ZLI	Zona limitans intrathalamica

TABLE OF CONTENTS

LIST OF FIGURES

LIST OF TABLES

1. GENERAL INTRODUCTION

1.1. NEURAL INDUCTION

1.1.1. Introduction

How does a single cell (the fertilised egg) give rise to the multicellular organism? This question has fascinated mankind for hundreds of years. Over these years, the works of great scientists have significantly contributed to getting us closer to the answer. Although, classically developmental biologists studied embryonic development by conducting explant and grafting experiments, nowadays the great advances in molecular biology and our ever expanding knowledge of various genomes with their complex DNA and protein networks, have all revolutionised the way we look at solving this puzzle. At any point in time, we can say that we are getting closer to completing the picture, which ultimately clarifies this central question. However, it will not come as a surprise that the field of developmental biology is at the present time much more complex than before, being divided into many branches and side-branches, each concerning itself with the development of a different organ or part of the embryo. Each one of these divisions is faced with a complex picture, involving many mechanisms, genes and signalling pathways all pointing to the same endpoint. It is, therefore, crucial to elucidate what all this data means and it is important to always go back to the question that started it all.

1.1.2. Establishment of the Central Nervous System

One of the most fascinating of these systems is the development of the central nervous system (CNS) and in particular the brain. Given its function in the adult organism, it is not surprising that it is one of the most complex of the embryonic structures to develop. Although, every organ has its own amazingly intricate pattern of formation, involving many molecular cues, it is this organ (the brain) that has undergone many changes in function, structure and capability among the various phyla in the animal kingdom. This divergence in evolutionary terms has meant the emergence of more complex structures within the brain such as the forebrain (see section 1.2) among the vertebrates, and the further expansion of the forebrain region in birds and mammals. This system has provided a perfect stepping stone for understanding the processes of gastrulation, pattern formation and morphogenesis.

The development of the CNS starts with the process of neural induction or neuralisation. This is the process by which epiblast cells become specified as neural stem or precursor cells. During this process, the primitive ectoderm undergoes morphogenetic changes and starts to express early neural markers, resulting in the cells becoming more columnar in appearance and rising above the adjacent cell layer, and subsequently becoming what is known as the neural plate (the precursor of brain and spinal cord).

Other processes such as gastrulation (the formation of the three principle germ layers: ectoderm, mesoderm and endoderm), and subsequent patterning of the axes also play crucial parts in CNS development. There are three axes in the developing embryo, including the anterior-posterior (A-P: running from head to tail), the dorsal-ventral (D-V: running from back to belly) and the left-right (L-R) axes (Gilbert, 2006). What is surprising, however, is that the mechanism and signalling pathways involved in patterning the axes in the embryo is very much conserved from the invertebrate chordate amphioxus, to the vertebrate mammal. Of these, the A-P axis is the most conserved and even in species without a true CNS such as Hydra, A-P axis formation follows the same basic steps as in mammals (Niehrs, 2004).

1.1.3. The organiser

The birth of "neural induction" can be traced back to the identification of the organiser, by the famous experiments carried out in Hans Spemann's lab (Spemann and Mangold, 1924). In these experiments, a small portion of the dorsal blastopore lip from one species of newt, was grafted into the ventral side of a different species of newt, and resulted in the formation of a second axis with a complete CNS. It was found that most of this secondary axis was derived from the host organism, except a portion called the notochord, which was from the grafted tissue. This part of the embryo, able to induce another axis, was termed Spemann's organiser in amphibians and since then equivalent regions have been found in other vertebrate species. In fish, this region is called the embryonic shield and in birds it is Hensen's node (Koshida et al., 1998; Stern, 2005). In mouse, the equivalent region was first found to be the node, a region in the distal tip of the epiblast at late streak stages derived from mesoderm (Beddington, 1994). However, following this work and taking it a stage

earlier, when the primitive streak is just forming (at early streak stages), it was found that a population of cells in the anterior side of primitive streak (which will form the node by late streak stages), is more likely to correspond to the organiser, this region is termed the early gastrula organiser or EGO (Tam et al., 1997).

Although, all the named animal models have shed light on the process of neural induction, many of the founding experiments were done in *Xenopus*. It is, therefore, important to review these ground breaking studies before moving to other species such as the mouse, where mechanisms of neuralisation are being elucidated relatively recently.

1.1.4. Studies in *Xenopus*

The mystery, surrounding the function of the organiser, arose very soon after its discovery. The question was how the organiser carries out its complex task of making the three embryonic axes in the three germ layers simultaneously. Many groups started to isolate and characterise genes, which were abundant in the organiser, in the hope of identifying the "neural-inducing" material. The result was the discovery of a number of genes found in this region of the embryo. These can be classified as transcription factors or secreted molecules (Figure 1.1).

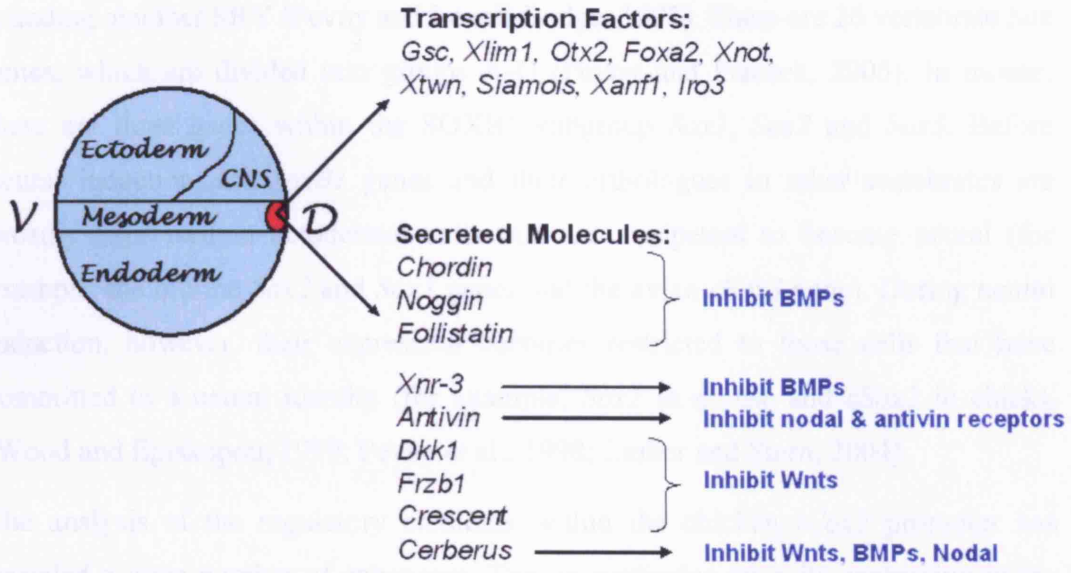

Figure 1.1 – The *Xenopus* organiser expresses a number of transcription factors and secreted molecules. Schematic representation of a gastrula-stage embryo. The organiser (red) is a group of cells in the dorsal marginal zone, which patterns the three germ layers (ecto-, meso- and endoderm). A number of transcription factors and secreted molecules are illustrated, which have been isolated from the organiser and contribute to its function. The secreted molecules antagonise different signalling pathways (shown in blue). Figure is adapted from De Robertis and Kuroda, 2004.

1.1.4.1. Transcription factors

The first organiser gene to be isolated in *Xenopus* was *goosecoid* (Blumberg et al., 1991; Niehrs et al., 1993). Overexpression of *gsc* in *Xenopus* results in a partial secondary axis (Cho et al., 1991). There have also been other genes identified, such as *Xlim1/Lhx1* (Taira et al., 1992) and *Foxa2/HNF3β* (Dirksen and Jamrich, 1992). These all encode transcription factors that can influence neighbouring cells to adopt dorsal fates. The role of transcription factors in neural induction has not been studied to the same extent as the role of signalling molecules (which are discussed below). Transcription factors do have a major role as the regulators of many of these signalling events. It is, therefore, important to study their regulation as well as the targets of these proteins.

An example of such a study includes the investigation of the regulation of the neural transcription factor *Sox2* in chick. SOX family of transcription factors all contain a

HMG domain with at least 50% sequence similarity to the HMG domain of the founding member SRY (Pevny and Lovell-Badge, 1997). There are 26 vertebrate *Sox* genes, which are divided into groups A-G (Pevny and Placzek, 2005). In mouse, there are three genes within the SOXB1 subgroup *Sox1*, *Sox2* and *Sox3*. Before neural induction, the *SoxB1* genes and their orthologues in other vertebrates are broadly expressed in ectodermal cells that are competent to become neural (for example, the murine *Sox2* and *Sox3* genes and the avian *cSox3* gene). During neural induction, however, their expression becomes restricted to those cells that have committed to a neural identity (for example, *Sox1* in mouse and *cSox2* in chick), (Wood and Episkopou, 1999; Pevny et al., 1998; Linker and Stern, 2004).

The analysis of the regulatory elements within the chicken *cSox2* promoter has revealed a large number of enhancers. Two in particular drive its expression in the neural plate. N1 drives its caudal expression, whilst N2 is responsible for its more anterior expression within the neural plate (Uchikawa et al., 2003). The N1 enhancer has been shown to contain binding sites for members of the WNT and FGF signalling pathways, although the exact mechanism of its regulation remains to be elucidated (Takemoto et al., 2006).

1.1.4.2. TGF-β antagonists

In addition, there are a number of secreted factors that have been isolated from Spemann's organiser, the first being *noggin* (Smith and Harland, 1992). This was followed by the identification of *chordin* (Sasai et al., 1994), *follistatin* (Hemmati-Brivanlou et al., 1994) and *xnr-3* (Smith et al., 1995). These and other factors can all be grouped together as they antagonise TGF-β signalling. In particular, they inhibit members of the Bone Morphogenetic Proteins (BMPs). Since BMPs promote epidermal fates, their inhibition leads to the induction of neural tissue. Generally, the downregulation of these BMP inhibitory proteins results in a reduction in CNS tissue, specifically a smaller head and enlarged tail structures, as seen in *Xenopus* embryos treated with *chordin* morpholinos (Oelgeschlager et al., 2003), as well as in zebrafish *chordino* mutants (Schulte-Merker et al., 1997).

In contrast, the inhibition of members of the BMP family results in defects in the trunk (Reversade et al., 2005) and in more extreme cases, in an enlarged brain

(Reversade and De Robertis, 2005). As will be discussed, BMP4 has a major role in neural induction (section 1.1.5). There is, however, redundancy between different members of the BMP family (BMP 2, 4, 7 and ADMP).

Lefty/antivin (Meno et al., 1997) is also a TGF-β signalling inhibitor found in the organiser, however, it antagonises nodal and activin receptors. Nodal is a member of the TGF-β superfamily, distinct from BMPs, and it plays roles in establishing the mesoderm and endoderm layers, as well as having roles in axis formation (De Robertis and Kuroda, 2004; Chea et al., 2005; Tian and Meng, 2006).

1.1.4.3. WNT antagonists

Members of the frizzled related proteins or FRPs such as *frzb1* (Leyns et al., 1997), *frzb2/crescent* (Pera and De Robertis, 2000), *sizzled2* (Bradley et al., 2000), *XfrzA* (Xu et al., 1998b) are also expressed in the organiser. *Dickkopf1 (dkk1)* (Glinka et al., 1998) is another organiser gene, which can be grouped with the above FRP members, as they all antagonise the Wnt/β-catenin signalling pathway. *Cerberus* (Bouwmeester et al., 1996) is found in the organiser and is unique, in that it acts as an antagonist of three separate pathways involved in trunk formation, by binding and inhibiting *Xenopus* nodal-related 1 and 2, WNT8 and BMP4 (Piccolo et al., 1999). *Cerberus* is required for head induction, as the treatment of *Xenopus* with *cerberus* antisense morpholino oligos, inhibits head development without affecting the trunk/tail (Kuroda et al., 2004).

Wnt/β-catenin signalling has many different functions during early embryonic development. Before gastrulation, Wnt/β-catenin signalling plays a role in establishing D-V axis in lower vertebrates (Marikawa, 2006). In frogs, β-catenin is accumulated in the future dorsal side of the embryo before the appearance of the organiser, triggering the transcription of organiser-specific genes such as *siamois* and *Xtwin* (Larabell et al., 1997). This activated Wnt/β-catenin signalling in the dorsal side, along with the action of other proteins from the vegetal side of the embryo such as VegT, creates a gradient of nodal-related gene expression in the endoderm (De Robertis et al., 2000). These events are thought to lead to the formation of the Nieuwkoop centre, a region of the dorsal endoderm, which induces the organiser in *Xenopus* and zebrafish. Indeed, ectopic expression of *Xwnt8* induces a secondary axis

in *Xenopus* (Sokol et al., 1991; Christian et al., 1992). As it will be discussed later, WNTs regulate neural induction by blocking the neural inducing ability of FGFs. Wnt/β-catenin signalling also plays a role in A-P axis formation (section 1.2.2.2).

1.1.5. Mechanisms of neural induction and the "default model"

The discovery of "organiser-genes" and their functions initially resulted in a large amount of data, but failed to identify a single "neural-inducing" agent. The first breakthrough came after a number of these findings were linked in a simple model for neural induction. In particular, two sets of experiments were crucial in elucidating this mechanism. It was found that if *Xenopus* animal cap cells (precursors of ectoderm) are cultured alone they become epidermal cells, whilst if they are dissociated and then allowed to re-aggregate, they follow a neural fate (Grunz and Tacke, 1989; Godsave and Slack, 1989). Later, it was found that overexpression of a dominant negative activin receptor (a TGF-β type II receptor) blocks mesoderm formation and the animal cap cells develop a neural character (Hemmati-Brivanlou and Melton, 1992; Hemmati-Brivanlou and Melton, 1994).

These discoveries, led to the formulation of the "default model" of neural induction (Munoz-Sanjuan and Brivanlou, 2002), which states that ectodermal cells are destined to form neural tissue; however, this is prevented by an inhibitory substance. This inhibition needs to be removed in order, for the nascent neural fate to be followed by these cells; this is the role played by the organiser, which produces molecules to antagonise the inhibiting substance.

This inhibitory molecule, was found to be the BMP protein and in particular BMP4. As mentioned above, a number of factors identified in the organiser are BMP antagonists. BMP4 inhibits neural fate, whilst promoting cells to form the epidermis (Hawley et al., 1995; Wilson and Hemmati-Brivanlou, 1995). Additionally, the expression pattern of BMP4 in *Xenopus* is consistent with the model. It is initially expressed in the entire ectoderm but then as the organiser forms, its transcripts are excluded from the neural plate (Fainsod et al., 1994).

The "default model" of neural induction became the accepted mechanism by which the initial neural character takes shape. Although, its main principles still apply, the

decade that has now followed its original proposal, has seen the appearance of a number of studies implicating other factors in the induction of neural character. As it can be seen from the above section, most of the common signalling pathways are involved and their roles can sometimes be in the inhibition, and other times in the induction of neural character. It seems that not only, are signalling pathways other than BMPs (FGF, canonical WNT and Notch) involved, but the timing during embryonic development at which they act is also critical for the process of neural induction. It is the order and timing of these events, which eventually leads to the acquisition of neural fate.

1.1.6. Looking beyond BMPs

It is established that in all systems BMP inhibition leads to the induction of neural fate (Harland, 2000). However, there is conflicting data on whether BMP inhibition is sufficient for the process. For example, it has been shown that if FGF signalling is simply inhibited by injection of a dominant negative form of FGF receptor in *Xenopus*, the neural-inducing properties of *noggin* and *chordin* are lost (Launay et al., 1996; Sasai et al., 1996). Additionally, in ES cells, inhibition of FGF signalling blocks neural differentiation (Ying et al., 2003).

The data emerging on FGFs is also complex. For example, there is some evidence suggesting that FGFs can act as neural inducers independent of BMPs (Linker and Stern, 2004; Delaune et al., 2005). Whilst, other groups have shown that downregulation of FGFs by a dominant negative FGF receptor does not prevent neural induction, as it should, if FGF signalling was sufficient for neural induction (Cox and Hemmati-Brivanlou, 1995; Pownall et al., 2003).

The reasons underlying this inconsistency are still unclear and are speculated among the leading scientists of this field. Evidently, the picture is complex with the possibility that many, as yet, unknown factors are involved. Moreover, the identified factors possibly act through more than one pathway, with interactions among them. A series of recent studies explain these conflicting data at the level of Smad1 phosphorylation. It was previously shown that a simple manipulation/wounding of amphibian embryos, activates the MAPK pathway (LaBonne and Whitman, 1997). This implicates FGF/IGF signalling, in those early dissociation experiments, as an additional inhibitor of BMP signalling, as they cause phosphorylation of the linker

region of Smad1, through the activation of MAPK (Pera and De Robertis, 2000; Reversade et al., 2005). However, studies using mouse mutants, have shown that it is the C-terminus phosphorylation of Smad1 by BMP receptors that is crucial for development, whilst mutations that disrupt the linker phosphorylation of Smad1 by MAPK, do not cause neural defects (Aubin et al., 2004).

Additionally, Smad1 linker region contains phosphorylation sites for GSK3, which cause inhibition of Smad1 function (Fuentealba et al., 2007). This new finding indicates that one possible mechanism of the canonical WNT pathway, in regulating neural induction, is to stabilise the Smads. Hence, Smad phosphorylation provides a regulatory step in neural induction, linking many of the signalling pathways.

Another issue is timing; there is still no firm evidence on when the process of neural induction initiates. The assumption was that it is coincident with gastrulation, however, there are indications that it starts even before the appearance of the organiser. For example, removal of the organiser does not completely abolish the formation of the neural plate in a number of vertebrates (Shih and Fraser, 1996; Sater and Jacobson, 1990; Davidson et al., 1999). If that is the case, then BMPs would have a relatively "late" stabilising role to play in neural induction. It is mostly work in chick and mouse that has implicated other factors, such as WNTs and FGFs, as independent neural inducers, although there is also supporting evidence from amphibians and zebrafish (Wilson et al., 2001; Wilson and Edlund, 2001; Stern, 2005; Stern, 2006).

It has also been shown that in both fish and frog at least, trunk neural induction requires only inhibition of BMPs whilst head neural induction involves inhibition of both TGF-β and WNTs (Glinka et al., 1997; Fekany-Lee et al., 2000; Niehrs, 1999). As mentioned above, the organiser contains a cocktail of factors such as TGF-β antagonists, WNT antagonists, FGFs and a number of transcription factors. It is not inconceivable, that it possibly contains a number of other, as yet unidentified, proteins. Therefore, the use of any one of these factors on their own or even in combination cannot replicate the function of the organiser. This leads to ambiguous data, which are difficult to interpret.

A neat model has been proposed for neural induction, using data available on a number of model organisms, which places FGF signalling as an active neural

inducer, with WNT antagonists as regulators and BMP antagonists as stabilisers of the process (Wilson and Edlund, 2001). In this model, cells are thought to be specified as neural or epidermal according to their position at blastula stages, before the appearance of the organiser. Medial epiblast cells at this stage express FGFs, which activate two pathways. Both pathways promote neural fate; one is through the inhibition of BMPs, whilst the other is independent of BMPs, leading to neural specification through a direct or as yet unknown pathway.

Lateral epiblast cells, on the other hand, express both FGFs and WNTs. In these cells, high levels of WNT signalling, prevents FGF from repressing BMPs. Under these conditions BMPs are able to promote epidermal fates. At lower WNT levels, FGF is still unable to repress BMPs, however FGF can promote neural fate through its independent pathway, hence BMP antagonists act as potent neural inducers in these cells.

1.1.7. Neural induction in mammals

Around 40% of all mammalian species are in the order Rodentia (Tam and Gad, 2004). The mammalian model used to study gastrulation and neural induction is the house mouse *Mus musculus*. Before looking at neural induction in mammals, therefore, it is important to have an understanding of early embryonic development and patterning in the mouse. Rodents' early gastrula differs from other amniotes studied, in that it forms a cup-shaped embryo compared to the flat embryos of chick and humans. The study of neural induction in mammals was behind other species mainly because of the very small size of the early blastula, and the subsequent difficulties in manipulation, as development takes place inside the uterus. However, the last three decades has seen some of the most intricate experimentation techniques used, resulting in an increase in information about mouse neural induction.

1.1.7.1. Early mouse development

From the start, mammalian development differs somewhat from other vertebrates, in that the second and subsequent cleavages are rotational rather than radial (Gilbert, 2006). Additionally, the mammalian zygotic genome is activated much earlier than other vertebrates (at the two-cell stage), whilst the rate of cleavage is much slower

(Beddington and Robertson, 1999). This, along with the fact that the blastomeres do not all divide at the same time and intermix extensively, means that the appearance of the mass of dividing cells after fertilisation looks disorganised, and indeed it is so until compaction occurs in the 16-cell morula. At this stage, although the individual cells are pluripotent (they can give rise to all cells of the embryo if placed in the correct environment), the cells inside of the morula go on to form the inner cell mass (ICM) and the ones on the outside become the trophectoderm.

By the 64-cell stage, these two cell populations have formed two separate layers, marking the first differentiation event in the early mammalian embryo. Cavitation then creates the blastocyst and with it, the proximal-distal axis of the conceptus takes shape (Figure 1.2). After hatching from the zona pellucida, the blastocyst attaches to the uterine wall and post-implantation development begins.

It is only after implantation, when the embryo has taken its famous cylindrical form, that the patterning and axis formation in the embryonic part becomes apparent. The two early axes of the conceptus are the embryonic-abembryonic (proximal-distal) and the animal-vegetal axes. There is growing evidence to suggest that the proximal-distal axis becomes the anterior-posterior, but it is not yet clear whether the axes defined during pre-implantation directly affect later embryonic axes (Beddington and Robertson, 1998; Beddington and Robertson, 1999; Brennan et al., 2001).

After implantation, the early egg cylinder has two cell layers. The trophectoderm contributes entirely to the extraembryonic tissues (the maternal and foetal parts of the placenta). The ICM later divides to become the hypoblast (or primitive endoderm) which, again contributes entirely to the extraembryonic tissues (parietal and visceral endoderm) and epiblast from which the entire embryo proper is derived but it also gives rise to the extraembryonic mesoderm. The shape and polarity of the conceptus at this stage forms the D-V axis of the embryo. The side of the epiblast in contact with the proamniotic cavity is the future dorsal side, whilst the outer surface will be the ventral side, it is therefore, necessary for these sides to switch at some point during development; this occurs during "turning" of the embryo after gastrulation (Kaufman, 1992).

Part of the hypoblast (or primitive endoderm) moves to cover the inside of trophectoderm and later becomes the Reichert's membrane, whilst the rest forms the

visceral endoderm, which covers the egg cylinder. The extraembryonic ectoderm derived from trophectoderm then acts like a cap. An early landmark of the mammalian embryo, which appears just prior to gastrulation at the pre-streak stage (~5.5 dpc), is a population of visceral endoderm cells which move from the distal tip of the cup proximally and to one side, forming a thickening at the future anterior side of the embryo (Thomas et al., 1998), a region called the anterior visceral endoderm (AVE). It is not known what drives this cell migration although the extraembryonic ectoderm and the epiblast may play roles (Rodriguez et al., 2005; Srinivas et al., 2004). This extraembryonic tissue is later displaced by the embryonic gut endoderm (Beddington and Robertson, 1998).

The AVE has been shown to be required in the anterior patterning of the embryo and has often been thought of as a separate head organiser, although it is now known to cooperate with the node and EGO in order to induce anterior head structures (Martinez-Barbera and Beddington, 2001; Tam and Steiner, 1999). After the appearance of the AVE, at early streak stages (~6.5 dpc), a group of epiblast cells at the proximal rim of the embryo move to the opposite side and undergo an epithelial to mesenchymal transition to generate a mesoderm. This region is called the primitive streak and marks the future posterior side of the embryo; it also signifies the start of gastrulation. Therefore, even before the start of gastrulation, the A-P, D-V and consequently L-R axes of the embryo are established. Whether or not these axes are a direct result of the earlier animal-vegetal and proximal-distal axes in the blastocyst is still unclear.

A

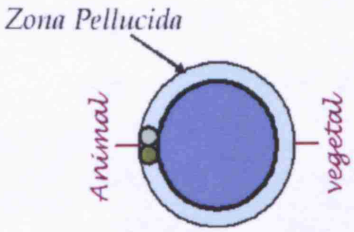

Fertilised egg
0 hrs

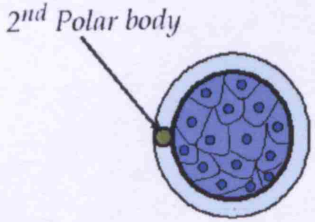

Compacted morula
3.0 dpc

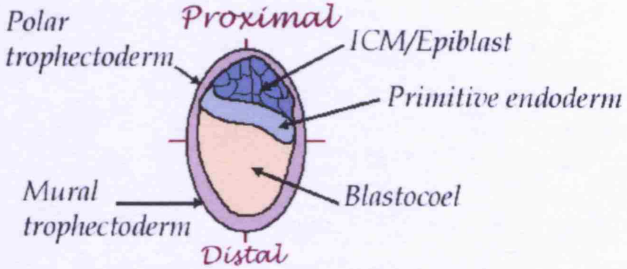

Implanting blastocyst
4.5 dpc

B

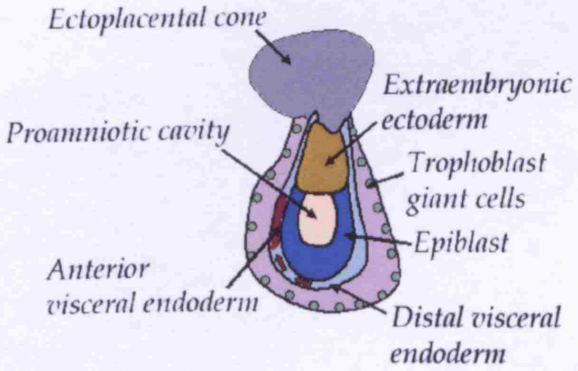

Pre-streak
6.0 dpc

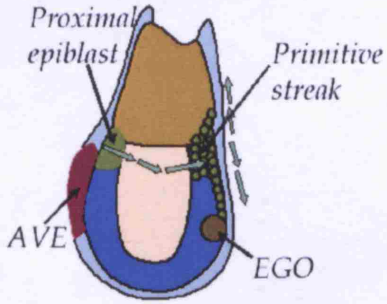

Early streak
6.5 dpc

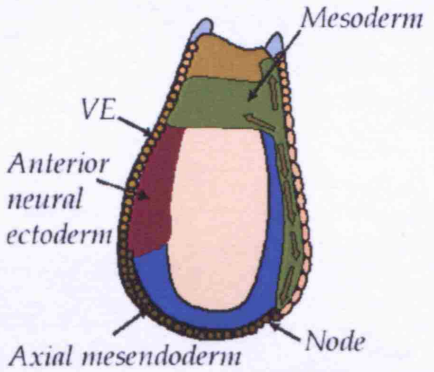

Late streak
7.5 dpc

Figure 1.2 – Early mouse development. A) Pre-implantation development. The animal and vegetal poles of the fertilised egg are determined by the position of the polar bodies. By the time of implantation, the blastocyst contains three distinct cell lineages: (1) the inner cell mass (ICM); (2) the trophectoderm and (3) the primitive endoderm. B) Post-implantation development. The appearance of the anterior visceral endoderm (AVE) and later the primitive streak, mark the future anterior and posterior sides of the embryo, respectively. As gastrulation starts (~6.5 dpc), cell movements (green arrows) through the primitive streak, result in the expansion of the mesoderm layer and subsequent formation of the early gastrula organiser (EGO). By 7.5 dpc, the node has formed at the distal tip of the growing mesoderm wings (green region), and the axial mesendoderm extends anteriorly, displacing the visceral endoderm (VE). At this point, the epiblast cells adjacent to the AVE, have acquired an anterior neural identity.

1.1.7.2. Neural induction in mouse

1.1.7.2.1. The mouse organiser

A number of findings, from studies on neural induction in mouse, differ from those in *Xenopus*, implicating that perhaps in mammals the mechanisms of neural induction have somewhat diverged from other vertebrates. In mouse, the transplantation of EGO or node, results in a secondary axis minus the mid- and forebrain regions (Beddington, 1994; Tam and Steiner, 1999). Additionally, many factors which cause axis duplication in *Xenopus* (such as WNTs) only duplicate a partial secondary axis in mouse, lacking the anterior forebrain (Popperl et al., 1997).

As discussed above, the mouse AVE is a structure which appears before the primitive streak and a number of genes have been discovered in this region with head inducing properties (these are discussed in more detail in section 1.2; Table 1.1). Chimeric studies show the requirement of a number of these genes in the visceral endoderm for the induction of the anterior forebrain, although this also requires the presence of the node (Martinez-Barbera and Beddington, 2001). Consequently, it is difficult to separate A-P axis specification from neural induction, as they increasingly overlap during early development. Although, the signalling pathways involved are common to both these processes, they often play different roles and at different times during development. For example, there are several WNT ligands expressed in the mouse primitive streak, such as *Wnt3*, *Wnt2b* *Wnt5a*, *Wnt8a* and *Wnt11*, where they are indicative of an activate Wnt/β-catenin signalling (Marikawa, 2006). This is essential for neural induction and a pre-requisite for gastrulation in this species. Moreover, as will be discussed, Wnt/β-catenin signalling subsequently plays a role in A-P axis specification as a caudalising factor (section 1.2.2.2).

A number of genes (*T*, *Cripto* and *nodal*) are expressed in the proximal rim of the epiblast and later in the posterior side where the primitive streak forms. It is unclear what induces the primitive streak but a combination of signals from the extraembryonic tissues (such as *Bmp4* from the extraembryonic ectoderm) and cell movements may contribute to the expression of these early primitive streak markers and its subsequent formation (Beddington and Robertson, 1998; Beddington and Robertson, 1999).

1.1.7.2.2. Wnt/β-catenin signalling

One of the first cases of axis duplication or twinning was reported in *Kinky* mice in 1949 by Gluecksohn-Schoenheimer. The gene was later identified as one of the alleles at the *Fused* locus and renamed *Axin1*, a negative regulator of the Wnt/β-catenin pathway and shown to cause partial axis duplication in mouse (Zeng et al., 1997). Adenomatous polyposis coli (Apc) is another negative regulator of Wnt/β-catenin pathway. Embryos homozygous for a hypomorphic allele of *Apc*, exhibit expansion of node and partial axis duplication (Ishikawa et al., 2003). *Tcf3*$^{-/-}$ (also a negative regulator of the pathway) embryos form an enlarged primitive streak and multiple neural folds (Merrill et al., 2004). The expression of chick *Wnt8c* gene under the human *β-Actin* promoter in mouse also causes some axis duplication, although the new axis lacks the most anterior structures as shown by the absence of the forebrain marker *Hesx1* (Popperl et al., 1997).

These results, collectively demonstrate that, upregulation of the Wnt/β-catenin pathway causes partial axis duplication, probably caused by an expansion in primitive streak and node, since mouse embryos with a constitutively active β-catenin show a premature transition of epithelial-mesenchymal cells (Kemler et al., 2004). Therefore, the activation of this pathway is important for the formation of the primitive streak and subsequently the node. This is further demonstrated by mouse models with under-active Wnt/β-catenin signalling. *Wnt3*$^{-/-}$ mutant mice do not form a primitive streak or node and hence lack mesoderm or definitive endoderm; the AVE in these embryos is, however, correctly specified and patterned, although the embryonic ectoderm does not subsequently acquire an anterior neural character (Liu et al., 1999b). β-catenin is also important for primitive streak formation. Mice lacking *β-catenin*, do not form a mesoderm but also display defects in A-P axis formation, reiterating the importance of this pathway in both processes (Huelsken et al., 2000).

1.1.7.2.3. BMPs

As previously mentioned, the initial neural inductive event in all systems studied is BMP inhibition. Although, there are indications of this also taking place in mammals, BMPs have not been shown to have such a central role as in lower vertebrates such as

amphibians. In fact, it is inhibition of BMPs, WNTs and nodals together, which plays a crucial part in induction of neural tissue in mice (Tam and Gad, 2004). A redundancy for the roles of *Noggin* and *Chordin* has also been demonstrated by the mouse knockouts of these genes. Neither *Nog* nor *Chrd* homozygous null mice, show a severe gastrulation defect but the double mutants show a range of defects affecting all three embryonic axes, although they are able to form a neural plate (McMahon et al., 1998; Bachiller et al., 2000; Bachiller et al., 2003). Additionally, the analysis of *HNF3β* mutant mice has demonstrated that although these mice lack a node and its derivatives, and hence do not express *Noggin* or *Chordin*, neural induction and A-P axis patterning takes place (Ang and Rossant, 1994; Klingensmith et al., 1999).

A recent study, however, highlights the sole role of BMP signalling in mammalian neural induction. *Bmpr1a* (or *Alk3*) is a type I BMP receptor, expressed in the epiblast of the implanting mouse embryo. Mice lacking *Bmpr1a* show ectopic expression of anterior neural marker such as *Hesx1*, *Six3* and *Sox1*; as well as a downregulation of pluripotency markers such as *Oct4*, *Nanog*, *Nodal* and *Cripto* (Di Gregorio et al., 2007). This phenotype is similar to that of *Nodal*$^{-/-}$ mice, where anterior neural markers such as *Hesx1* are prematurely and ectopically expressed (Camus et al., 2006). These data suggest that, mouse neural induction requires an early inhibition of BMPs (prior to gastrulation), and that Nodal signalling acts downstream of BMPs in this process.

Collectively, these data increasingly imply that the process of neural induction is more complex than previously thought. A number of the signalling molecules (BMPs, FGFs and WNTs) are involved and their interactions, spatially and temporally, impose the correct cellular identity on the ectoderm layer. As shown in mice, cellular movement is also essential for this process, and together with molecular cues from both embryonic and extraembryonic tissues, lead to the formation of mesoderm, which is a requirement for neural induction.

Despite differences between species, it is still highly likely that the mechanisms of neural induction and that of axis specification are conserved among all vertebrates. The disparities may be due to different experimental procedures as well as timing. Additionally, the importance of extraembryonic tissues for signalling and the cup-shape of the mammalian gastrula create apparent differences, which may prove to be an adaptable mechanism to viviparity rather than differences in the mechanisms of neural induction between mammals and other vertebrates.

1.2. FOREBRAIN INDUCTION, PATTERNING AND DEVELOPMENT

1.2.1. Introduction

In birds and mammals, the forebrain is enlarged at the expense of hindbrain compared to teleosts and amphibians. Although, this added complexity creates differences in gene regulation between species resulting in differences in capability of the mature brain, amazingly the mechanisms of anterior neural induction and patterning during embryonic development are conserved from frogs to mammals, mostly involving the same key players.

The neural plate is first visibly divided during the process of neurulation, when the neural tube is closing. Ring-like constrictions mark the first set of boundaries that divide the neural tube, anterior to posterior, into forebrain (prosencephalon), midbrain (mesencephalon), hindbrain (rhombencephalon) and spinal cord (Figure 1.3). Each of these regions is further subdivided into both longitudinal and transverse partitions, characterised by their own set of markers, which incidentally interact with each other positively and/or negatively to give the CNS a grid-like pattern of gene expression. The longitudinal subdomains consist of, ventral to dorsal, the floor, basal, alar and roof plates (Figure 1.4A).

The forebrain has been proposed to be transversally divided into compartments called prosomeres (Rubenstein et al., 1998). These are thought to be similar to the rhomobomeres, which are separate territories in the developing hindbrain. However, cell lineage restriction has not been solidly proven in the prosomeres and these boundaries are therefore hypothetical (Figure 1.4B-C).

Anatomically, the developing forebrain consists of the telencephalon, which will form the cerebral hemispheres, basal ganglia, hippocampus and olfactory bulbs in the mature brain, and the diencephalon, which gives rise to the epithalamus, thalamus and hypothalamus (Figure 1.5). Eyes and the pituitary gland develop in close association with the forebrain, although they are not entirely of neural origin (section 1.4 looks at the development of the pituitary gland). The mature forebrain controls basic functions, and in humans, it is where the highest cognitive functions, including intelligence, memory and emotions reside.

After the initial induction and early maintenance of anterior character, local signalling centres develop within the brain primordium. These are sources of signals that act on the adjacent cells to further maintain and refine regionally restricted cellular identity. This results in compartments where populations within a cell lineage are restricted to a particular position (Lumsden and Krumlauf, 1996). Among the signalling centres in the brain are the anterior neural ridge (ANR), which is a source of *Fgf8* and WNT antagonists, the zona limitans intrathalamica (ZLI), which signals through *Shh*, and the midbrain-hindbrain boundary (MHB) or isthmic organiser, which expresses *Fgf8* (Rhinn et al., 2006).

The ANR includes the cells in the rostral margin of the neural plate or the row-1 cells (Houart et al., 1998). *Fgf8* expression in this region seems to regulate telencephalic markers such as *Bf1* (Shimamura and Rubenstein, 1997). However, the relatively late onset of *Fgf8* expression, redundancy between different FGFs, as well as the identification of WNT antagonists such as *tlc*, all indicate that the induction of telencephalon by ANR is more complex and involves an array of signalling molecules. Nevertheless, it is very likely that *Fgf8* expression in the ANR has a similar role to its expression in the isthmus, where it is required for A-P patterning (Liu et al., 1999a). The importance of *Fgf8* in the ANR for normal forebrain development is further demonstrated in *Hesx1*$^{-/-}$ and *Hex*$^{-/-}$ mutants, which show a reduction or absence of *Fgf8* expression in this region (Martinez-Barbera and Beddington, 2001).

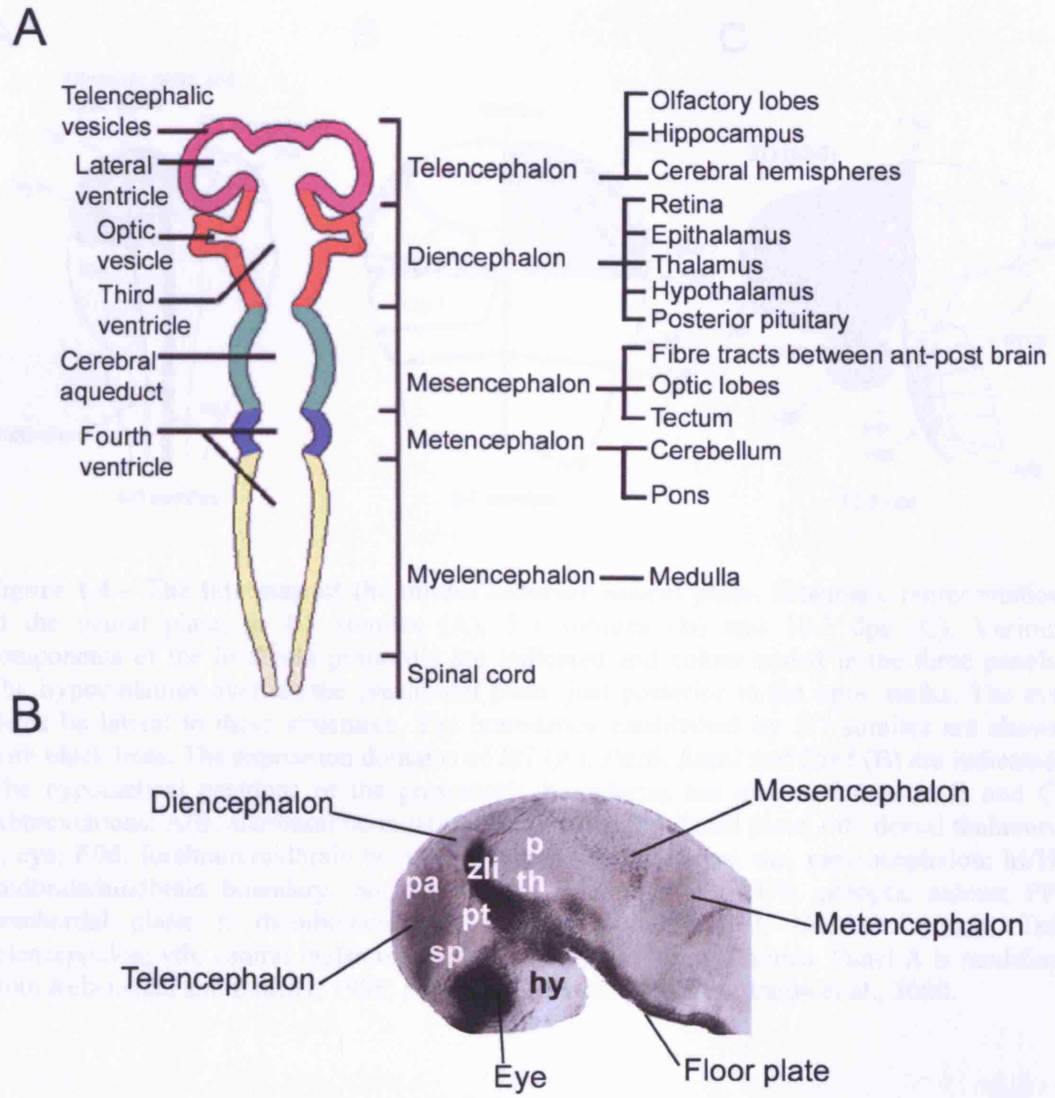

Figure 1.3 – Divisions of the neural plate in the developing vertebrate embryo. A) Schematic representation of the developing neural plate. The divisions of the neural plate at embryonic stages are indicated on the left and the structures they give rise to in the adult, are shown on the right. B) Lateral view of a zebrafish embryo after in-situ hybridisation with *shh* (dark staining). Various structures of the developing brain are indicated. Abbreviations: p, pretectum; pa, pallium; pt, prethalamus; sp, subpallium; th, thalamus; zli, zona limitans intrathalamica. Panel A is adapted from developmental biology online (University of Guelph) and panel B is modified from Wilson and Houart, 2004.

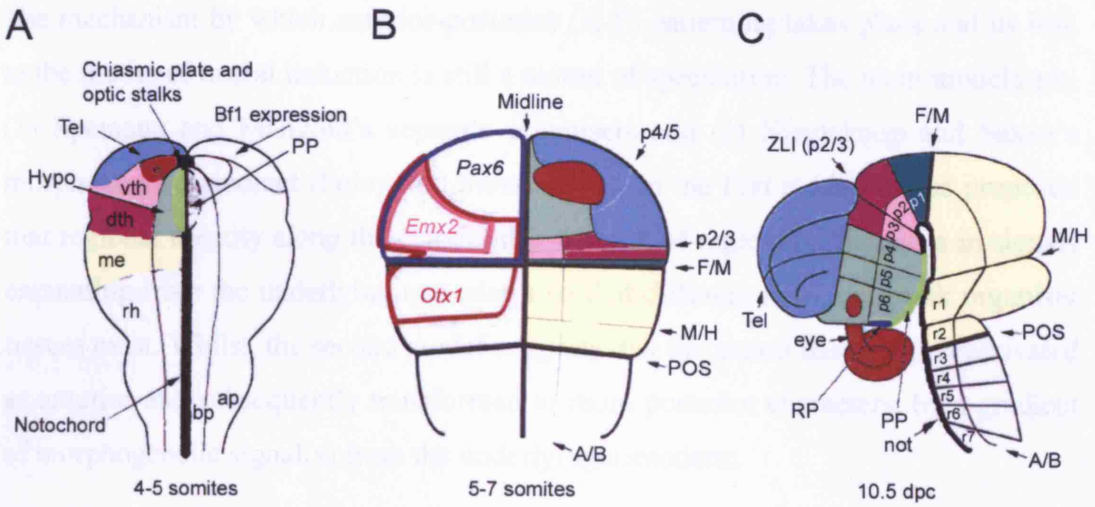

Figure 1.4 – The fate map of the mouse anterior neural plate. Schematic representation of the neural plate, at 4-5 somites (A), 5-7 somites (B) and 10.5 dpc (C). Various components of the forebrain primordia are indicated and colour coded in the three panels. The hypothalamus overlies the prechordal plate, just posterior to the optic stalks. The eye fields lie lateral to these structures. The boundaries established by 5-7 somites are shown with black lines. The expression domains of *Bf1* (A), *Pax6*, *Emx2* and *Otx1* (B) are indicated. The hypothetical positions of the prosomeric boundaries are also indicated in B and C. Abbreviations: A/B, alar/basal boundary; ap, alar plate; bp, basal plate; dth, dorsal thalamus; e, eye; F/M, forebrain/midbrain boundary; Hypo, hypothalamus, me, mesencephalon; M/H, midbrain/hindbrain boundary; not, notochord; p, prosomere; POS, preoptic sulcus; PP, prechordal plate; r, rhombomere; rh, rhombencephalon; RP, Rathke's pouch; Tel, telencephalon; vth, ventral thalamus; ZLI, zona limitans intrathalamica. Panel A is modified from Rubenstein and Beachy, 1998; panels B-C are adapted from Inoue et al., 2000.

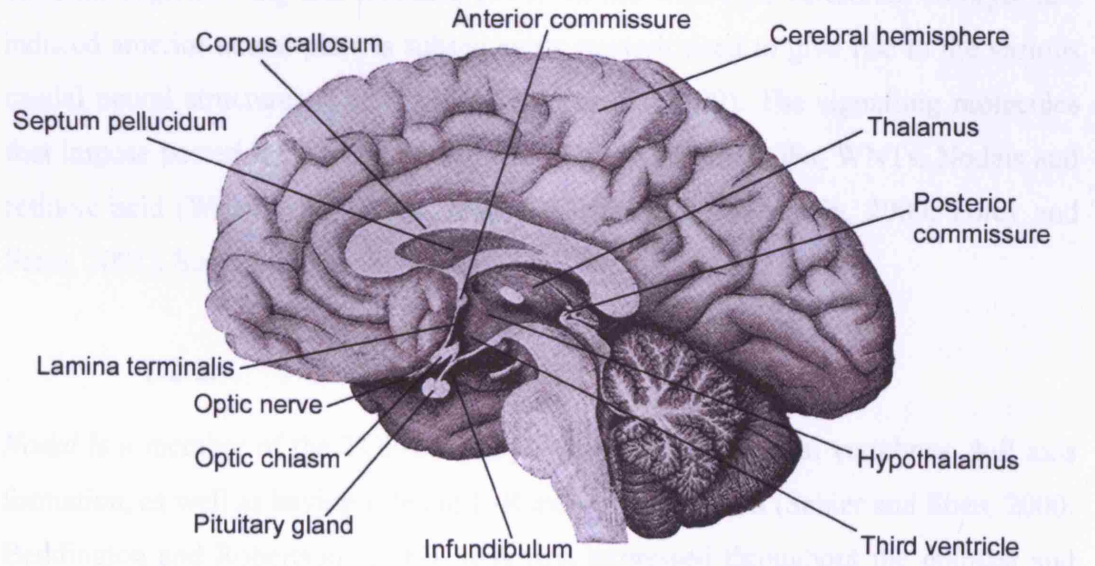

Figure 1.5 – Midline structures of the human forebrain. Median, sagittal plane section through a human brain, showing the midline components of the forebrain. Figure is modified from Gray's anatomy of the human body, 1918 (Bartleby.com).

The mechanism by which anterior-posterior (A-P) patterning takes place and its link to the model of neural induction is still a matter of speculation. The main models are: (1) Spemann and Mangold's separate organisers and (2) Nieuwkoop and Saxen's morphogenetic gradient (Foley and Stern, 2001). In the first model, it was proposed that regional identity along the ectoderm is a result of regional differences in signals emanating from the underlying mesoderm so that different head and trunk organiser tissues exist. Whilst, the second model suggests that the neural tissue is first activated as anterior and subsequently transformed to more posterior characters, by a gradient of morphogenetic signal(s) from the underlying mesoderm.

Whether the first model is taken into account or the second or indeed an interpretation of both, what is clear is that the signals involved are the selected few that have repeated roles during development. In addition, there is the possibility that other, as yet unidentified, factors are also involved in the process.

1.2.2. Anterior-posterior patterning of the neural plate

A number of studies suggest that the induced neural plate initially possesses an anterior identity. For example, the expression pattern of markers such as *Otx2* is initially in the entire neural plate and consequently restricted to the forebrain and midbrain regions (Ang and Rossant, 1994). In the wild-type vertebrate embryo, this induced anterior neural plate is subsequently posteriorised to give rise to the various caudal neural structures (Stern, 2001; Muhr et al., 1999). The signalling molecules that impose posterior character on the neural plate are the FGFs, WNTs, Nodals and retinoic acid (Wilson and Houart, 2004; Wilson and Rubenstein, 2000; Foley and Stern, 2001). Some of them are discussed below.

1.2.2.1. Nodal signalling

Nodal is a member of the TGF-β family, which is important in vertebrate A-P axis formation, as well as having roles in L-R axis determination (Schier and Shen, 2000; Beddington and Robertson, 1999). It is first expressed throughout the epiblast and the visceral endoderm and later in development it becomes restricted to the future posterior side of the embryo, hence it acts to promote posterior cell fates. It has additional roles in the maintenance of patterning in the extraembryonic ectoderm and

visceral endoderm. The latter role is Smad2 dependent and is important in the specification of anterior identity in the embryo (Brennan et al., 2001). A recent study has shown that in the absence of nodal, the epiblast prematurely acquires an anterior neural character, indicating both a requirement for nodal inhibition in anterior neural development and the involvement of nodal in the default model of anterior neural induction in mouse (Camus et al., 2006).

Mice lacking *Cripto* (a nodal co-receptor) show a phenotype where distal epiblast cells never move proximally to their AVE location and proximal cells destined to form the primitive streak also never make this transition. Interestingly, anterior forebrain tissue develops in *Cripto* mutants, although at a more posterior position. This results in embryos exhibiting a head without a trunk phenotype (Ding et al., 1998). These findings indicate that lack of nodal signalling prevents the cell movements essential for A-P axis elongation, as well as disrupting caudalising signals essential in mesendoderm formation. The result is the "default" formation of forebrain but in a more posterior location. Although, working through a different mechanism, a similar phenotype is seen in $Fgf8^{-/-}$ mutant mice, in which there is no anterior movement of the AVE, resulting in the absence of hindbrain at the expense of fore- and midbrain (Sun et al., 1999).

Cerberus-like, expressed in the mouse AVE, acts as an anti-nodal and anti-BMP but does not display the anti-WNT ability of *Xenopus cerberus*. Another anti-nodal in the AVE is *Lefty1*. Neither *Cerberus-l* nor *Lefty1* homozygous mice show gastrulation defects; however, the double mutants display a lack of head development, as ectopic trunk mesoderm is formed in the head region. If nodal is reduced, then these defects are partially rescued as shown in $Nodal^{+/-};Cer\text{-}l^{-/-};Lefty1^{-/-}$ mutants (Belo et al., 2000; Perea-Gomez et al., 2002).

Work in zebrafish also mostly correlates with the mouse data. *One-eyed pinhead* (*oep*) is the orthologue of *Cripto* while *cyclops* and *squint* are orthologues of nodal ligands in zebrafish. These mutants also display more caudally located and enlarged forebrain structures (Gritsman et al., 1999).

1.2.2.2. Wnt/β-catenin signalling

Evidence from zebrafish and *Xenopus*, as well as growing evidence from mouse and chick, has shown that Wnt/β-catenin signalling is required for normal A-P patterning. For example, mice deficient in *β-catenin* (apart from a failure to form primitive streak) display an A-P patterning defect, where the expressions of *Hex* and *Hesx1* never appear and *Cer-l* remains distal at 6.5 dpc. Chimeric studies show the requirement of *β-catenin* in the epiblast for the correct movement of visceral endoderm cells to the future anterior side of the embryo (Huelsken et al., 2000).

A phenotype is seen in *Wnt3a*$^{-/-}$ and *Lef1*$^{-/-}$;*Tcf1*$^{-/-}$ mice (all positive regulators of Wnt/β-catenin signalling), where mesoderm is not specified (Takada et al., 1994; Galceran et al., 1999). Interestingly, a hypomorph of *Wnt3a* called *Vestigial tail* shows a dosage dependent role of *Wnt3a* in the development of more posterior structures such as the tail and somites, where increasing *Wnt3a* is required for the development of more posterior structures (Greco et al., 1996).

The role of Wnt/β-catenin signalling in A-P patterning is unequivocally demonstrated in the development of the anterior forebrain. For example, in *Six3*$^{-/-}$ mice, rostral structures such as the telencephalon are lost and there is evidence of enhanced WNT activity in these mutants (Lagutin et al., 2003). In zebrafish *tlc* (a sFRP family member) mutants, there is a delay and reduction in telencephalic markers (Houart et al., 2002). Also *masterblind* and *headless* mutants with disruptions to their *axin1* and *tcf3* loci respectively, show a lack of telencephalon and eyes (van de et al., 2001; Kim et al., 2000). Similarly *bozozok* mutants show reduction or absence of anterior neural fates (Fekany et al., 1999). The products of all these genes act through the negative regulation or antagonism of the Wnt/β-catenin pathway.

In chick, the role of Wnt/β-catenin signalling is elegantly demonstrated using neural plate explants and embryo culture (Nordstrom et al., 2002). In this study, WNTs are shown to directly impose caudal identity on neural cells. A gradient of WNT signalling, in combination with FGFs is shown to progressively specify caudal forebrain, midbrain and rostral hindbrain.

Generally, in all organisms tested: *Xenopus* (Fredieu et al., 1997; Hamilton et al., 2001); zebrafish (Kelly et al., 1995; Kim et al., 2000; Heisenberg et al., 2001; van de

et al., 2001); chick (Roeser et al., 1999) and mouse (Popperl et al., 1997), activation of Wnt/β-catenin signalling after gastrulation (overexpressing *β-catenin* or inactivating WNT antagonists *tcf3* and *axin1* or treatment with Li^+ ions), leads to a reduction in anterior structures. Interestingly, these studies show that within the anterior forebrain, the eye is particularly sensitive to Wnt/β-catenin signalling.

Inversely, overexpression of WNT antagonists results in enlarged heads and shortened trunks (Leyns et al., 1997), indicating that Wnt/β-catenin signalling has an inhibitory influence over neural fate acquisition and anterior structure formation after gastrulation.

1.2.2.3. Transcription factors

In mouse, the idea of separate head and trunk organisers was first proposed as the two signalling centres are physically separated. However, in light of the information discussed thus far, it is believed that this physical separation is a necessity to protect the anterior forebrain from caudalising factors that are secreted by the node such as the WNTs, FGFs, Nodals and RA.

The disruption of cell movement or signalling in the AVE results in the lack of anterior CNS. The importance of this tissue in normal anterior patterning is demonstrated by ablation experiments in mouse, where the removal of the AVE impairs the expression of forebrain markers such as *Hesx1* (Thomas and Beddington, 1996). There is, therefore, an array of genes whose absence from the visceral endoderm results in anterior head truncations in mouse (Table 1.1). These include *Lim1/Lhx1* (Shawlot and Behringer, 1995; Perea-Gomez et al., 1999), *Otx2* (Acampora et al., 1995; Matsuo et al., 1995; Rhinn et al., 1998), *HNF3β* (Dufort et al., 1998), *Smad2* (Waldrip et al., 1998; Nomura and Li, 1998) and *Nodal* (Varlet et al., 1997a; Brennan et al., 2001).

Lim1, *Otx2* and *HNF3β* are three transcription factors required in the AVE for anterior neural plate induction. Mice mutant for these genes lack structures rostral to otic vesicles. *HNF3β* and *Lim1* are both expressed in the entire VE before gastrulation and subsequently in the AVE, primitive streak and node. $HNF3\beta^{-/-}$ mice do not develop a head and also display D-V patterning defects (Ang and Rossant, 1994). $Lim1^{-/-}$ mice also show a headless phenotype (Shawlot and Behringer, 1995). Double homozygous mouse mutants ($HNF3\beta^{-/-};Lim1^{-/-}$) show a phenotype more

severe than each of the single mutants, with the primitive streak being abnormally expanded (Perea-Gomez et al., 1999).

Otx2 is expressed in the epiblast and VE before gastrulation and subsequently in the AVE, anterior epiblast and the node (Ang et al., 1994). Similarly *Otx2*$^{-/-}$ mouse mutants do not develop a head (Acampora et al., 1995). Moreover, there is a direct protein-protein interaction of OTX2 with HNF3β and LIM1 (Nakano et al., 2000). It is, therefore, highly likely that these three transcription factors work in the same pathway in the VE in order to regulate transcription of genes required for normal head development. Later, *Otx2* is expressed in the forebrain and midbrain, stopping sharply at the mid/hindbrain boundary. Its negative interaction with *Gbx2* in this region is thought to have important roles in the positioning of the isthmus as well as the patterning of the forebrain (Martinez-Barbera et al., 2001).

Other than the genes discussed above, there are two additional transcription factors expressed in the AVE, *Hex* and *Hesx1*, which are also required for normal forebrain development (Martinez-Barbera and Beddington, 2001). *Hex* is one of the earliest markers expressed in the AVE. Its expression is seen in the distal VE before the appearance of the primitive streak. This expression then moves to a medial strip of the AVE. With the start of gastrulation, *Hex* transcripts are also seen in anterior definitive endoderm, which then extends rostrally to displace the AVE. *Hesx1* expression is first detected in the AVE at the start of gastrulation. The transcripts then extend to the axial mesendoderm and overlying anterior neural ectoderm. In the absence of either of these genes, the development of the most anterior forebrain structures is affected. However, the mechanism is distinct from *Lim1*, *Otx2* and *HNF3β*. The role of *Hesx1* is discussed in detail in section 1.3, suffice to say here that *Hesx1* is not required in the AVE but its action in epiblast derivatives (most likely in the ANE) is essential for forebrain development (Martinez-Barbera et al., 2000). Similarly, *Hex* is unlikely to be required in the AVE. The ADE and AME are not specified properly in *Hex*$^{-/-}$ mice and it is the requirement of *Hex* in these tissues which leads to the forebrain defects seen in the mutants. The *Hex* mutant emphasises the role of vertical signals emanating from the underlying mesendoderm tissues in the specification of neural character in the ectoderm.

Table 1.1 – Genes implicated in neural induction and axis specification during mouse gastrulation.

Gene	Expression	Mouse mutant	References
Transcription factors			
Hesx1	AVE at the onset of gastrulation and in the anterior AME and anterior neural ectoderm during and after gastrulation	Forebrain truncations	(Hermesz et al., 1996; Thomas and Beddington, 1996; Martinez-Barbera and Beddington, 2001)
Hex	Distal VE and AVE before gastrulation, AVE and ADE during gastrulation	Forebrain truncations	(Thomas et al., 1998; Martinez-Barbera and Beddington, 2001)
Otx2	Entire epiblast and VE before gastrulation, and restricted to anterior epiblast and AVE and EGO during gastrulation	Headless	(Acampora et al., 1995; Matsuo et al., 1995; Ang et al., 1994)
Lim1	VE before gastrulation and AVE, anterior primitive streak, EGO, node and mesoderm wings during gastrulation	Headless[1]	(Shawlot and Behringer, 1995; Perea-Gomez et al., 1999)
HNF-3β	VE before gastrulation and AVE, anterior primitive streak, EGO, node and axial mesoderm derivatives during gastrulation	Headless and D-V patterning defects[1,2]	(Ang et al., 1993; Ang and Rossant, 1994)
Goosecoid	AVE before gastrulation, AVE and EGO during gastrulation	No brain defects[2]	(Belo et al., 1997; Filosa et al., 1997)
Six3	Anterior neural plate during and after gastrulation	Forebrain truncations	(Oliver et al., 1995; Lagutin et al., 2003)
Brachyury/T	Proximal epiblast before gastrulation and posterior epiblast, primitive streak and node during gastrulation	Mesoderm formation and migration defects	(Wilkinson et al., 1990; Thomas et al., 1998; Wilson et al., 1995)

Wnt signalling			
Wnt3	Proximal epiblast before gastrulation, primitive streak and mesoderm during gastrulation	Lack of primitive streak, node and their derivatives as well as anterior neural patterning defects	(Liu et al., 1999b; Thomas et al., 1998)
Wnt3a	Primitive streak and EGO	Posterior truncation and defects in paraxial mesoderm and somite formation	(Takada et al., 1994; Greco et al., 1996)
Wnt5a	Primitive streak and EGO	A-P axis extension defects	(Yamaguchi et al., 1999)
Wnt8	EGO	No mouse mutant available	(Bouillet et al., 1996)
Wnt11	Node and extraembryonic mesoderm	No mouse mutant available	(Kispert et al., 1996)
β-catenin	Ubiquitous	Defects in mesoderm, ectoderm and A-P axis formation	(Huelsken et al., 2000; Haegel et al., 1995)
Lef1	Primitive streak	No neural defects[3]	(Oosterwegel et al., 1993; van Genderen et al., 1994; Galceran et al., 1999)
Wnt antagonists			
Frzb1	Primitive streak and EGO	No mouse mutant available	(Leyns et al., 1997; Hoang et al., 1998)
Dkk1	AVE and ADE as well as prechordal mesoderm	Forebrain truncations	(Glinka et al., 1998; Mukhopadhyay et al., 2001)
Axin1	Ubiquitous	Partial axis duplication	(Zeng et al., 1997)
Tcf3	Primordia of fore-, mid- and hinbrain	Enlarged primitive streak and multiple neural folds of posterior character	(Galceran et al., 1999; Merrill et al., 2004)

TGFβ antagonists

Noggin	Node	Single mutants do not display neural/patterning defects[4]	(Rhinn et al., 1998; Shawlot et al., 1998; Bachiller et al., 2000)
Chordin	EGO and node		
Cerberus-l	AVE and ADE before and during gastrulation	Single mutants do not display neural/patterning defects[5]	(Belo et al., 1997; Belo et al., 2000; Shawlot et al., 1998; Meno et al., 1996; Perea-Gomez et al., 2002; Oulad-Abdelghani et al., 1998)
Lefty1	AVE before and during gastrulation		

Other signalling molecules

Nodal	AVE and entire epiblast before gastrulation, restricted to proximal and posterior epiblast and node during gastrulation	Failure to establish primitive streak, premature neural induction	(Varlet et al., 1997b; Conlon et al., 1994; Camus et al., 2006)
Cripto	AVE and entire epiblast before gastrulation, restricted to proximal and posterior epiblast during gastrulation	Head without a trunk	(Ding et al., 1998)
Bmp7	EGO and node	No neural defects	(Dudley et al., 1995; Arkell and Beddington, 1997)
Bmp4	Primitive streak	Lack of primitive streak and posterior structures	(Winnier et al., 1995)
Smad2	Ubiquitous during gastrulation	Lack of embryonic mesoderm and AVE formation	(Waldrip et al., 1998)
Shh	Node, prechordal plate and ventral forebrain	Midline structure defects	(Chiang et al., 1996)
Fgf8	Primitive streak and AVE	Head without a trunk, posterior patterning defects	(Crossley and Martin, 1995; Sun et al., 1999)

1: *Lim1*$^{-/-}$;*HNF3β*$^{-/-}$ mutants have expanded primitive streak at the expense of anterior regions.
2: *Gsc*$^{-/-}$;*HNF3β*$^{-/-}$ mutants show D-V patterning defects along the length of CNS.
3: *Lef1*$^{-/-}$;*Tcf1*$^{-/-}$ mutants show defects in paraxial mesoderm formation similar to *Wnt3a*$^{-/-}$.
4: *Nog*$^{-/-}$;*Chrd*$^{-/-}$ mutants display forebrain deletions.
5: *Cerl*$^{-/-}$;*Lefty1*$^{-/-}$ mutants show a lack of head development at the expense of trunk mesoderm.

1.2.3. Dorso-ventral patterning of the neural plate

Following the induction of anterior neural identity, a number of signals and mechanisms are involved in A-P (as discussed above) and D-V patterning of the neural plate, as well as the regionalisation within local domains. Fate mapping studies have shown that after the establishment of the A-P axis, soon after gastrulation, a second axis is formed that runs medial to lateral. These are the forerunners of the ventral and dorsal regions of the neural tube, respectively. Hence within the prosencephalic neural plate region, medial cells constitute the ventral forebrain whilst, lateral cells go on to colonise the dorsal forebrain (Rubenstein et al., 1998).

Just as extraembryonic tissues, such as the AVE, play important roles in patterning of the neural plate, vertical signals from underlying tissues, such as the axial and paraxial mesoderm and endoderm, play essential roles in both A-P and D-V patterning of the neural plate/tube (Placzek et al., 1993; Itasaki et al., 1996). For example, the notochord underlying the spinal cord specifies medial/ventral cell fates (Tanabe and Jessell, 1996; Placzek, 1995). In the anterior regions this role is played by the prechordal plate, which is the mesendormal tissue underlying the medial prosencephalic neural plate.

An important signal secreted by the entire length of axial mesendoderm (prechordal plate and notochord) is sonic hedgehog (SHH). Graded activity of this morphogen establishes expression of transcription factors in distinct domains along the D-V axis of the neural tube, resulting in the differentiation of different neuronal cell types (Placzek and Briscoe, 2005; Ingham and Placzek, 2006). Although *Shh* is the ventral regulator in caudal neural tube, it displays the same role in more rostral regions, where it induces ventral forebrain/hypothalamus (Ericson et al., 1995).

It is still unclear what makes the same signal (*Shh* in this case) induce different identities, depending on its position along the A-P axis. One explanation is that the competence of the overlying neurectoderm cells is different along the rostral-caudal length of the neural tube. Although there is no firm evidence for this, the possibility should not be ruled out. Additionally, there is evidence suggesting that the vertical signals from the axial mesendoderm are different along the length of the A-P axis. For example, *Bmp7* is expressed in the prechordal plate but not in the more caudal

mesendoderm (Dale et al., 1999; Vesque et al., 2000). BMP7 along with SHH is thought to promote hypothalamic identity at the expense of floor plate, as shown in explant experiments (Dale et al., 1997; Dale et al., 1999).

The forebrain is a very complex structure; this is also reflected in its development and patterning during embryogenesis. Fate mapping studies, as well as genetic and molecular analyses of mutants have demonstrated that although, mammals have evolved more complex features such as the neocortex, the patterning of the forebrain is essentially conserved among vertebrates. Such studies have shown that A-P patterning in the embryo starts before the onset of gastrulation. At the start of gastrulation, neural induction gives rise to the neural plate that has an anterior identity. Subsequently, tissues such as the axial mesendoderm as well as the neurectoderm itself emit signals to further maintain and embellish the A-P (WNTs, FGFs, Nodals, RA) and subsequently D-V (SHH and BMPs) pattern. As a result, specific transcription factors are expressed in restricted domains of the developing neural plate that in turn confer the correct cellular identity. This results in the appearance of signalling centres that further pattern the adjacent regions and give rise to compartments within the brain and spinal cord. The correct spatio-temporal interaction among these signals and processes is essential for normal CNS development.

1.3. MOUSE *Hesx1*

1.3.1. The *Hesx1* gene

As seen in previous sections, a large number of genes are involved in the induction and patterning of the CNS in the early vertebrate embryo. Although most of the genes discussed encode secreted factors involved in signalling pathways, their targets play the ultimate role in conferring a particular cellular identity. One class of these target genes encode transcription factors, which are proteins that bind specific DNA sequences in order to activate and/or repress a set of target genes. Transcription factors comprise a large family of proteins that are divided into groups according to their structure and function. They also represent one of the four major groups of proteins whose mutations are associated with human disease (Chi, 2005; Jimenez-Sanchez et al., 2001).

Homeobox transcription factors are distinguished by the presence of the homeobox, which encodes a motif called the homeodomain. The homeodomain is a conserved 60 amino acid domain that recognises and binds target DNA sequences containing the core binding site TAAT. The homeodomain folds into four alpha helices, the third helix binds to the DNA major groove, whilst the first helix contacts the minor groove of the DNA double helix (Holland and Takahashi, 2005). Homeodomain specificity is thought to be aided in part by the interaction of transcription factors with other proteins, including the formation of homodimers (Wolberger, 1996; Wilson et al., 1993). Homeobox genes have important roles in development of both vertebrate and invertebrate species, conferring positional value along the embryonic A-P axis.

Hesx1 encodes a transcriptional repressor, belonging to the paired-like family of homeobox transcription factors. *Hesx1* was first isolated in mouse ES cells, showing homology to the *Xenopus Xanf1* gene (Thomas and Rathjen, 1992; Zaraisky et al., 1992) and was localised to mouse chromosome 14 (Webb et al., 1993). It was subsequently, isolated from the Rathke's pouch and hence named *Rpx* (Hermesz et al., 1996). The other homologues of *Hesx1* are *Ganf* in the chick (Knoetgen et al., 1999), *Danf/Zanf* in zebrafish (Spieler et al., 2004; Reim and Brand, 2002) and *HESX1* in humans (Dattani et al., 1998).

1.3.2. The expression of *Hesx1*

Hesx1 is absent in invertebrates and its rostral expression pattern in vertebrate embryos is dynamic, reflecting its essential role in the early patterning and development of forebrain and related structures (Hermesz et al., 1996; Thomas and Beddington, 1996; Kazanskaya et al., 1997; Knoetgen et al., 1999). In the mouse, it is first detected at the onset of gastrulation at 6.5 dpc in the AVE (Figure 1.6). Half a day later, its transcripts are detected in the axial mesendoderm and by 7.5 dpc its expression pattern is broadened to also cover the anterior neural ectoderm. 8.5 dpc is the stage when *Hesx1* transcripts are abundant in the rostral neural ectoderm and oral ectoderm and by 9.0 dpc, *Hesx1* expression is in ventral diencephalon and Rathke's pouch anlage. It remains exclusively in the Rathke's pouch from 10.5-13.5 dpc, after which point the transcripts are no longer detected (Martinez-Barbera and Beddington, 2001; Hermesz et al., 1996; Dattani et al., 1998; Thomas and Beddington, 1996). The expression of *Anf* genes in other vertebrates follow similar patterns (Knoetgen et al., 1999; Kazanskaya et al., 1997; Martynova et al., 2004).

This spatio-temporal expression of *Hesx1* transcripts during early vertebrate development is in part regulated by conserved *cis*-elements in 3', 5' and intragenic sequences of *Hesx1* (Eroshkin et al., 2002; Hermesz et al., 2003; Chou et al., 2006). Distinct regulatory elements are required for *Hesx1* expression in the ANE/AME and the Rathke's pouch. These works also demonstrate possible binding sites for a number of factors, which could be involved in the regulation of *Hesx1* expression, such as LIM homeodomain, OTX2, PITX2, GATA and SOX proteins.

A
B
C
D
E
F
G
RP
H
I
J

Figure 1.6 – *Hesx1* expression in the developing mouse embryo. (A-F) Whole mount in-situ hybridisation with *Hesx1*, in the developing forebrain from 6.5-9.5 dpc. (G-J) Section in-situ hybridisation with *Hesx1*, in the developing pituitary from 9.5-14.5 dpc. A) *Hesx1* transcripts are first detected in the AVE at the onset of gastrulation at ~6.5 dpc. B) At late-streak stages (~7.0 dpc), *Hesx1* is expressed in the anterior axial mesendoderm. C) By head fold stages (~7.5 dpc) the *Hesx1* expression domain also covers the anterior neural ectoderm. D) At early somite stages (~8.5 dpc), the expression of *Hesx1* is very strong in the prospective forebrain region. E) At ~9.0 dpc, *Hesx1* transcripts are restricted to the ventral diencephalon. (F,G) By ~9.5 dpc, *Hesx1* expression is only detected in the invaginating Rathke's pouch (RP). (H-J) This expression in the RP continues until ~12.5 dpc, when a high dorsal to low ventral gradient of *Hesx1* transcripts are observed in the RP (I). After this point, *Hesx1* transcripts are no longer detected, as shown in the ~14.5 dpc RP (J). Panels A-D are taken from Martinez-Barbera and Beddington, 2001; panels G-J are taken from Dasen et al., 2001; panels E-F are from Sajedi.

1.3.3. *Hesx1*$^{-/-}$ mice

Chimeric studies, as well as the deletion of *Hesx1* in mouse, have provided insights into the function of *Hesx1* in the developing forebrain and pituitary gland (Dattani et al., 1998; Martinez-Barbera et al., 2000; Andoniadou et al., 2007). Mouse embryos lacking *Hesx1* show a fully penetrant phenotype, displaying a range of defects affecting forebrain structures such as the telencephalic vesicles, optic vesicles, and olfactory pits, as well as midline defects affecting the floor of hypothalamus and the Rathke's pouch (Dattani et al., 1998).

The onset of forebrain defects is at 8.5 dpc, when there is a reduction in forebrain tissue and optic vesicles fail to develop. By 9.5 dpc these defects become more evident as the telencephalic and optic vesicles are either absent or abnormally small. The phenotype is highly variable with ~50% of homozygous embryos showing a complete absence of telencephalic vesicles, olfactory placodes, eyes and frontonasal mass and the remaining embryos showing a milder phenotype with some degree of reduction in these structures (Figure 1.7) (Dattani et al., 1998 and our own observations). The eye and telencephalic defects are frequently asymmetric, with the right side being generally more severely affected (Andoniadou et al., 2007).

Hesx1$^{-/-}$ mice do not survive to weaning stages and in fact almost all null mutants die perinatally, although this along with the severity of the phenotype is background dependent. The adults and neonate *Hesx1*$^{-/-}$ mice (in specific backgrounds), show a similar range of defects with abnormal telencephalic midline structures (anterior commissures, septum pellucidum and corpus callosum), hypoplastic nasal cavities, olfactory bulbs and olfactory neuroepithelium (Figure 1.7). Eye defects, such as microphthalmia/anophthalmia and defects in the anterior pituitary gland are also fully penetrant in the neonates.

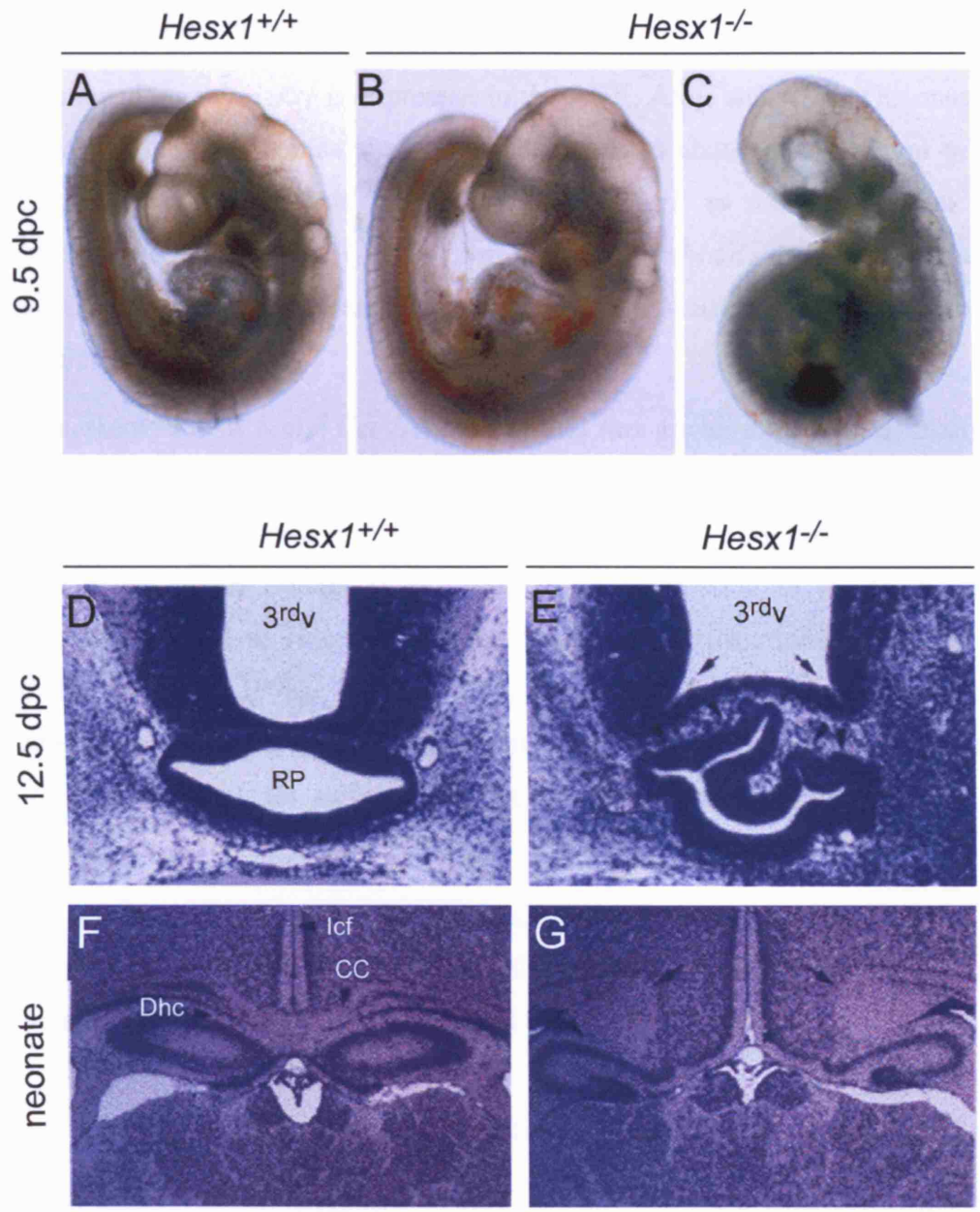

Figure 1.7 – Forebrain and pituitary defects associated with *Hesx1*$^{-/-}$ mutant mice. A) Lateral view of a wild-type 9.5 dpc embryo, with anterior to the left. (B,C) *Hesx1*$^{-/-}$ embryos displaying mild (B) and severe (C) phenotypes. The telencephalic and optic vesicles are either reduced or absent in the null mutants. D) Transverse section through the hypothalamus and Rathke's pouch (RP) of a wild-type 12.5 dpc embryo, stained with hematoxylin and eosin. E) Equivalent transverse section through a *Hesx1*$^{-/-}$ embryo, showing lateral expansion and bifurcation of the RP (arrowheads) as well as bifurcations of the wall of the third ventricle (3rdv, arrows). F) Coronal section through the corpus callosum (CC) and dorsal hippocampal commissures (Dhc) of a wild-type neonate, stained with hematoxylin and eosin. G) Equivalent section through a *Hesx1*$^{-/-}$ brain, showing that the CC is absent (asterisk), although the nerve fibres have formed (arrows). The intercerebral fissure (Icf) is continuous with the third ventricle and the Dhc do not cross the midline. Panels A-C are taken from Martinez-Barbera et al., 2000; panels D-G are taken from Dattani et al., 1998.

1.3.4. The function of *Hesx1*

As mentioned above, *Hesx1* is expressed in the AVE, AME and ANE. The onset of phenotype at the early somite stages coincides with its abundant expression in the ANE. The use of chimeras has shown that *Hesx1* is not required in the extraembryonic derivatives (AVE), for normal forebrain development as a predominantly wild-type visceral endoderm fails to rescue the defects (Martinez-Barbera et al., 2000).

Early markers such as *Lim1*, *Cer-l*, *Shh*, *Six3* and *Rax* are all expressed normally in *Hesx1*$^{-/-}$ at presomitic stages. It is only at early somite stages that the forebrain fails to be maintained and there is a reduction in *Six3* and *Rax* expression (Martinez-Barbera et al., 2000; Dattani et al., 1998). *Fgf8* expression in the forebrain is significantly reduced in *Hesx1*$^{-/-}$ embryos at 4-5 somites (Martinez-Barbera et al., 2000; Dattani et al., 1998). These data highlight the distinct mechanism of *Hesx1* function in forebrain development, indicating that *Hesx1* is required in the anterior neural ectoderm, not for initial induction but for subsequent expansion of the forebrain.

This is also consistent with data in *Xenopus*, where the overexpression of *Xanf1* has been shown to cause expansion of the neural plate at the expense of neural crest and epidermis, without affecting non-ectodermal tissues (Ermakova et al., 1999).

1.3.5. The mechanism of *Hesx1*

The mechanism by which *Hesx1* achieves its function(s) has been somewhat of a speculation until recently. As discussed in section 1.2, evidence from mouse (but also from chick, zebrafish and frog), has provided growing support for Nieuwkoop's "activation-transformation" model. In light of this, *Hesx1* function seems to play an important role in maintaining the anterior neural character of the neural plate and is, therefore, a counterforce to the posterior "transformation" signals that act on the neural plate. Indeed, recent work from our group provides strong support for the hypothesis that HESX1 acts as an anti-Wnt/β-catenin signalling factor (Andoniadou et al., 2007). A new finding is that before the appearance of a morphological defect in *Hesx1*$^{-/-}$ embryos at 2-3 somites, neural crest markers *Pax3* and *Foxd3* are both anteriorised. Additionally, both the WNT ligand *Wnt1* and the Wnt/β-catenin

signalling targets *Axin2* and *Sp5* are anteriorised at these early stages, covering the most rostral tip of the neural plate, where they are not normally expressed.

These data indicate that in the absence of *Hesx1*, the anterior forebrain loses its identity in favour of more posterior ones, in particular the neural crest. By 8.5 dpc, when the reduction in forebrain tissue is evident, the anterior forebrain is already transformed into a posterior fate (the posterior diencephalon), as shown by the anterior expansion of posterior markers *Pax3*, *Foxd3*, *Wnt1* and *Wnt3a* and the reduction of the anterior domains of markers such as *Pax2*, *Fgf8*, *Pax6* and *Six3*.

Fate mapping experiments show that the normal fate of *Hesx1*-expressing cells is to colonise the anterior forebrain (telencephalon, eyes, ventral thalamus and hypothalamus). Only occasionally cells reach posterior forebrain regions (Andoniadou et al., 2007). In the absence of *Hesx1*, however, there is a fate transformation and more of these cells reach the posterior forebrain, giving rise to the neural crest that populate the first branchial arch.

Interestingly, although *Hesx1* is unable to transform posterior forebrain into anterior fates, overexpression studies in mice have shown that it is able to rescue the posterior transformation seen in *Hesx1*$^{-/-}$. In these experiments, the eyes require a higher dosage of *Hesx1* than the telencephalon for a complete rescue.

Recent findings in *Xenopus* also support a role for the *Hesx1* orthologue *Xanf1* in suppressing posterior fates in anterior forebrain (Ermakova et al., 2007). This work shows that *Xanf1* downregulates expression of *Otx2* and *Pax6* (posterior forebrain markers) in the anterior forebrain. In the knockdown morphant embryos, these factors are anteriorised, whilst rostral markers such as *Bf1*, *Bf2*, *Fgf8* and *Nkx2.4* are dowregulated. This demonstrates that *Hesx1* function is conserved in *Xenopus*. The role of *Hesx1* as a Wnt/β-catenin antagonist has, however, not been demonstrated in other species, but given the conservation of signalling pathways, it is very probable that *Hesx1* mechanism is conserved in all vertebrates.

1.3.6. The HESX1 protein

HESX1 protein functions as a repressor, in-vivo and in-vitro; although to date its target genes have not been identified (Brickman et al., 2001; Dasen et al., 2001; Carvalho et al., 2003). There are two repressor domains within HESX1; one is

located in its amino-terminal (eh1 and HRPW/CD2 motifs) and the other is located in the homeodomain (Figure 1.8). Eh1 and HRPW/CD2 domains of HESX1 interact with the mammalian orthologue of Groucho, Transducin-like enhancer of split (TLE1), and the homeodomain mediates repression by association with the nuclear receptor co-repressor complex N-CoR/mSin3/HDAC1/2 (Dasen et al., 2001; Xu et al., 1998a).

As discussed above, experiments both in mouse and frog, have demonstrated that the repressor activity of HESX1 is required in-vivo for the normal patterning of anterior neurectoderm (Andoniadou et al., 2007; Ermakova et al., 1999). Additionally, HESX1 functions as a repressor in the pituitary primordium but its interactions and targets could be distinct to those of the early neurectoderm. TLE1 is temporally and spatially co-expressed with *Hesx1* in Rathke's pouch and this interaction is required and sufficient for proper HESX1 function at this stage of embryonic development (the role of *Hesx1* in pituitary organogenesis is discussed in more detail in section 1.4.4.1.1).

These works highlight the broad role of HESX1 as a repressor, in establishing normal development and patterning of forebrain and pituitary gland. This is further supported by the fact that specific mutations within *HESX1* are linked with different phenotypes in humans (section 1.5). In-vitro assays have also shown that the DNA binding ability and/or repressor activity of HESX1 are affected by different mutations. These assays make use of a palindromic sequence called PIII (Dattani et al., 1998; Sornson et al., 1996). In the absence of a well characterised HESX1 target in-vivo, the in-vitro assays using PIII have provided helpful insights into the behaviour of the wild-type and mutant proteins.

The following section looks at the intricate network of signals involved in pituitary development, since this organ develops in close association with the forebrain. Specific reference is also be made to *Hesx1* function during pituitary development. The successive section will return to *HESX1* mutations and human disease with reference to defects in forebrain and the pituitary gland.

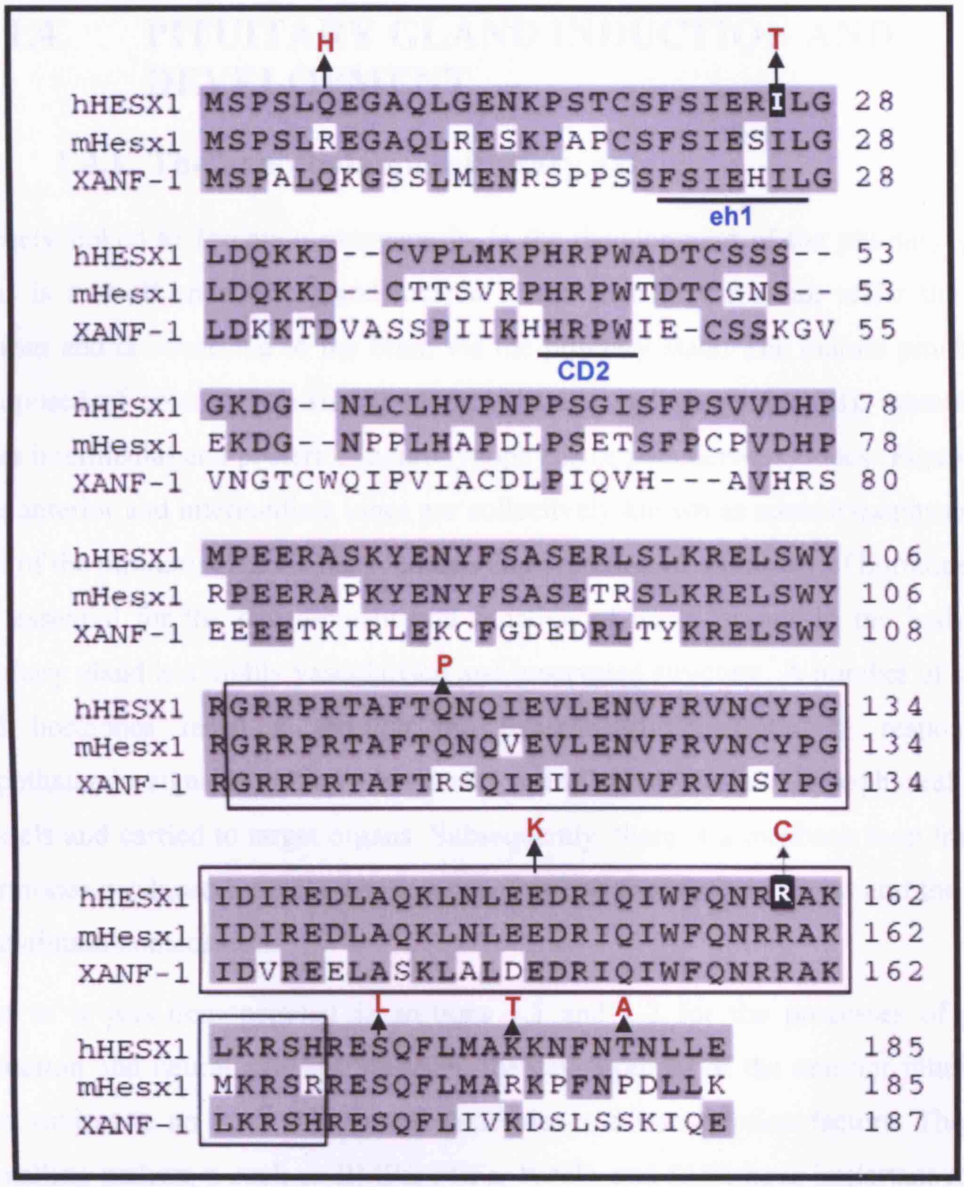

Figure 1.8 – The primary structure of HESX1 protein from three different species. The amino acid sequences of human (hHESX1), mouse (mHesx1) and frog (XANF-1) proteins are aligned, displaying regions of homology (grey). HESX1 contains two conserved repressor sequences (eh1 and CD2), located in the N-terminus of the protein, which are underlined in the figure. The boxed region is the homeodomain, located in the C-terminus of the protein. Eight point mutations have been associated with SOD and hypopituitarism in humans (section 1.5), these are indicated in red. Two of these residues, I26 and R160 (highlighted), are strictly conserved between the three species and are positioned in the two conserved domains of the protein. Figure is modified from Dattani et al., 1998.

1.4. PITUITARY GLAND INDUCTION AND DEVELOPMENT

1.4.1. The hypothalamic-pituitary axis

Closely linked to forebrain ontogenesis, is the development of the pituitary gland. This is a small endocrine gland located at the base of the brain, under the optic chiasm and is connected to the brain via the pituitary stalk. The mature pituitary is composed of anterior (consisting of pars distalis and pars tuberalis), intermediate (pars intermedia) and posterior (neurohypophysis or pars nervosa) lobes (Figure 1.9). The anterior and intermediate lobes are collectively known as adenohypophysis. The role of the pituitary gland is the synthesis and secretion of a number of hormones that are essential for the development and function of many organs in the body. The pituitary gland is a highly vascularised and innervated structure. A number of signals and hormones reach it through the hypothalamic neurons. In response to hypothalamic signals, pituitary hormones are released into the hypophyseal blood vessels and carried to target organs. Subsequently, there is a feedback loop from the hormones produced by these target organs back to the pituitary gland and the brain, to maintain homeostasis.

Just as it was demonstrated in sections 1.1 and 1.2 for the processes of neural induction and neural axis specification, the development of the anterior pituitary is also subject to an array of secreted molecules and transcription factors. The same signalling pathways such as BMPs, FGFs, WNTs and SHH have important roles in pituitary organogenesis. Gradients of these factors are established along the local axes of the developing gland. Subsequently, transcription factors are expressed in distinct regions and they act collectively to stimulate the transcription of hormone-encoding genes in the correct time point and region of the gland.

The pituitary gland contains six distinct cell type populations, which are distinguished by the hormone they produce and secrete (Table 1.2). Five of these cell types (somatotropes, lactotropes, gonadotropes, corticotropes and thyrotropes), reside in the anterior lobe. Intermediate lobe contains melanotropes, which is the sixth hormone secreting cell type of adenohypophysis (Zhu et al., 2007). The two major hypothalamic nuclei (paraventricular and supraoptic) send magnocellular neuron axons that terminate in the neurohypophysis, where they release the two hormones

oxytocin and vasopressin (also known as antidiuretic hormone or ADH). The parvocellular neurons of the hypothalamus regulates cell proliferation, hormone synthesis and secretion of the pituitary gland by secreting hypophysiotropic hormones that reach the pituitary through the hypophyseal portal system (Rizzoti and Lovell-Badge, 2005; Dasen and Rosenfeld, 2001).

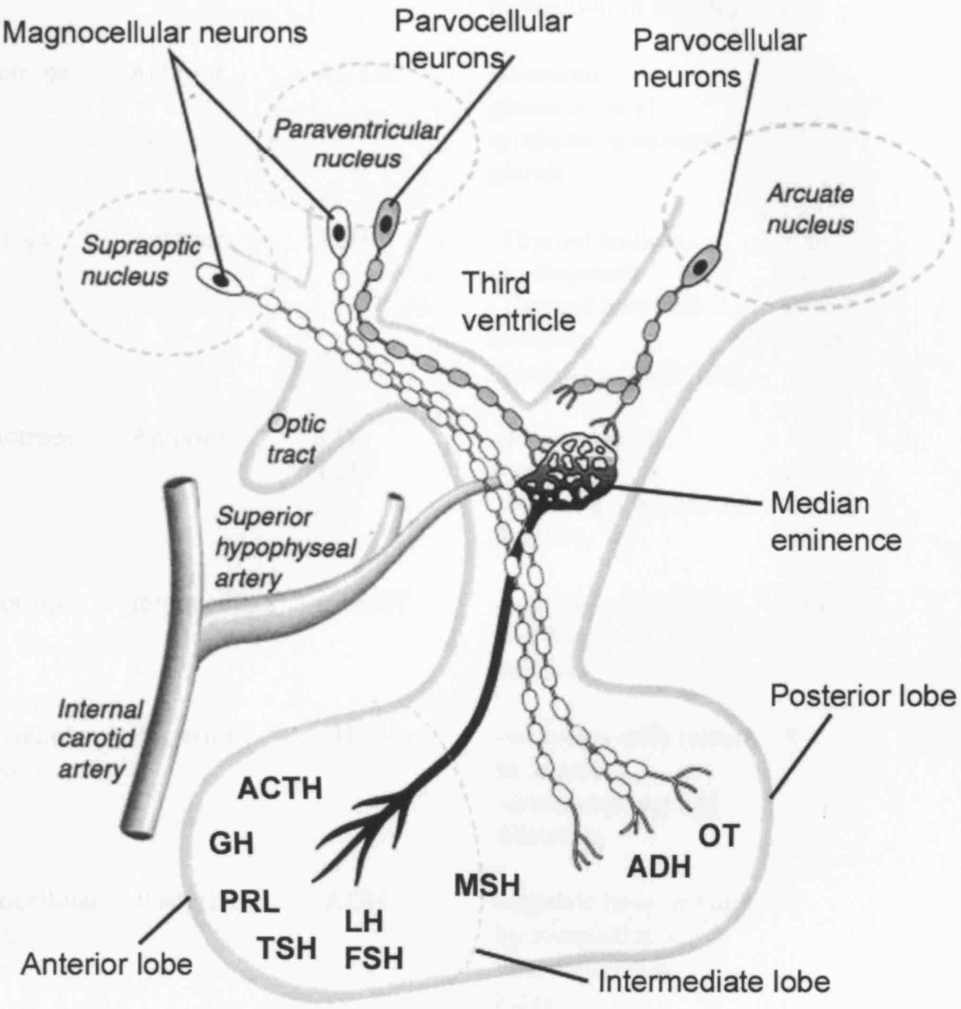

Figure 1.9 – The hypothalamic-pituitary axis. Schematic representation of the pituitary gland and its connections to the brain. The magnocellular neurons of the paraventricular and supraoptic nuclei from the hypothalamus extend their axons directly into the posterior lobe of the pituitary gland, secreting oxytocin (OT) and antidiuretic hormone (ADH). The parvocellular neurons secrete hypophysiotropic hormones into the capillaries of the median eminence, which reach the anterior and intermediate lobes through the portal system. Cells in the intermediate lobe produce α-melanocyte-stimulating hormone (MSH). Five cell types in the anterior lobe are responsible for the secretion of six hormones: growth hormone (GH); prolactin (PRL); adrenocorticotrophic hormone (ACTH); thyroid-stimulating hormone (TSH); luteinising hormone (LH) and follicle-stimulating hormone (FSH). Figure is adapted from Andersen and Rosenfeld, 2001.

Table 1.2 – Anterior and posterior pituitary cell types and hormones.

Pituitary cell type	Pituitary lobe	Hormone produced	Hormone action	TF involved in cell type determination
Somatotrope	Anterior	GH	-regulate linear growth -regulate metabolism	*Pit1* *Prop1*
Lactotrope	Anterior	PRL	-regulate milk production in females	*Pit1* *Prop1*
Corticotrope	Anterior	ACTH[1]	-stimulate glucocorticoid synthesis in adrenal glands	*Tbx19* *NeuroD1* *Pitx1*
Thyrotrope	Anterior	TSH[2]	-Thyroid follicle development -Thyroid hormone secretion -Skeletal remodelling	*Pitx2* *Pit1* *Prop1* *Gata2*
Gonadotrope	Anterior	LH[2] FSH[2]	-initiate sexual maturation -maintain reproductive function	*Pitx1* *Prop1* *Gata2* *Sf1*
Melanotrope	Intermediate	α-MSH[1]	-regulate production and distribution of melanin	*Tbx19*
Magnocellular neurons	Posterior	OT	-promotes milk release in females -stimulates cervical dilatation	?
Magnocellular neurons	Posterior	ADH	-regulate body volume by stimulating water re-absorption in kidneys	?

1: ACTH and α-MSH are both derivatives of proopiomelanocortin (POMC).
2: TSH, LH and FSH are heterodimeric glycoproteins made from the common subunit α-GSU (also known as Cga) and a hormone specific subunit (TSHβ, LHβ, FSHβ).
Abbreviations: GH, growth hormone; PRL, prolactin; ACTH, adrenocorticotrophic hormone; TSH, thyroid-stimulating hormone; LH, luteinizing hormone; FSH, follicle-stimulating hormone; α-MSH, α-melanocyte stimulating hormone; OT, oxytocin; ADH, antidiuretic hormone (also known as vasopressin); TF, transcription factor.

1.4.2. Organogenesis

Like the eye, the pituitary gland has a dual embryonic origin. The posterior lobe is derived from a neural primordium, whilst the anterior and intermediate lobes are of ectodermal origin. Fate mapping experiments from various species (amphibians, chick and mammals) have shown that the ectodermal anlage of the pituitary originates from the hypophyseal placode, located at the midline of the ANR (Baker and Bronner-Fraser, 2001; Kawamura et al., 2002; Rubenstein et al., 1998).

The hypophyseal placode appears at 7.5 dpc and among the early pituitary markers expressed in this region in the mouse are *Hesx1*, *Six3*, *Pitx1/2*. The neural plate just posterior to this region will give rise to the neural aspect of the gland. Although, in lower vertebrates such as fish and frog, development of the pituitary is directly from the placode and the adjacent neural plate, in chick and mammals these two regions are displaced by the expansion of the cranial neural tube and head morphogenesis. The placodal ectoderm ends up as part of the oral ectoderm at the roof of the mouth and the adjacent neural plate is displaced to be positioned in the ventral diencephalon.

At around 8.5 dpc in mouse, the first sign of pituitary development becomes apparent when oral ectoderm thickens and subsequently invaginates by 9.0 dpc to form a structure called Rathke's pouch (RP), the primordium of the anterior and intermediate lobes. At the same time that the RP is invaginating, the ventral diencephalon also evaginates and forms what is known as the infundibulum, which goes on to become the neural posterior lobe of the gland. By 9.5 dpc, these two structures come into direct contact as a result of cellular movements and proliferation (Figure 1.10). This contact is thought to be a pre-requisite for the development of the pouch, and is required for terminal differentiation of all endocrine cell types.

Although, the signal(s) and/or mechanism that initially induce the formation of infundibulum are still unknown, there is a large number of evidence highlighting the requirement of dorsal signalling molecules in the induction of RP (Rizzoti and Lovell-Badge, 2005; Zhu et al., 2007; Dasen and Rosenfeld, 2001). For example, *Nkx2.1*$^{-/-}$ mice show defects in the ventral diencephalon and the differentiation of the anterior pituitary is also affected (Kimura et al., 1996). In frogs, the ablation of the infundibulum results in a lack of differentiation of cell types in the pouch

(Kawamura and Kikuyama, 1998). In chick and mouse explant studies, the ventral diencephalon is able to induce RP, which is subsequently able to express a range of differentiated pituitary cell types. The ectoderm from a number of regions in the head (not just the oral ectoderm) is competent to this inducing activity of the infundibulum (Gleiberman et al., 1999). In human embryos, the contact between infundibulum and RP occurs by the fifth week of gestation.

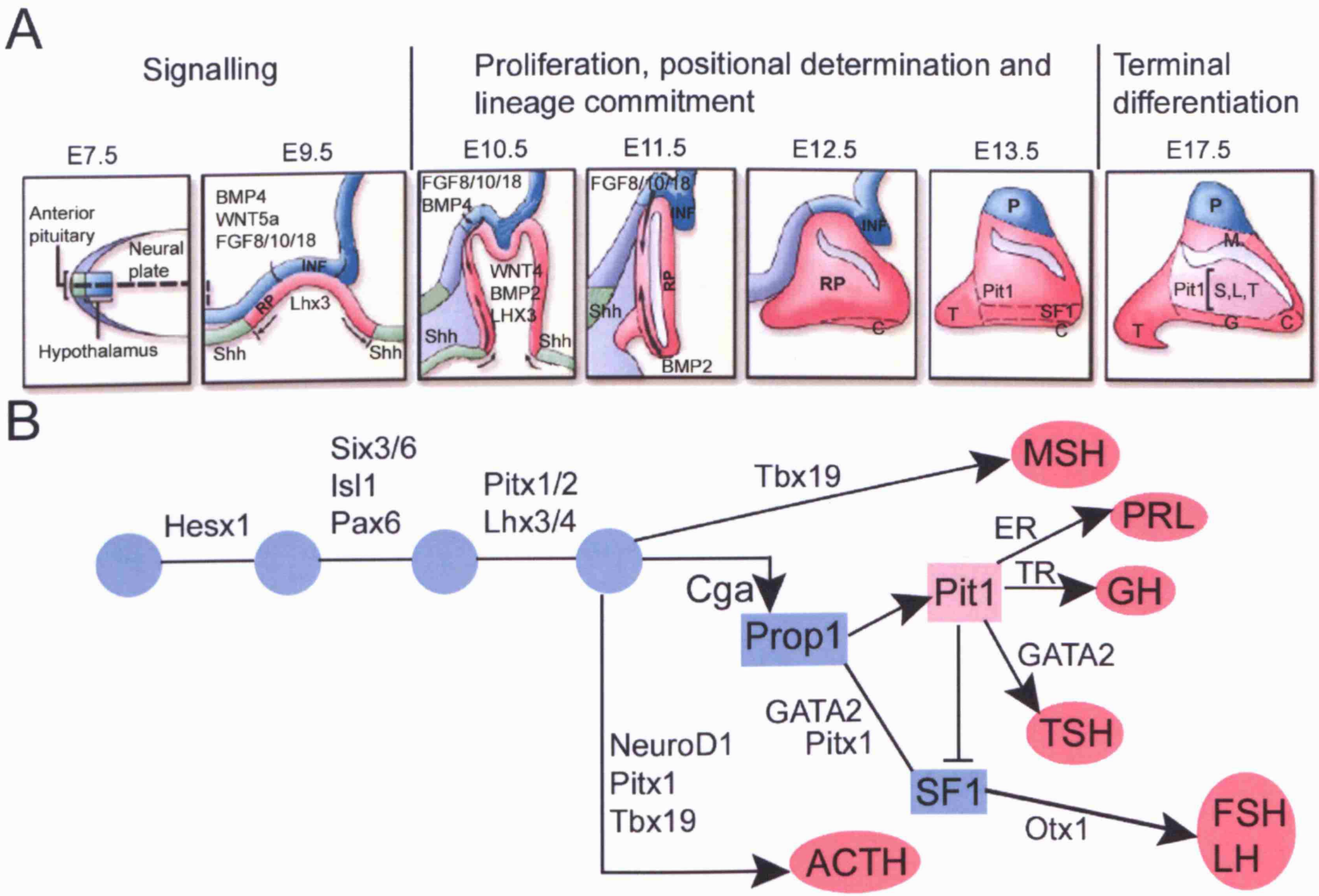
A
Signalling
Proliferation, positional determination and lineage commitment
Terminal differentiation
E7.5
E9.5
E10.5
E11.5
E12.5
E13.5
E17.5
Anterior pituitary
Neural plate
Hypothalamus
BMP4
WNT5a
FGF8/10/18
INF
RP
Lhx3
Shh
FGF8/10/18
BMP4
WNT4
BMP2
LHX3
BMP2
P
M
Pit1
S,L,T
T
C
G
SF1
B
Six3/6
Isl1
Pax6
Hesx1
Pitx1/2
Lhx3/4
Tbx19
MSH
ER
PRL
TR
GH
Cga
Prop1
Pit1
GATA2
TSH
GATA2
Pitx1
NeuroD1
Pitx1
Tbx19
SF1
Otx1
FSH
LH
ACTH

Figure 1.10 – Signalling and transcriptional regulation during mouse pituitary organogenesis. A) Cartoon representation of the steps in pituitary development from 7.5 dpc to terminal determination at 17.5 dpc. The origins of the anterior pituitary can be traced back to the anterior neural ridge. The adjacent midline region gives rise to the posterior pituitary and the hypothalamus. Pituitary development starts at 9.5 dpc, when a thickening and invagination of the oral ectoderm forms the Rathke's pouch (RP). A thickening from the ventral diencephalon forms the infundibulum (INF), which expresses a number of signalling molecules (*Bmp4*, *Wnt5a*, *Fgf8/10/18*), as indicated in the blue region. The direct contact between the RP and INF induces the expression of a number of signalling molecules and transcription factors (*Wnt4*, *Bmp2*, *Lhx3*) in the RP, which are indicated in the pink region. *Shh* is expressed in the oral ectoderm adjacent to the RP (green region). By 12.5 dpc, the pouch has detached from the oral ectoderm and corticotropes start to appear in the ventral side. The spatial and temporal expression of transcription factors (which influence proliferation and cell lineage determination) is regulated by the opposing dorsal and ventral gradients of signals and continues until all the pituitary cell types have differentiated by 17.5 dpc. B) A model of cell lineage determination during pituitary development. The cascade of signalling molecules and transcription factors shown in A, result in a stepwise appearance and subsequent proliferation and determination of the six different endocrine cell types (dark pink). The development of somatotropes, lactotropes and thyrotropes is dependent on *Pit1*. Note that the rostral tip thyrotropes are independent of *Pit1*. *Prop1* is important for the induction of *Pit1*, and it is also required for the development of gonadotropes. *Lhx3* and *Tbx19* are important factors for the development of adrenocorticotropes and melanotropes. Various other factors needed in the intermediate steps are indicated in the figure. Figure is modified from Zhu et al., 2007.

1.4.3. Extrinsic and intrinsic signals

The surrounding ectoderm, the underlying mesenchyme and endoderm have all been shown to play important roles in pituitary organogenesis (Withington et al., 2001; Gleiberman et al., 1999). Both the RP and the infundibulum express a number of signalling molecules. Among members of the signalling pathways expressed in the ventral diencephalon are *Shh*, *Bmp4*, *Fgf 3*, *8*, *10*, *18* and *Wnt5a* (Treier et al., 1998; Treier et al., 2001; Ericson et al., 1998). The RP, on the hand, expresses *Bmp2* and *Wnt4* (Treier et al., 1998). *Shh* is expressed in the ectoderm adjacent to the RP; although it is absent from the pouch itself, it is thought to play important roles in proliferation and cell type determination in the anterior pituitary (Treier et al., 2001). In addition, several members of the Notch signalling pathway are expressed in both the infundibulum and the RP, such as *Dll1*, *Jag1*, *Notch 1*, *2*, *3* and *Hes1* (Raetzman et al., 2004; Zhu et al., 2006).

As a result of the spatio-temporal expression of these molecules, a number of transcription factors are up- or downregulated at specific time points in either the RP or the infundibulum, resulting in the overall shaping of the gland, as well as the induction and terminal differentiation of the endocrine cell types. The evidence, which has aided our understanding of the function of these genes and the proteins they encode, has mainly come from work in mouse.

1.4.3.1. BMPs

To date, two members of this signalling pathway (BMP2 and 4), have been shown to play direct roles in the development of the pituitary gland. However, both *Bmp2*$^{-/-}$ and *Bmp4*$^{-/-}$ mutant mice die early (Zhang and Bradley, 1996; Winnier et al., 1995). Evidence has, therefore, largely come from other analyses. The ectopic expression of *Noggin* (a BMP antagonist) in the pouch, results in the arrest of RP development at 10.0 dpc and the subsequent lack of all pituitary cell types. Misexpression of a dominant negative BMP receptor in the RP, results in a hypoplastic anterior lobe and the absence of ventral cell types (*Pit1* lineage). *Bmp2* expression normally decreases at 14.5 dpc, the maintenance of *Bmp2* beyond that, results in the induction of ventral cell types but disrupts their terminal differentiation (Treier et al., 1998).

These results demonstrate the requirement of *Bmp2* in specifying ventral cell fate proliferation but their terminal differentiation only takes place when *Bmp2* is downregulated, whilst *Bmp4* is required for initial organ commitment.

1.4.3.2. Sonic Hedgehog

Shh$^{-/-}$ mice show a massive distortion of head structures and the ventral diencephalon is dramatically affected in these mutants (Chiang et al., 1996). Due to the early effect of *Shh* on midline structures, it is difficult to specifically establish the role of hedgehog signalling on pituitary development using this model. However, *Gli2*$^{-/-}$ mice show variable loss of the pituitary, whilst *Gli1*$^{-/-}$;*Gli2*$^{-/-}$ mice show a more severe absence of pituitary tissue (Park et al., 2000). Consistently, misexpression of *Hip* (a *Shh* inhibitor) in the pouch prevents RP growth. Moreover, *Bmp2* expression in RP is lost and endocrine cell lineages do not appear in this model (Treier et al., 2001).

On the other hand, ectopic expression of *Shh* in the pouch results in hyperplasia and expansion of ventral cell types such as gonadotropes and thyrotropes at the expense of somatotropes (Treier et al., 2001). *Patched1* (downstream of *Shh*) is expressed in the RP, indicating that although *Shh* is not expressed in the pouch, its signalling indirectly promotes ventral cell type specification and expansion.

1.4.3.3. FGFs

The main signalling molecule in the ventral diencephalon seems to be *Fgf8*, as it can mimic the activities of the infundibulum (induction of proliferation). In explant studies, *Fgf8* can maintain *Lhx3* expression and repress *Islet1* and *Cga* (Ericson et al., 1998). Ectopic expression of *Fgf8* in the pouch results in the expansion of *Pomc* expression and absence of other cell types, as well as the appearance of multiple pouches and branching in the pituitary (Treier et al., 1998). Inversely, inhibiting FGF signalling with SU5402, results in the downregulation of *Lhx3*, reduced cell proliferation and ectopic differentiation of ventral cell types (Norlin et al., 2000).

Fgf10$^{-/-}$ (Ohuchi et al., 2000) and *FgfrIIIb*$^{-/-}$ (De Moerlooze et al., 2000) mice show an arrest of RP development with increased apoptosis and subsequent agenesis of the pituitary gland. Additionally, *Titf1*$^{-/-}$ (*Nkx2.1*$^{-/-}$) mice lack the expression domains of

Fgf8/10 and as a result, *Lhx3/4* expression never appear and the pouch itself degenerates due to apoptosis (Takuma et al., 1998).

These results demonstrate the requirement of FGF signalling from the ventral diencephalon, in patterning and development of RP and specifically in dorsal cell type proliferation.

1.4.3.4. WNTs

As mentioned above, several components of the Wnt/β-catenin signalling pathway are expressed in the developing pituitary, showing the importance of this pathway in pituitary organogenesis. The conditional deletion of *β-catenin* in the anterior pituitary, using the *Pitx1-Cre* transgenic line, results in the absence of *Pit1* and its three lineages and subsequent reduction in gland size. It has been shown that PROP1 interacts with β-catenin and they both associate on a *Pit1* enhancer element to induce *Pit1* expression. LEF1 inhibits this action of PROP1/β-catenin and indeed *Lef1*$^{-/-}$ mice show elevated levels of *Pit1*, *Gh* and *Tshb*. The PROP1/β-catenin complex also acts to inhibit *Hesx1* expression, thus allowing the appearance of ventral cell lineages (Sornson et al., 1996; Olson et al., 2006).

Wnt4 is expressed in the RP and *Wnt4*$^{-/-}$ mice have pituitary hypoplasia with reduction in some cell types (somatotropes, thyrotropes and *Cga*-expressing cells), whilst corticotropes are expressed normally (Treier et al., 1998).

Wnt5a is expressed in the ventral diencephalon from 9.5 dpc. *Wnt5a*$^{-/-}$ mice die neonatally and display an abnormal pituitary shape among other defects (Yamaguchi et al., 1999). The pituitary gland of these mutants exhibits abnormal branching of the dorsal aspects by 11.5 dpc, although all the pituitary markers are expressed normally (Cha et al., 2004).

Tcf3, Tcf4 and *Frizzled2* are other members of this pathway, which are expressed in the pituitary gland. Targeted deletion of *Tcf4* results in hyperplasia of the anterior lobe, as well as elevated expression of *Prop1* (Brinkmeier et al., 2003).

Overall, these data indicate that the Wnt/β-catenin signalling pathway is crucial for pituitary gland growth and Pit1 lineage determination.

1.4.4. Transcription factors

The actions of the secreted factors mentioned above, result in the spatial and temporal expression of a number of transcription factors during pituitary development. Transcription factors encode proteins that in turn determine cell identity by activating and/or repressing a set of target genes. They are assisted by another set of proteins, which act as co-activators or co-repressors. A number of these transcription factors are briefly described below with reference to pituitary development.

1.4.4.1. Paired-like homeobox genes

1.4.4.1.1. *Hesx1*

Hesx1 is one of the earliest markers of the pituitary gland, being expressed in the early pituitary primordium, the anterior neural ectoderm, from as early as 7.5 dpc (Thomas and Beddington, 1996). By 9.0 dpc in mouse embryonic development, *Hesx1* is prominently expressed in the invaginating Rathke's pouch and the ventral diencephalon. At 10.5 dpc, it is restricted to the RP where it remains until 13.5 dpc (Figure 1.6). Given the expression pattern of *Hesx1* and the closely linked development of the pituitary with the forebrain, it is not surprising that *Hesx1*$^{-/-}$ mice display defects in the pituitary gland. Consistently, a number of mutations in *HESX1* have been linked with SOD and hypopituitarism in humans (section 1.5).

Pituitary defects, like other defects in *Hesx1*$^{-/-}$ embryos, are variable. The vast majority of the mutant embryos show an enlarged RP with bifurcations and multiple lumens (Dasen et al., 2001 and our own observations). Moreover, it was reported that in ~5% of null embryos, RP induction does not take place and the pituitary gland is subsequently absent. The enlarged pituitary gland (a feature of the majority of null mutants) is possibly the result of the expansion of *Fgf8/10* expression domain in the diencephalon, which leads to the recruitment of additional oral ectoderm in the RP. However, increased proliferation is thought to be the main reason underlying pituitary defects in *Hesx1* mutants (Gaston-Massuet et al., in press). Based on these observations it was suggested that *Hesx1* has a role during pituitary development as a factor, which restricts the expression of *Fgfs* in the infundibulum at around 10.5 dpc.

As mentioned above, co-factor proteins are crucial for the function of transcription factors. Thus, the importance of some of these has also been demonstrated in pituitary organogenesis, in particular the members of the *Tle* gene family, which include *Tle1-4* and *Aes*. For example, *Aes*$^{-/-}$ mice display pituitary dysmorphology and growth retardation (Brinkmeier et al., 2003).

HESX1 is a repressor and it has been shown to interact with TLE1 and the N-CoR complex through two separate repressor domains. Interestingly, *Tle1* is co-expressed with *Hesx1* in the RP. By 13.5 dpc when the endocrine cell types are starting to appear, their expression in the RP is extinguished. Ectopic expression of either *Hesx1* or *Tle1* under the *Pitx1* regulatory elements results in a minor phenotype. However, overexpression of both genes, as shown in *Pitx1/Hesx1:Pitx1/TLE1* transgenic embryos, results in the absence of *Pit1*, *Gh*, *Tshb* and *Cga* (the ventral cell lineages). It has been suggested that the repressing activity of HESX1, through its interaction with TLE1 in the pituitary gland, serves to prevent PROP1 from initiating the differentiation of the four ventral cell types (somatotropes, lactotropes, thyrotropes and gonadotropes).

1.4.4.1.2. *Prop1*

Prop1 (Prophet of *Pit1*) is a another paired-like transcription factor expressed in the RP from 10 dpc, its expression peaks when *Hesx1* transcripts are diminishing, and it is itself extinguished at 15.5 dpc. Different domains of the protein have activating and repressing properties, indicating that PROP1 can be both an activator and a repressor. For example, the PROP1/β-catenin complex can act as an activator of *Pit1* and a repressor of *Hesx1* (Olson et al., 2006).

Ames dwarf mice carry a mutation (S83P) in the *Prop1* locus; these mice show a small pituitary gland with reduced numbers of somatotropes, lactotropes, thyrotropes and a delay in gonadotrope development. *Prop1* is also required for the induction of *Pit1* expression, as there is a lack of *Pit1* activation and subsequent failure of the Pit1 lineage determination in *Prop1*$^{df/df}$ embryos. Additionally, *Hesx1* expression is prolonged in these mutants (Sornson et al., 1996).

Prop1 is, therefore, necessary to activate genes that are required for the determination and proliferation of four ventral cell types (i.e. the three *Pit1* lineages

as well as gonadotropes). Premature expression of *Prop1* in the RP (*Pitx1/Prop1*), leads to agenesis of the anterior pituitary (similar to the severe *Hesx1*$^{-/-}$ phenotype), possibly due to an early inhibition of *Hesx1* (Dasen et al., 2001). Prolonged expression of *Prop1*, in *αGSU/Prop1* mice, results in a decrease in gonadotropes (Cushman et al., 2001). Therefore, although PROP1 activity is required for ventral cell type induction, its downregulation is necessary for their later expansion.

Finally, mutations within the *PROP1* gene in humans are the most common cause of CPHD.

1.4.4.1.3. *Pitx* genes

There are three paralogous *Pitx* gene members in vertebrates (*Pitx1*, *2* and *3*) encoding paired-like, Otx-related homeodomain transcription factors (Gage et al., 1999). They show distinct expression patterns in the mouse embryo with some overlap, notably in the eye (*Pitx2* and *3*) and in the pituitary (*Pitx1* and *2*).

Pitx1 is expressed in the RP from 9.5 dpc and continues to be expressed in the adult anterior pituitary (Szeto et al., 1996). It interacts with the N-terminal of PIT1, as well as binding and activating the *Pomc* promoter (Lamonerie et al., 1996). *Pitx1*$^{-/-}$ mice show defects in hindlimbs and craniofacial development, as well as in the anterior pituitary. Although, RP induction and development take place normally, there is a reduction in *Fshb*, *Lhb* and *Tshb* expression and an increase in ACTH (Szeto et al., 1996; Cohen and Radovick, 2002a; Cohen and Radovick, 2002b).

Pitx2 is expressed in the oral ectoderm and epithelium from 8.5 dpc, followed by expression in the RP as well as in the mesenchyme near the optic eminence. *Pitx2*$^{-/-}$ mutants show various defects affecting the heart, teeth, eyes and the pituitary. The RP forms in these embryos, furthermore, *Lhx3*, *Hesx1*, *Pitx1* and *Cga* are induced normally but the gland does not progress further. *Prop1* is expressed at low levels, whilst *Pit1* and *Lhx4* are absent in these embryos (Zhu et al., 2007).

Role of *Pitx1* and *2* in the pituitary seems to be in cell proliferation after initial induction and commitment. *Ptx1*$^{+/-}$;*Ptx2*$^{+/-}$, *Ptx2*$^{-/-}$ and *Ptx1*$^{-/-}$;*Ptx2*$^{neo/neo}$ (*Ptx2-neo* is a hypomorphic allele of *Ptx2*) all show reduced proliferation and smaller gland size. Moreover, overexpression of *Pitx2* under *Pit1* and *Cga* regulatory elements, results in increase in somatotropes and gonadotropes (Zhu et al., 2007). Additionally *Pitx2*

expression is induced by the Wnt/β-catenin pathway, which in turn converts PITX2 into an activator to regulate the induction of cyclin D2 gene and promote proliferation (Kioussi et al., 2002).

There is, however, redundancy between the roles of *Pitx1* and *2* in pituitary development. One of their redundant roles is in controlling the expression of *Lhx3* in the RP (Charles et al., 2005). Moreover, they are both able to activate the promoters of *Cga*, *Fshb*, *Lhb*, *Tshb*, *Prl* and *Gh* (Tremblay et al., 2000). However, *Pitx2* plays a predominant role in the pituitary, as its inactivation in mouse results in a more severe pituitary phenotype than its counterpart (*Pitx1*).

Several mutations in the human *PITX2* gene (*RIEG*) have been associated with an autosomal dominant condition called Rieger's syndrome. Patients show defects in a number of organs such as the eyes and teeth, as well as mental retardation and pituitary defects (Semina et al., 1996a; Semina et al., 1996b).

1.4.4.2. *Poulf1*

Poulf1 (*Pit1*) belongs to the POU homeodomain transcription factors. Its expression starts at 13.5 dpc in the RP and persists in the adult pituitary in three distinct anterior pituitary endocrine lineages, namely somatotrope, lactotrope and thyrotrope. It is essential for both the terminal differentiation and the subsequent proliferation of these three cell types. *Pit1* is also able to bind and activate *Gh*, *Prl*, *Tshb* and *Ghrh* promoters as well as its own promoter (Andersen and Rosenfeld, 2001).

Two transgenic mouse lines have shed light on the function of *Pit1*. The Snell dwarf mouse ($Pit1^{dw/dw}$) has a point mutation (W261C) in the *Pit1* gene. The three *Pit1* lineages and corresponding hormones (GH, PRL, TSHβ) are absent in these mice. There is, however, a low level of *Pit1* expression but this cannot be maintained since protein levels are too low for its autoregulatory function (Rhodes et al., 1993).

The Jackson dwarf mouse ($Pit1^{dwJ/dwJ}$) has a recessive null mutation as a result of a rearrangement in the *Pit1* locus. These animals have a hypoplastic anterior pituitary and *Gh*, *Prl*, *Tshb* and *Pit1* expression are absent (Li et al., 1990).

A number of mutations in the *POU1F1* gene have also been linked to CPHD in humans (Cohen and Radovick, 2002a; Cohen and Radovick, 2002b; Dattani, 2005).

1.4.4.3. LIM homeobox genes

Islet-1, *Lhx3* (*P-Lim*) and *Lhx4* are three members of the LIM homeodomain transcription factors expressed in the RP, with important roles in pituitary development. *Isl1* is expressed in the oral ectoderm and RP between 8.5-9.5 dpc, but becomes restricted to the ventral region of the pouch by 10.5 dpc. Its expression is regulated by signalling from the ventral diencephalon and from within the RP: *Bmp2* induces *Isl1* expression, whilst *Fgf8* represses it (Ericson et al., 1998). *Isl1*$^{-/-}$ embryos show various defects in the heart, pancreas and motor neurons. In these embryos, RP is induced but with a thin epithelium (Takuma et al., 1998).

Lhx3 is expressed in many other regions of the embryo, including the RP from 9.5 dpc and continues to be expressed in the adult adenohypophysis. In *Lhx3*$^{-/-}$ embryos, RP is induced but development is arrested shortly after. *Hesx1* expression is diminished early and expression of *Pit1*, *Cga*, *Tshb* and *Gh* is not induced showing an important role in organ commitment and growth (Sheng et al., 1996; Sheng et al., 1997). Hence, *Lhx3* is thought to positively regulate *Hesx1* expression. It has also been shown that LHX3 activates *Cga* together with PITX1 and activates *Prl*, *Tshb* and *Pit1* together with PIT1. There are also human mutations in *LHX3*, which lead to CPHD (Cushman et al., 2002; Dattani, 2005).

Lhx4 is also expressed in the pouch at 9.5 dpc, but its transcripts disappear by 15.5 dpc. In *Lhx4*$^{-/-}$ embryos, there is increased cell death in the pouch at 12.5 dpc and by 18.5 dpc, most of the endocrine cell types are reduced and the anterior lobe is hypoplastic. *Lhx3*$^{-/-}$;*Lhx4*$^{-/-}$ embryos show more severe pituitary defects, with an earlier arrest of pituitary development (Sheng et al., 1997).

1.4.4.4. *Sox* genes

The SoxB1 family of *Sox* genes were briefly mentioned in section 1.1.4.1, as they are some of the earliest neural markers with important roles in neuronal determination. *Sox2* and *Sox3* are two genes within this family that are implicated in pituitary development. *Sox3* is expressed in the ventral diencephalon and infundibulum, and in *Sox3*$^{-/-}$ mice, the RP is bifurcated by 11.5 dpc, resulting in extra clefts in the pituitary gland (Rizzoti et al., 2004). The expression domains of *Fgf8* and *Bmp4*, in the ventral

diencephalon, are transiently expanded at 10.5 dpc. These mice have a range of other abnormalities, including craniofacial and midline defects. There is also the occurrence of lethality before weaning, although ~57% of mutants survive. Some of the surviving animals are smaller or infertile and the pituitary levels of GH, LHβ, FSHβ and TSHβ are lower compared with wild-type.

Sox2, on the other hand, is expressed in the ventral diencephalon and infundibulum as well as the RP (Avilion et al., 2003). *Sox2*$^{-/-}$ mutants die at peri-implantation stages, however, heterozygous embryos display similar pituitary defects to *Sox3*$^{-/-}$, although these defects are less severe in *Sox2*$^{+/-}$ (Kelberman et al., 2006). Pituitary levels of LHβ and GH are moderately reduced in the heterozygous animals.

Human mutations in *SOX3* result in X-linked mental retardation and GH deficiency, whilst *SOX2* human mutations cause hypothalamic-pituitary and reproductive defects (Kelberman and Dattani, 2007a; Kelberman and Dattani, 2007b).

1.4.4.5. *Six* homeobox genes

Six1, *Six3*, *Six4* and *Six6* belong to the Six family of transcription factors (homologues of the *Drosophila melanogaster* sine oculis homeobox genes), which are expressed in the developing pituitary. However, *Six1*$^{-/-}$ and *Six4*$^{-/-}$ mutants do not display any pituitary defects, possibly owing to redundancy between the different *Six* genes (Laclef et al., 2003a; Laclef et al., 2003b; Ozaki et al., 2001).

Six6 is expressed in the developing hypothalamus, pituitary, eyes, and optic stalks (Jean et al., 1999). *Six6*$^{-/-}$ mutants display retina and optic nerve defects, as well as pituitary hypoplasia (Li et al., 2002). *Six3* is expressed in the anterior neural plate (Table 1.1), however, by 9.5 dpc its expression is in the developing retina, hypothalamus and the RP (Oliver et al., 1995). Human mutations in *SIX3* have been shown to cause holoprosencephaly (Wallis et al., 1999). Similarly, *Six3*$^{-/-}$ mice show severe forebrain defects as early as 9.5 dpc. Therefore, a direct role of this gene in pituitary development has not been demonstrated. Recent work from our group indicates a requirement of *Six3* in normal pituitary development, as *Hesx1*$^{Cre/+}$;*Six3*$^{+/-}$ compound heterozygotes display a range of defects in the developing pituitary. This results in dwarfism, as well as impaired development of the thyroid and gonads (Gaston-Massuet et al., in press).

1.5. HUMAN *HESX1*

1.5.1. Septo-optic dysplasia and hypopituitarism

Septo-optic dysplasia (SOD), also known as de Morsier Syndrome, was first described by Reeves in 1941 in a human patient. It is a highly heterogeneous condition, defined by any combination of: (1) optic nerve hypoplasia; (2) midline neuroradiological abnormalities and (3) pituitary hypoplasia. A diagnosis is made when at least two of these features are present (Kelberman and Dattani, 2007a; Kelberman and Dattani, 2007b). Approximately 30% of cases show the complete range of defects, 62% have some form of hypopituitarism and 60% have an absent septum pellucidum. Optic nerve hypoplasia can be bilateral, which is more common (88%) or unilateral (12%). Neurological defects are present in 75% of patients with optic nerve hypoplasia. Midline defects include agenesis of corpus callosum and absence of septum pellucidum (Dattani and Robinson, 2002). The incidence of SOD is rare (1 in 10,000 births) and is generally sporadic, although very rare familial cases have been described (Dattani et al., 2000).

Pituitary gland is a midline structure and hence congenital midline brain defects (such as SOD) are often associated with pituitary hypoplasia. It is, however, important to note that pituitary hypoplasia can also occur in the absence of any other brain abnormalities. Pituitary hypoplasia, associated with SOD or in isolation, results in hypopituitarism, which is itself highly variable. It can range in severity, resulting in variable hormone deficiencies. In the extreme case of panhypopituitarism, none of the anterior pituitary hormones are produced. In other cases, these endocrinopathies may evolve with time such as in evolving panhypopituitarism. Finally, the least severe forms are the isolated hormone deficiencies (IHD), with the most common being isolated growth hormone deficiency (IGHD), reported to occur between 1 in 4,000-10,000 live births (Dattani, 2005). Combined pituitary hormone deficiencies (CPHD) cover the range between these two extremes (i.e. IHD to panhypopituitarism).

Additionally, defects in the hypothalamus are known to cause hypopituitarism (Dattani, 2004; Dattani, 2005). Human patients generally develop well with hormone replacement therapies, although if untreated these syndromes can result in death. The

cause of SOD and hypopituitarism is multifactorial, with the involvement of both environmental and genetic components.

1.5.2. *HESX1* and disease

The resemblance between the *Hesx1*$^{-/-}$ phenotype in mice and SOD in humans prompted the analysis of the *HESX1* locus in patients with SOD and/or hypopituitarism. Indeed, the closest mouse model for SOD is the *Hesx1* null mouse line (Dattani et al., 1998) and to date thirteen mutations in *HESX1* have been reported in human patients with hypopituitarism both in association with SOD and without it (Figure 1.11).

Eight are point mutations (I26T, R160C, Q6H, E149K, S170L, T181A, Q117P, K176T); one results in the deletion of a guanine at position 175 (1684delG); another mutation results in the insertion of an Alu element in the homeodomain (Alu); two further mutations result from the insertion or deletion of two nucleotides (306/307insAG and 449/450delAC); the final mutation results in a T to C transition in exon 2, affecting a splice donor site in intron 2. (Dattani et al., 1998; Thomas et al., 2001; Brickman et al., 2001; Carvalho et al., 2003; Cohen et al., 2003; Tajima et al., 2003; Dattani, 2004; Sobrier et al., 2005; Sobrier et al., 2006; Coya et al., 2007). These *HESX1* mutations cause both missense and frameshift changes in the protein and include recessive and dominant mode of inheritance, resulting in phenotypes with variable penetrance and severity.

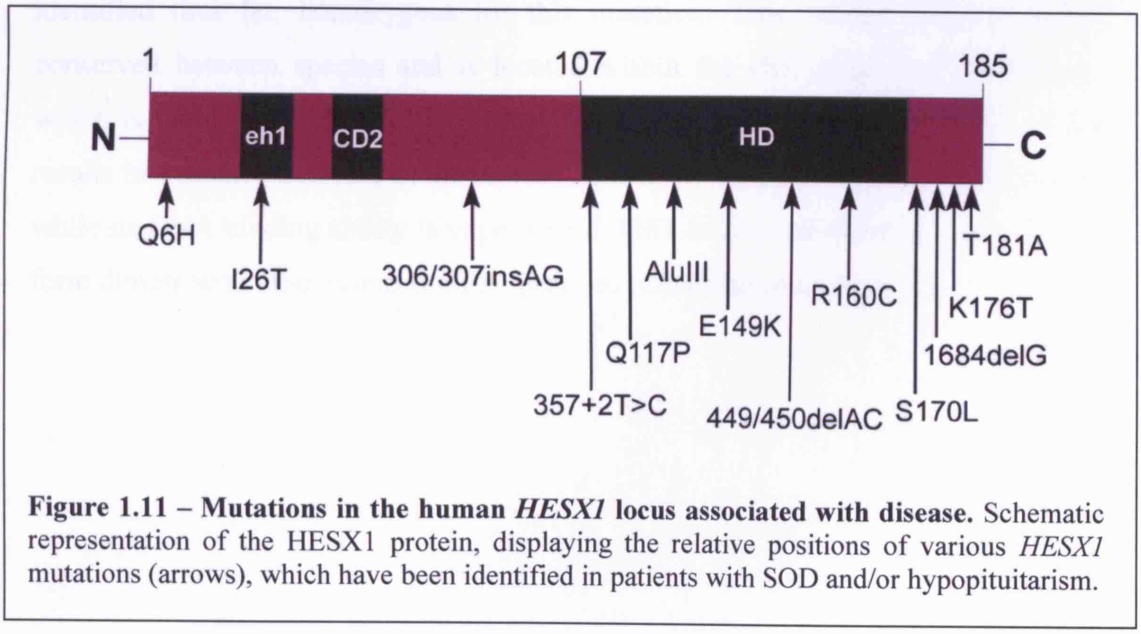

Figure 1.11 – Mutations in the human *HESX1* locus associated with disease. Schematic representation of the HESX1 protein, displaying the relative positions of various *HESX1* mutations (arrows), which have been identified in patients with SOD and/or hypopituitarism.

Of these, two recessive point mutations are relevant to this thesis. A homozygous mutation, resulting in the substitution of arginine by cysteine at position 160 (R160C), is present in two siblings, previously diagnosed with SOD (Wales and Quarrell, 1996). MRI scans of their brains, show optic nerve hypoplasia, agenesis of the corpus callosum and abnormal septum pellucidum, as well as hypoplasia of the anterior pituitary, an ectopic/undescended posterior pituitary and abnormal sella turcica (Figure 1.12). Interestingly, the corpus callosum and pituitary abnormalities differ between the two siblings, although this does not manifest in differences in severity of their defects. Additionally, the optic nerve and chiasm abnormalities do not have a clinical impact (Dattani et al., 1998; Brickman et al., 2001).

R160 is a highly conserved residue, located at position 53 of the homeodomain and is thought to be involved in contacting the DNA double helix in other homeodomain proteins (Wilson et al., 1993). Indeed, the mutant protein is unable to bind DNA in-vitro and abrogates the DNA binding ability of the wild-type protein (Dattani et al., 1998; Brickman et al., 2001). Although, nine human cases heterozygous for the mutation do not show a phenotype, this dominant negative behaviour raises questions about the true nature of this mutant protein in-vivo.

A further missense mutation, resulting in the homozygous substitution of isoleucine by threonine at position 26 (I26T), was identified in a girl with evolving CPHD (Carvalho et al., 2003). MRI scans show anterior pituitary hypoplasia, a thin pituitary stalk and an undescended posterior pituitary (Figure 1.12). She is the only patient identified thus far, homozygous for this mutation. This residue (I26) is highly conserved between species and is located within the eh1 domain of the protein, which is involved in the HESX1/TLE1 interaction. In effect, the disruption of I26 results in a marked decrease in the repressing activity of HESX1 in mammalian cells, while its DNA binding ability is unperturbed. I26T is also unable to recruit TLE1, or form dimers with other homeodomain proteins (Carvalho et al., 2003).

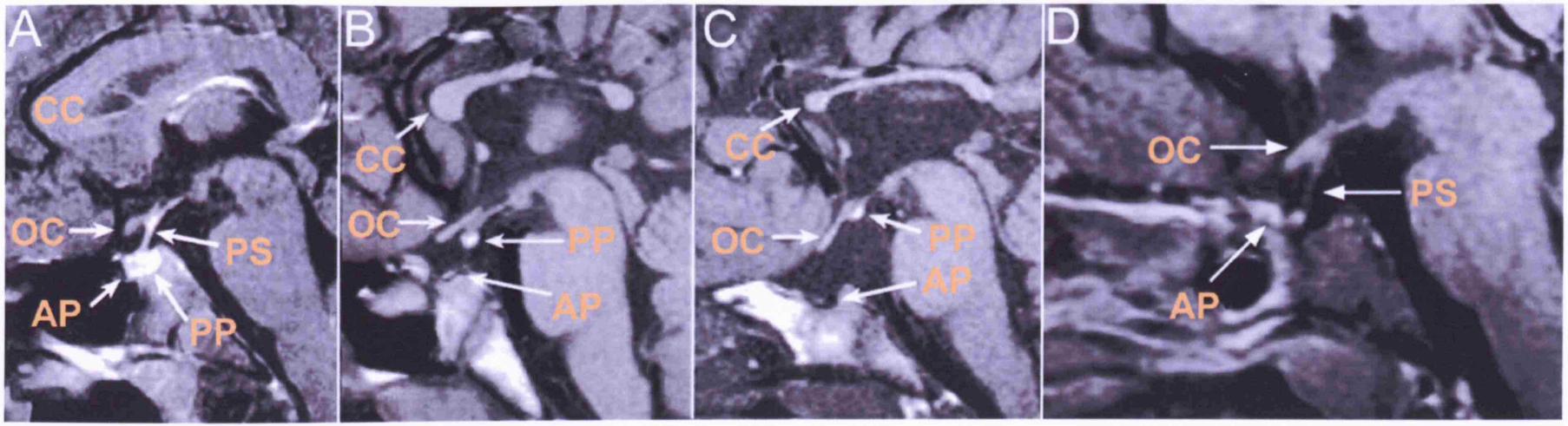

Figure 1.12 – Forebrain and pituitary defects in human *HESX1*$^{R160C/R160C}$ and *HESX1*$^{I26T/I26T}$ patients. A) Sagittal MRI scan of the head from a normal child, showing normal corpus callosum (CC), optic chiasm (OC), anterior pituitary (AP), pituitary stalk (PS) and posterior pituitary (PP). (B-C) Equivalent MRI scans of two siblings with a homozygous R160C mutation in *HESX1*. In both siblings, the CC is hypoplastic and the PP is ectopic/undescended. The OC and the AP are hypoplastic. The sella turcica and the pituitary stalk are also abnormal. However, note that these defects are more severe in sibling 2 (C), compared with sibling 1 (B). D) Sagittal MRI scan of a patient with a homozygous I26T mutation in *HESX1*. The AP is severely hypoplastic. The PS is thin and the PP is undescended (not shown). However, the OP and the CC (not shown) are normal. Note that image D is a higher magnification compared with A-C, showing only the hypothalamic-pituitary region. A-C are taken from Brickman et al., 2001; D is taken from Carvalho et al., 2003.

1.6. THESIS AIMS

Since its discovery just over a decade ago, great progress has been made at characterising the function of *Hesx1*; however, there are still a number of unanswered questions. The overall aim of this study is to investigate the role of *HESX1/Hesx1* during forebrain and pituitary development. Two different and complementary approaches were used in this thesis.

The first aim was to use the yeast two-hybrid system, in order to identify and characterise the proteins that interact with HESX1. Chapter 2 contains the details of the screen, whilst chapter 3 looks at the verification of these interactions and their implications regarding HESX1 function in-vivo.

The second aim was to analyse and characterise two mouse models carrying two of the human *HESX1* mutations, namely *Hesx1-I26T* and *Hesx1-R160C*. Chapters 4 and 5 contain the details of these analyses.

The mouse models, *Hesx1-I26T* and *Hesx1-R160C*, were generated by Dr. J.P. Martinez-Barbera and Mr. M. Signore. This work was mostly carried out before the initiation of my PhD, and I therefore, only made a minor contribution by cloning and generating the final *Hesx1-R160C* construct (Appendices, Figure 8.1). Nevertheless, the bulk of the results chapters are purely my own work, although wherever the work documented was not performed by me, I have given credit to the contributor(s).

2. IDENTIFICATION OF PROTEIN PARTNERS OF HESX1 BY A YEAST TWO-HYBRID SCREEN

2.1. INTRODUCTION

When studying the role of a protein in-vivo, it is very important to remember that proteins rarely function as a single, isolated unit in order to carry out their task(s). Instead, they cooperate with other proteins and molecules, often forming complexes. The interaction within a complex is dependent on the biological function that is being carried out and can change with time, so that the complex may appear transiently and disappear once the function has been accomplished. These protein-protein interactions form the basis of many biological processes that are crucial for the survival of an organism whether prokaryotic or eukaryotic. During development, the disruption of these interactions can be lethal or in some cases can cause disease. Transcription factors in particular, have been shown to cooperate with other proteins in order to activate/repress the transcription of their target genes (Rual et al., 2005; Rosenfeld et al., 2006; Tan et al., 2007).

It is already known that the eh1 domain in the amino terminal of HESX1, can mediate its interaction with Transducin-like enhancer of split 1 (TLE1), which is a mammalian orthologue of Groucho (Dasen et al., 2001). Additionally, the homeodomain of HESX1 is involved in its interaction with the nuclear corepressor complex N-CoR/mSin3/HDAC1/2 (Dasen et al., 2001; Xu et al., 1998a).

What has been missing concerning HESX1 is a large scale screen in order to identify protein(s) that interact with it. The importance of such a screen is clear, since in doing so, a deeper understanding of HESX1 function is achieved. This is in turn important for elucidating the mechanism and pathway(s) through which it regulates other genes as a transcriptional repressor. The screen has also the potential of identifying other genes, which may have a role in the aetiology of SOD and/or other forms of hypopituitarism. To achieve this, a yeast two-hybrid screen was carried out.

2.1.1. The yeast two-hybrid system

The yeast two-hybrid was first introduced in 1989 by Fields and Song (Fields and Song, 1989). They took advantage of a number of properties of transcription factors, shown in research carried out a few years earlier. Firstly, transcriptional activators are made up of two separate domains, one that recognises and binds a specific DNA sequence (DNA-binding domain or DBD) and a second domain, which activates transcription (activation domain or AD) (Brent and Ptashne, 1984 and 1985). Secondly, these two domains have separate roles and fold independently. Hence, they do not have to be present within the same polypeptide chain in order to activate target genes. Provided that the two domains are within close proximity of each other, activation takes place (Figure 2.1) (Stern et al., 1989; Triezenberg et al., 1988a; Triezenberg et al., 1988b).

Since then, much effort and research has been conducted, in order to improve this technique for a wide range of applications. This has meant the availability of many different engineered host yeast strains, with plasmids and libraries compatible to each strain (Brent and Finley, Jr., 1997; Van Criekinge and Beyaert, 1999). As a result, when employing the yeast two-hybrid system, several important components need to be chosen carefully, depending on the application used.

The first important component is the choice of host yeast. Host strains contain inducible promoters fused to reporter genes in order to select for protein interactions. In this study the yeast host strain PJ69-4A (James et al., 1996) was available to us. This strain has been engineered to carry three inducible promoters: (1) *Gal1* promoter driving the histidine (*his3*) reporter gene; (2) *Gal2* promoter driving the adenine (*ade2*) reporter gene; (3) *Gal7* promoter driving the *lacZ* reporter gene. All three promoters have upstream sequences, which make them responsive to GAL4. Along with mutations in their endogenous adenine and histidine genes, this strain is ideal for selecting for interactions using media deficient in histidine and adenine and supplemented with X-α-Gal. Finally, this yeast strain has mutations in uracil, leucine, methionine and tryptophan genes, which allow for selection of a wide range of "bait" and "prey" plasmids.

The other two important components are the "prey" and the "bait" vectors. The "bait" plasmid carries the gene of interest fused in-frame with either Gal4-DBD

(Chien et al., 1991) or LexA-DBD (Vojtek et al., 1993). In our case, two "baits" were constructed carrying either full-length HESX1 (aa 1-185), or HESX1 lacking the homeodomain (aa 1-107), in-frame with Gal4-DBD in the pGBDUC-3 vector, which carries an *ura3* gene making it compatible with PJ69-4A (Appendices, Figure 8.7).

The "prey" vectors carry sequences for genes encoding proteins that act as potential interactors, fused in-frame with either B42-AD, GAL4-AD (Chien et al., 1991) or VP16-AD (Dalton and Treisman, 1992). In our case, the "prey" was a mouse embryonic library at stages 9.5 and 10.5 dpc (Hollenberg et al., 1995). In these libraries, the cDNAs are fused in-frame with VP16-AD in a pVP16 vector, which carries a *leu2* gene and hence can be selected in PJ69-4A (Appendices, Figure 8.8). The yeast strain and the mouse embryonic libraries were kindly given to us by Prof. P. Scambler, Molecular Medicine Unit, ICH, UCL (Magnaghi et al., 1998).

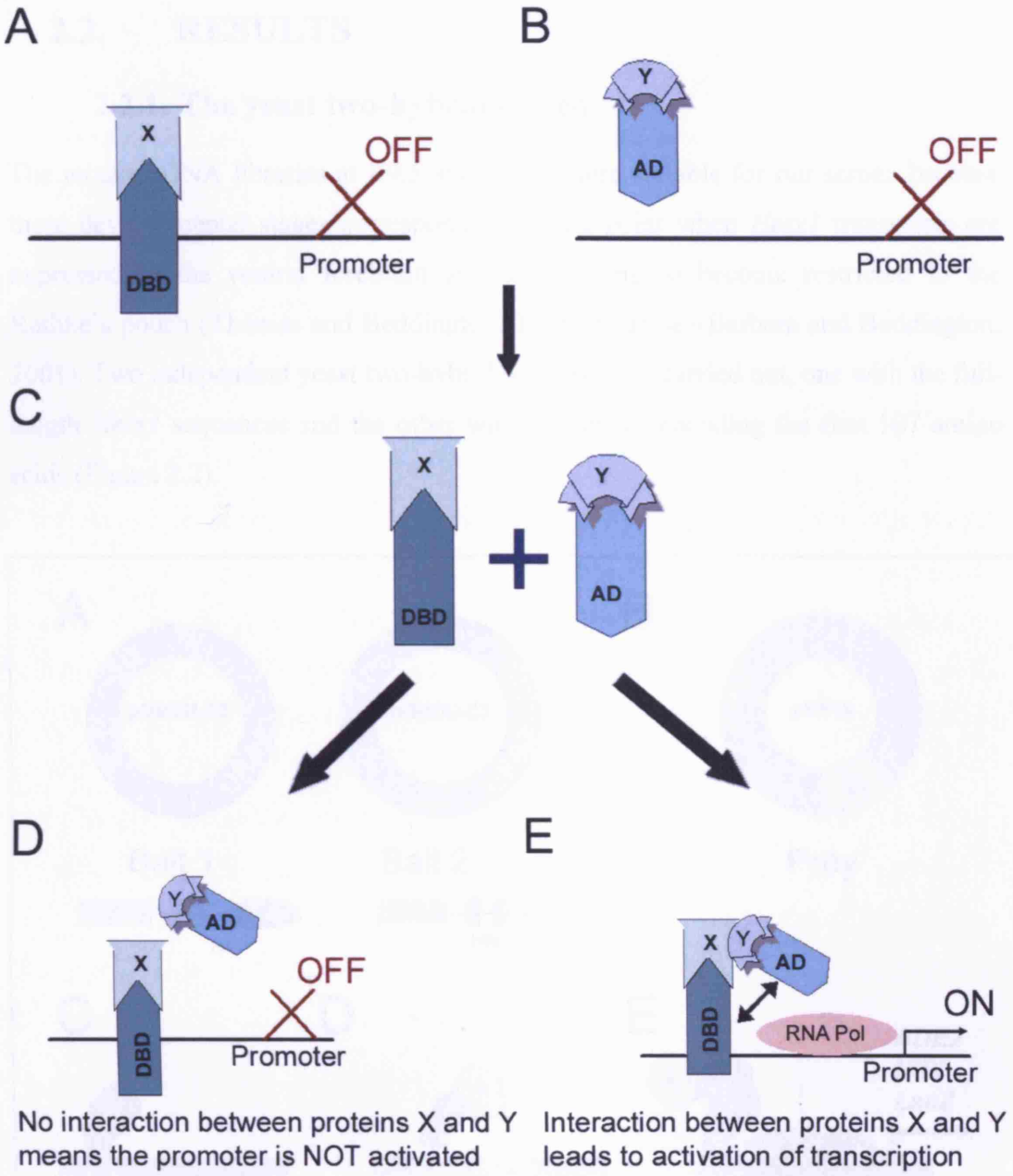

Figure 2.1 – The yeast two-hybrid system. A) Protein X is fused to the DNA-binding domain (DBD) of either Gal4 or LexA transcription factors. Without the activation domain this fusion protein is unable to activate downstream genes. B) Protein Y is fused to the activation domain (AD) of B42, Gal4 or VP16. This fusion protein is also unable to activate downstream genes in the absence of a DBD. C) Both fusion proteins are expressed in yeast. D) In the absence of an interaction between proteins X and Y, AD and DBD are not in close proximity of each other and therefore, downstream genes remain silent. E) Activation of downstream genes is only achieved when proteins X and Y interact.

2.2. RESULTS

2.2.1. The yeast two-hybrid screen

The mouse cDNA libraries at E9.5 and E10.5 were suitable for our screen because these developmental stages correspond to a time point when *Hesx1* transcripts are expressed in the ventral forebrain and are starting to become restricted to the Rathke's pouch (Thomas and Beddington, 1996; Martinez-Barbera and Beddington, 2001). Two independent yeast two-hybrid screens were carried out, one with the full-length *Hesx1* sequences and the other with sequences encoding the first 107 amino acids (Figure 2.2).

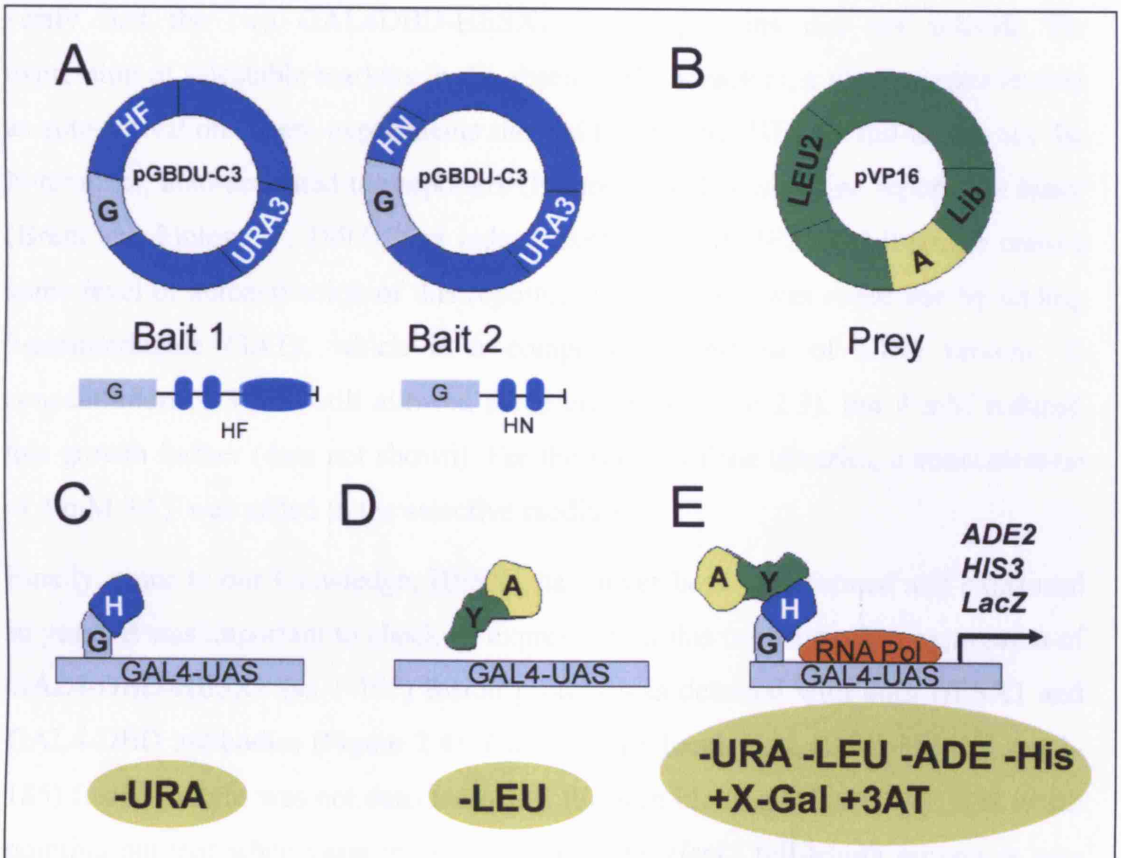

Figure 2.2 – Schematic representation of the yeast two-hybrid strategy used to identify HESX1-interacting proteins. A) Two "baits" were constructed by fusing either the full-length *Hesx1* sequences (HF, Bait 1) or sequences encoding its first 107 amino acids (HN, Bait 2) in-frame with Gal4DBD (G) in a pGBDU-C3 vector. B) The "prey" was the embryonic mouse cDNA library at 9.5-10.5 dpc. In these libraries, cDNA fragments are fused to the VP16-AD (A) in a pVP16 vector. C) The Gal4-HESX1 fusion proteins are selected on medium lacking uracil, but reporter genes are not activated. D) The "prey" is selected on medium lacking leucine, but reporter genes are not activated. E) Interaction between HESX1 (H) and a protein Y leads to the activation of reporter genes and can be selected by using media lacking uracil, leucine, adenine, histidine and supplemented with 3AT and X-α-Gal.

Initially, however, three important experiments were carried out: (1) phenotyping of the yeast strain PJ69-4A; (2) Assessing the absence of autoactivation of reporters by the baits; (3) checking that the baits are expressed in the yeast strain PJ69-4A.

Phenotyping of the yeast strain PJ69-4A involved assessing its growth on selective media, lacking the amino acids essential for the selection of interacting clones. It was confirmed that the yeast strain PJ69-4A (James et al., 1996) was unable to grow on selective media (SD -ura, -leu, -met, -tryp, -his and -ade), while it was able to grow on media supplemented with all the amino acids (data not shown).

Absence of auto-activation of the reporters was also demonstrated. This was to verify that the two GAL4DBD-HESX1 fusion proteins did not activate the expression of selectable markers in the absence of interactors, a phenomenon known as auto-activation. These experiments showed that neither HESX1 full-length nor the N-terminal, auto-activated the reporters (Figure 2.3). The histidine reporter is leaky (Brent and Finley, Jr., 1997), and indeed expression of HESX1 full-length caused some level of autoactivation of this reporter. The problem was overcome by adding 3-aminotriazole (3AT), which is a competitive inhibitor of HIS3 protein. A concentration of 3 mM still allowed some growth (Figure 2.3), but 4 mM reduced this growth further (data not shown). For the screen of the libraries, a concentration of 4 mM 3AT was added to the selective medium.

Finally, since to our knowledge, HESX1 has never been transformed and expressed in yeast, it was important to check its expression in this organism. The expression of GAL4-DBD-HESX1 (aa 1-107) fusion protein was detected with both HESX1 and GAL4-DBD antibodies (Figure 2.4). On the other hand, GAL4DBD-HESX1 (aa 1-185) fusion protein was not detected using Western blotting (Figure 2.4). It is worth pointing out that when yeast transformed with the *Hesx1* full-length sequences was grown in liquid culture, it always showed a slower growth rate compared to yeast expressing HESX1 N-terminal protein. This suggested that HESX1 full-length, but not the N-terminal, is toxic in this yeast strain. However, the screen was carried out using both "baits" since the effect was not lethal and the HESX1 (aa 1-107) expression was detectable.

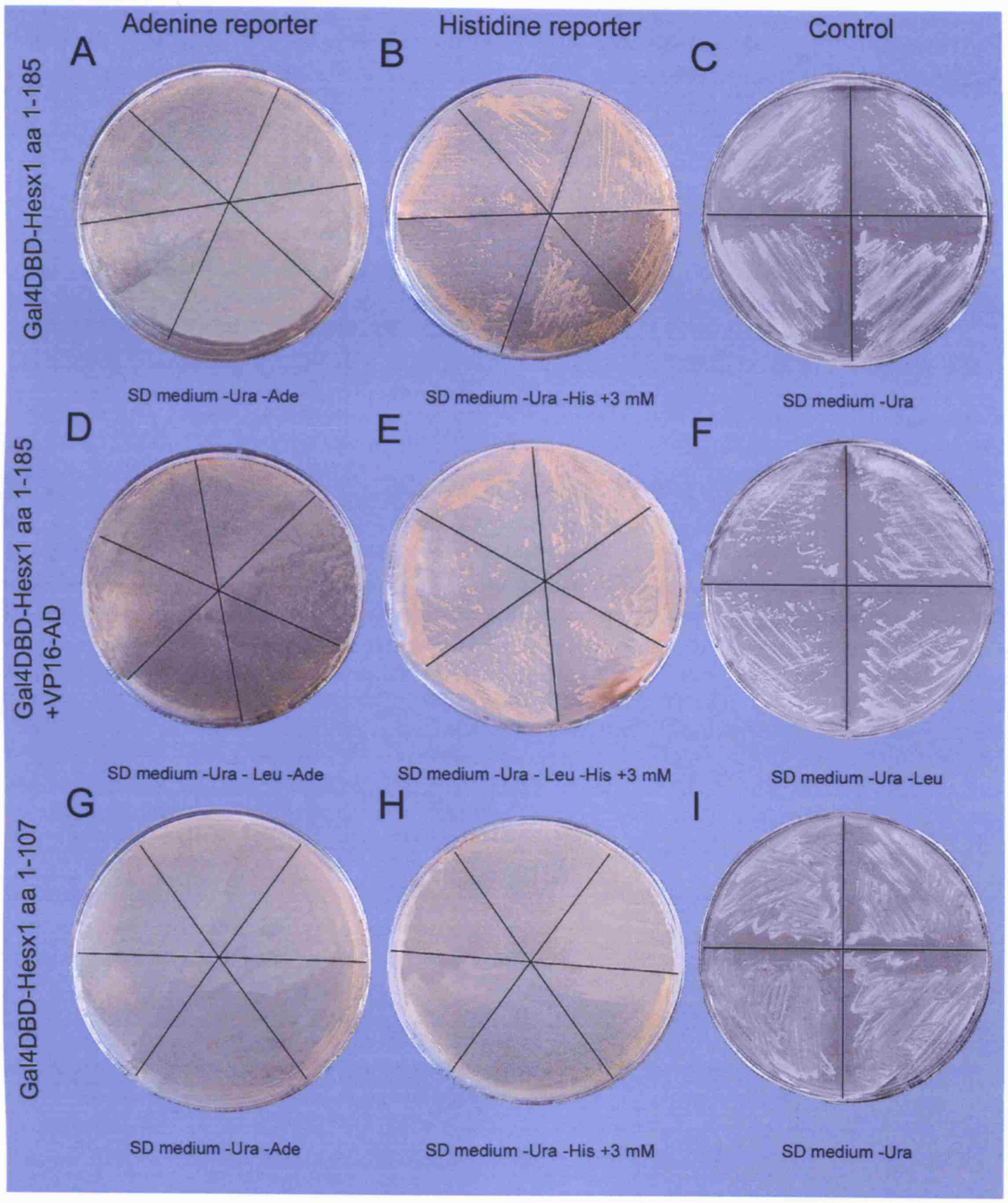

Figure 2.3 – Assessment of autoactivation of histidine and adenine reporters by the two "bait" vectors. (A-C) Yeast transformed with GAL4DBD-HESX1 aa 1-185 and grown on SD medium lacking the following amino acids: A) uracil/adenine; B) uracil/histidine; C) uracil. (D-F) Yeast transformed with GAL4DBD-HESX1 aa 1-185 and the empty prey plasmid (VP16-AD) and grown on SD medium lacking the following amino acids: D) uracil/leucine/adenine; E) uracil/leucine/histidine; F) uracil/leucine. (G-I) Yeast transformed with GAL4DBD-HESX1 aa 1-107 vector and grown on SD medium lacking the following amino acids: G) uracil/adenine; H) uracil/histidine; I) uracil. Note that even in the presence of 3 mM 3AT, there is some autoactivation of histidine by HESX1 aa 1-185 (B and E), due to the "leakiness" of the histidine reporter. A concentration of 4 mM 3AT was used in the screen (not shown).

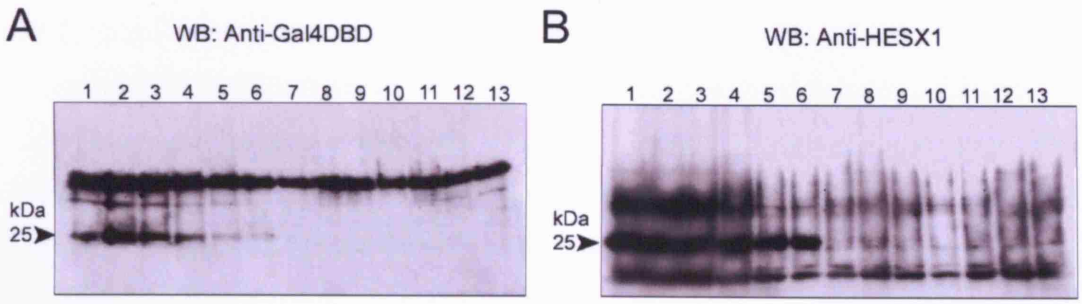

Figure 2.4 – Expression of HESX1 protein in yeast PJ69-4A. GAL4DBD antibody (A) and a HESX1 antibody (B) were used in Western blot analysis to detect the fusion proteins. (A-B) Expression of HESX1 is detected using both antibodies in clones transformed with the Gal4DBD-HESX1 aa 1-107 fusion protein, as indicated by arrowheads in lanes 1-6 (A and B). No expression is detected in yeast clones transformed with Gal4DBD-HESX1 aa 1-185 (lanes 7-12 in A and B). Lane 13 is a negative control, containing protein extracts from yeast transformed with plasmid carrying Gal4DBD-empty.

Initially, after the two screens were carried out, 200 clones were picked, isolated and sequenced. The sequences were analysed for homology to other cDNAs by BLAST search (http://www.ncbi.nlm.nih.gov/blast). At this stage some of the clones were discarded as they did not match any known sequences in the database. Additionally, some sequences were not in-frame with the VP16-AD sequence and were also discarded. The result was the identification of nine proteins (Table 2.1), as potential interactors of HESX1. It was very promising at this stage to observe the occurrence of clones encoding different regions of the same protein.

Table 2.1 – Results from the yeast two-hybrid screens.

HESX1-interacting protein	Accession Number	Number of clones	No. of overlapping clones
Scaffold Attachment Factor β 1 (SAFB1)	XM_128715	20	3
Serum Response Factor Binding Protein 1 (SRFBP1)	NM_026040	17	4
DNA Methyltrasferase 1 (DNMT1)	NM_010066	14	3
Lon Peptidase 2, Peroxisomal (LONP2)	BC049090	3	2
Zinc Finger Protein 592 (ZFP592)	BC059073	3	2
Zinc Finger, MIZ-type containing 1 (ZMIZ1)	BC058646	3	1
Ring Finger Protein 2 (RNF2)	NM_011277	6	3
BTB (POZ) Domain Containing 2 (BTBD2)	BC055704	6	1
Nuclear Receptor Binding Protein 2 (NRBP2)	BC012437	1	1

2.2.2. Selecting the positive interactors

In order to confirm that these interactions are a specific result of binding to HESX1 sequences and not Gal4-DBD or activation of reporters on their own, the interacting clones were re-introduced in yeast alone as well as with Gal4DBD-HESX1 aa 1-185, Gal4DBD-HESX1 aa 1-107 and Gal4-DBD.

The results are demonstrated in Figure 2.5, showing the reproducible interaction for a number of clones including DNA methyltransferase 1 (DNMT1), Scaffold/matrix Attachment Factor β1 (SAFB1), Serum Response Factor Binding Protein 1 (SRFBP1), Zinc finger protein 592 (ZFP592), Lon Peptidase 2 Peroximal (LONP2), Zinc Finger MIZ-type containing 1 (ZMIZ1) and BTB (POZ) Domain Containing 2 (Table 2.1). At this stage, two of the interacting clones were eliminated (Figure 2.5B). Ring Finger Protein 2 (RFP2) showed an interaction with GAL4-DBD and Nuclear Receptor Binding Protein 2 (NRBP2) only showed a weak interaction with HESX1 (aa 1-185) and was only picked once in the screen (Table 2.1).

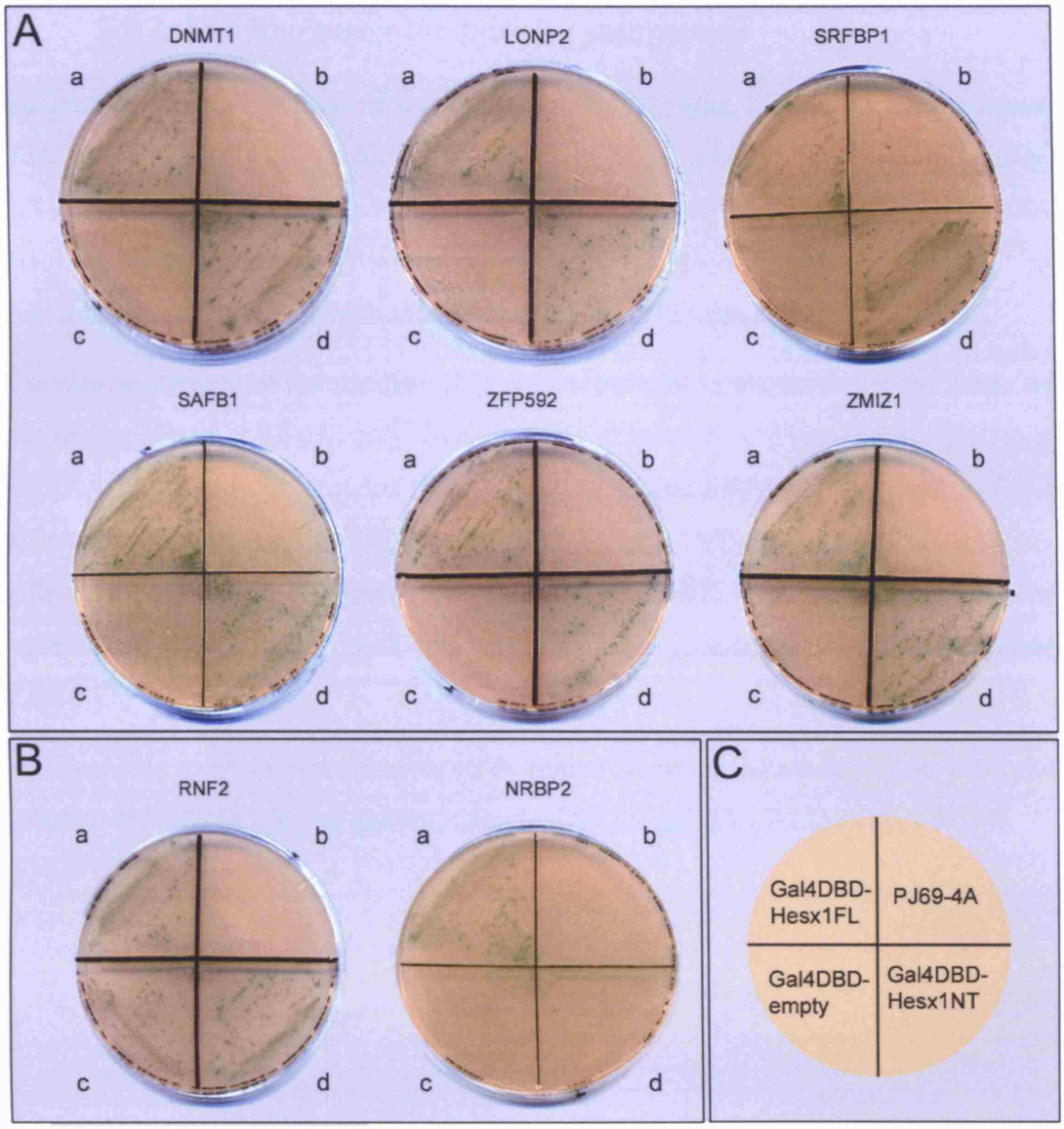

Figure 2.5 – Interaction in yeast is reproducible for a number of interacting clones. Clones picked from the screen were sequenced and those in-frame with VP16-AD were analysed further. A) Specific interactions were observed with: DNMT1, LONP2, SRFBP1, SAFB1, ZFP592, ZMIZ1 and BTBD2 (data not shown), as shown by growth of yeast transformed only with Gal4DBD-HESX1 aa 1-185 and Gal4DBD-HESX1 aa 1-107 (sections a and d, respectively). B) RNF2 and NRBP2 are false positives. RNF2 shows an interaction with Gal4DBD (section c). NRBP2 only showed a weak interaction with Gal4DBD-HESX1 aa 1-185, and was only identified once in the screen. C) The corresponding transformations are shown in this schematic. Interactors were transformed with (a) yeast expressing Gal4DBD-HESX1 aa 1-185, (b) yeast PJ69-4A (c) yeast expressing Gal4DBD-empty and (d) yeast expressing Gal4DBD-HESX1 aa 1-107. G: Gal4-DBD.

2.2.3. In-vitro assay for positive interactors

Following the confirmation of these interactions in yeast, it is important to assess whether HESX1 directly interacts with each of these proteins in an in-vitro assay. GST pull-down experiments were carried out using GST-HESX1 aa 1-185, GST-HESX1 aa 1-107 and GST alone, as well as the in-vitro translated (IVT) ^{35}S-methionine-labelled full-length interactor proteins (See Materials and Methods).

Coomassie staining of the purified GST fusion proteins is shown in Figure 2.6A. As shown in Figure 2.6B-H, only five proteins displayed a direct interaction with HESX1. Three of these proteins (DNMT1, LONP2 and SRFBP1) exhibited a higher affinity for the full-length HESX1 (GST-HESX1 aa 1-185). SAFB1 showed a higher affinity for the amino-terminal (GST-HESX1 aa 1-107). Finally, ZFP592 showed equal levels of binding to both full-length and amino-terminal of HESX1 (Figure 2.6B-F).

Again at this stage, it was possible to eliminate some of the clones as they did not interact with HESX1 in this system, namely ZMIZ1 and BTBD2 (Figure 2.6G,H).

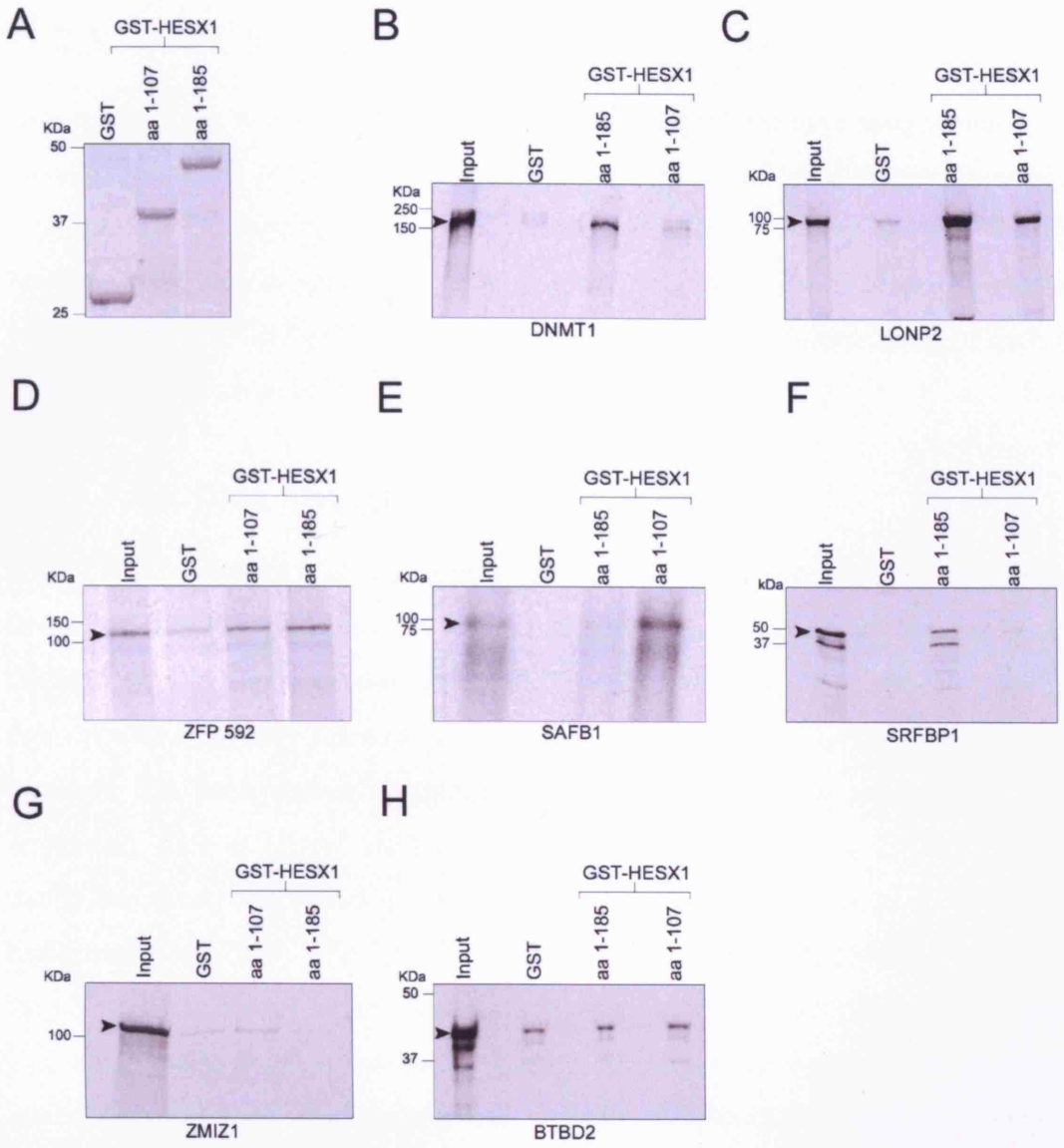

Figure 2.6 – GST pull-down assays, using HESX1 and the putative partner proteins. A) Representative Coomassie stain, showing the proteins used in the subsequent GST pull-down experiments. (B-H) ^{35}S-methionine-labelled interacting proteins were incubated with either GST alone, GST-HESX1 aa 1-107 or GST-HESX1 aa 1-185. 1/10 of the labelled protein, used in the pull-down experiment, was loaded as control (lane 1). Specific binding to HESX1 sequences were observed with DNMT1 (B), LONP2 (C), ZFP592 (D), SAFB1 (E) and SRFBP1 (F). (G-H) ZMIZ1 and BTBD2 did not specifically bind to HESX1 in this assay. Molecular weight markers are shown on the left of each panel.

2.3. SUMMARY

As a result of the two yeast two-hybrid screens, five proteins have been identified as putative interactors of HESX1. These five proteins were identified several times with different and overlapping clones in the screens (Table 2.1). They showed specific binding to HESX1 sequences in yeast (Figure 2.5), as well as a direct interaction with HESX1 in a GST pull-down assay (Figure 2.6). A brief description of each of these proteins is given below.

2.3.1. DNA Methyltransferase 1 (DNMT1)

DNMT1 is a member of the methyltransferase family of proteins comprising DNMT1, DNMT2 and DNMT3a, 3b and 3L (Hermann et al., 2004; Bestor, 2000). DNMT1 is the largest of the family (1620 aa) consisting of a large N-terminal domain with regulatory functions and a smaller C-terminal catalytic domain. The N-terminus has been shown to interact with multiple proteins involved in gene repression, such as HDAC (histone deacetylases), retinoblastoma, DNMAP (DNA methyltransferase-associated protein 1) among others (Leonhardt et al., 1992; Robertson et al., 2000). The catalytic domain catalyses the methylation of cytosine at the C5 position, mainly in the short canonical sequence 5'-CG-3', and rarely in non-CG sites. DNA methylation has a variety of important functions in mammals including control of gene expression, cellular differentiation and development. Indeed, *Dnmt1*$^{-/-}$ mutants are stunted, developmentally delayed and do not survive past midgestation (Li et al., 1992).

HESX1 interacts with the first 150 aa of the N-terminus, a unique region in DNMT1 that is not present in the other members of the family. The HESX1-DNMT1 interaction raises interesting questions about the mechanisms responsible for the HESX1 repressing activity.

2.3.2. Lon Peptidase 2, Peroxisomal (LONP2)

This cDNA encodes an unknown protein. Bioinformatics databases identified homology between a portion of the protein and certain conserved domains present in some ATP-dependent proteases. It is likely that it belongs to the large family of AAA proteases (for ATPases Associated with diverse cellular Activities). This large family

of proteins has been associated with proteolysis, membrane fusion and DNA replication. Human LON proteases have been shown to bind mitochondrial promoters when presented in a single stranded form, suggesting that perhaps they are involved in mitochondrial gene expression, by targeting the degradation of regulatory proteins (Fu and Markovitz, 1998). No details on the expression pattern during mouse development have been reported. HESX1 interacts with a fragment contained within the N-terminal part of the protein.

2.3.3. Scaffold/Matrix attachment factor β 1 (SAFB1)

SAFB1 is a nuclear protein with multiple functions (Townson et al., 2004). It was originally cloned on the basis of its ability to bind to AT-rich scaffold/matrix attachment regions (S/MARs) (Nayler et al., 1998). S/MARs have been proposed to potentially contribute to a higher-order chromatin structure by mediating the attachment of chromatin to the nuclear matrix, thereby folding chromatin into topologically independent loop domains, which are thought to be implicated in regulation of gene expression. SAFB1 also interacts with RNA processing proteins and with RNA Polymerase II. For this reason, it has been suggested that SAFB1 can be part of the "transcriptosome" complex, bringing together transcription and RNA processing (Arao et al., 2000). SAFB1 can repress transcription of estrogen receptor alpha responsive promoters (Townson et al., 2004). A related protein, SAFB2 has a similar structure and function to SAFB1. HESX1 interacts with a region in the C-terminal of SAFB1, which shows around 60% similarity to SAFB2.

The HESX1-SAFB1 interaction might be highly significant in normal development. Most *Safb1*$^{-/-}$ mutants die during development and perinatally, but some survive weaning. These animals are smaller than wildtype littermates, IGF-1 (insulin-like growth factor 1) levels are significantly reduced and the mice also exhibit gonadal defects. These anomalies are compatible with hypopituitarism in *Safb1*$^{-/-}$ mutants, but neither the brain nor the pituitary gland have been analysed (Ivanova et al., 2005).

2.3.4. Serum Response Factor Binding Protein 1 (SRFBP1)

SRFBP1 is a transcription factor that was identified very recently in a yeast two-hybrid screen aiming to identify proteins that interact with Serum response factor (SRF) (Zhang et al., 2004). Little is known about this gene. It is conserved in

mammals and vertebrates, and widely expressed in adult mouse tissues, but no data exists on its expression pattern during development. In transient transfection experiments SRFBP1 interacts with SRF to modulate, by either enhancing or reducing, SRF activating action on a variety of promoters. The interaction of this protein with HESX1 suggests that *Srfbp1* is expressed during embryogenesis in anterior neural tissues. HESX1 binds with the same region of SRFBP1 that is involved in its interaction with SRF.

2.3.5. Zinc Finger Protein 592 (ZFP592)

Zinc finger domains are nucleic acid-binding protein structures first identified in the transcription factor TFIIIA (Brown et al., 2004; Nakamura et al., 2004). These domains have since been found in numerous nucleic acid-binding proteins. Many classes of zinc fingers are characterised according to the number and positions of the histidine and cysteine residues involved in the zinc atom coordination. ZFP592 belongs to the kruppel C2H2-type zinc-finger protein family. HESX1 interacts with the N-terminus, whereas the zinc-fingers are located in the C-terminus. No information about its function or expression pattern during development is available.

3. PUTATIVE INTERACTORS OF HESX1

3.1. INTRODUCTION

The yeast two-hybrid is ideal for identifying interacting partners of a particular protein from a pool of potentials. However, once the list is narrowed down, it is very important to confirm these interactions and investigate their functional relevance in the correct biological setting.

Although, yeast itself is a eukaryotic organism, it is standard practice to validate the interactions identified in yeast by alternative methods. Several techniques exist to achieve this, in this study we decided to first map the region of HESX1, which makes direct contact with each of these proteins, using GST pull-down assays. We then moved on to assess if these interactions take place in mammalian cells using co-immunoprecipitation experiments and luciferase assays. We also looked at the localisation of the proteins with respect to HESX1 in mammalian cells using immunofluorescence techniques, as well as the localisation of the RNA transcripts in embryos using whole mount and section in-situ hybridisation and RT-PCR.

We decided to focus on the interaction of HESX1 with DNMT1 and attempted to characterise this binding further, by mapping the region of interaction in mammalian cells. An attempt was also made at elucidating the functional relevance of this interaction in-vivo by analysing *Dnmt1*$^{+/-}$;*Hesx1*$^{+/-}$ mice. Finally, we assessed whether the interactions (between HESX1 and the five identified proteins) are affected by seven existing human *HESX1* mutations.

3.2. RESULTS

3.2.1. Mapping the region of HESX1 interaction in-vitro

The region(s) of HESX1, responsible for binding to each of the five proteins, was depicted using GST pull-down assays. In this way, a more detailed analysis of the interactions was made, and it was anticipated to increase our understanding of the functional domains of HESX1. This also stemmed from the observation that in the previous GST pull-down experiment, the two GST-HESX1 fusion proteins (GST-HESX1 aa 1-185 and aa 1-107) displayed variable binding affinities to the five proteins (Figure 2.6).

The assay was conducted much in the same way, as previously described (Chapter 2). Firstly, however, six additional GST fusion proteins were constructed, each encompassing different regional domains of the HESX1 protein (Figure 3.1A). Using these eight GST-HESX1 fusion proteins and the ^{35}S-Met-labelled IVT full-length protein for each of the five putative interactors, we observed some variation in binding affinity between the proteins and the different domains of HESX1.

DNMT1 showed the highest affinity to HESX1 full-length protein, whilst binding to all the other HESX1 fragments was weaker and at equal levels (Figure 3.1C). It seems likely, therefore, that the whole tertiary structure of HESX1 is involved in this interaction.

SAFB1 and ZFP592 both showed strong binding to HESX1 full-length, but also to fragments aa 50-107 and aa 108-185 (Figure 3.1E,G). These fragments encompass a section of the amino-terminal adjacent to the homeodomain and the homeodomain itself, respectively.

SRFBP1 also interacted strongly with the full-length HESX1 and additionally, with the fragment containing only the homeodomain (aa 108-185) (Figure 3.1F).

Finally, LONP2 bound the full-length HESX1, but also showed a strong interaction with fragments aa 1-107 and aa 50-107, which cover the entire amino-terminal portion of HESX1 (Figure 3.1D).

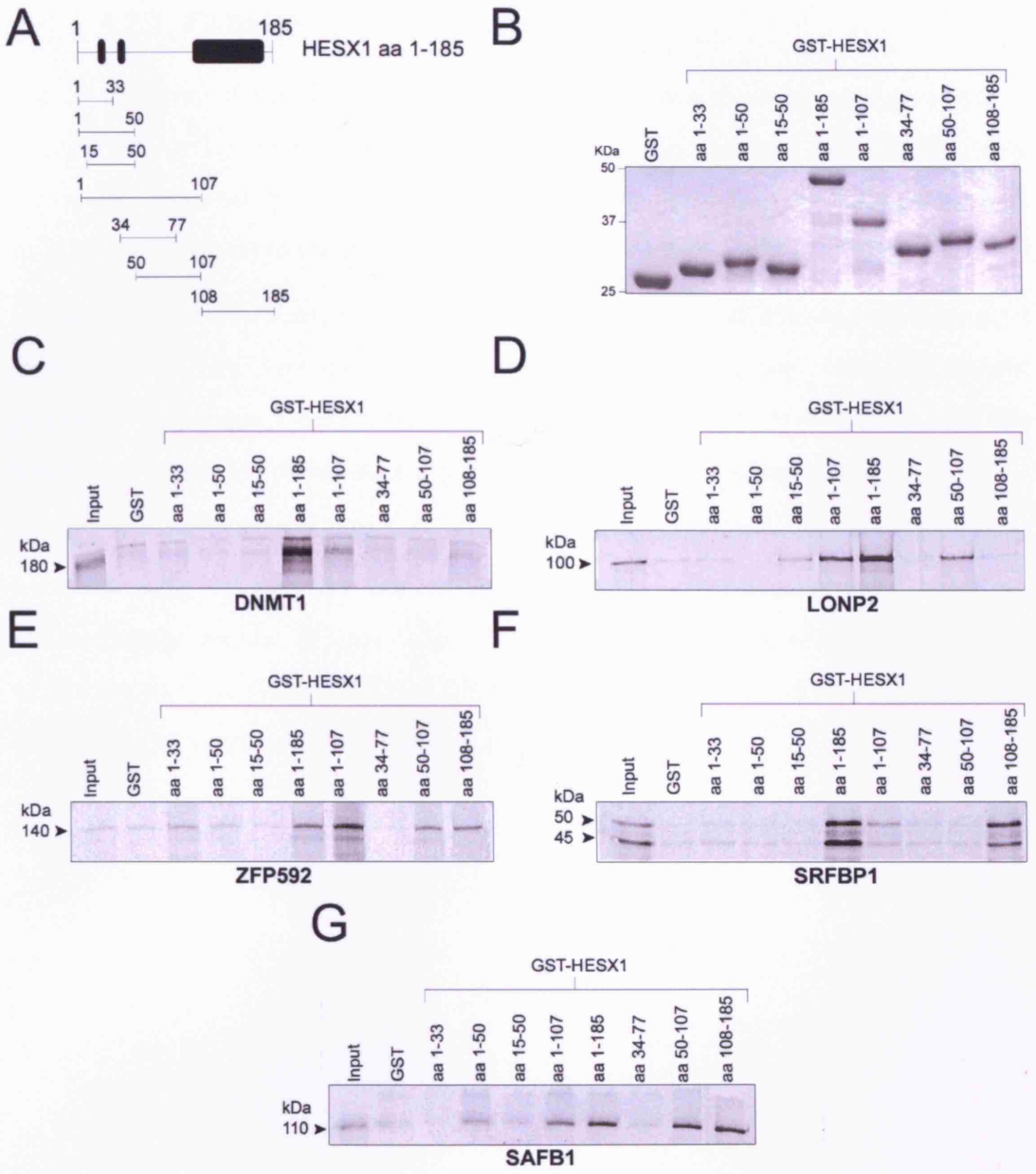

Figure 3.1 – Mapping the interacting regions of HESX1 by GST pull-down experiments. A) Schematic representations of HESX1 fragments expressed as GST fusion proteins. B) Representative Coomassie stain of the GST-HESX1 fusion proteins used in subsequent panels. Molecular weight marker is indicated on the left. C) DNMT1 strongly interacts with GST–HESX1 (aa 1–185), whilst binding to other GST-HESX1 fragments weakly. D) LONP2 shows a strong interaction with the N-terminal of HESX1 (fragments 1-107 and 50-107). E) ZFP592 shows an interaction with HESX1 aa 50-107 and the homeodomain (aa 108-185). F) SRFBP1 shows an interaction with the homeodomain (aa 108-185). G) SAFB1 shows an interaction with HESX1 aa 50-107 and the homeodomain (aa 108-185). As input, 1/10 of the total amount of ^{35}S-Met-labelled protein was used in panels C-G (arrowheads). The approximate sizes of the proteins are indicated on the left of each panel. Note the presence of a smaller band in F, which may correspond to a spliced isoform of the SRFBP1 protein.

3.2.2. Cellular localisation studies

The localisation of the five putative HESX1-interacting proteins was analysed in mammalian cells, with respect to HESX1. The localisation of DNMT1 was previously reported in 3T3 and other mammalian cell lines to be nuclear and dynamic with respect to the phase of the cell cycle (Muromoto et al., 2004).

CHO cells were co-transfected with HA-tagged HESX1 and Flag-tagged interactor proteins. Anti-HA and anti-Flag primary antibodies, along with fluorescent secondary antibodies, were used in immunocytochemistry experiments and the localisation of each protein was analysed using a confocal microscope.

HESX1 protein was predominantly nuclear (Figure 3.2). All of the interactors co-localised with HESX1 in the nucleus. DNMT1, SAFB1, ZFP592 were all predominantly nuclear (Figure 3.2), SRFBP1 localised to the nucleolar structures within the nucleus (Figure 3.2J). LONP2 co-localised with HESX1 in the nucleus, but it was also present in the cytoplasm (Figure 3.2F).

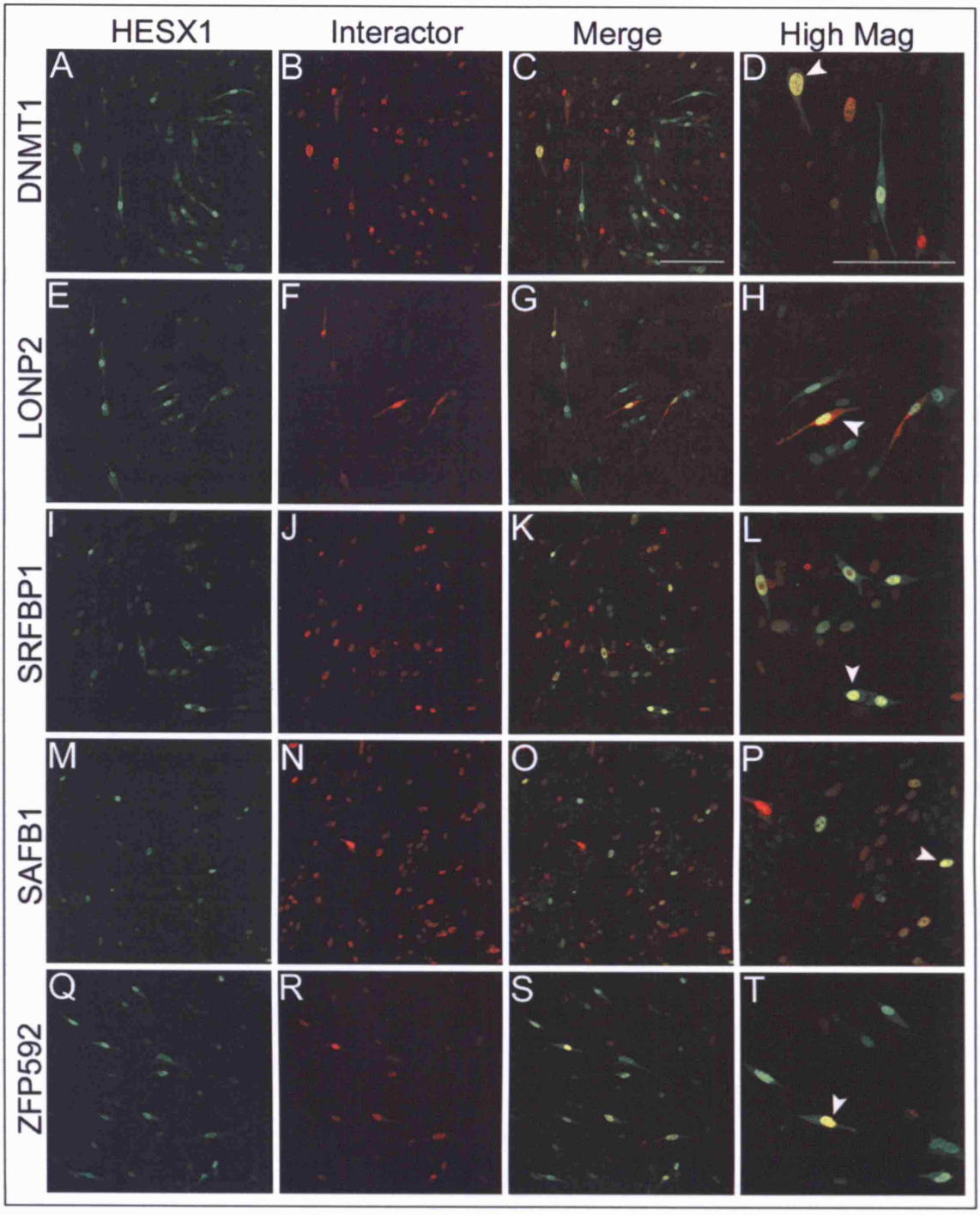
HESX1
Interactor
Merge
High Mag
DNMT1
LONP2
SRFBP1
SAFB1
ZFP592
A
B
C
D
E
F
G
H
I
J
K
L
M
N
O
P
Q
R
S
T

Figure 3.2 – Co-localisation of HESX1 with the interacting proteins in mammalian cells. CHO cells were transfected with HA-HESX1 and Flag-interactor proteins followed by immunofluorescence with Alexa fluor 488 and 594 secondary antibodies. HESX1 staining (A,E,I,M,Q) is mainly detected in the nucleus, although there is sporadic cytoplasmic staining in some cells. The interactors (indicated on the left hand side of the panel) all co-localise with HESX1 in the nucleus as shown in the merged images (C,G,K,O,S). Individual nuclei showing co-localisation of both proteins (yellow staining) are indicated with arrowheads in the higher magnification views (D,H,L,P,T). DNMT1, SRFBP1, SAFB1 and ZFP592 are all predominantly nuclear, LONP2 is additionally found in the cytoplasm. Scale bars shown in C and D correspond to 100 μm.

3.2.3. Co-immunoprecipitation studies

The ability of each of the proteins to interact with HESX1 in mammalian cells was tested in co-immunoprecipitation experiments. 293T cells were transfected with HA-tagged HESX1 and Flag-tagged interactor proteins. The complexes were then analysed for co-immunoprecipitation, using anti-HA and anti-Flag antibodies after immunoprecipitation with protein G beads.

HA-HESX1 formed a complex with both Flag-DNMT1 and Flag-SRFBP1 (Figure 3.3). However, further attempts to co-immunoprecipitate HESX1 with LONP2 (Figure 3.4), SAFB1 and ZFP592 (data not shown), revealed that the expression levels of these proteins were very low. As shown in Figure 3.4, immunoprecipitation of Flag-LONP2 with anti-flag resulted in a very weak band.

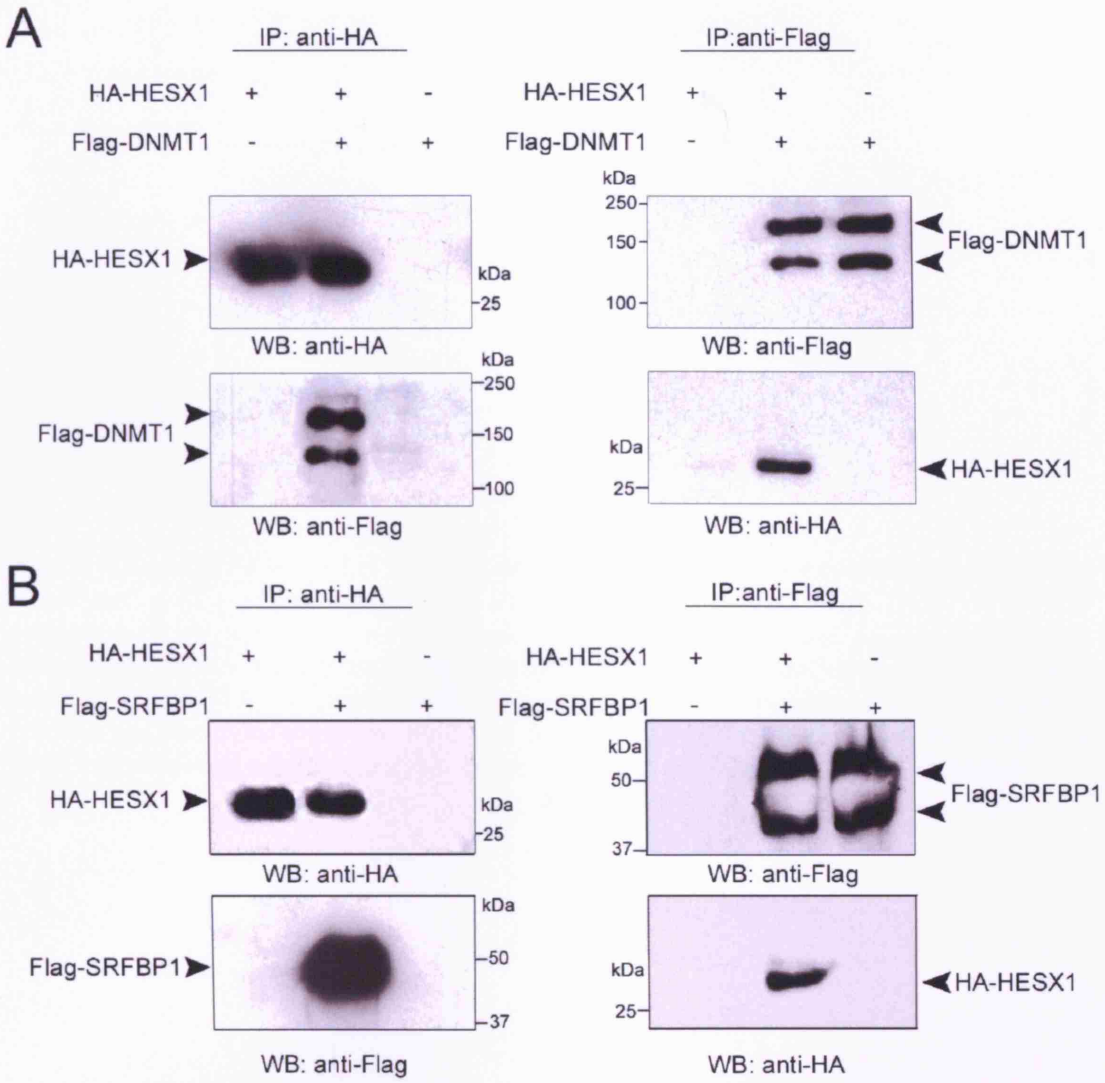

Figure 3.3 – DNMT1 and SRFPB1 interact with HESX1 in 293T cells. A) Cells were transfected with plasmids carrying *Ha–Hesx1* sequences and/or *Flag–Dnmt1* sequences (indicated by + or −) and immunoprecipitated (IP), with anti-Flag and anti-HA antibodies. Immunoprecipitates were blotted and detected with anti-HA or anti-Flag HRP-conjugated antibodies. Specific immunoreactive bands are indicated with arrowheads. B) Cells were transfected with plasmids carrying *Ha–Hesx1* sequences and/or *Flag–Srfbp1* sequences (indicated by + or −) and a similar co-immunoprecipitation experiment to the one described in (A) was carried out. The molecular weight markers are shown on the sides. Note that two bands were detected for both Flag-DNMT1 and Flag-SRFBP1, which correspond to spliced isoforms of the proteins or degradation products.

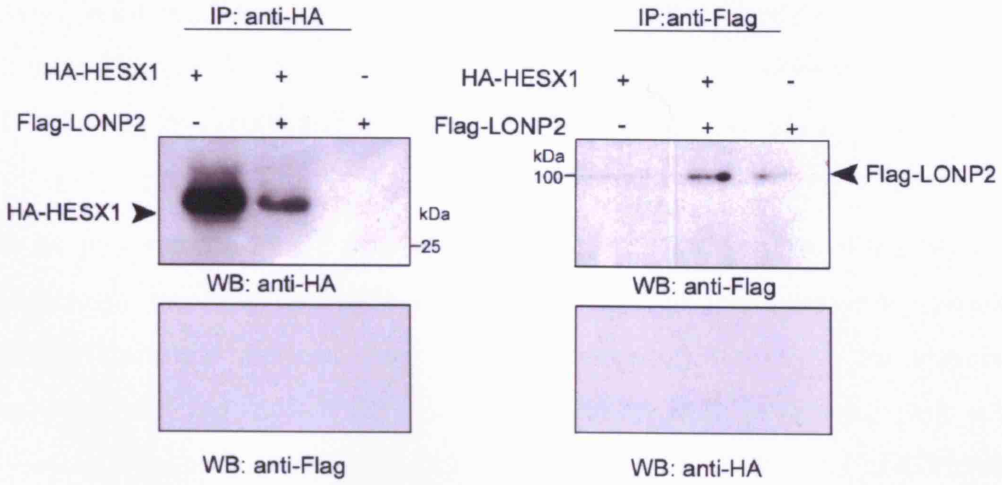

Figure 3.4 – LONP2 is weakly detected in immunoprecipitation experiments. Cells were transfected with plasmids carrying *Ha–Hesx1* and/or full-length *Flag–Lonp2* sequences (indicated by + or −) and immunoprecipitated with anti-Flag and anti-HA antibodies. Immunoprecipitates were blotted and detected with anti-HA or anti-Flag HRP-conjugated antibodies. Specific immunoreactive bands are indicated with arrowheads. Molecular weight markers are shown on the sides. Note that the Flag-LONP2 band is very weak, especially when co-transfected with HA-HESX1. No co-immunoprecipitated bands were detected.

Likewise, Western blot analysis of the cellular lysates after transfection showed that these three proteins (LONP2, SAFB1 and ZFP592) were not present at detectable levels, whereas the controls (HESX1 and DNMT1) showed abundant bands (Figure 3.5).

There are two possibilities for these observations, either the proteins of interest were not expressed by these cells following transfection, or they were not extracted efficiently from the nucleus. In order to investigate this, both the extracted (supernatant) and the nuclear (pellet) protein extracts from transfected cells were analysed by Western blotting. This analysis revealed that SAFB1 and LONP2 were expressed, as shown by detectable bands in the nuclear extracts (Figure 3.6), although it seemed that the cells were unable to express these proteins at high levels. However, the lysis buffer was unable to extract them as they remained in the nuclear fraction. ZFP592 was, on the other hand, absent from the nucleus indicating that the cells were unable to express this protein at detectable levels (Figure 3.6).

Five different conditions were set up to extract SAFB1 and LONP2 from transfected cells (Appendices, Table 8.6), and CHO cells were used as an alternative mammalian cell line. As Figure 3.7 shows, one of the extraction methods (condition 3) yielded in minimal levels of SAFB1 protein in the immunoprecipitated product. However, it was not possible to detect a co-immunoprecipitated complex between HESX1 and SAFB1 with any of the five conditions. A similar result was found with LONP2 (data not shown). Therefore, it was not possible to show an interaction between HESX1 and SAFB1, LONP2 and ZFP592 in mammalian cells using this technique.

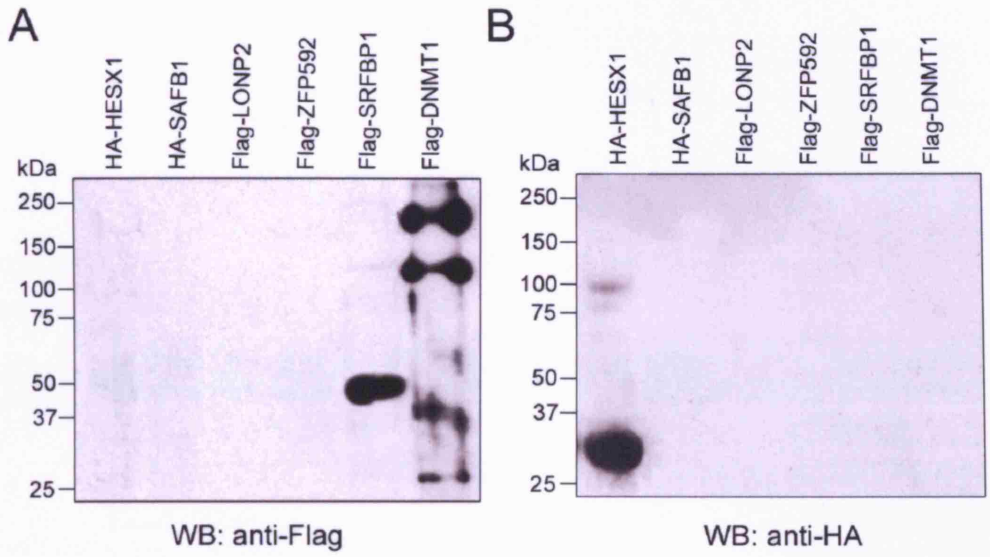

Figure 3.5 – Extraction of proteins from the nucleus. 293T cells were transfected with various tagged proteins (indicated above each lane). Cells were lysed in 1 ml lysis buffer and spun at low speed. Equal amounts of the cell lysates (supernatant) were loaded. The Western blot analysis with anti-Flag (A) and anti-HA (B) antibodies shows abundant bands corresponding to HA-HESX1, Flag-DNMT1 and Flag-SRFBP1. However, Flag-LONP2, HA-SAFB1 and Flag-ZFP592 were not detected. Note the presence of several bands in the Flag-DNMT1 lane, reflecting truncated proteins or partial degradation products.

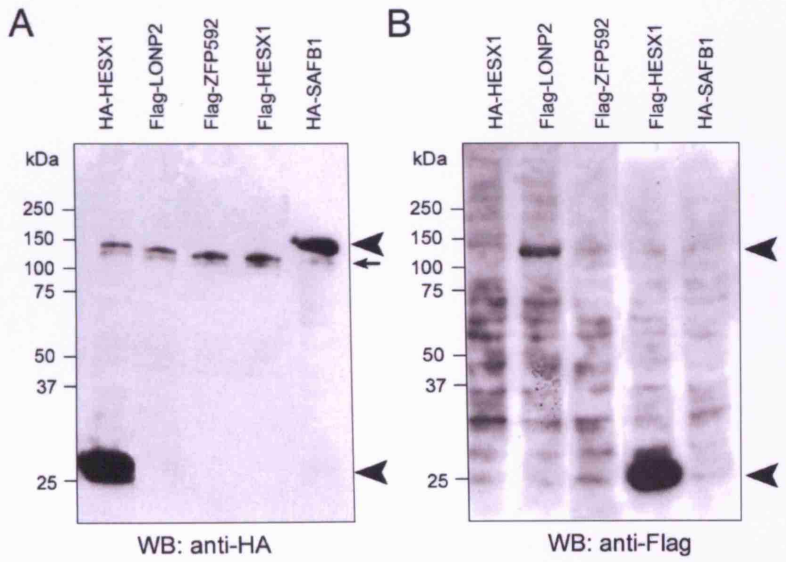

Figure 3.6 – Analysis of the nuclear extracts. 293T cells were transfected with various tagged proteins (indicated above each lane). Cells were lysed in 1 ml lysis buffer and spun at low speed. The nuclear fraction (pellet) was denatured by adding 50 µl Laemmli buffer, heating at 100°C for 3-5min and passing through a shredder. The maximum and equal amounts of samples were loaded. The Western blot analysis with anti-HA (A) and anti-Flag (B) antibodies shows strong bands, corresponding to HA-HESX1, HA-SAFB1, Flag-HESX1 and weak expression of Flag-LONP2 (arrowheads). However, Flag-ZFP592 was not detected. There is a non-specific band at ~150 kDa in A (arrow).

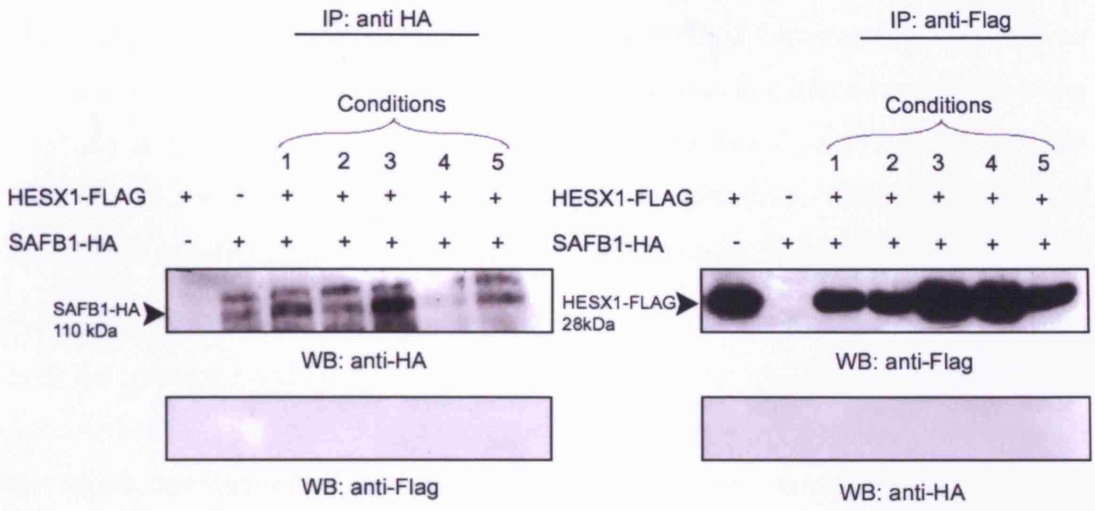

Figure 3.7 – Co-immunoprecipitation of HESX1 and SAFB1. Cells were transfected with plasmids carrying full-length *Flag–Hesx1* and/or full-length *Ha–Safb1* sequences (indicated by + or −) and immunoprecipitated with anti-Flag and anti-HA antibodies. Immunoprecipitates were blotted and detected with anti-HA or anti-Flag HRP-conjugated antibodies. Five different lysis buffers were used to extract the proteins from the nucleus (conditions 1-5). Note that condition 3 results in the extraction of a higher amount of HA-SAFB1; however, no co-immunoreactive bands were detected. The five conditions are described in Table 8.6.

3.2.4. Mammalian two-hybrid assay

The mammalian two-hybrid assay is an elegant method for detecting interactions between two proteins in a mammalian setting. This system essentially uses the same principle as the yeast two-hybrid in a mammalian cell line (Figure 3.8). Only when HESX1 and the interacting protein are bound to each other, VP16-AD is able to activate the reporter (usually firefly luciferase) and a signal is detected.

Activation of the luciferase reporter was not significantly higher when expressing both the interactor and HESX1 together, compared with HESX1 on its own (Figure 3.9). Although, sequences carrying both the full-length and truncated (covering only the region that was initially identified in the yeast screen) versions of the interactor proteins were used and the amount of DNA was varied, it was not possible to detect a statistically significant activation of luciferase activity (data not shown). The use of TLE1, a protein previously shown to interact with HESX1 (Dasen et al., 2001), resulted in a significant increase in luciferase activity when co-transfected with HESX1 (Figure 3.9). This positive control confirmed that the assay was valid.

Since the studies both in-vitro (GST pull-down and yeast) and in cells (co-localisation in cells and co-IP for DNMT1 and SRFBP1) showed binding between HESX1 and these proteins, it is possible that in this luciferase assay the conditions are not optimal for detecting these interactions. Alternatively, the in-vitro assay may be unable to replicate an in-vivo scenario where such an interaction may take place (see Chapter 6 for further discussion).

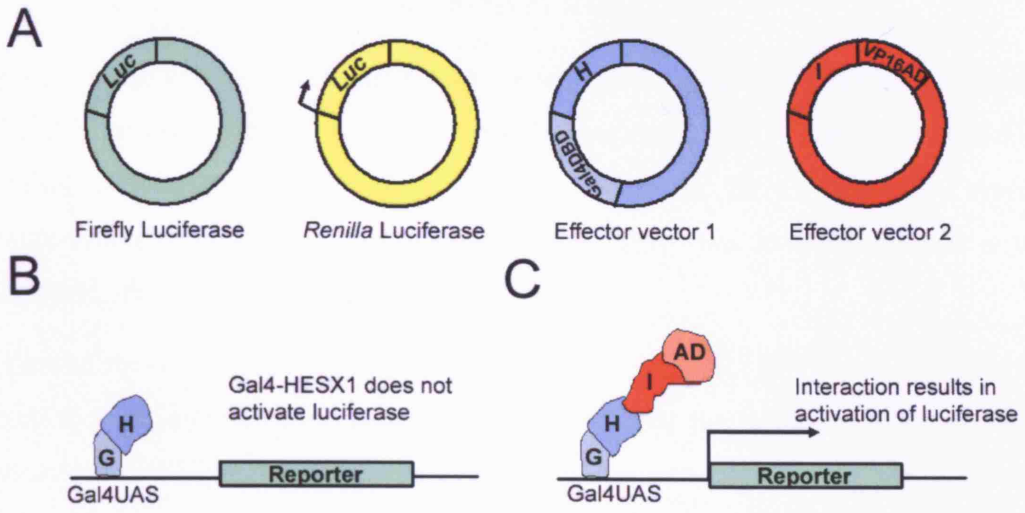

Figure 3.8 – Schematic representation of the mammalian two-hybrid assay. A) Cells are transfected with four different effector vectors in different combinations: (1) a plasmid carrying the firefly luciferase reporter gene that is not constitutively active; (2) a plasmid carrying the *Renilla* luciferase reporter gene for normalisation of the signal; (3) a plasmid carrying *Gal4DBD-Hesx1* sequence; (4) a plasmid carrying VP16AD-interactor sequences. B) Gal4DBD-HESX1 binds Gal4BS sequences. However, this does not activate the reporter and only a basal level of reporter expression is detected. C) Only when HESX1 (H) and the interactor (I) bind, there is an activation of reporter activity (arrow).

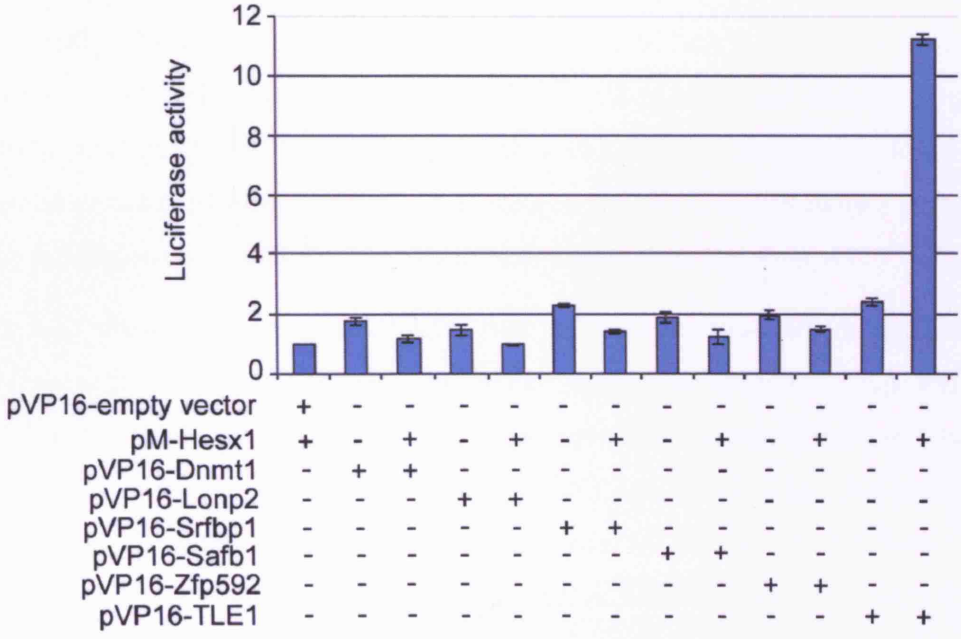

Figure 3.9 – Mammalian two-hybrid assay. CHO cells were transfected with pGL4/NOSV40 and pRL/SV40 plasmids and two effector vectors carrying *Hesx1* and/or the interactor sequences (indicated by + or −). pVP16-empty vector was the control. Co-expression of HESX1 with the interacting proteins did not result in a significant increase in reporter activity. TLE1 is a positive control that results in a 6 fold increase in reporter activity when co-expressed with HESX1.

3.2.5. Mammalian one-hybrid assay

Another application of the luciferase system is the one-hybrid assay (Figure 3.10). HESX1 has been shown to bind an artificial sequence, PIII (TAATYNRATTA) using EMSA (Dattani et al., 1998). The use of this sequence allows HESX1 to repress the transcription of a gene placed downstream of PIII, and luciferase offers a way of measuring this repressor activity.

Three of the interactors, namely DNMT1, SAFB1 and SRFBP1 have functions linking them to gene repression or silencing. DNMT1 keeps the repressed state of a gene by methylation of DNA. SAFB1 is involved in the repression of certain promoters, namely estrogen receptor alpha promoters. SRFBP1 has been shown to both enhance and inhibit the activity of serum response factor on various promoters. Finally, LONP2 shows homology to a family of proteases and might, therefore, be involved in repression through its proteolytic activity if indeed it has one. Thus, it is possible that the functionality of some or all of these interactions lies in cooperative regulation of HESX1 target genes. It was, therefore, postulated that the interaction between HESX1 and the interactor may repress reporter activity (either through PIII or Gal4-BS) by a higher factor, than HESX1 or the interactor alone.

It was found that incubating the cells 24 hrs after transfection was optimal for detecting a HESX1 dose-dependent repression (Figure 3.11). 10 ng of the plasmid carrying *Hesx1* sequences resulted in a ~50% reduction in reporter activity. This was the ideal amount of plasmid to use in subsequent one-hybrid assays, although, additionally 1 ng was used lest the repression caused by the interactors was higher than anticipated.

Figure 3.12 shows an experiment where two different amounts of plasmids carrying *Dnmt1* sequences (10 and 100 ng) and *Hesx1* sequences (1 and 10 ng) were used. HESX1 represses luciferase activity in a dose dependent manner (first three bars). As expected, DNMT1 has no effect on its own. HESX1 and DNMT1 together also have no significant effect on the level of repression mediated by HESX1. Additionally, the use of 10 times more DNMT1 with the same amount of HESX1 caused an opposite effect and slightly "de-repressed" luciferase activity.

The same was repeated with the other four interactors with similar findings. Altering the amount of DNA and using truncated instead of full-length proteins (expressing only the region that showed interaction in the yeast two-hybrid screen), did not cause significant deviation from the results discussed above (data not shown).

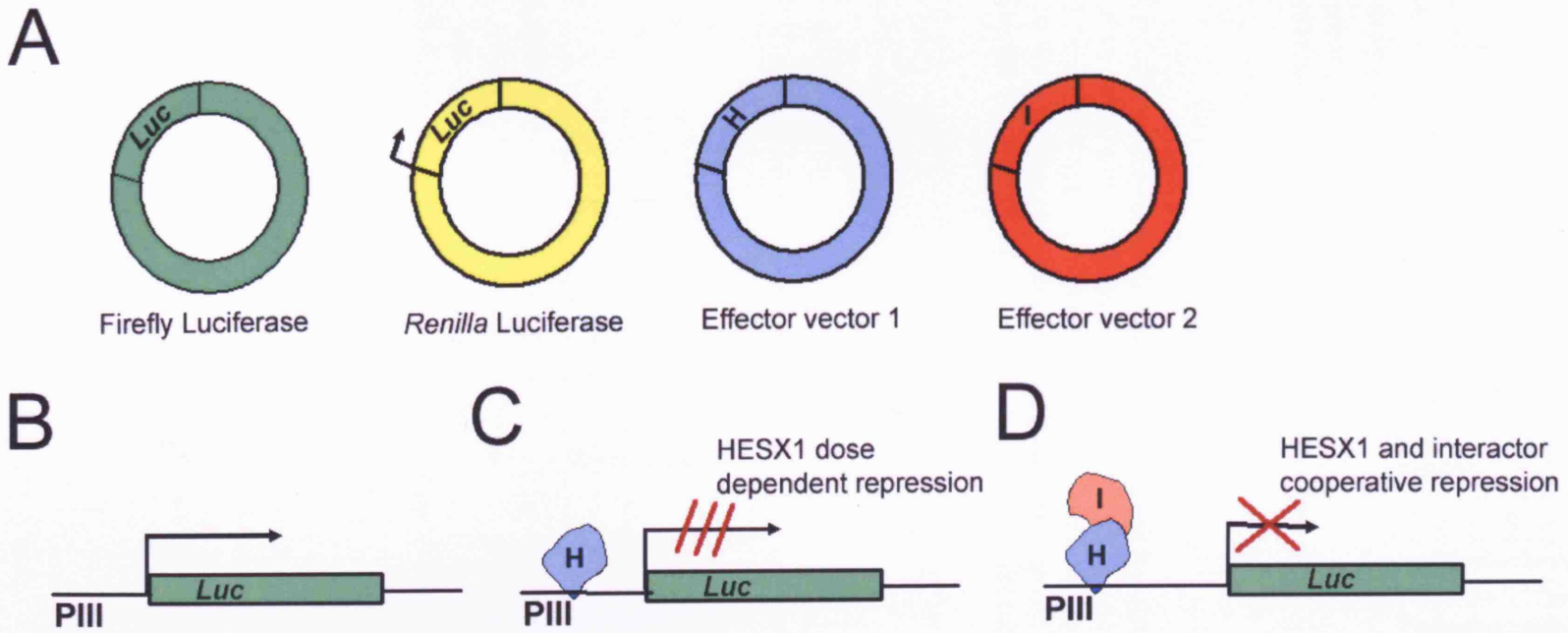

Figure 3.10 – Schematic representation of the mammalian one-hybrid assay. A) Cells are transfected with four different effector vectors in different combinations: (1) a plasmid carrying firefly luciferase reporter gene that is constitutively active under the SV40 promoter; (2) a plasmid carrying the *Renilla* luciferase reporter gene for normalisation of the signal; (3) a plasmid carrying *Hesx1* sequences; (4) a plasmid carrying interactor protein sequences. B) Luciferase is active and is preceded by either Gal4BS or the PIII sequences. C) HESX1 (H) binds the PIII sequence. This results in a HESX1-mediated repression of reporter activity. D) When HESX1 (H) binds to the interactor (I), there is the possibility of a second level of repression, resulting from the cooperative repressing activity, mediated by the interaction.

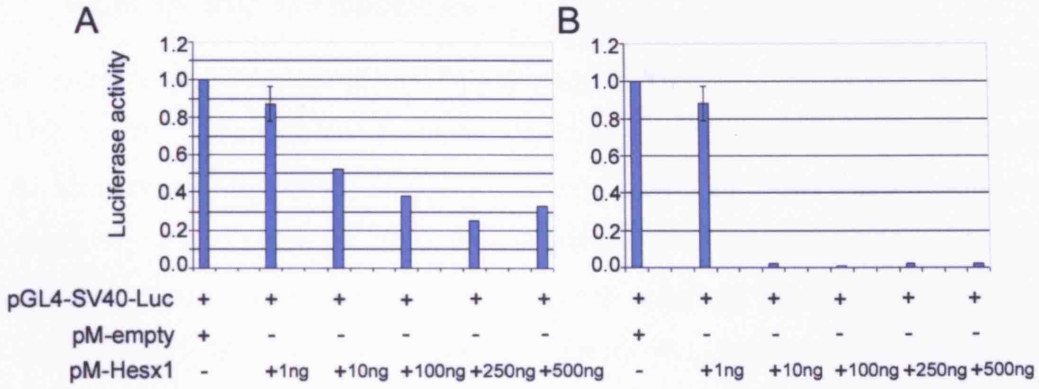

Figure 3.11 – Dose-dependent repression, mediated by HESX1. Cells were transfected with pGL4/SV40 and pRL/SV40 and varying amounts of plasmids carrying *Hesx1* sequences (indicated from 1-500 ng). Cells were lysed 24 hrs (A) or 48 hrs (B) after transfection. Lysis of cells 24 hrs after transfection is optimal for detection of a dose-dependent repression mediated by HESX1 (A). 10 ng of plasmid resulted in ~50% reduction in luciferase activity.

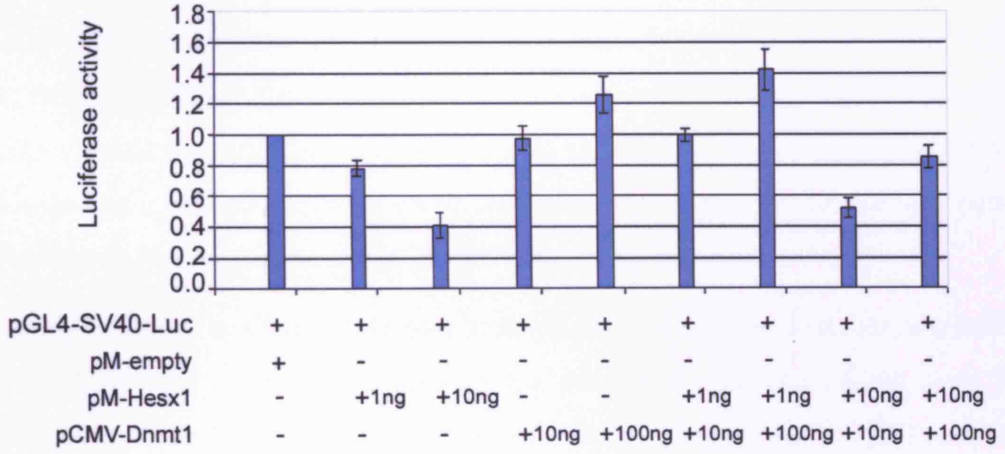

Figure 3.12 – Mammalian one-hybrid assay. CHO cells were transfected with pGL4/SV40 and pRL/SV40 and varying amounts of the plasmid carrying *Hesx1* sequences (indicated from 1-10 ng) and *Dnmt1* sequences (indicated from 10-100 ng). Co-transfection of cells with HESX1 and DNMT1 did not result in an increase in the HESX1-mediated repression of reporter activity.

3.2.6. In-situ hybridisation

Hesx1 shows a very dynamic pattern of expression during mouse development (Chapter 1). This pattern is also reflected by its role in forebrain and pituitary development, since in its absence the structures whose primordia expressed *Hesx1* during embryonic development, are missing or abnormal in embryos and neonates. In mice, *Hesx1* transcripts are predominantly expressed in anterior forebrain tissues at 8.5 dpc (Figure 3.13A,B). At 12.5 dpc, *Hesx1* is expressed in the RP in a gradient of high dorsal to low ventral (Figure 3.13M). We analysed the expression of the interactors with respect to *Hesx1* at 8.5-9.0 dpc using whole mount in-situ hybridisation and at 12.5 dpc in the Rathke's pouch using section in-situ hybridisation.

Whole mount in-situ hybridisation showed that the transcripts for all of the five interactors were present throughout the embryo at 8.5 dpc (Figure 3.13A-L). *Srfbp1* and *Zfp592* appeared to be expressed at lower levels compared to *Dnmt1*, *Lonp2* and *Safb1*, which were highly and ubiquitously expressed in the embryo at these stages (Figure 3.13).

At 12.5 dpc, *Dnmt1* transcripts were seen in various structures in the head including the lens, neural retina and the cortex (data not shown), and were also predominant in the Rathke's pouch in a high dorsal to low ventral pattern similar to *Hesx1* (Figure 3.13N). The expression of *Safb1* also followed the same high dorsal to low ventral pattern of expression as *Hesx1* and *Dnmt1*, in the RP (Figure 3.13O).

Similarly, RT-PCR analysis of embryo heads at 8.5 and 12.5 dpc, further confirmed that the transcripts for all five interactors were present in the head along with *Hesx1*. Although, quantitative PCR was not carried out, it appeared that *Srfbp1* and *Zfp592* transcripts were present in lower amounts compared to *Dnmt1*, *Lonp2* and *Safb1* (Figure 3.14).

While, transcripts for all five interactors were present in a wide range of tissues during mouse embryonic development (as it can be expected given their broad cellular functions), what is shown here is that at 8.5 dpc, they were co-expressed with *Hesx1* in the most anterior part of forebrain including the primordia of optic and telencephalic vesicles. By 12.5 dpc, *Dnmt1* and *Safb1* followed an expression pattern in the RP pouch, which was strikingly similar to *Hesx1* at this stage, whilst the transcripts for *Lonp2*, *Srfbp1* and *Zfp592* started to decrease considerably by 12.5 dpc.

Hesx1
Dnmt1
Safb1
Srfbp1
Zfp592
Lonp2
A
C
E
G
I
K
B
D
F
H
J
L
M
N
O
8.5 dpc
12.5 dpc
Lateral
Rostral
Sagittal

Figure 3.13 – Expression analysis of the interactors in wild-type mouse embryos using in-situ hybridisation. (A-B) Whole mount in-situ analysis of *Hesx1* transcripts in the forebrain at 8.5 dpc (A lateral view, B rostral view). (C-L) Whole mount in-situ analysis of the interactors (indicated on top of the panel), demonstrating that they are co-expressed with *Hesx1* in the forebrain. Top row shows the lateral view with anterior to the left, bottom row shows the rostral view. M) Expression of *Hesx1* transcripts in the Rathke's pouch of the wild-type embryo at 12.5 dpc. *Dnmt1* (N) and *Safb1* (O) transcripts are expressed in a similar pattern to *Hesx1* in the RP (high dorsal to low ventral).

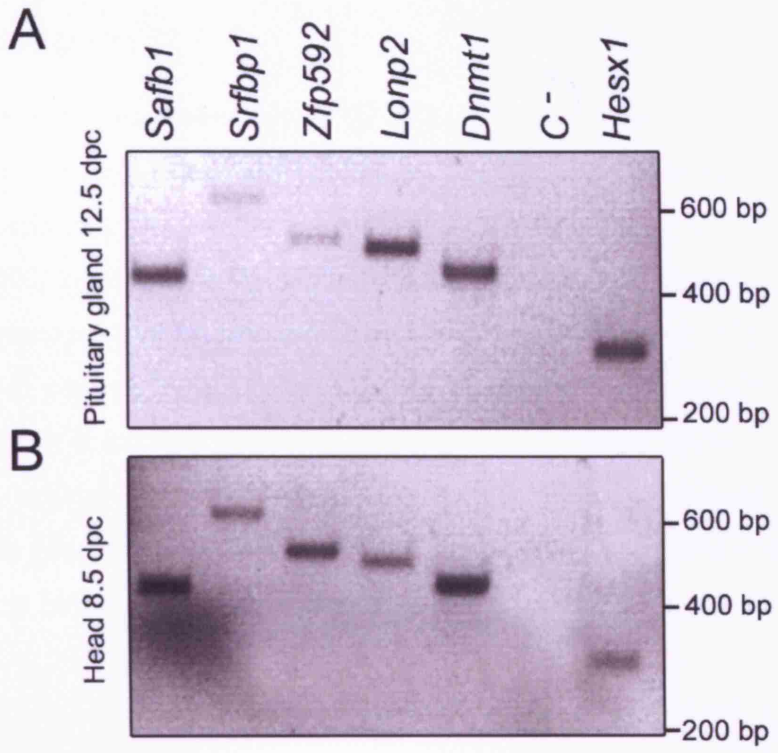

Figure 3.14 – Expression analysis of *Hesx1* and the interactors in wild-type mouse embryos using RT-PCR. RT-PCR from RNA samples purified from mouse pituitary tissues at 12.5 dpc (A) and mouse heads at 8.5 dpc (B) for *Hesx1* and the five interactors (indicated on top of the panel). Amplification of the RNA samples prior to retrotranscription (c-) demonstrates the absence of DNA contamination. The RT-PCR experiment was carried out by M. Signore.

3.2.7. DNMT1

Of the five identified interactors of HESX1, DNMT1 is possibly the most widely studied. It is apparent from these studies that DNMT1 has an important role in gene regulation and in particular gene silencing through, its CpG methylation activity (Bestor, 2000; Meehan, 2003). DNMT1 does not have any specific targets, it has been contemplated that its role is in keeping the repressed state of genes that have already been marked by other DNA methyltransferases such as DNMT3A and B and/or by other transcription factors. We hypothesised that HESX1 partly exerts its repressing activity through its interaction with DNMT1, thereby, altering the methylation patterns of its target genes. We, therefore, concentrated our studies on DNMT1 and further defined this interaction.

3.2.7.1. Mapping the DNMT1 interacting region

3.2.7.1.1. GST pull-down assay

The GST pull-down assay carried out with various fragments of HESX1 (Figure 3.1), indicated that the whole tertiary structure of HESX1 is involved in its interaction with DNMT1. Since DNMT1 is a much larger protein, with various functional domains, it is possible that its interaction with HESX1 is specific to particular domain(s). In order to understand this further, a series of GST-DNMT1 fusion proteins, each spanning different functional domain of the DNMT1 protein (Figure 3.15A), were used in GST-pull-down assays along with ^{35}S-Met-labelled HESX1 full-length protein.

HESX1 showed a strong affinity to the first 748 amino acids of DNMT1. This region of the protein contains several functional domains, including the PCNA binding domain, the targeting sequence and the cysteine rich region. The region adjacent to this, which includes the two bromo-homology (BH) domains showed no interaction with HESX1, although when both BH1 and BH2 were present, a very weak interaction was observed. Finally, the region containing the C-terminal catalytic domain of DNMT1 also showed binding to HESX1 (Figure 3.15C).

Overall, it is evident that a portion of the N-terminal region of the protein encompassing the first 748 amino acids, as well as the catalytic C-terminal tail of DNMT1 are involved with its interaction with HESX1.

A further confirmation of the direct interaction between HESX1 and DNMT1 was demonstrated using mouse ES cells. Untransfected mouse ES cells express both *Hesx1* and *Dnmt1*. GST-HESX1 (aa 1-185) bound on GST beads, were used in a GST pull-down assay with protein extracts from untransfected ES cells. This experiment showed that endogenous DNMT1 was able to bind to GST-HESX1 (aa 1-185), but not to GST alone (Figure 3.15D).

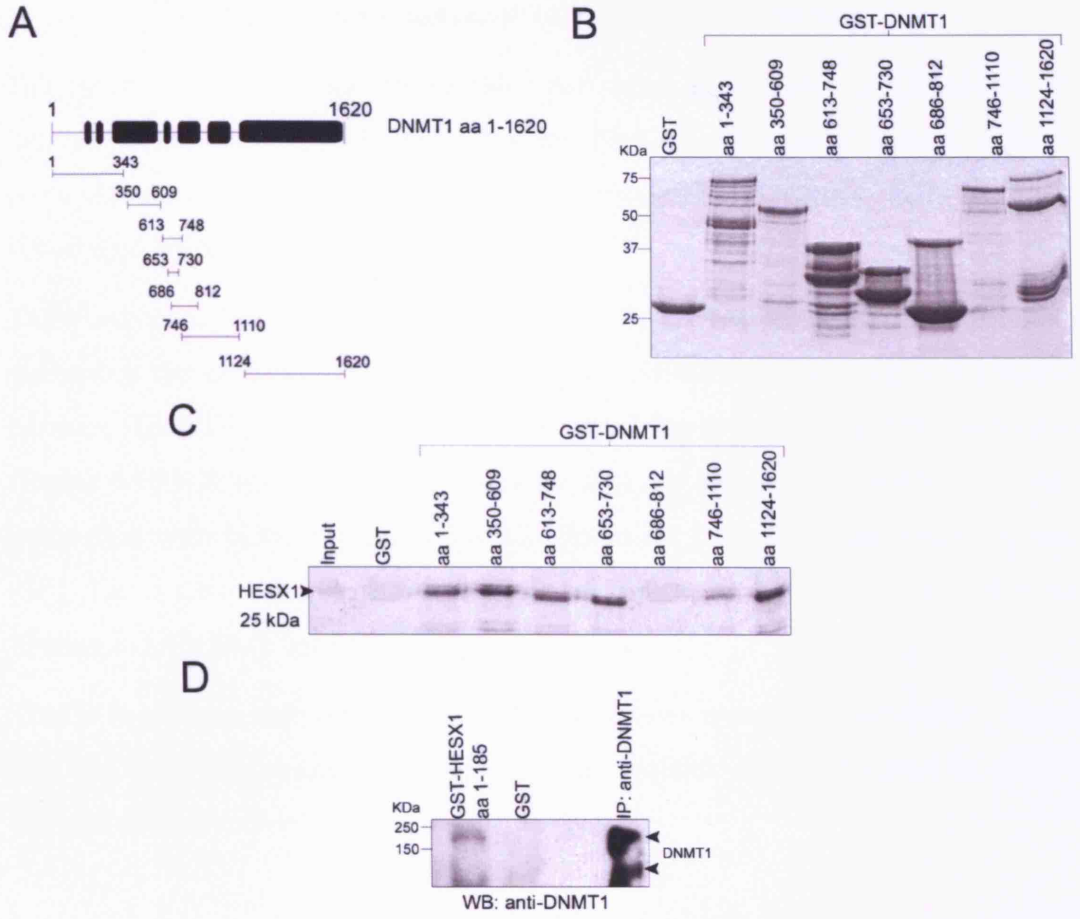

Figure 3.15 – Mapping the interacting regions of DNMT1 with HESX1 by GST pull-down experiments. A) Schematic representation of DNMT1 fragments expressed as GST fusion proteins. B) Representative Coomassie stain of the GST–DNMT1 fusion proteins used in C. C) GST pull-down experiments. Strong interaction is observed between HESX1 and DNMT1 fragments containing the first 748 amino acids (aa 1–343, aa 350–609, aa 613–7480 and aa 653–730) and the catalytic domain (aa 1124–1620). No binding was detected with a DNMT1 fragment containing the BAH1 domain (aa 686–812). DNMT1 fragment including BAH1 and BAH2 domains (aa 746–1110) exhibited weak binding. D) Approximately 1 mg of protein extracts obtained from untransfected ES cells was incubated with either an anti-DNMT1 antibody (IP: anti-DNMT1), GST or GST–HESX1 (aa 1–185), and bound proteins analysed by Western blot, using an anti-DNMT1 antibody. Only GST–HESX1 (aa 1–185), but not GST, interacts with endogenous DNMT1 (arrowheads). Molecular weight markers are indicated on the left. As input, 1/10 of the total amount of ^{35}S-Met-labelled protein was used in panel C (arrowhead). Experiments in ES cells (D) were carried out by Dr. Martinez-Barbera.

3.2.7.1.2. Co-immunoprecipitation experiments

The results obtained in the above GST pull-down assays were confirmed by co-immunoprecipitation experiments. Several Flag-tagged deleted mutant DNMT1 proteins were constructed (Figure 3.16A) and used to transfect 293T cells along with HA-tagged HESX1.

These experiments confirmed that a portion of the N-terminal and the C-terminal containing the catalytic domain, interact with HESX1. No binding was observed between HESX1 and a DNMT1 fragment containing only the first 158 amino acids (Figure 3.16B). Expanding this, to cover the first 296 amino acids, resulted in a weak interaction with HESX1 (Figure 3.16C). Fragment containing the target sequence (TS), the cysteine rich and the catalytic domains (aa 296-1620) showed strong binding to HESX1 (Figure 3.16F).

This is in concert with the previous GST pull-down assays and altogether, suggest that the three dimensional structure of both proteins come into play in order to achieve this interaction.

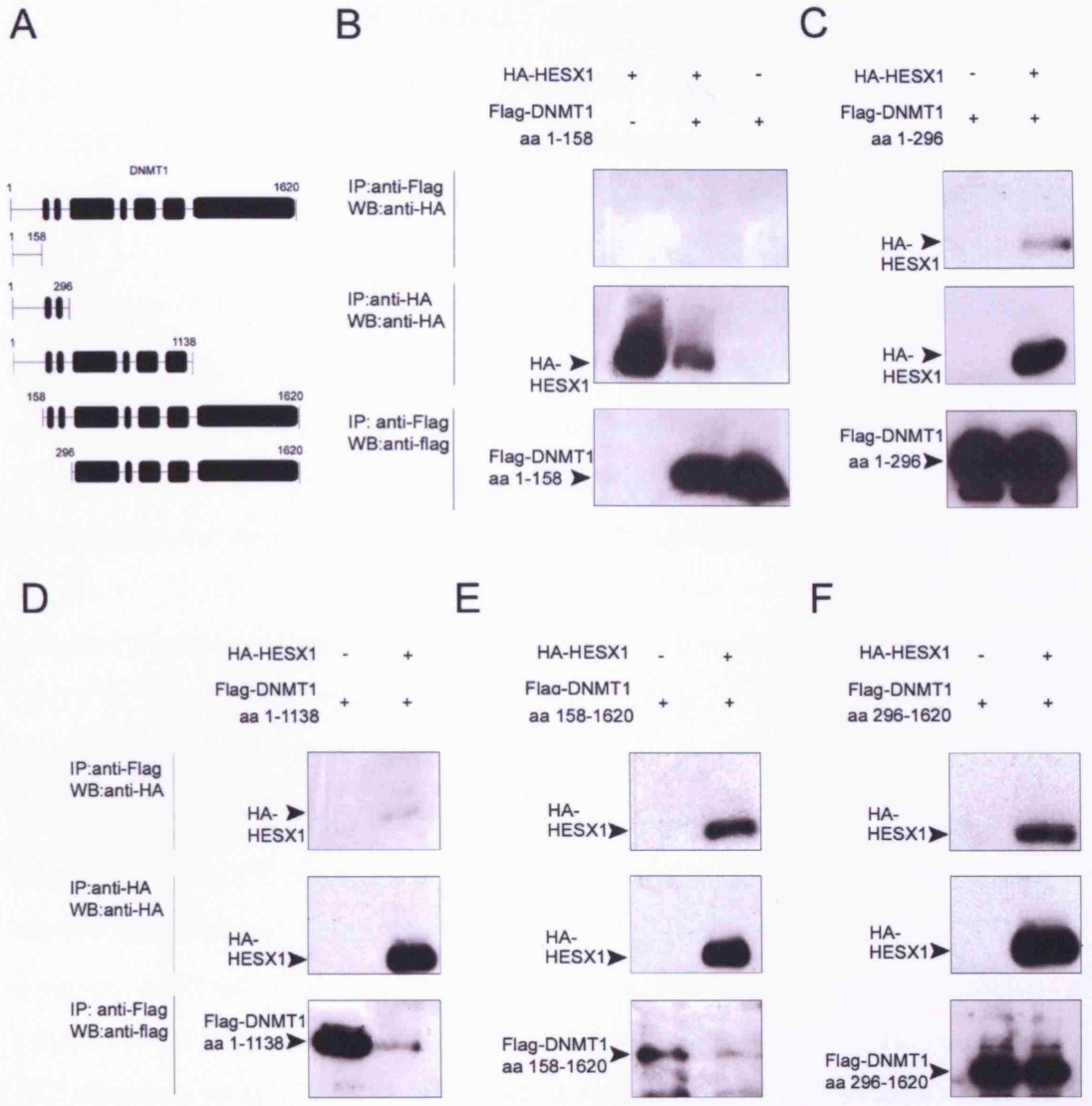

Figure 3.16 - Mapping the interacting regions of DNMT1 with HESX1 by co-immunoprecipitation experiments. A) Schematic representation of full-length DNMT1 (aa 1–1620) and fragments used in these experiments. Cells were transfected with full-length HA–HESX1 and/or several Flag–DNMT1 deletion proteins, as indicated (+ or −) and immunoprecipitated with anti-Flag or anti-HA antibodies. The presence of HESX1–DNMT1 complexes was analysed by Western blotting the anti-Flag immunoprecipitates with an HRP-conjugated anti-HA antibody. The approximate sizes of the DNMT1 fragments in kDa are: 18 (aa 1-158), 33 (aa 1-296), 125 (aa 1-1138), 160 (aa 158-1620), 145 (aa 296-1620). Specific immunoreactive bands of correct sizes are indicated with arrowheads. Fragments containing part of the N-terminus and the catalytic domain of DNMT1 (aa 158–1620 and aa 296–1620) strongly interact with HA–HESX1. Immunoprecipitation with anti-HA antibody was used to verify the presence of HA–HESX1 in the lysates.

3.2.7.2. *Dnmt1*$^{+/-}$;*Hesx1*$^{+/-}$ compound heterozygous mice

It has been reported that *Dnmt1* is crucial for early embryonic development as disruption of the *Dnmt1* locus in mouse results in embryonic lethality (Li et al., 1992). Heterozygous mice are normal, whilst homozygous embryos do not develop beyond 9.5 dpc. The interaction between HESX1 and DNMT1 in-vivo was explored by analysing *Dnmt1*$^{+/-}$;*Hesx1*$^{+/-}$ compound heterozygous embryos and adult mice.

Table 3.1 demonstrates the results obtained from crosses between *Dnmt1*$^{+/-}$;*Hesx1*$^{+/-}$ and C57BL6/J wild-type mice. This data illustrates that the number of pups obtained at weaning for each genotype followed the expected Mendelian ratios. However, interestingly, we detected a phenotype in ~17% of both *Dnmt1*$^{+/-}$;*Hesx1*$^{+/-}$ (n=59) and *Hesx1*$^{+/-}$ (n=36) genotypes (Table 3.2). This phenotype resembled the unilateral anophthalmia/severe microphthalmia that is associated with a number of *Hesx1*$^{I26T/I26T}$ mice (see chapter 4). One *Dnmt1*$^{+/-}$;*Hesx1*$^{+/-}$ animal was small and died by weaning stages.

We took the study further to embryonic stages in order to identify the onset of this phenotype. From 122 embryos analysed at 12.5-18.5 dpc, numbers of each genotype matched the expected Mendelian ratio (Table 3.3). Of the twenty *Dnmt1*$^{+/-}$;*Hesx1*$^{+/-}$ embryos analysed (Table 3.4), five showed eye defects (microphthalmia or anophthalmia) (Figure 3.17B) and one was developmentally delayed, resembling a 10.5 dpc embryo at 12.5 dpc. However, it was surprising to also find six *Hesx1*$^{+/-}$ embryos (n=18) with similar eye defects (microphthalmia or anophthalmia) (Figure 3.17C).

At 10.5 dpc, some embryos displayed forebrain abnormalities affecting the telencephalic vesicles, which were smaller than in the wild-type (Figure 3.17E, F). Surprisingly, this phenotype was seen in a similar proportion of both *Dnmt1*$^{+/-}$;*Hesx1*$^{+/-}$ and *Dnmt1*$^{+/-}$ embryos. Furthermore, at this stage, one *Dnmt1*$^{+/-}$;*Hesx1*$^{+/-}$ and one *Dnmt1*$^{+/-}$ embryo displayed a completely truncated forebrain (Figure 3.17G). This phenotype was more severe than the anterior forebrain truncations associated with *Hesx1*$^{-/-}$ mutants, at a similar stage.

In summary, it seems that this system is not suitable for studying the interaction between HESX1 and DNMT1. Contrary to the published data, it was found here that a small number of *Dnmt1*$^{+/-}$ embryos display abnormal telencephalic vesicles. We

also find a higher percentage of *Hesx1*$^{+/-}$ embryos and mice with eye defects, than previously reported. These discrepancies may be due to the mixed genetic background, created by crossing these two lines.

Table 3.1 - Genotype of mice obtained from *Dnmt1*$^{+/-}$;*Hesx1*$^{+/-}$ X C57BL6/J crosses.

Genotype	No. of mice obtained			Expected
	♀	♂	Total (%)	
WT	31	29	60 (~22)	68.5
Hesx1$^{-/-}$	33	35	68 (~25)	68.5
Dnmt1$^{-/-}$	31	30	61 (~25)	68.5
Dnmt1$^{-/-}$; *Hesx1*$^{-/-}$	37	48	85 (~31)	68.5
Total	132	142	274	274

Table 3.2 - Frequency of observable phenotypes associated with *Dnmt1*$^{+/-}$;*Hesx1*$^{+/-}$ and *Hesx1*$^{+/-}$ mice.

Phenotype	Frequency			
	Female ♀		Male ♂	
	Dnmt1$^{-/-}$; *Hesx1*$^{-/-}$	*Hesx1*$^{-/-}$	*Dnmt1*$^{-/-}$; *Hesx1*$^{-/-}$	*Hesx1*$^{-/-}$
Normal	29	14	30	22
Eye defect	7	4	2	2
Small with eye defect	1	0	0	0
Total	37	18	32	24

Table 3.3 - Genotype of embryos obtained from *Dnmt1*$^{+/-}$;*Hesx1*$^{+/-}$ X C57BL6/J crosses.

Stage	Genotype			
	WT	*Hesx1*$^{-/-}$	*Dnmt1*$^{-/-}$	*Dnmt1*$^{-/-}$; *Hesx1*$^{-/-}$
10.5 dpc	2	3	3	6
12.5 dpc	13	16	20	17
14.5 dpc	6	4	2	3
15.5 dpc	2	1	2	4
16.5 dpc	0	3	3	0
18.5 dpc	3	3	1	5
Total	26 (~21%)	30 (~25%)	31(~25%)	35 (~29%)

Table 3.4 - Frequency of observable phenotypes associated with *Dnmt1*$^{+/-}$;*Hesx1*$^{+/-}$ and *Hesx1*$^{+/-}$ embryos at stages 12.5-18.5 dpc.

Phenotype	Genotype	
	Dnmt1$^{-/-}$; *Hesx1*$^{-/-}$	*Hesx1*$^{-/-}$
Normal	14	12
Developmentally delayed	1	0
Right eye microphthalmia	1	2
Left eye microphthalmia	3	1
Both eye microphthalmia	0	3
Right eye anophthalmia	1	0
Total	20	18

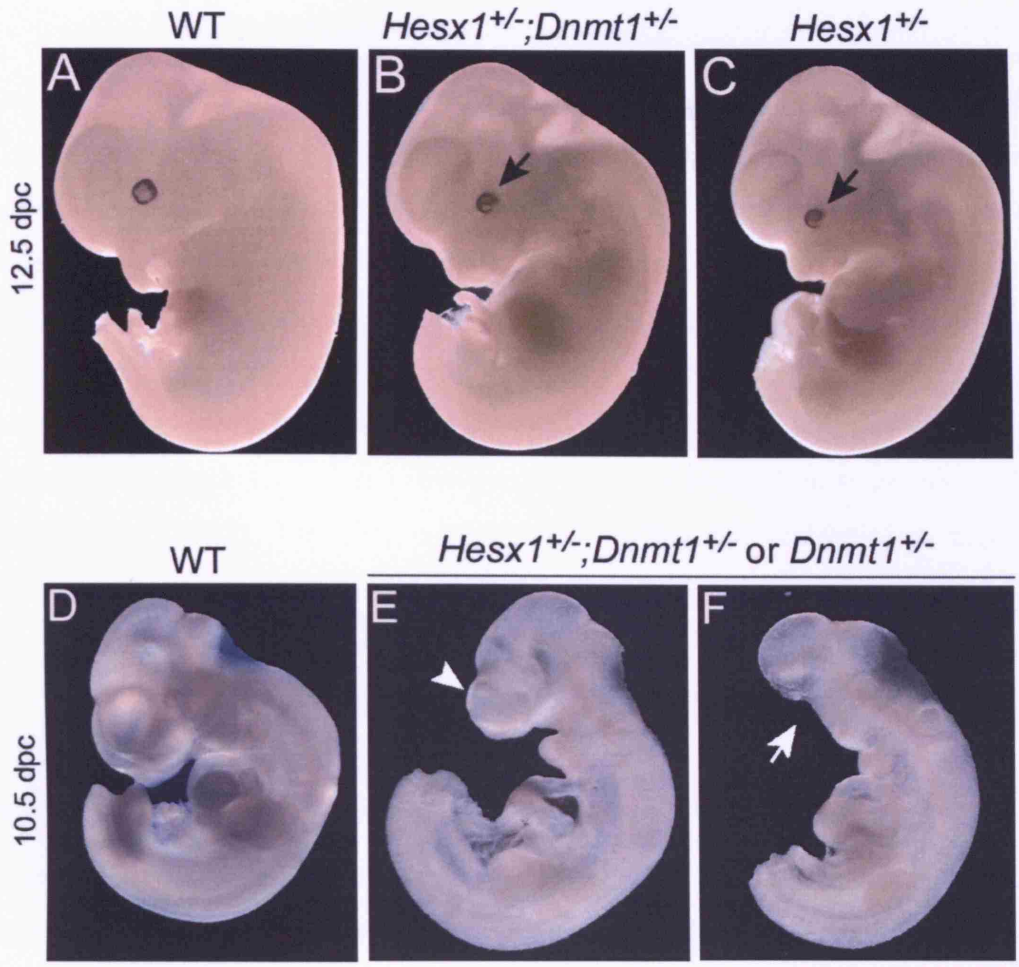

Figure 3.17 – Phenotypes associated with embryos from *Dnmt1*$^{+/-}$;*Hesx1*$^{+/-}$ X C57BL6/J crosses. A) Wild-type embryo at 12.5 dpc, with anterior to the left. Examples of eye defects (black arrows) associated with *Dnmt1*$^{+/-}$;*Hesx1*$^{+/-}$ and *Hesx1*$^{+/-}$ embryos are shown in panels B and C respectively. D) Wild-type embryo at 10.5 dpc, with anterior to the left. (E-F) Examples of the telencephalic defects (white arrowhead) seen in some *Dnmt1*$^{+/-}$;*Hesx1*$^{+/-}$ and *Dnmt1*$^{+/-}$ embryos. Note the severe forebrain truncations seen in a small number of these embryos (white arrow in F).

3.2.7.3. Diet experiments

Numerous studies have shown that in humans, prenatal and early postnatal diets affect susceptibility to disease in the newborn (Burdge et al., 2007). For example, insufficient intake of folic acid in pregnant women increases the risk of neural tube defects in the unborn child. This has also been shown in the mouse, although the effect seems to be strain dependent. Hence, a combination of genetic and environmental factors probably contributes to this phenomenon. The exact mechanism is still under investigation. A clue came from the study of a strain of agouti mice, which have a retrotransposon element inserted in their *agouti* locus (Wolff et al., 1998). The mice carrying this allele show variability in their coat colour, adiposity, glucose tolerance and tumour susceptibility. It has been shown that this variability is a direct result of the variable CpG methylation pattern of the transposable element in this locus. It was also illustrated that the use of a diet, rich in methyl donors, in pregnant mice affects this methylation pattern in the offspring and hence can be visualised by coat colour (Cooney et al., 2002).

Hesx1$^{-/-}$ embryos show variable degrees of truncation of anterior forebrain, affecting structures such as the telencephalic vesicles, the eyes, and the pituitary. This phenotype is caused by a posterior transformation of anterior forebrain (Andoniadou et al., 2007) as a result of activation of genes, which are normally repressed by HESX1. If indeed HESX1 cooperates with DNMT1 in repressing these loci, it is not inconceivable that by supplementing *Hesx1*$^{-/-}$ embryos with methyl donors, using a methyl rich diet in the mother, these targets might be hypermethylated. As a result, part or most of the mutant phenotype may be rescued.

Hesx1$^{-/-}$ dams were put on either a methyl supplement diet or a control diet (Harlan, Wolff et al., 1998) for three weeks prior to mating and were kept on the diets until the embryos were harvested. *Hesx1*$^{-/-}$ males were fed the normal diet used in the animal facility. As can be seen in Table 3.5, the occurrence of the mild and severe phenotypes associated with *Hesx1*$^{-/-}$ mutants was not significantly different between the embryos from the two different diets (n=47).

The same was repeated in *Hesx1*$^{R160C/R160C}$ embryos. These embryos display a phenotype identical to *Hesx1*$^{-/-}$ (Chapter 5), although the HESX1 protein is present

(in a mutant form). Similarly, there was no statistically significant difference between the two groups of embryos of this genotype (n=58, Table 3.6).

These data suggest that the use of a methyl-rich diet in *Hesx1*$^{+/-}$ and *Hesx1*$^{R160C/+}$ mice does not affect the phenotype seen in their homozygous offspring.

Table 3.5 – Phenotypes associated with *Hesx1*$^{-/-}$ embryos, obtained from females put on a methyl-rich diet compared to controls.

Phenotype	Control Diet	Methyl Supplement Diet
Normal	6 (30%)	13 (48%)
Microphthalmia	6 (30%)	5 (19%)
Microphthalmia and mild forebrain defects	1 (5%)	2 (7.5%)
Anophthalmia and severe forebrain defects	7 (35%)	5 (19%)
Exencephaly	0	2 (7.5%)
Total	20	27

Table 3.6 - Phenotypes associated with *Hesx1*$^{R160C/R160C}$ embryos, obtained from females put on a methyl-rich diet compared to controls.

Phenotype	Control Diet	Methyl Supplement Diet
Normal	16 (55%)	18 (62%)
Microphthalmia	6 (21%)	3 (10%)
Anophthalmia	4 (14%)	2 (7%)
Microphthalmia and mild forebrain defects	2 (7%)	0
Anophthalmia and severe forebrain defects	1 (3.5%)	6 (21%)
Exencephaly	0	0
Total	29	29

3.2.8. SOD and interruption of HESX1 interactions

As discussed in section 1.5, hypopituitarism is a highly heterogeneous condition that can be associated with SOD depending on the presence or absence of defects in forebrain structures, such as midline telencephalic commissures and corpus callosum, and optic nerves (Kelberman and Dattani, 2007a; Kelberman and Dattani, 2007b; Dattani et al., 2000). Familial cases of SOD and hypopituitarism have shed light on the genetic causes of this condition. A number of mutations in different genes have been shown to cause SOD and hypopituitarism including *HESX1*, *POU1F1* and *PROP1*, among others.

To date, 13 mutations in *HESX1* have been associated with SOD and/or hypopituitarism in humans (Dattani et al., 1998; Thomas et al., 2001; Brickman et al., 2001; Carvalho et al., 2003; Cohen et al., 2003; Tajima et al., 2003; Dattani, 2004; Sobrier et al., 2005; 2006; Coya et al., 2007; McNay et al., 2007). The resulting phenotypes are variable; one reason for such variability could be the involvement of other genes, which indirectly affect the phenotype in those patients who carry *HESX1* mutations. Potential candidates for such modifier genes are the interactors of HESX1.

In order to increase our understanding of these interactions, as well as to investigate their possible roles in the pathogenesis of SOD and hypopituitarism, their binding to seven human HESX1 mutant proteins was analysed in yeast. To achieve this, yeast strain PJ69-4A was transformed with each of these interactors on their own and additionally co-transformed with the following: (1) GAL4-DBD; (2) mouse HESX1; (3) human HESX1; (4) human HESX1-I26T; (5) human HESX1-R160C; (6) human HESX1-E149K; (7) human HESX1-Q6H; (8) human HESX1-T181A; (9) human HESX1-V129I; (10) human HESX1-306/307insAG. The strength of interaction was assessed by the rate and colour (blue) of the yeast growth. The results are displayed in Figure 3.18 and summarised in Table 3.7.

The interactions were initially identified using mouse *Hesx1* sequences, it was confirmed here that these proteins also interact with human *HESX1*. The strength of interaction was comparable between mouse and human sequences for four of the interactors, namely DNMT1, LONP2, ZFP592 and SAFB1 (Figure 3.18). However, SRFBP1 interaction with human HESX1 was weaker compared with mouse HESX1, as suggested by the poor growth after 48 hrs, although the interaction was present after 96 hrs (Figure 3.18). As Figure 3.18 demonstrates, certain interactions were disrupted by some of the mutations.

T181A was found in a heterozygous patient with isolated growth hormone deficiency (Thomas et al., 2001); this mutation did not cause disruption to any of the five interactions.

V129I was found in a patient with hypogonadotrophic hypogonadism. It is suspected to be a polymorphism as it does not have any effect in functional assays compared with the wild-type (Dattani M.T., unpublished data). Similarly in this study, this mutation did not affect any of the interactions, possibly further supporting it to be a polymorphism.

E149K was found in a heterozygous patient with isolated growth hormone deficiency (McNay et al., 2007). The interactions with ZFP592 and SRFBP1 were reduced but not completely lost.

Q6H was observed in a heterozygous patient with multiple hormone deficiency (Thomas et al., 2001) and it was found that the interactions with SRFBP1, ZFP592 and SAFB1 were reduced but not completely lost.

I26T was identified in a homozygous patient with evolving panhypopituitarism (Carvalho et al., 2003). This mutant protein failed to interact with SRFBP1 and the interaction with DNMT1 was reduced.

R160C is a mutation that was observed in two homozygous patients with SOD and panhypopituitarism (Dattani et al., 1998). The interaction of this mutant protein with SRFBP1 and LONP2 were lost and its interaction with DNMT1 was reduced.

306/307insAG is a frameshift mutation resulting in a truncated protein, lacking the homeobox. The heterozygous patient displays panhypopituitarism, as well as optic nerve defects (Tajima et al., 2003). The resulting protein failed to interact with LONP2 and SAFB1. Its interactions with DNMT1 and ZFP592 were very weak. However, strikingly, its interaction with SRFBP1 remained as strong.

In summary, it appears that mutations in human *HESX1* sequences cause disruptions in protein-protein interactions. This is possibly one of the reasons underlying the variable nature of phenotypes seen in human patients. For example, the interaction with LONP2 is lost with the two mutant HESX1 proteins (R160C and 306/307insAG), which cause the more severe clinical features in humans. Additionally, the disruption of more protein interactions appears to be associated with more severe phenotypes in humans.

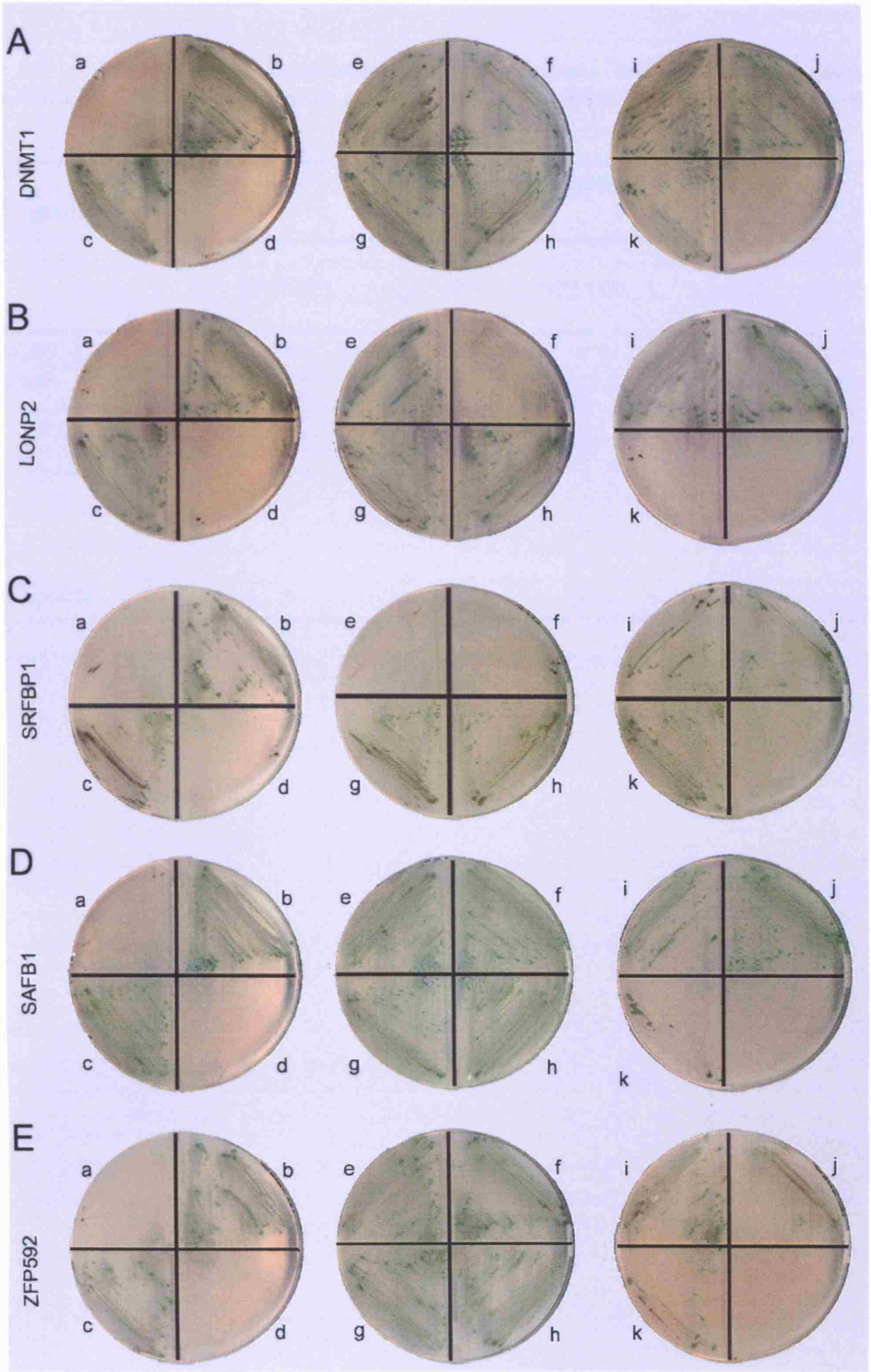

Figure 3.18 – Interactions with HESX1 mutants in yeast. (A-E) Yeast PJ69-4A was transformed with pVP16-Interactor plus the following: (a) No other plasmid (i.e. PJ69-4A); (b) mouse *Hesx1* full-length sequences; (c) human *HESX1* full-length sequences; (d) *Gal4DBD* sequences; (e) human *HESX1-I26T*; (f) human *HESX1-R160C*; (g) human *HESX1-V129I*; (h) human *HESX1-T181A*; (i) human *HESX1-Q6H*; (j) human *HESX1-E149K*; (k) human *HESX1-306/307insAG*. The name of the interactor is indicated on the left of each panel. Interaction is displayed by the blue/green growth of yeast in each corresponding section.

Table 3.7 – Summary of protein-protein interactions between human mutations associated with SOD or hypopituitarism and five known HESX1-interacting proteins.

HESX1 protein	Interactor				
	DNMT1	LONP2	SRFBP1	SAFB1	ZFP592
WT mouse	+++	+++	+++	+++	+++
WT human	+++	+++	++	+++	+++
R160C	+	-	-	+++	++
I26T	+++	+++	-	+++	+++
E149K	+++	+++	+	+++	+
Q6H	+++	+++	+	++	++
V129T	+++	+++	+++	+++	+++
T181A	+++	+++	+++	+++	+++
306/307insAG	+	-	++	-	+

4. ANALYSIS OF THE *Hesx1-I26T* MOUSE LINE

4.1. INTRODUCTION

Embryologists have always relied on and used a wide variety of animal systems ranging from flies and amphibians to birds and mammals in order to expand our knowledge on the big question of all: how does a single cell give rise to the complex organism? What these studies have shown is that although the development of an embryo varies from species to species, many of the key processes are conserved from flies to mammals. As it is difficult to use human embryos for such studies, this conservation in developmental mechanisms, presents a clear advantage for embryologists, geneticists and clinicians alike. Another advantage concerning the study of human embryo development comes from naturally occurring abnormalities. Up to 5% of human births are associated with some form of visible malformation. The study of these birth defects has long been used to broaden our knowledge of the mechanisms of human development and to shed light into the causes of the disease, which in turn aids the design of successful therapies.

In the past, most animal studies have relied on the use of teratogens in creating random mutants. Advances in both molecular biology and stem cell technology have allowed for the generation of targeted mutations in a desired locus within the genome. This technology has been increasingly used in the mouse, where it is now possible to use gene targeting and mouse embryonic stem cells to generate a wide range of mouse models carrying deletions, mutations or insertions in almost any gene. This is of course great for studying the fundamentals of embryonic development and patterning, but as mentioned before, animal models also play a key role in elucidating the mechanisms underlying human syndromes.

This technology has, therefore, allowed for the generation of a wide range of mouse models of human diseases. There are many benefits to this approach. In many human cases where the causative gene is known, the deletion or mutation of that gene in the mouse has shown a very similar, if not identical, phenotype. The mouse models in these cases allow for a thorough investigation of the phenotype(s) as well as the underlying developmental mechanisms, leading to the discovery of the the gene function in development and disease and even subsequent design of therapy. Additionally, the number of human patients with a particular gene mutation or deletion leading to a specific disease phenotype is limited (sometimes limited to only one person). In these cases the use of a mouse model, creates a large cohort of

affected mice and a statistically significant investigation of the phenotype can be made. In some cases, the genetic cause of a disease has been discovered from the similarity in phenotype between the human syndrome and a mouse model.

As mentioned in chapter 1, the *Hesx1* locus has been previously deleted in the mouse. The resulting *Hesx1*$^{-/-}$ mice are the closest existing animal model for SOD, and their analysis has shed light into the function of *Hesx1* in forebrain patterning as well as its role in the aetiology of SOD and hypopituitarism. These conditions are highly heterogeneous and *Hesx1*$^{-/-}$ mice also show variability in their phenotypes. The underlying cause of this variability is still unclear. It is clear, however, that a number of different genes and different mutations within the same gene, as well as environmental factors could contribute to the aetiology of SOD and hypopituitarism.

Patients carrying different mutations in *HESX1* show variable phenotypes, from IGHD to severe panhypopituitarism and SOD. We decided to generate mouse models for two homozygous *HESX1* mutations, namely I26T and R160C. The reasoning behind this choice stems from the phenotype of the patients as well as the point mutations themselves. Firstly, both mutations result in a single amino acid substitution of two different residues, both of which are strictly conserved in (Chapter 1). They are also both located in conserved and functionally important, but different domains of the HESX1 protein. Secondly, the patients display two strikingly different phenotypes, where the pituitary gland abnormalities are profound, however, forebrain defects which are seen in the *HESX1*$^{R160C/R160C}$ patients are absent in the *HESX1*$^{I26T/I26T}$ patient. We are, therefore, hoping to use these mouse models to:

1. Investigate the function of the different domains of HESX1 protein (eh1 and homeodomain) in achieving its role as an important transcriptional repressor during forebrain and pituitary development; as such a differential study is not achievable using *Hesx1*$^{-/-}$ mice alone.
2. Carry out a detailed analysis of the phenotype caused by each mutation since a coherent study is not possible based on only three human patients.
3. Investigate this genotype-phenotype relationship in elucidating the broad role *Hesx1* plays in development as well as in the pathogenesis and variability of SOD and hypopituitarism.

4.2. RESULTS

4.2.1. Genotypic and morphological analysis of *Hesx1*$^{I26T/I26T}$ mice

Genotypic analysis of the *Hesx1-I26T* mouse line showed that *Hesx1*$^{I26T/+}$ (n=124) animals were viable and normal. The vast majority of *Hesx1*$^{I26T/I26T}$ pups survived weaning and went on to produce viable offspring. However, closer inspection on the number of weaners of each genotype from *Hesx1*$^{I26T/+}$ intercrosses, showed a slight deviation from the expected Mendelian ratios for the number of homozygous animals (Table 4.1). Although, there was an indication that a small percentage of *Hesx1*$^{I26T/I26T}$ (~7%) died, this was not statistically significant (Table 4.1).

Gross morphological analysis of the *Hesx1*$^{I26T/I26T}$ mice (n=50), showed that the majority of them (~74%) displayed eye defects, ranging from microphthalmia to anophthalmia. This eye phenotype appeared both uni- and bilaterally (Table 4.2;Table 4.3; Figure 4.1A). Apart from eye defects, the homozygous mice appeared normal, growing to a normal size and age, they were also fertile and went on to produce viable offspring. The remaining (~26%) *Hesx1*$^{I26T/I26T}$ animals did not display any defects (Table 4.3; Figure 4.1B).

Histological analysis of adult *Hesx1*$^{I26T/I26T}$ brains showed no abnormalities in the corpus callosum and anterior commissures (n=8, Figure 4.2).

Table 4.1 - Genotype of mice resulting from *Hesx1*$^{I26T/+}$ intercrosses.

Genotype	No. of mice obtained (%)	Expected
Hesx1$^{+/+}$	97 (~36)[a]	68
Hesx1$^{I26T/+}$	124 (~46)	135
Hesx1$^{I26T/I26T}$	50 (~18)[b]	68
Total	271	271

a: Significant deviation from the expected Mendelian ratios (Chi-squared test, $p<0.03$)
b: No Significant deviation from the expected Mendelian ratios (Chi-squared test)

Table 4.2 - Observable phenotypes of *Hesx1*$^{I26T/I26T}$ mice after weaning.

Phenotype	Frequency
Normal eyes	13
Both eyes anophthalmia	21
Right eye anophthalmia	7
Left eye anophthalmia	4
Both eyes microphthalmia	1
Right eye microphthalmia	3
Left eye microphthalmia	1
Total	50

Table 4.3 - Phenotypes associated with *Hesx1*$^{I26T/I26T}$ mice.

Phenotype	Frequency (n=50)
Normal eyes	26%
Unilateral eye defect	44%
Right eye defect	20%
Left eye defect	10%

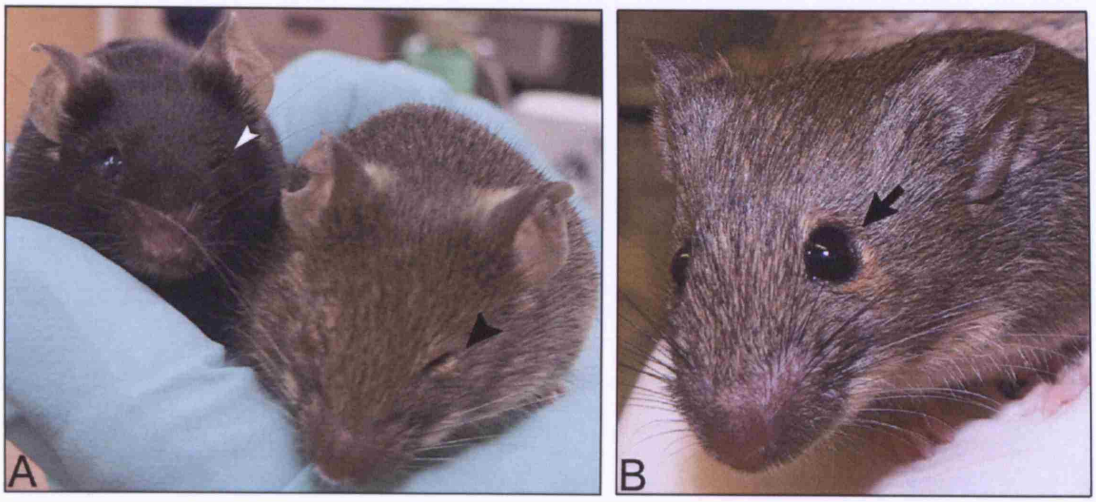

Figure 4.1 – Eye defects in *Hesx1*$^{I26T/I26T}$ mice. A) Majority of *Hesx1*$^{I26T/I26T}$ mice display microphthalmia and/or anophthalmia, which are seen both symmetrically (black arrowhead) and asymmetrically (white arrowhead). Apart from these eye defects, the mice were viable and fertile, growing to a normal size compared with their wild-type littermates. B) ~26% of *Hesx1*$^{I26T/I26T}$ mice do not show visible eye abnormalities (arrow).

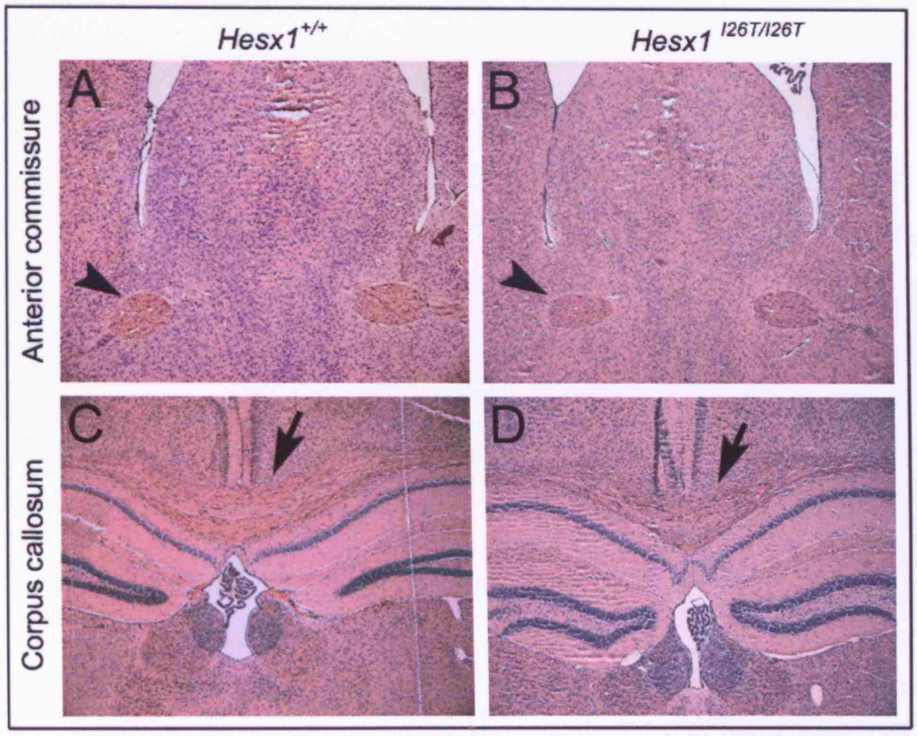

Figure 4.2 – Intercerebral commissures in *Hesx1*$^{I26T/I26T}$ adult brains. A) Coronal section through a wild-type adult brain, at the level of anterior commissures (arrowhead). B) A similar section from a *Hesx1*$^{I26T/I26T}$ adult brain, showing normal anterior commissures (arrowhead). C) Coronal section through a wild-type adult brain, at the level of the corpus callosum (arrow). D) Corpus callosum (arrow) is normal in *Hesx1*$^{I26T/I26T}$ adult brains.

4.2.2. *Hesx1*$^{I26T/I26T}$ embryos

A similar analysis was carried out at embryonic stages 8.5-17.5 dpc. The numbers obtained for each genotype followed the expected Mendelian ratios (Table 4.4). Gross morphological analysis at 12.5-17.5 dpc showed that the key phenotypic feature in *Hesx1*$^{I26T/I26T}$ embryos is the eye defect, appearing in ~77% of homozygotes (n=42;Table 4.5).

This eye phenotype was not fully penetrant, i.e. ~22% of the embryos at 12.5 dpc (n=23) showed no apparent defects (Table 4.5; Figure 4.3E). Moreover, these defects were highly variable in nature appearing both symmetrically and asymmetrically. In order to characterise the defects observed in *Hesx1*$^{I26T/I26T}$ embryos, the phenotypes were broadly divided into five groups and the total frequency of embryos displaying each phenotype was assessed at stages 12.5-17.5 dpc (Table 4.5).

Microphthalmia was itself highly variable, and can be further subdivided into three classes, the range of which is shown in Figure 4.3. The least severe form (mild microphthalmia), was seen as an abnormality in the shape of the pigmented retina (Figure 4.3D), followed by moderate microphthalmia, which was manifested in the form of a small eye (Figure 4.3C). Finally, severe microphthalmia was defined by the absence or almost absence of eye structure (Figure 4.3I and J). For simplicity, these were all grouped together as microphthalmia, and were found in ~60% of 12.5-17.5 dpc embryos.

The most severe eye defect was the complete absence of any eye structure or pigment. This was classified as anophthalmia (Figure 4.3B) and was found in ~17% of the cases. Finally, ~21% of embryos showed no defects presumably corresponding to the 25% adult mice that displayed normal eyes (Figure 4.3E). Histological analysis of these normal homozygous embryos at 15.5 dpc showed that the optic nerve was present in these embryos (Figure 4.4).

These eye defects were observed in the absence of any other forebrain abnormalities. The telencephalic vesicles in 12.5 dpc homozygous embryos developed normally and the severe forebrain truncations, which are a feature of some *Hesx1*$^{-/-}$ mutants were not seen in *Hesx1*$^{I26T/I26T}$ embryos. The same was true for both younger and older embryos, although only one embryo at 17.5 dpc (corresponding to ~2% of total embryos), showed severe craniofacial defects resembling the severe *Hesx1*$^{-/-}$ and

Hesx1$^{R160C/R160C}$ phenotype, which will be discussed in more detail in the next chapter.

The eye defects were harder to see in younger embryos, but morphological analysis of 9.5-10.5 dpc mutants showed that these embryos had small or absent optic vesicles, appearing both symmetrically and asymmetrically (data not shown). Reducing the dosage of the I26T allele by 50% in *Hesx1*$^{I26T/-}$ embryos resulted in an increase in both severity ($p<0.01$) and penetrance ($p<0.05$) of eye and telencephalic defects (Figure 4.3G-J). All the mutants analysed at 12.5-14.5 dpc (n=19) displayed either severe microphthalmia (~26%) or anophthalmia (~48%). Additionally, the appearance of telencephalic defects was now observed in ~26% of embryos (Figure 4.3G).

In summary, *Hesx1*$^{I26T/I26T}$ mice are mostly viable and fertile. Both at the embryonic level and in the adult, they display eye defects, manifested in the form of microphthalmia and anophthalmia. This eye phenotype is highly variable and occurs both symmetrically and asymmetrically, although unilateral defects are more abundant (~44% in adults). ~26% of *Hesx1*$^{I26T/I26T}$ mice and 21% of embryos at 12.5-17.5 dpc (n=42) have normal eyes macroscopically, although the functionality of this has not been tested. Aside from these eye defects, the telencephalon and other aspects of the forebrain develop normally in the mutants. Similarly, the analysis of forebrain commissural tracts in the adult homozygous mice revealed that these animals have a normal corpus callosum and anterior commissures.

Table 4.4 - Genotype of embryos resulting from *Hesx1*$^{I26T/+}$ intercrosses at stages 8.5-17.5 dpc.

Stage	Genotype		
	Hesx1$^{+/+}$	*Hesx1*$^{I26T/+}$	*Hesx1*$^{I26T/I26T}$
8.5 dpc	17	24	10
10.5 dpc	3	9	5
12.5 dpc	20	49	23
15.5 dpc	15	29	11
17.5 dpc	14	24	13
Total	69 (~26%)	135 (~51%)	62 (~23%)

Table 4.5 – Phenotypes associated with *Hesx1*$^{I26T/I26T}$ and *Hesx1*$^{I26T/-}$ embryos.

Phenotype	*Hesx1*$^{I26T/I26T}$	*Hesx1*$^{I26T/-}$
	12.5-17.5 dpc	12.5-14.5 dpc
Severe forebrain defects[a]	1[f]	2
Anophthalmia and other forebrain defects[b]	0	3
Anophthalmia[c]	7	9
Microphthalmia[d]	25	5
No defects[e]	9	0
Total	42	19

a: Absent telencephalic vesicles, anophthalmia and considerably smaller frontonasal mass (Figure 4.3F). This phenotype generally, manifests in the form of severe craniofacial defects by 17.5 dpc (Figure 5.3).
b: Anophthalmia in association with reduced telencephalic vesicles and/or frontonasal mass (Figure 4.3G,H).
c: Anophthalmia with no other forebrain defects (Figure 4.3B).
d: Microphthalmia with no other forebrain defects (Figure 4.3C,D,J).
e: Phenotypically normal (Figure 4.3E).
f: 17.5 dpc.

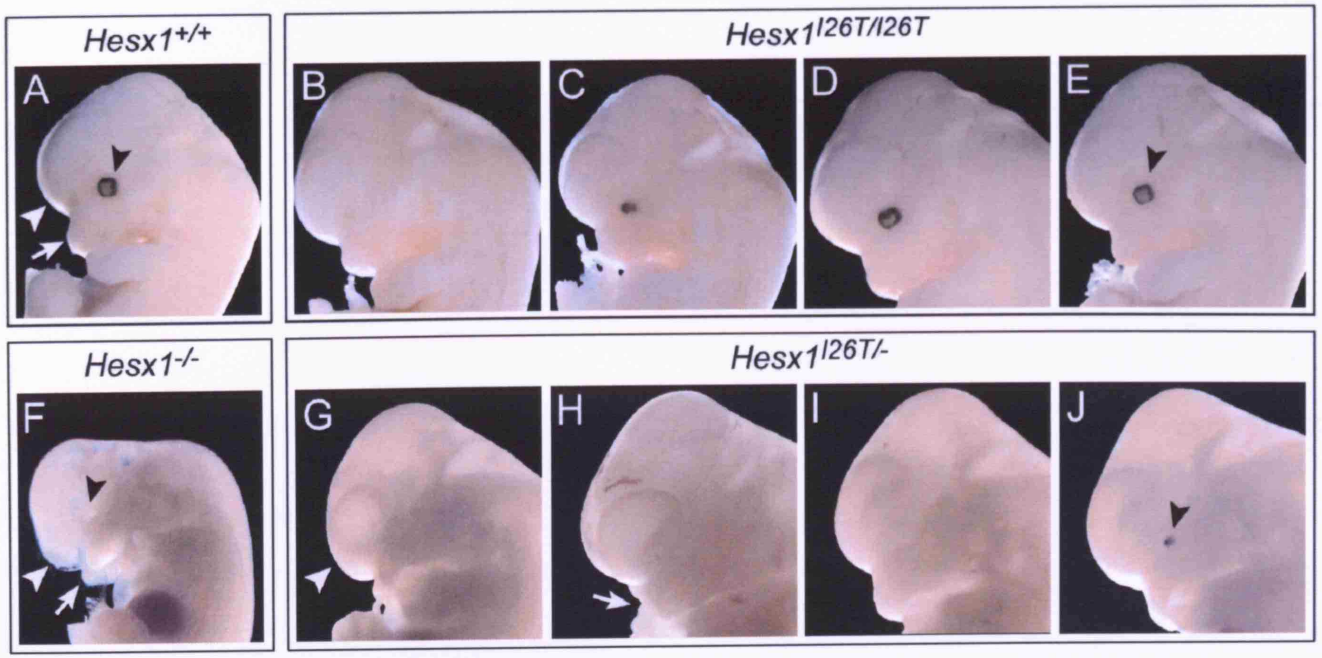

Figure 4.3 – Forebrain defects observed in *Hesx1*$^{I26T/I26T}$ and *Hesx1*$^{I26T/-}$ embryos at 12.5 dpc. A) Wild-type embryo, displaying normal eyes (black arrowhead), telencephalic vesicles (white arrowhead) and frontonasal mass (white arrow). (B-E) *Hesx1*$^{I26T/I26T}$ embryos show eye defects, ranging from anophthalmia (B) and severe microphthalmia (C) to mild microphthalmia (D). E) Some embryos have normal eyes (arrowhead). Note that the other forebrain structures such as telencephalic vesicles and frontonatal mass are unaffected in *Hesx1*$^{I26T/I26T}$ embryos. F) *Hesx1*$^{-/-}$ embryo at 12.5 dpc, showing a severe phenotype with absent eyes (black arrowhead), telencephalic vesicles (white arrowhead) and frontonasal mass (white arrow). (G-J) *Hesx1*$^{I26T/-}$ embryos, display a range of defects from small telencephalic vesicles (arrowhead in G) and small fontonasal mass (arrow in H) to severe microphthalmia (arrowhead in J). Notice that the range of defects is shifted to a more severe spectrum in *Hesx1*$^{I26T/-}$ mutants, compared with *Hesx1*$^{I26T/I26T}$ embryos.

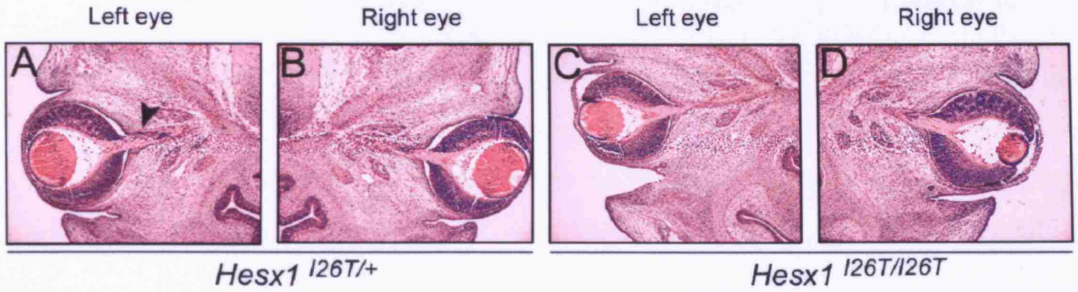

Figure 4.4 – Optic nerves appear normal in *Hesx1*$^{I26T/I26T}$ embryos that show no eye phenotypes. (A-D) Hematoxylin and eosin staining on transverse sections of the head of 15.5 dpc embryos at the level of the eyes. Note that the optic nerves (arrowhead in A), develop normally in *Hesx1*$^{I26T/I26T}$ (C,D) compared with *Hesx1*$^{I26T/+}$ control embryo (A,B).

4.2.3. Early forebrain patterning in *Hesx1*$^{I26T/I26T}$ embryos

Forebrain defects in *Hesx1*$^{-/-}$ embryos are observed as early as 8.0 dpc, when there is a clear reduction in anterior forebrain tissue (Dattani et al., 1998; Martinez-Barbera et al., 2000). Marker and cell fate analyses have shown that this defect is due to a transformation of the anterior to posterior forebrain. There is also growing evidence indicating that this transformation is due to ectopic activation of the Wnt/β-catenin signalling in the rostral region of the *Hesx1*$^{-/-}$ forebrain before the onset of phenotype at 8.0 dpc (Andoniadou et al., 2007). Cell fate and marker analyses were carried out, in order to establish the onset as well as the nature of the phenotype caused by *I26T* mutation as compared with *Hesx1*$^{-/-}$.

4.2.3.1. Cell Fate analysis of *Hesx1*-expressing cells in *Hesx1-I26T* embryos

First, we took advantage of two mouse lines available to us to investigate the fate of *Hesx1*-expressing cells in *Hesx1*$^{I26T/I26T}$ compared to null and control embryos: (1) In the *Hesx1-Cre* mouse line, *Cre* replaces the *Hesx1* coding region so that *Hesx1*$^{Cre/Cre}$ embryos are phenotypically identical to *Hesx1*$^{-/-}$ mutants (Andoniadou et al., 2007); (2) In the *Rosa26*$^{Cond\text{-}lacZ}$, *lacZ* is activated by CRE-mediated excision of a transcriptional stop sequence, the result being that the *Cre*-expressing cells and their descendants express *lacZ* permanently, and can be detected by X-Gal staining (Soriano, 1999).

The *Hesx1*$^{Cre/+}$;*R26*$^{Cond\text{-}lacZ/+}$ (phenotypically normal) and *Hesx1*$^{Cre/I26T}$;*R26*$^{Cond\text{-}lacZ/+}$ (equivalent to *Hesx1*$^{I26T/-}$) compound embryos were generated and X-Gal stained at 10.5 dpc. In *Hesx1*$^{Cre/+}$;*R26*$^{Cond\text{-}lacZ/+}$ embryos, *lacZ*-positive cells localised to the anterior forebrain structures such as the telencephalon, eyes and ventral diencephalon (Figure 4.5A,C), as was reported previously (Andoniadou et al., 2007). In *Hesx1*$^{Cre/I26T}$;*R26*$^{Cond\text{-}lacZ/+}$ embryos, however, a higher proportion of *lacZ*-expressing cells colonised posterior forebrain regions and the 1st branchial arch (Figure 4.5B,D). This is very similar to the pattern seen in the absence of *Hesx1* in *Hesx1*$^{Cre/-}$;*R26*$^{Cond\text{-}lacZ/+}$ embryos (equivalent to *Hesx1*$^{-/-}$).

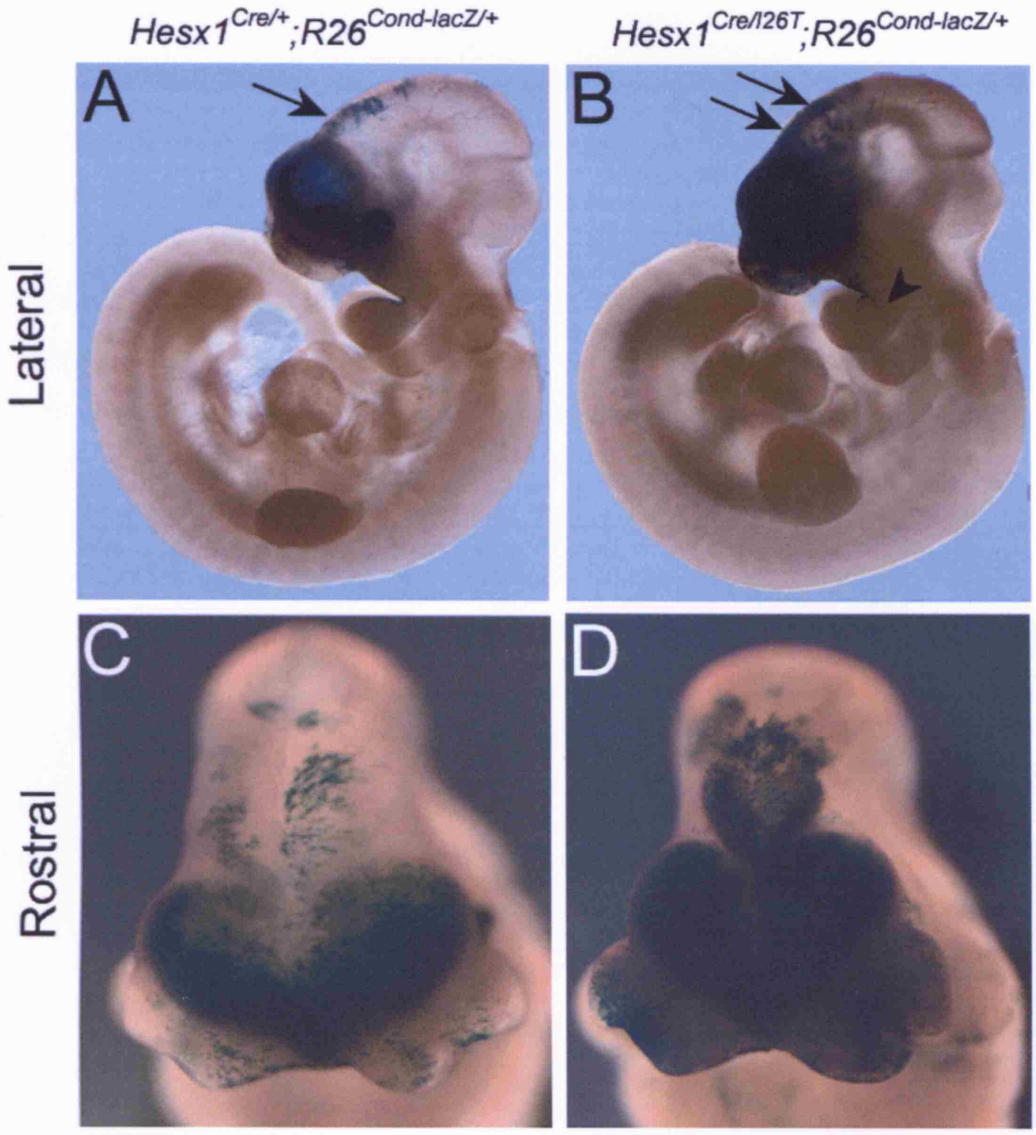

Figure 4.5 – Cell fate analysis in *Hesx1*$^{Cre/I26T}$;*R26*$^{Cond\text{-}lacZ/+}$ embryos. A) X-Gal staining of a *Hesx1*$^{Cre/+}$;*R26*$^{Cond\text{-}lacZ/+}$ embryo at 10.5 dpc, note that the descendants of *Hesx1*-expressing cells in a control embryo mainly colonise the anterior forebrain, with some reaching the posterior forebrain (arrow). B) An equivalent analysis in a *Hesx1*$^{Cre/I26T}$;*R26*$^{Cond\text{-}lacZ/+}$ embryo, note that now more cells reach the posterior forebrain (arrows), with some colonising the first branchial arch (arrowhead). C and D are the frontal views of embryos depicted in A and B, respectively.

4.2.3.2. Early marker analysis in *Hesx1*$^{I26T/I26T}$ embryos

We set out to investigate the onset of this phenotype, by using specific early neural markers, in whole mount in-situ hybridisation at 8.5-9.5 dpc. As previously mentioned, morphologically, the phenotype of the homozygous embryos at these early stages of development was variable. The majority of embryos displayed a mild abnormality in the forebrain region, whilst the remainder appeared normal. The expression pattern of markers in the latter set of embryos was the same as that seen in the wild-type and presumably corresponds to those embryos, which appeared normal later at 12.5 dpc; hence they are not shown here. On the other hand, the analysis of markers in embryos with phenotypic defects was relatively consistent, although some variability existed. This variability was dependent on the abnormality in the development of the presumptive eye tissue, which was the only defective forebrain tissue in these embryos. Therefore, the results discussed below correspond to this representative latter group of embryos.

Hesx1 is a marker of anterior forebrain at 8.0 dpc and by 9.0 dpc its transcripts are detected in the ventral diencephalon and proximal regions of optic stalks. At 8.0 dpc, *Hesx1* expression domain was slightly reduced laterally in *Hesx1*$^{I26T/I26T}$ embryos (Figure 4.6B). By 9.0 dpc this reduction was specific to the developing optic vesicles whilst in the anterior forebrain *Hesx1* was expressed normally in these embryos compared with controls (Figure 4.6D).

Wnt1 is an early marker important for midbrain formation, its expression in the 8.0-9.0 dpc head is restricted to the midbrain and posterior forebrain. In *Hesx1*$^{I26T/I26T}$ embryos, the expression of *Wnt1* was anteriorised (Figure 4.6F,H). The same rostral expansion of *Wnt1* expression is seen in *Hesx1*$^{-/-}$ embryos (Andoniadou et al., 2007).

Finally, the expression domain of *Pax6* in the anterior forebrain was reduced in the *Hesx1*$^{I26T/I26T}$ embryos at 9.0 dpc. The optic vesicles were abnormal in these mutant embryos, whilst the surrounding forebrain tissue expressed *Pax6* normally (Figure 4.6J).

Two possible scenarios exist with regard to the onset of phenotype in *Hesx1*$^{I26T/I26T}$ embryos. One possibility is that early on, at 8.0 dpc, only the presumptive eye field is reduced, whilst the remaining anterior forebrain tissue (i.e. the telencephalic precursors) is correctly specified, hence leading to the eye defects seen later.

Alternatively, the anterior forebrain tissue in *Hesx1*$^{I26T/I26T}$ could be reduced early on (as is the case in *Hesx1*$^{-/-}$), but the telencephalic primordial may catch up at later stages so that by 10.5 dpc, the only defect seen is the eye phenotype.

The first possibility seems to be more likely in this case, as the expression of markers such as *Pax6*, *Bf1* and *Fgf8* in the prospective telencephalon are similar in control and *Hesx1*$^{I26T/I26T}$ embryos at early stages (Figure 4.6J and data not shown).

Collectively, these results indicate that in *Hesx1*$^{I26T/I26T}$ embryos, the early anterior neural patterning defects affect the presumptive eye regions, whilst the developing telencephalon is specified properly. This is supported by the morphological analysis of embryos as well as the expression patterns of *Hesx1*, *Pax6* and *Bf1*. In these studies, the expression domains of *Hesx1* and *Pax6* are reduced in the developing optic vesicles, whilst the developing telencephalic tissue expresses these markers as well as *Bf1* normally. This indicates that the eye is more sensitive to HESX1 impaired function than the other anterior forebrain structures.

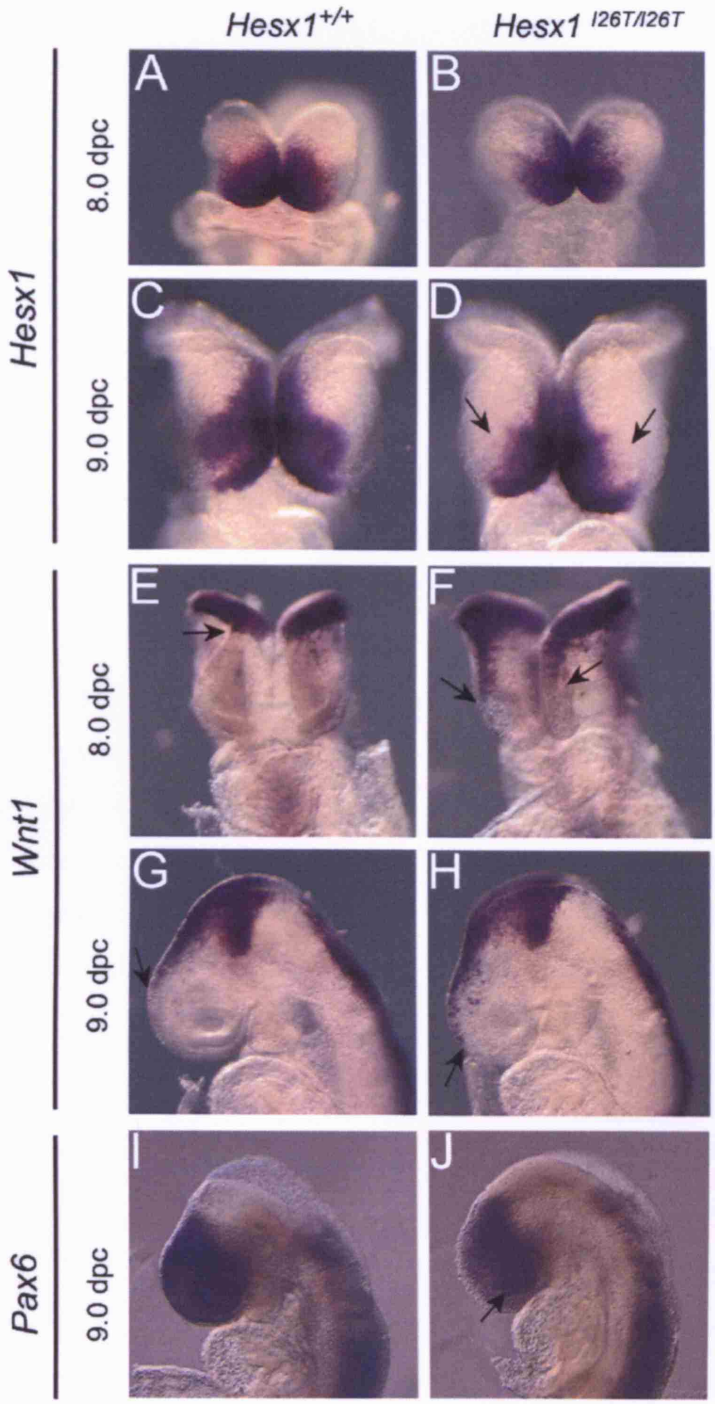

Figure 4.6 – Early forebrain patterning defects in *Hesx1*$^{I26T/I26T}$ embryos. Whole mount in-situ hybridisation in 8.0 dpc (A,B,E,F) and 9.0 dpc (C,D,G-J) embryos with different markers. The riboprobes used are indicated on the left hand side. A-F are rostral views, G-J are lateral views with anterior to the left. (A-D) *Hesx1* expression is slightly reduced in the lateral aspects of the forebrain tissue at 8.0 dpc in *Hesx1*$^{I26T/I26T}$ embryos. By 9.0 dpc, this reduction is more pronounced and it is restricted to the developing optic cups in the mutants compared with the wild-type (arrows in D). (E-H) *Wnt1* expression is anteriorised in *Hesx1*$^{I26T/I26T}$ embryos (arrows in F and H). (I-J) Note the expression domain of *Pax6* is reduced in the anterior forebrain of *Hesx1*$^{I26T/I26T}$ embryos; the optic vesicles are smaller in the mutants compared with the wild-type (arrow in J).

4.2.4. Morphological and molecular analysis of pituitary defects in *Hesx1*$^{I26T/I26T}$ embryos

The *HESX1*$^{I26T/I26T}$ homozygous human patient displays evolving hypopituitarism. Our analysis of the *Hesx1*$^{I26T/I26T}$ mice showed that these animals are mostly viable and fertile growing to a healthy size. Although, the pituitary hormone levels have not been analysed, there is so far no indication of any hormone deficiencies in these adult mice. Hence, the embryonic development of the pituitary gland was investigated in these animals.

Morphological analysis of the developing pituitary gland in *Hesx1*$^{I26T/I26T}$ embryos showed that unlike the eye defects, pituitary abnormalities were fully penetrant in the mutants between 12.5-17.5 dpc (n=30). Although, the phenotype was variable at these stages, the severity of RP defects was relatively consistent. Hematoxylin and eosin staining on sections at the level of the developing pituitary gland showed that by 12.5 dpc, RP was bifurcated and contained multiple lumens (Figure 4.8B). At 15.5 dpc the anterior pituitary was enlarged with disorganised cells expanding ventrally into the sphenoid cartilage (Figure 4.8D). The sphenoid bone failed to fuse by 17.5 dpc (Figure 4.8F) and the pituitary was larger, as it covered more anterior to posterior sections when compared with controls (data not shown).

The expression patterns of *Lhx3* (in the RP) and *Fgf8* (in the ventral diencephalon) at 10.5 dpc were used to analyse the induction of RP in *Hesx1*$^{I26T/I26T}$ embryos. Both markers displayed similar expression domains in the mutants compared with wild-type (Figure 4.7). This suggests that the induction of Rathke's pouch (RP) took place normally in these embryos.

At 12.5 dpc most of the pituitary-specific markers (*Lhx3, Hesx1* and *Prop1*) were expressed, indicating that cell lineages were properly specified (Figure 4.9). The only exception at this stage was the expression of *Pomc*, which was reduced in the ventral diencephalon but was normally expressed in the RP (Figure 4.9J,L). *Lhx3* expression was expanded, reflecting the presence of extra anterior pituitary tissue (Figure 4.9B).

By 15.5-16.5 dpc *Pit1, Cga, Prop1, Lhx3* and *Pomc* were all expressed, indicating that the cell lineages were specified properly (Figure 4.10 and data not shown).

By 17.5 dpc, the hormone producing cells were properly differentiated, as shown by normal expression of *Gh, Prl, Lhb, Cga, Tshb* and *Pomc* (Figure 4.11).

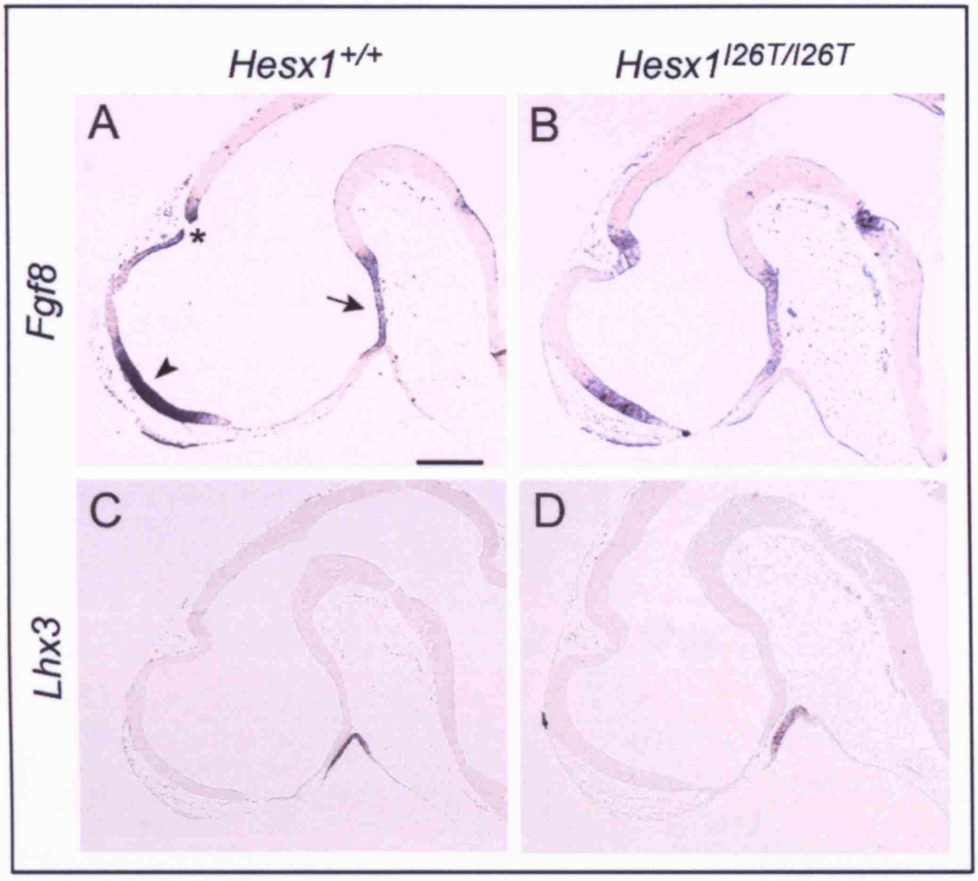

Figure 4.7 – Analysis of *Fgf8* and *Lhx3* in *Hesx1*$^{I26T/I26T}$ embryos at 10.5 dpc. In-situ hybridisation on sagittal sections of 10.5 dpc embryos, at the level of Rathke's pouch (RP), with anterior to the left. A) Wild-type embryo, displaying *Fgf8* expression in the commissural plate of the forebrain (arrowhead), roof of the telencephalon (asterisk) and the ventral diencephalon/infundibulum (arrow). B) The *Fgf8* expression domain in the ventral diencephalon in *Hesx1*$^{I26T/I26T}$ embryos is similar to the wild-type. The neuroepithelium of the depicted mutant appears slightly thicker due to the angle of the section. C) Wild-type embryo, showing *Lhx3* expression in the RP. D) *Lhx3* is expressed in the RP of *Hesx1*$^{I26T/I26T}$ embryos. *Lhx3* expression domain appears reduced in caudal levels possibly due to a slight developmental delay in the mutant compared with the wild-type embryo. Scale bar: 0.1 mm.

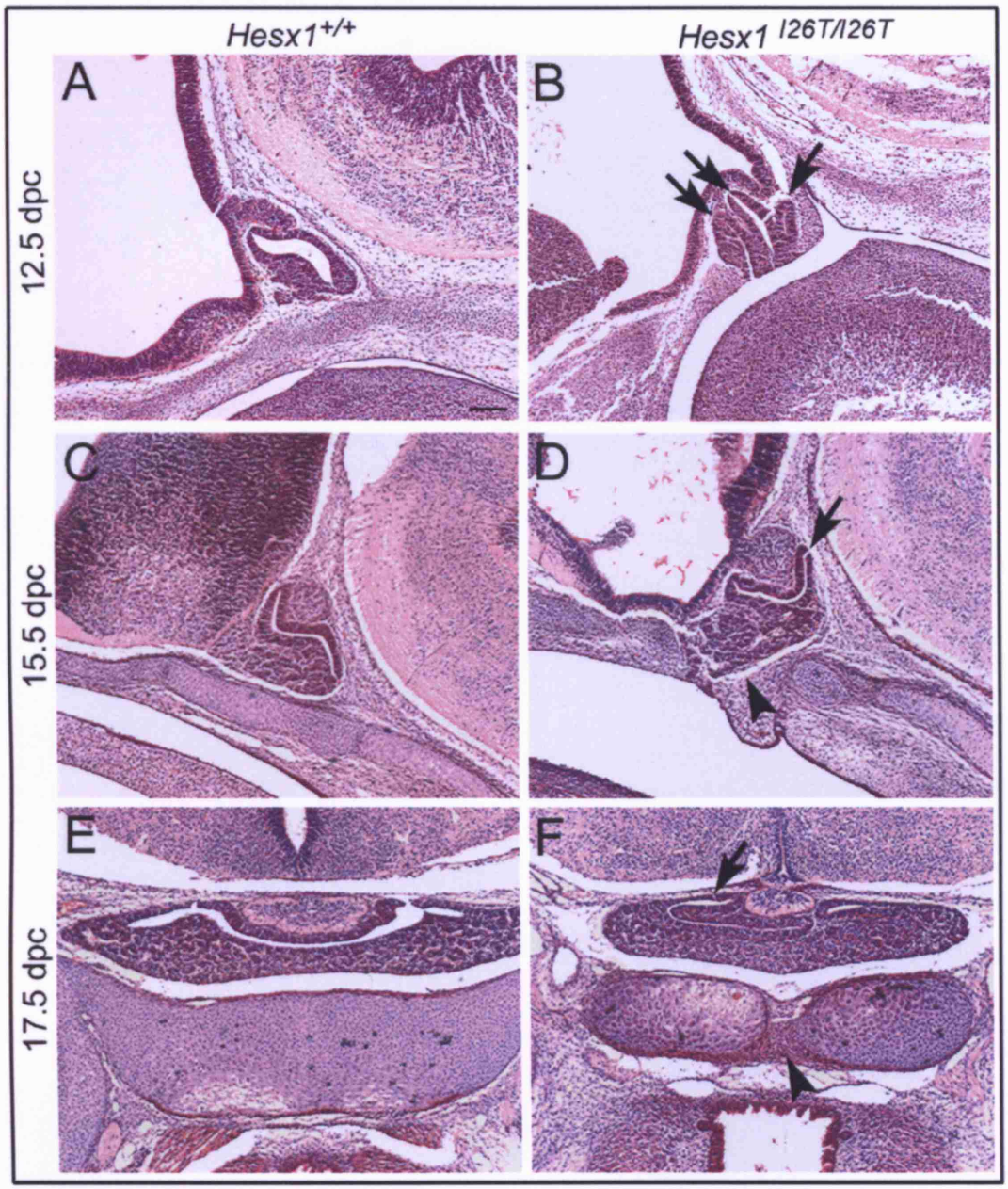

Figure 4.8 – Morphological Rathke's pouch defects in *Hesx1*$^{I26T/I26T}$ embryos. Hematoxylin and eosin staining on sagittal sections (anterior to the left), of the wild-type Rathke's pouch at 12.5 dpc (A), 15.5 dpc (C) and on coronal sections at 17.5 dpc (E). B) Defects are seen in RP at 12.5 dpc in *Hesx1*$^{I26T/I26T}$ embryos, with bifurcations and multiple lumens (arrows). The cells in the ventral side of the pouch are often disorganised and expanded. D) By 15.5 dpc, the developing anterior lobe has clearly expanded, preventing the sphenoid bone from fusing (arrowhead). The lumen is abnormal and bifurcated (arrow). F) This phenotype persists at 17.5 dpc, when the anterior pituitary, the sphenoid bone (arrowhead) and the lumen (arrow) display abnormalities. Scale bar: 0.1 mm.

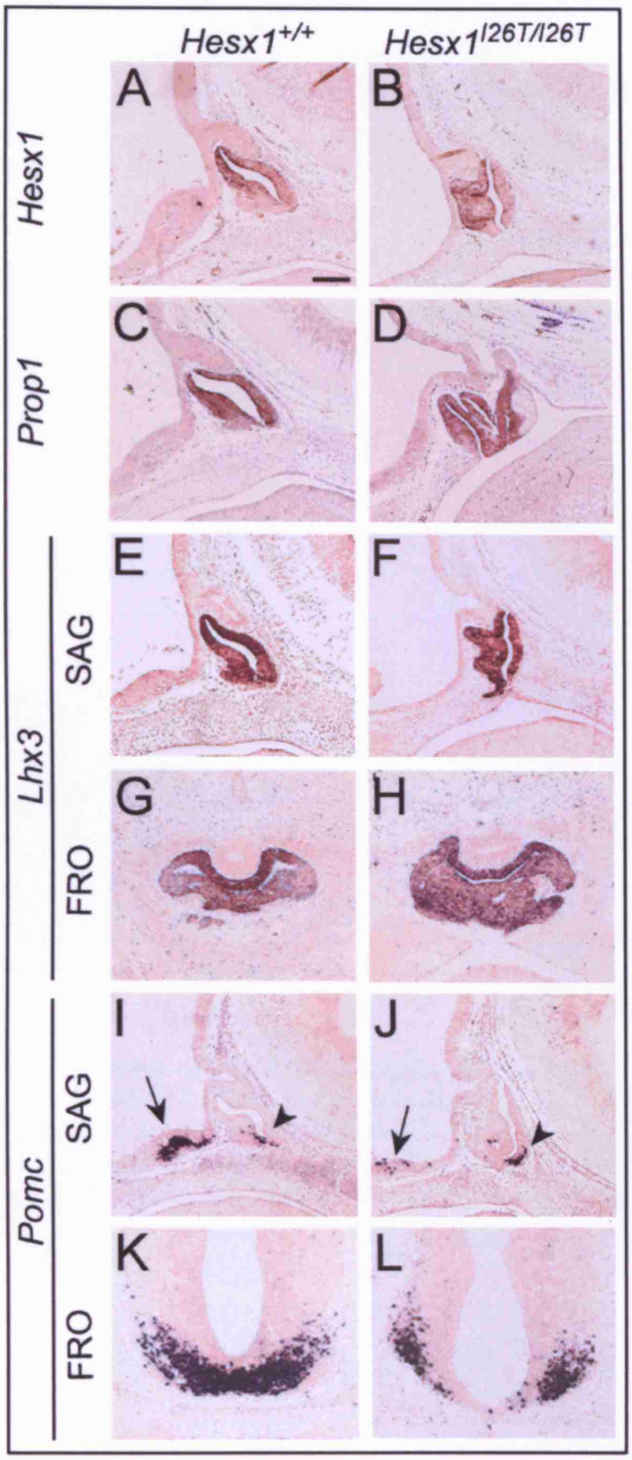

Figure 4.9 – Analysis of pituitary gland markers at 12.5 dpc in *Hesx1*$^{I26T/I26T}$ embryos. In-situ hybridisation on sagittal sections (SAG) with anterior to the left (A-F, I-J) and on frontal sections, FRO (G-H, K-L). The riboprobes used are indicated on the left hand side. *Hesx1* (B), *Prop1* (D) and *Lhx3* (F, H) are expressed in *Hesx1*$^{I26T/I26T}$ RP at this stage. The expression of these markers is increased as the cells in the ventral aspect of the pouch are expanded compared with the wild-type (A-G). J) Expression of *Pomc* is normal in the pouch (arrowhead), but it is reduced in the hypothalamus (arrow). This is clearly seen in the frontal view (compare L with K). Scale bar: 0.1 mm.

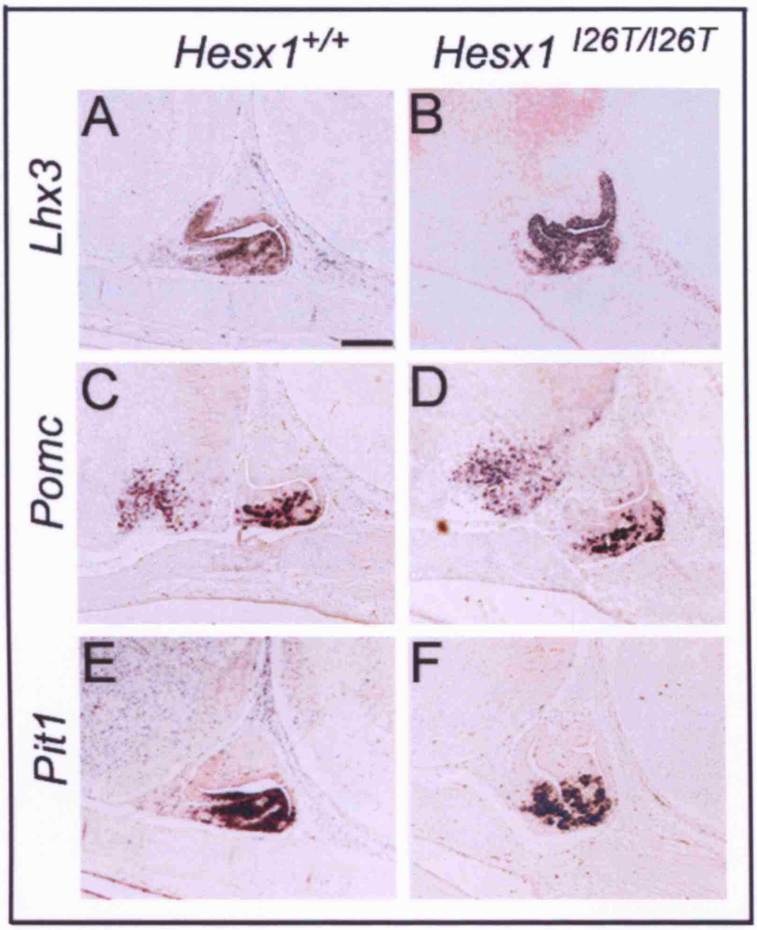

Figure 4.10 – Analysis of pituitary gland markers at 15.5 dpc in *Hesx1*$^{I26T/I26T}$ embryos. In-situ hybridisation on sagittal sections, with anterior to the left. The probes used are indicated on the left hand side. (A, B) *Lhx3* is expressed in *Hesx1*$^{I26T/I26T}$ RP at this stage. (C, D) *Pomc* expression in *Hesx1*$^{I26T/I26T}$ embryos is similar to wild-type, both in the RP and in the ventral diencephalon. (E, F) The Pit1 lineage is been specified in *Hesx1*$^{I26T/I26T}$ embryos, as shown by the correct expression of *Pit1*. Scale bar: 0.1 mm.

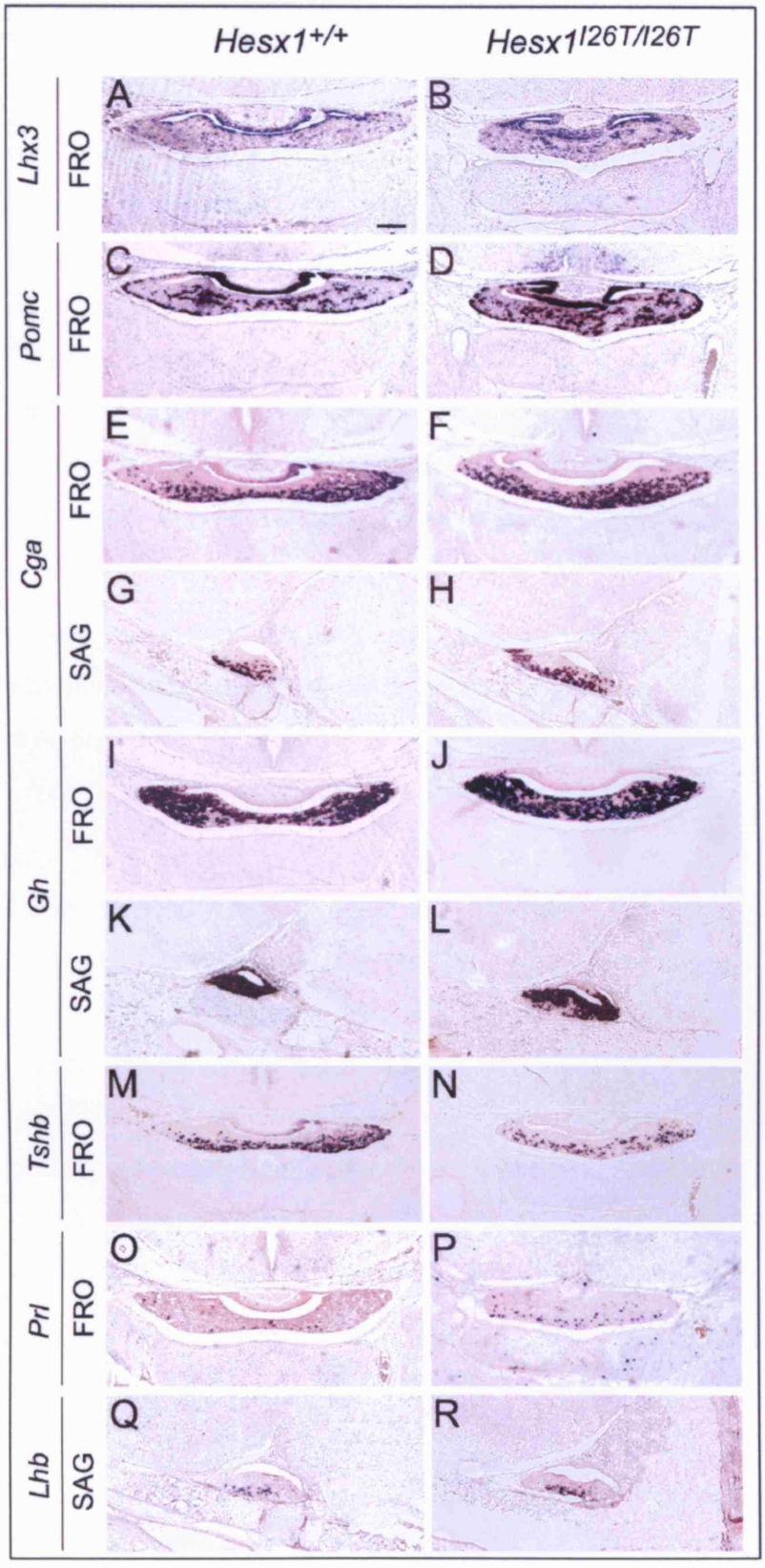

Figure 4.11 – Analysis of terminal differentiation markers at 17.5 dpc in *Hesx1*$^{I26T/I26T}$ embryos. In-situ hybridisation on frontal (Fro) and sagittal (Sag) sections, of *Hesx1*$^{I26T/I26T}$ and wild-type embryos. *Lhx3* (A,B), *Pomc* (C,D), *Cga* (E-H), *Gh* (I-L), *Tshb* (M,N), *Prl* (O,P) and *Lhb* (Q,R) are all expressed to same extent in the pituitary glands of the mutant and control embryos. Scale bar: 0.1 mm.

4.3. CONCLUSION

The results presented in this chapter show that *Hesx1*$^{I26T/I26T}$ animals display a range of defects, mainly affecting the eye and the pituitary gland. The other structures in the forebrain such as the telencephalic vesicles and the frontonasal mass appear essentially normal in the embryos and structures such as the corpus callosum and the anterior commissures are unaffected in the adult mutant mice. Eye defects in *Hesx1*$^{I26T/I26T}$ embryos and mice are variable in nature, ranging from microphthalmia to anophthalmia and appear both symmetrically and asymmetrically. These defects are not fully penetrant as ~26% of mice (n=50) and 21% of embryos (n=42) have normal eyes. Pituitary defects, on the other hand, appear in 100% of the embryos (n=30).

Analysis of early markers of the fore- and midbrain and fate mapping in these embryos, indicate an early anterior neural patterning defect at 8.0 dpc. This primarily affects the eye precursors and therefore, appears milder than the patterning defect observed in *Hesx1*$^{-/-}$ mutants, which carry a null allele (Andoniadou et al., 2007).

The analysis of the Rathke's pouch in the homozygous embryos shows that it is initially induced correctly at 10.5 dpc, but becomes abnormal as shown by bifurcations and multiple lumens at 12.5 dpc. By 15.5 dpc and through to 17.5 dpc, this abnormality is manifested in an enlarged anterior lobe that expands ventrally causing the sphenoid cartilage to break open. Interestingly, this phenotype does not affect the specification of anterior pituitary cell types, as all the early and terminal pituitary markers are expressed correctly at embryonic stages. Moreover, the majority (~93%) of homozygous animals survive to a normal adult size and are fertile, possibly indicating a functionally normal pituitary gland.

These data indicate that the *Hesx1-I26T* is a hypomorphic allele. It also shows that the various forebrain structures display different sensitivities to compromised HESX1 function with the pituitary gland being the most sensitive, followed by the eyes and finally the telencephalon and frontonasal mass. These results are further discussed in Chapter 6 following the analysis of *Hesx1-R160C* mice.

5. ANALYSIS OF THE *Hesx1-R160C* MOUSE LINE

5.1. RESULTS

5.1.1. Genotypic and morphological analysis of *Hesx1*$^{R160C/R160C}$ mice

The number of mice obtained from *Hesx1*$^{R160C/+}$ intercrosses is shown in Table 5.1. This analysis showed that *Hesx1*$^{R160C/+}$ mice (n=94) were viable and normal, although there was one case of bilateral microphthalmia in a *Hesx1*$^{R160C/+}$ mouse, which did not affect its viability or fertility. Therefore, although *Hesx1-R160C* allele clearly displayed a dominant negative effect in-vitro (Brickman et al., 2001) and was lethal in heterozygosity in ES cells (section 7.5.3), in mice this effect was not observed, as the *Hesx1*$^{R160C/+}$ animals were predominantly normal. These crosses also revealed a significant deviation from the expected Mendelian ratios for *Hesx1*$^{R160C/R160C}$ numbers (Table 5.1). Only ~3% of homozygous mice survived weaning indicative of perinatal lethality in the vast majority of these pups ($P<0.001$).

Some *Hesx1*$^{R160C/R160C}$ neonates displayed severe craniofacial defects, which resulted from a complete truncation of their anterior forebrain structures during development. They had an abnormal/small head with a significantly small nose and "eye-like" protrusions appeared dorsally, where the cranium is situated. This resembles the phenotype seen in cyclopic embryos, although in *Hesx1*$^{R160C/R160C}$ embryos both symmetric and asymmetric bulges were present indicating that the mechanism is distinct from cyclopia (i.e. the failure to divide the eye field). This is the exact phenotype displayed in some *Hesx1*$^{-/-}$ neonates, which die perinatally.

It should also be noted that not all the dead neonates displayed this severe phenotype, signifying that although a proportion of these deaths was due to craniofacial abnormalities; these defects alone cannot be responsible for the perinatal lethality seen here. A further ~2% of *Hesx1*$^{R160C/R160C}$ animals were abnormally small and survived for ~10 days but died by weaning (Table 5.1).

Histological analysis of the surviving *Hesx1*$^{R160C/R160C}$ adult brains (n=5), revealed defects in the anterior commissures in one of the animals (Figure 5.1B). Although, the corpus callosum in these animals was present it appeared thinner (Figure 5.1D). However, it must be noted that these animals survived into adulthood and were hence among the ~3% least severely affected *Hesx1*$^{R160C/R160C}$ animals. Indeed, the analysis

of these intercerebral commissural tracts in homozygous embryos at 17.5 dpc (n=4), showed that they were either absent or severely abnormal (data not shown).

Table 5.1 - Genotype of mice resulting from *Hesx1*$^{R160C/+}$ intercrosses.

Genotype	No. of mice obtained (%)	Expected
Hesx1$^{-/-}$	47 (32)	37
Hesx1$^{R160C/+}$	94 (63)	74
Hesx1$^{R160C/R160C}$	7* (5)[a]	37
Total	148	148

*: Of these 7 *Hesx1*$^{R160C/R160C}$ mice, 2 died by weaning. From the 5 survivors, one was small and infertile with unilateral anophthalmia. The remaining four mice displayed uni- or bilateral eye defects (essentially like *Hesx1*$^{I26T/I26T}$ mice).
a: There was a significant deviation from the expected Mendelian ratios for the homozygous mice (Chi-squared test, $p<0.001$).

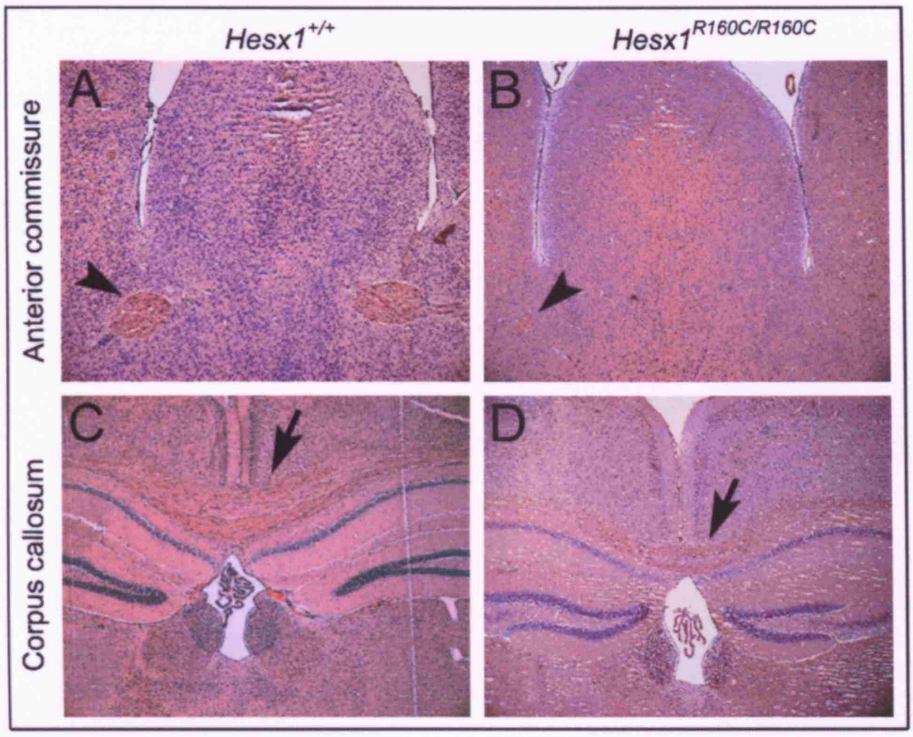

Figure 5.1 – Intercerebral commissures in *Hesx1*$^{R160C/R160C}$ adult brains. A) Coronal section through a wild-type adult brain, at the level of anterior commissures (arrowhead). B) A similar section through a *Hesx1*$^{R160C/R160C}$ adult brain, displaying hypoplastic anterior commissures (arrowhead). C) Coronal section through a wild-type adult brain, at the level of the corpus callosum (arrow). D) Corpus callosum (arrow) is thinner in the *Hesx1*$^{R160C/R160C}$ mutant. Note that these are the surviving *Hesx1*$^{R160C/R160C}$ mice; hence the brain defects are amongst the mildest within this genotype.

5.1.2. *Hesx1*$^{R160C/R160C}$ embryos

The numbers obtained from *Hesx1*$^{R160C/+}$ intercrosses followed the expected Mendelian ratios (Table 5.2), further indicating that the large proportion of homozygous mice were dying perinatally.

At 9.5-10.5 dpc, the telencephalic and optic vesicles were reduced or completely absent (data not shown). Gross morphological analysis of *Hesx1*$^{R160C/R160C}$ embryos at 12.5-17.5 dpc, showed a fully penetrant eye phenotype, albeit variable in nature (n=43). Moreover, these eye defects were associated with other forebrain abnormalities in the majority of cases (~67%). For simplicity, these phenotypes were divided into four broad groups (Table 5.3). The scale of severity of these defects is displayed in Figure 5.2 for 12.5 dpc embryos. Similar variability was observed in both younger and older embryos.

Overall, eye defects appeared both symmetrically and asymmetrically, and they were in the form of severe microphthalmia (Figure 5.2E) or anophthalmia (Figure 5.2B-D). Other forebrain defects affected the telencephalic vesicles and olfactory placodes in variable degrees (Figure 5.2C; Table 5.3).

Furthermore, a more severe class of forebrain defects was observed in ~7% of 12.5 dpc embryos (n=15), where the entire forebrain tissue was truncated (Figure 5.2B). This is also a feature of the severe *Hesx1*$^{-/-}$ embryos (Figure 5.2F). By 17.5 dpc, ~33% of the homozygous embryos showed a severe phenotype, where the entire frontonasal mass, eyes and telencephalon were absent (Figure 5.3), and as a result these embryos showed severe craniofacial defects (as described in p. 162 for the neonates).

The similarity between the *Hesx1* null and *Hesx1-R160C* alleles was further demonstrated in *Hesx1*$^{R160C/-}$ embryos. In these mutants, despite reducing *Hesx1-R160C* dosage by half, the severity and frequency of eye/forebrain phenotypes were not affected (Figure 5.2G-I). From the *Hesx1*$^{R160C/-}$ embryos analysed (n=15), the majority (~67%) displayed eye defects in association with other forebrain abnormalities.

In conclusion, *Hesx1*$^{R160C/R160C}$ mice and embryos display a much more severe phenotype compared to *Hesx1*$^{I26T/I26T}$ mice and somewhat reminiscent of the defects seen in *Hesx1*$^{-/-}$ mice. *Hesx1*$^{R160C/R160C}$ mice die perinatally and the embryos show a

fully penetrant phenotype, primarily affecting the eyes, but also the telencephalon and olfactory placodes in the majority of cases (~67%). In addition, ~21% of these homozygous embryos display severe craniofacial defects resulting from a failure to develop the most anterior forebrain structures. This latter phenotype is not compatible with life, although it does not solely account for the vast lethality observed in *Hesx1*$^{R160C/R160C}$ neonates.

Table 5.2 - Genotype of embryos resulting from *Hesx1*$^{R160C/+}$ intercrosses at stages 8.5 dpc-17.5 dpc.

Stage	Genotype		
	Hesx1$^{+/+}$	*Hesx1*$^{R160C/+}$	*Hesx1*$^{R160C/R160C}$
8.5 dpc	8	15	7
10.5 dpc	4	13	6
12.5 dpc	10	32	15
15.5 dpc	8	21	10
17.5 dpc	18	42	18
Total	48 (~21%)	123 (~54%)	56 (~25%)

Table 5.3 – Phenotypes associated with *Hesx1*$^{R160C/R160C}$ and *Hesx1*$^{R160C/-}$ embryos.

Phenotype	*Hesx1*$^{R160C/R160C}$	*Hesx1*$^{R160C/-}$
	12.5-17.5 dpc	12.5-14.5 dpc
Severe forebrain defects[a]	9	3
Anophthalmia and other forebrain defects[b]	20	7
Anophthalmia[c]	8	4
Microphthalmia[d]	6	1
No defects[e]	0	0
Total	43	15

a: Absent telencephalic vesicles, anophthalmia and considerably smaller/absent frontonasal mass (Figure 5.2B,F). This phenotype generally, manifests in the form of severe craniofacial defects by 17.5 dpc (Figure 5.3B,C,D).
b: Anophthalmia in association with reduced telencephalic vesicles and/or frontonasal mass (Figure 5.2C).
c: Anophthalmia with no other forebrain defects (Figure 5.2D).
d: Microphthalmia with no other forebrain defects (Figure 5.2E).

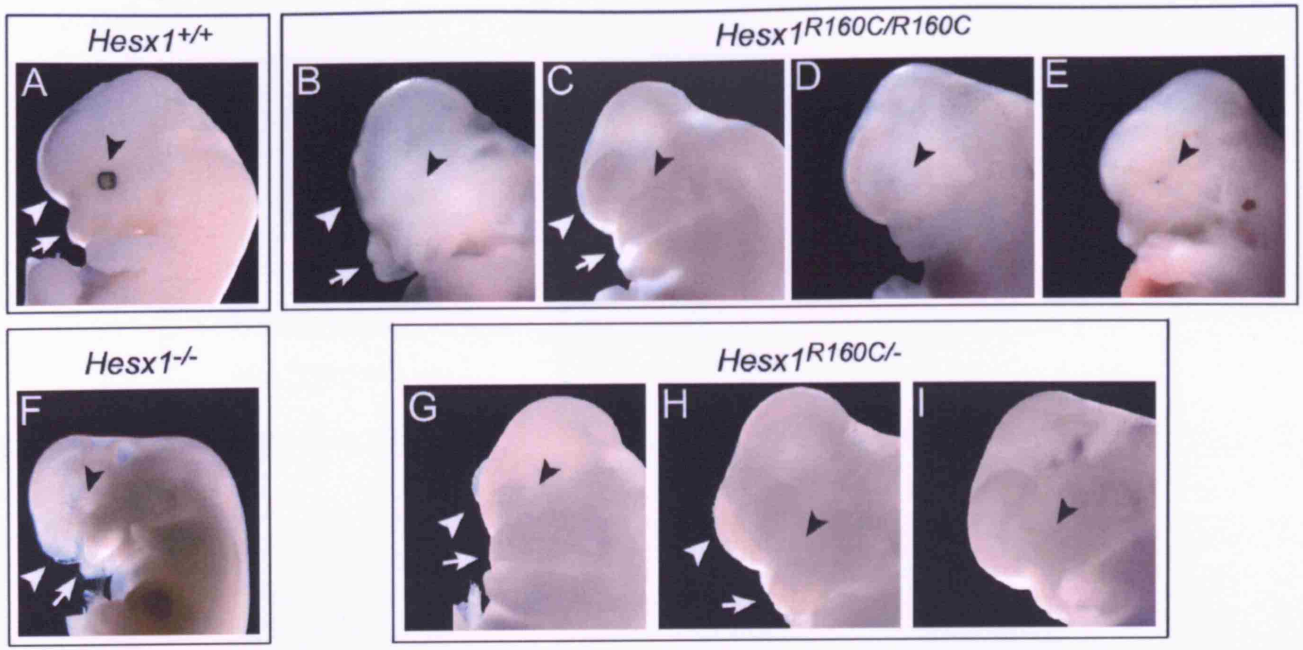

Figure 5.2 – Forebrain defects in *Hesx1*$^{R160C/R160C}$ and *Hesx1*$^{R160C/-}$ embryos at 12.5 dpc. A) Wild-type embryo, displaying normal eyes (black arrowhead), telencephalic vesicles (white arrowhead) and frontonasal mass (white arrow). (B-E) *Hesx1*$^{R160C/R160C}$ embryos show a range of defects: the eyes are absent (black arrowheads in B-D), the telencephalic vesicles are absent (white arrowhead in B) or small (white arrowhead in C), frontonasal mass is also either absent (white arrow in B) or small (white arrow in C). E) The mildest *Hesx1*$^{R160C/R160C}$ embryos only display severe microphthalmia (arrowhead). F) *Hesx1*$^{-/-}$ embryo, displaying a severe phenotype with absent eyes (black arrowhead), telencephalic vesicles (white arrowhead) and frontonasal mass (white arrow). (G-I) *Hesx1*$^{R160C/-}$ embryos show small or absent telencephalic vesicles (arrowhead in G and H), small or absent frontonasal mass (arrow in G and H). The mildest embryos only display severe microphthalmia (arrowhead in I). Notice that the range of defects is similar in Hesx1$^{R160C/-}$ and *Hesx1*$^{R160C/R160C}$ embryos.

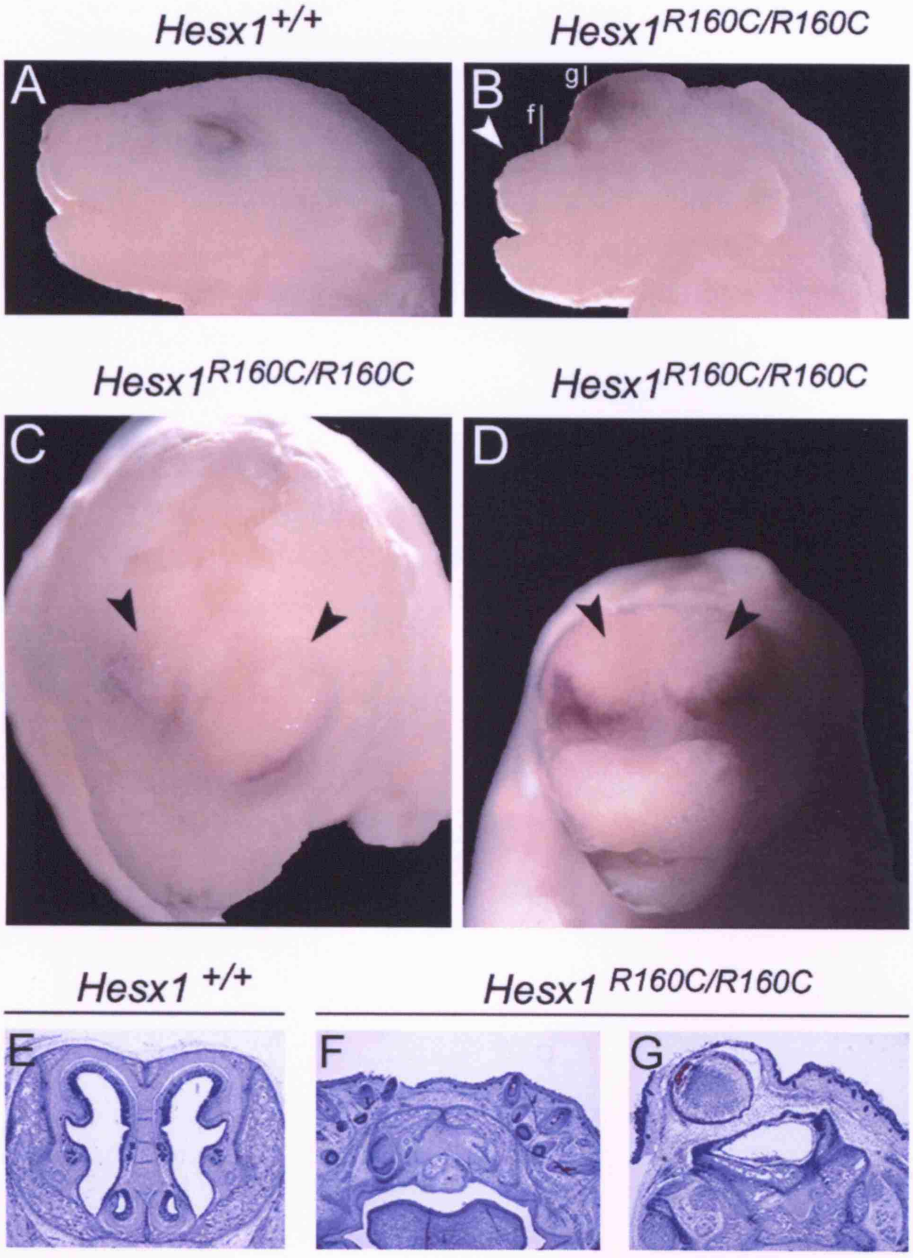

Figure 5.3 – Severe craniofacial defects in *Hesx1*$^{R160C/R160C}$ embryos at 17.5 dpc. A) Lateral view of a wild-type embryo at 17.5 dpc. B) Lateral view of a *Hesx1*$^{R160C/R160C}$ embryo at a similar stage. Notice that the nose is small (white arrowhead) and there are dorsal protrusions in the region of the telencephalon, which is itself small. (C-D) Dorsal and rostral views of *Hesx1*$^{R160C/R160C}$ embryos, demonstrating that these ectopic protrusions are seen both asymmetrically (black arrowheads in C) and symmetrically (black arrowheads in D). (E-G) Hematoxylin and eosin staining of frontal sections of the head of wild-type (E) and *Hesx1*$^{R160C/R160C}$ embryos (F,G) at the level indicated in B (f,g). There are defects in the development of nasal cavities (F) and the presence of a dorsal "eye-like" protrusion (G).

5.1.3. Cell Fate analysis of *Hesx1*-expressing cells in *Hesx1-R160C* embryos

The *Hesx1-Cre* and *Rosa26-floxstop-LacZ* mouse lines (see Chapter 4) were used to generate $Hesx1^{Cre/R160C};R26^{Cond\text{-}lacZ/+}$ embryos. These embryos were collected at 10.5 dpc and analysed after X-Gal staining. As previously reported, in $Hesx1^{Cre/+};R26^{Cond\text{-}lacZ/+}$ embryos (which are phenotypically normal), *lacZ*-positive cells colonise the anterior forebrain structures such as the telencephalon, eyes and ventral diencephalon (Figure 5.4A,C). However, in $Hesx1^{Cre/R160C};R26^{Cond\text{-}lacZ/+}$ embryos, a higher proportion of *lacZ*-expressing cells colonised posterior forebrain regions and the 1st branchial arch (Figure 5.4B,D). This is very similar to the pattern seen in $Hesx1^{Cre/-};R26^{Cond\text{-}lacZ/+}$ embryos (equivalent to $Hesx1^{-/-}$), and in $Hesx1^{Cre/I26T};R26^{Cond\text{-}lacZ/+}$ embryos (equivalent to $Hesx1^{I26T/-}$, Figure 4.5).

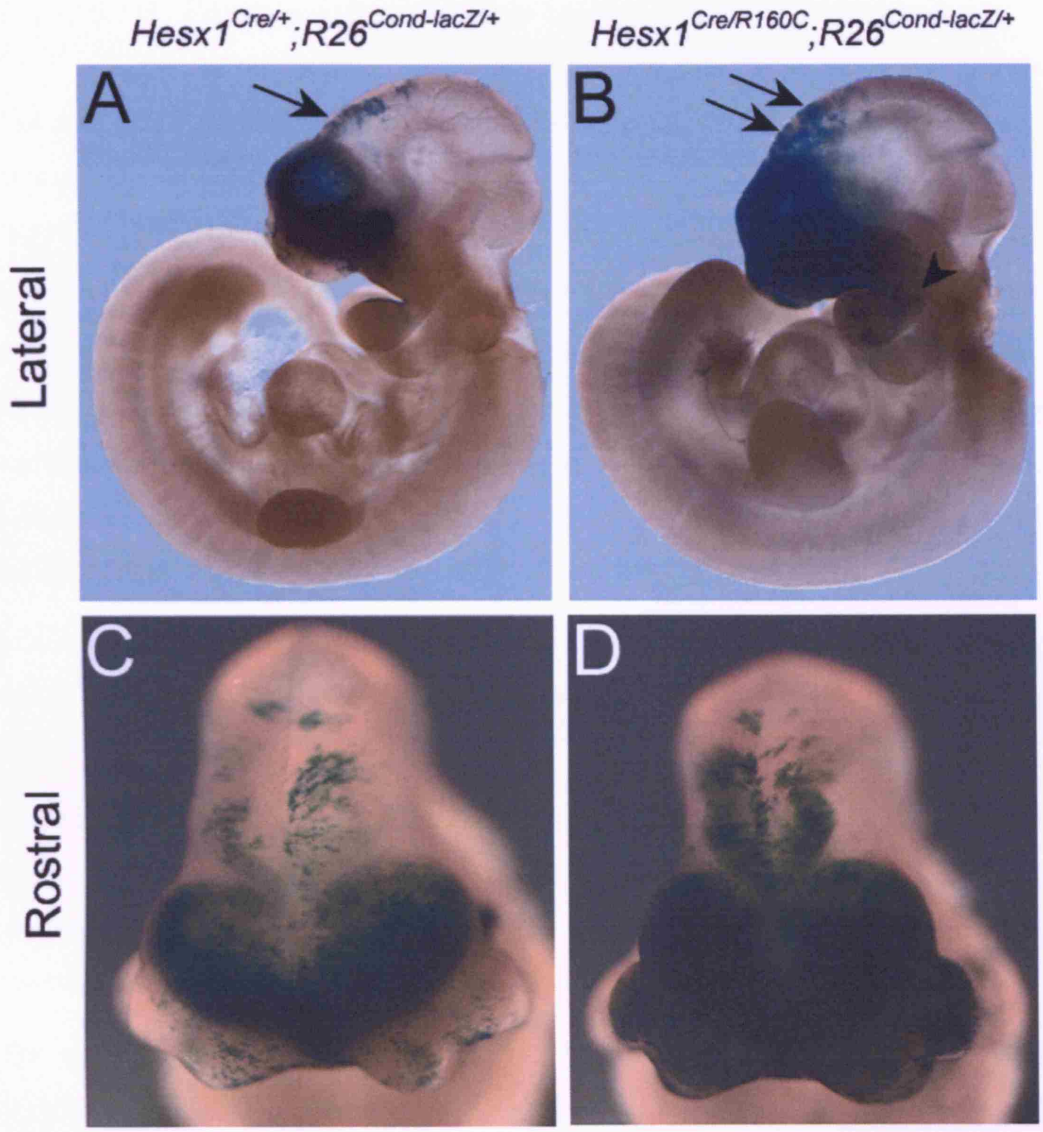

Figure 5.4 – Cell fate analysis in *Hesx1*$^{Cre/R160C}$;*R26*$^{Cond\text{-}lacZ/+}$ embryos. A) X-Gal staining of a *Hesx1*$^{Cre/+}$;*R26*$^{Cond\text{-}lacZ/+}$ embryo at 10.5 dpc, showing that the descendants of *Hesx1*-expressing cells in a control embryo mainly colonise the anterior forebrain, with some reaching the posterior forebrain (arrow). B) An equivalent analysis in a *Hesx1*$^{Cre/R160C}$;*R26*$^{Cond\text{-}lacZ/+}$ embryo, showing that more cells reach the posterior forebrain (arrows) and some colonise the first branchial arch (arrowhead). C and D are the frontal views of embryos depicted A and B, respectively.

5.1.4. Early marker analysis in *Hesx1*$^{R160C/R160C}$ embryos

The same early markers used in the analysis of *Hesx1*$^{I26T/I26T}$ embryos, were used to investigate the nature and onset of anterior neural patterning defects in *Hesx1*$^{R160C/R160C}$ embryos at 8.0-9.0 dpc, using whole mount in-situ hybridisation. In general, patterning defects were fully penetrant with little variability at these stages.

At 8.0 dpc, the *Hesx1* expression domain was significantly reduced in *Hesx1*$^{R160C/R160C}$ embryos (Figure 5.5B). This decrease in *Hesx1* expression correlated with the amount of missing anterior tissue. By 9.0 dpc, this reduction was evident in the anterior forebrain, affecting the future telencephalic vesicles as well as the eyes (Figure 5.5D).

In *Hesx1*$^{R160C/R160C}$ embryos, the expression of *Wnt1* was anteriorised at 8.0 and 9.0 dpc (Figure 5.5F,H). The same rostral expansion of *Wnt1* is seen in *Hesx1*$^{-/-}$ and *Hesx1*$^{I26T/I26T}$ embryos (Figure 4.6).

The expression domain of *Pax6* at 9.0 dpc was also reduced in both the presumptive eye and telencephalic tissues in *Hesx1*$^{R160C/R160C}$ embryos (Figure 5.5J). Furthermore, the expression of both *Fgf8* and *Bf1* were significantly reduced in the anterior forebrain affecting the future telencephalon (data not shown).

The analysis of these early markers in *Hesx1*$^{R160C/R160C}$ embryos revealed more dramatic defects at these stages compared to *Hesx1*$^{I26T/I26T}$ embryos. Neural patterning defects, affected telencephalic as well as the optic vesicles, as previously reported in *Hesx1*$^{-/-}$ mice (Andoniadou et al., 2007; Martinez-Barbera et al., 2000).

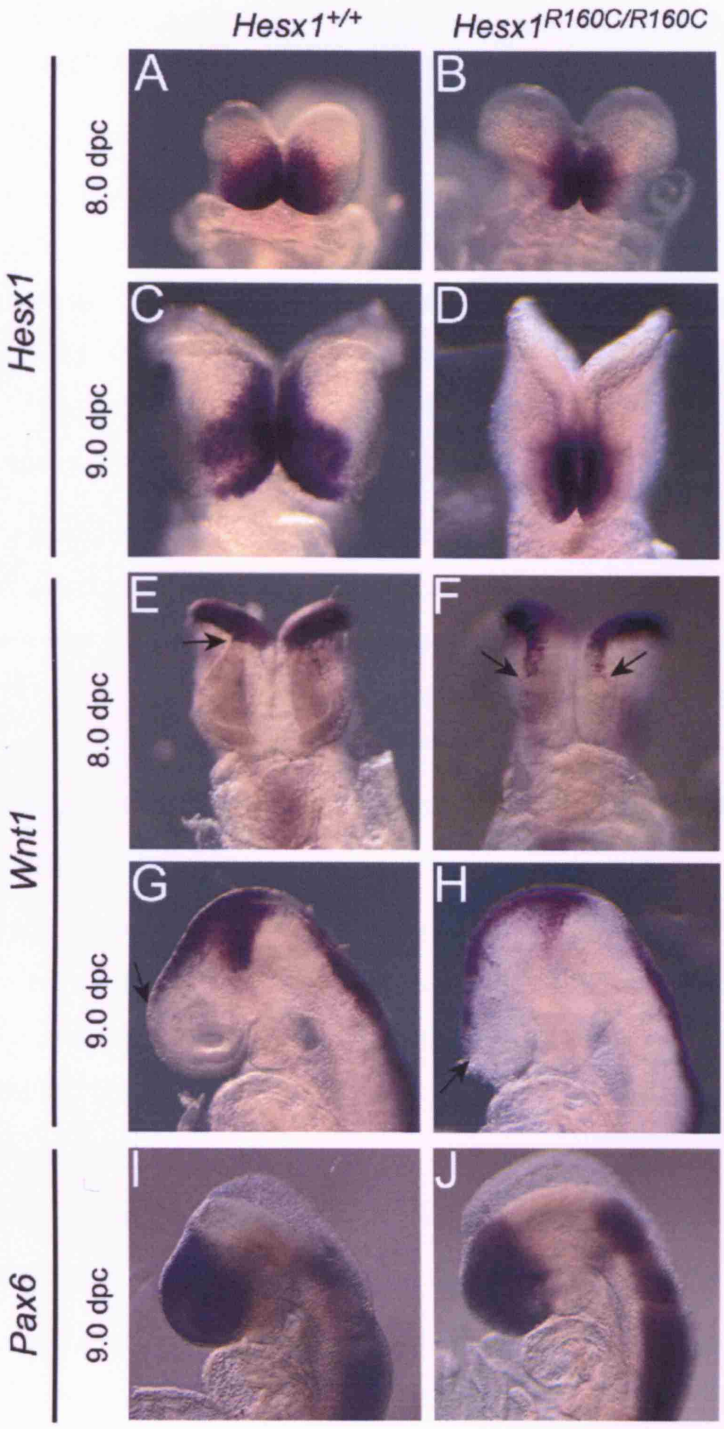

Figure 5.5 – Early forebrain patterning defects in *Hesx1*$^{R160C/R160C}$ embryos. Whole mount in-situ hybridisation in 8.0 dpc (A,B,E,F) and 9.0 dpc (C, D, G-J) embryos with different markers. The riboprobes used are indicated on the left hand side. A-F are rostral views, G-J are lateral views with anterior to the left. (A-D) *Hesx1* expression is reduced in the developing optic cups and anterior neural plate in *Hesx1*$^{R160C/R160C}$ embryos at 8.0-9.0 dpc. (E-H) *Wnt1* expression is anteriorised in *Hesx1*$^{R160C/R160C}$ embryos (arrows in F and H). (I-J) The expression domain of *Pax6* is reduced in the anterior forebrain of *Hesx1*$^{R160C/R160C}$ embryos including the developing optic vesicles as well as the surrounding prospective telencephalic tissues.

5.1.5. Morphological and molecular analysis of pituitary defects in *Hesx1*$^{R160C/R160C}$ embryos

Morphologically, the pituitary was found to be abnormal in all of the *Hesx1*$^{R160C/R160C}$ embryos analysed (n=25). In the majority (15 out of 21 embryos at 12.5-15.5 dpc) of cases, this abnormality was evident from 12.5 dpc when the RP was bifurcated and had multiple lumens. From 15.5 dpc and through to 17.5 dpc, the anterior pituitary was enlarged and its disorganised cells expanded ventrally into the sphenoid cartilage (Figure 5.6). This phenotype was identical in severity compared with that of *Hesx1*$^{I26T/I26T}$ embryos at similar stages of development (Figure 4.8).

Likewise, RP was induced properly at 10.5 dpc, as both *Lhx3* (in the pouch) and *Fgf8* (in the ventral diencephalon) were expressed in the correct domains (Figure 5.7). It should be noted that the expression of *Fgf8* in the anterior commissural plate in the *Hesx1*$^{R160C/R160C}$ embryos was very close to the RP, because of the severely dysmorphic anterior forebrain (Figure 5.7B). However this did not affect the expression domain in the ventral diencephalon, which was unaltered in the mutant compared with wild-type.

Lhx3, *Hesx1* and *Prop1* were expressed properly at 12.5 dpc, although expression domains were enlarged (Figure 5.8A-H). The only exception at this stage was the expression of *Pomc*, which was reduced in the hypothalamic area, but was normally expressed in the RP (Figure 5.8J,L).

By 15.5-16.5 dpc, *Pit1*, *Cga*, *Prop1*, *Lhx3*, and *Pomc* were all expressed in the mutants, indicating that the cell lineages have been specified properly (Figure 5.9 and data not shown).

By 17.5 dpc, the abnormal morphology of the pituitary persisted, but the hormone producing cells were properly differentiated, as shown by normal expression of *Gh*, *Prl*, *Lhb*, *Tshb*, *Cga* and *Pomc* (Figure 5.10).

Interestingly, a second class of RP defects was evident in some *Hesx1*$^{R160C/R160C}$ embryos. This phenotype was invariably correlated with those embryos displaying severe craniofacial defects. In these embryos, due to the severe truncation of forebrain structures as early as 12.5 dpc, RP development was delayed so that it was still attached to the oral ectoderm at this stage (Figure 5.11D). *Lhx3* expression was

expanded rostrally and *Pomc* expression was minimal (Figure 5.11F,H). This is identical to the severe *Hesx1*$^{-/-}$ embryos at a similar stage.

At 15.5 dpc, the craniofacial abnormalities became apparent in these "severe" embryos. As discussed before, the telencephalon and frontonasal mass were reduced or almost absent and in the most extreme case protrusions appeared dorsally, where the telencephalon normally develops. In these mutants, the pituitary gland was recognised as a mass of tissue in the nasopharyngeal cavity (Figure 5.12) and subsequently, it was found ectopically located at the roof of the nasopharynx by 17.5 dpc (Figure 5.13).

This ectopic "nasopharyngeal" pituitary gland can be easily missed in hematoxylin and eosin stained sections, as the structure is severely disorganised and it is also displaced. However, analysis of terminal markers at 17.5 dpc confirmed the presence of pituitary tissue in the dorsal epithelium lining the nasopharynx as *Pomc*, *Gh*, *Cga*, *Tshb*, *Lhb* and *Prl* were expressed there (Figure 5.14 and data not shown).

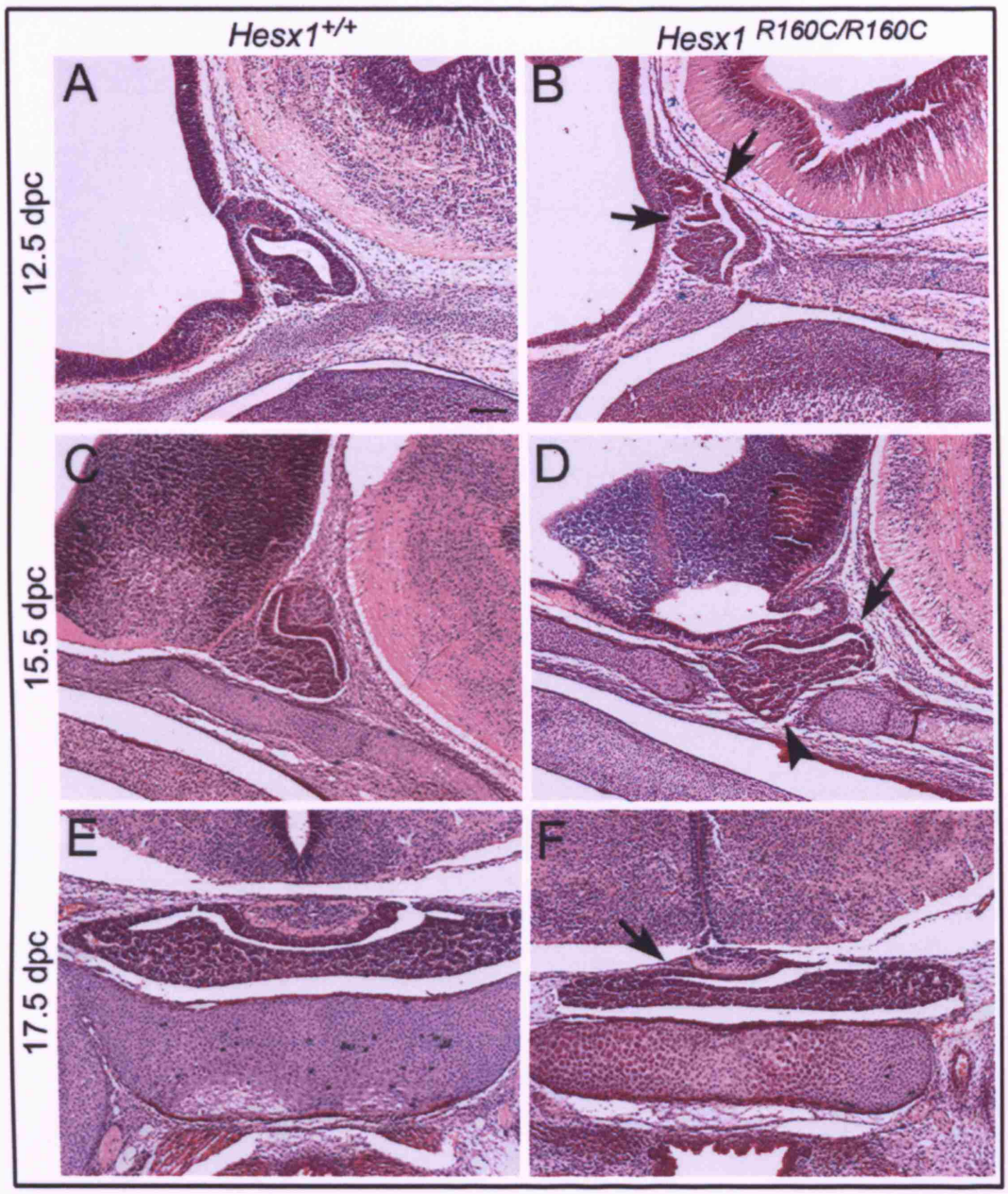

Figure 5.6 – Pituitary defects observed in *Hesx1*$^{R160C/R160C}$ embryos. Hematoxylin and eosin staining of sagittal sections (anterior to the left), showing wild-type Rathke's pouch (RP) at 12.5 dpc (A), 15.5 dpc (C) and in coronal sections at 17.5 dpc (E). B) Defects are seen in RP at 12.5 dpc in *Hesx1*$^{R160C/R160C}$ embryos, with bifurcations and multiple lumens (arrows). The cells in the ventral side of the pouch are often disorganised and expanded. D) By 15.5 dpc, the developing anterior lobe has clearly expanded, preventing the sphenoid bone from fusing (arrowhead). The lumen is abnormal and bifurcated (arrow). F) This abnormality persists at 17.5 dpc (arrow). This phenotype was observed in ~71% of *Hesx1*$^{R160C/R160C}$ embryos (n=21). Scale bar: 0.1 mm.

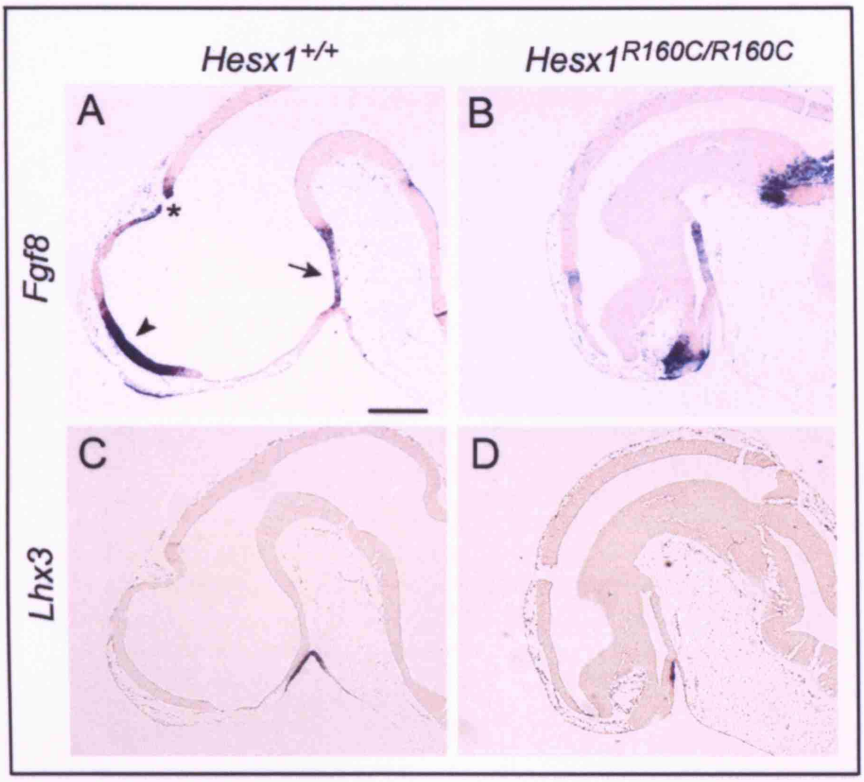

Figure 5.7 – Analysis of *Fgf8* and *Lhx3* in *Hesx1*$^{R160C/R160C}$ embryos at 10.5 dpc. In-situ hybridisation on sagittal sections of 10.5 dpc embryos, with anterior to the left. A) Wild-type embryo, displaying *Fgf8* expression in the commissural plate of the forebrain (arrowhead), roof of the telencephalon (asterisk) and the ventral diencephalon/infundibulum (arrow). B) *Fgf8* expression domain in the ventral diencephalon in *Hesx1*$^{R160C/R160C}$ embryos is similar to wild-type. However, note that the expression in the anterior commissural plate is located very near the pituitary due to the severely abnormal anterior forebrain. C) Wild-type embryo showing *Lhx3* expression in the Rathke's pouch. D) *Lhx3* is expressed in the RP in *Hesx1*$^{R160C/R160C}$ embryos, although the expression domain appears reduced in caudal levels possibly due to a slight developmental delay in the mutant compared with the wild-type embryo. Scale bar: 0.1 mm.

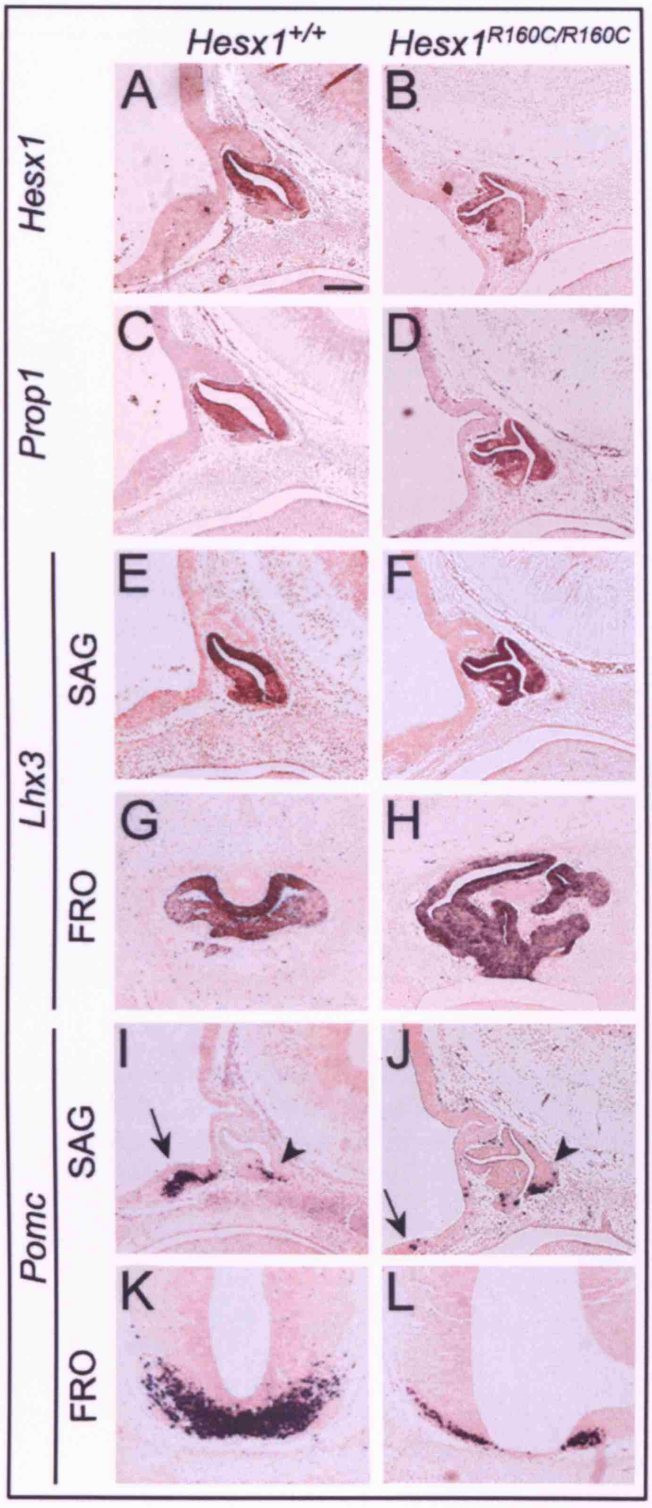

Figure 5.8 – Analysis of pituitary gland markers at 12.5 dpc in *Hesx1*$^{R160C/R160C}$ embryos. In-situ hybridisation on sagittal (SAG) sections, with anterior to the left (A-F, I-J) and on frontal (FRO) sections (G-H, K-L). The riboprobes used are indicated on the left hand side. *Hesx1* (B), *Prop1* (D) and *Lhx3* (F, H) are expressed in *Hesx1*$^{R160C/R160C}$ RP at this stage. The expression of these markers is increased, as the cells in the ventral aspect of the pouch are expanded compared with wild-type (A-G). J) Expression of *Pomc* is normal in the RP (arrowhead) compared with wild-type (I) but it is reduced in the diencephalon (arrow). This is clearly seen in the frontal view (compare L with K). Scale bar: 0.1 mm.

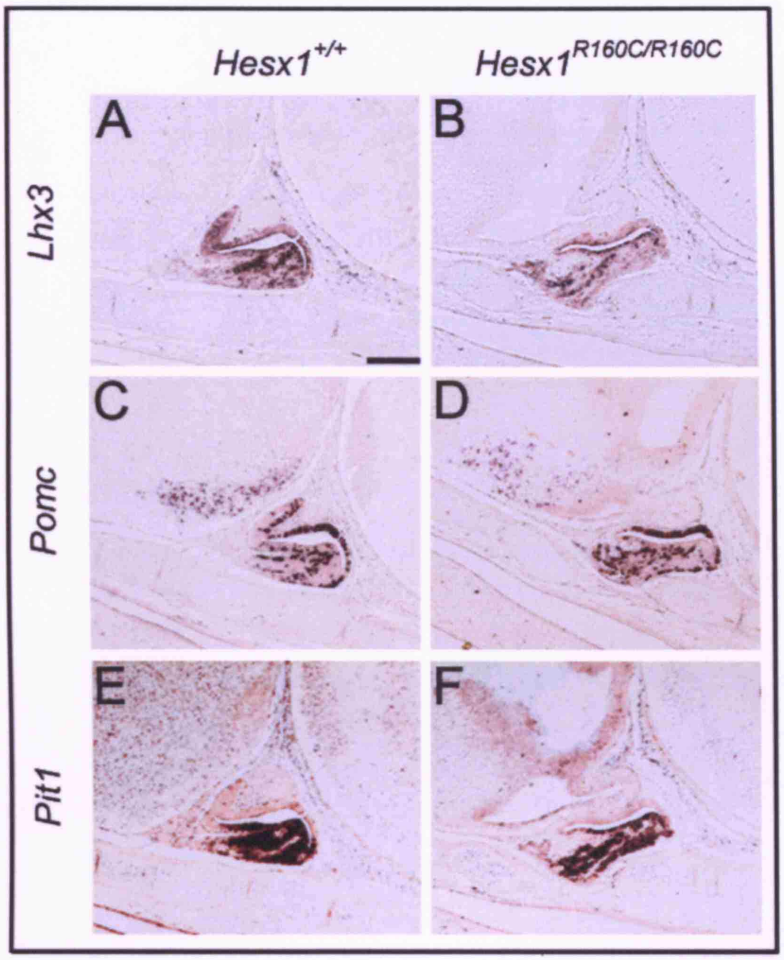

Figure 5.9 – Analysis of pituitary gland markers at 15.5 dpc in *Hesx1*$^{R160C/R160C}$ embryos. In-situ hybridisation on sagittal sections with anterior to the left. The riboprobes used are indicated on the left hand side. (A, B) *Lhx3* is expressed in *Hesx1*$^{R160C/R160C}$ RP at this stage. (C, D) *Pomc* expression in the ventral diencephalon and pituitary gland is similar between genotypes. (E, F) The Pit1 lineage has been specified in *Hesx1*$^{R160C/R160C}$ embryos as shown by correct expression of *Pit1*. Scale bar: 0.1 mm.

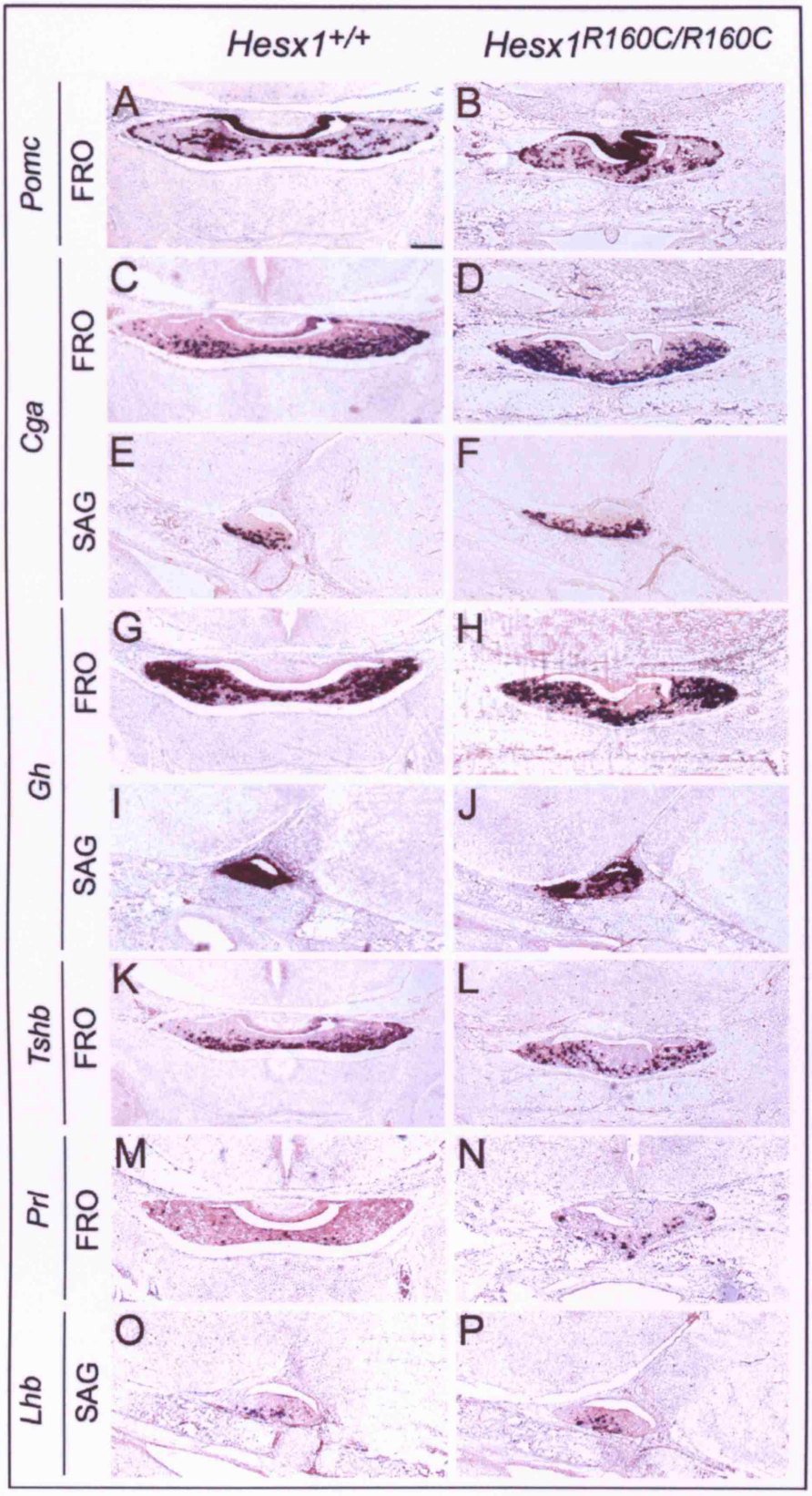

Figure 5.10 – Analysis of terminal differentiation markers at 17.5 dpc in *Hesx1*$^{R160C/R160C}$ embryos. In-situ hybridisation on frontal (FRO) and sagittal (SAG) sections, of *Hesx1*$^{R160C/R160C}$ and wild-type embryos. *Pomc* (A,B), *Cga* (C-F), *Gh* (G-J), *Tshb* (K-L), *Prl* (M-N) and *Lhb* (O-P) are all expressed to the same extent in the pituitary glands of the mutant and control embryos. Scale bar: 0.1 mm.

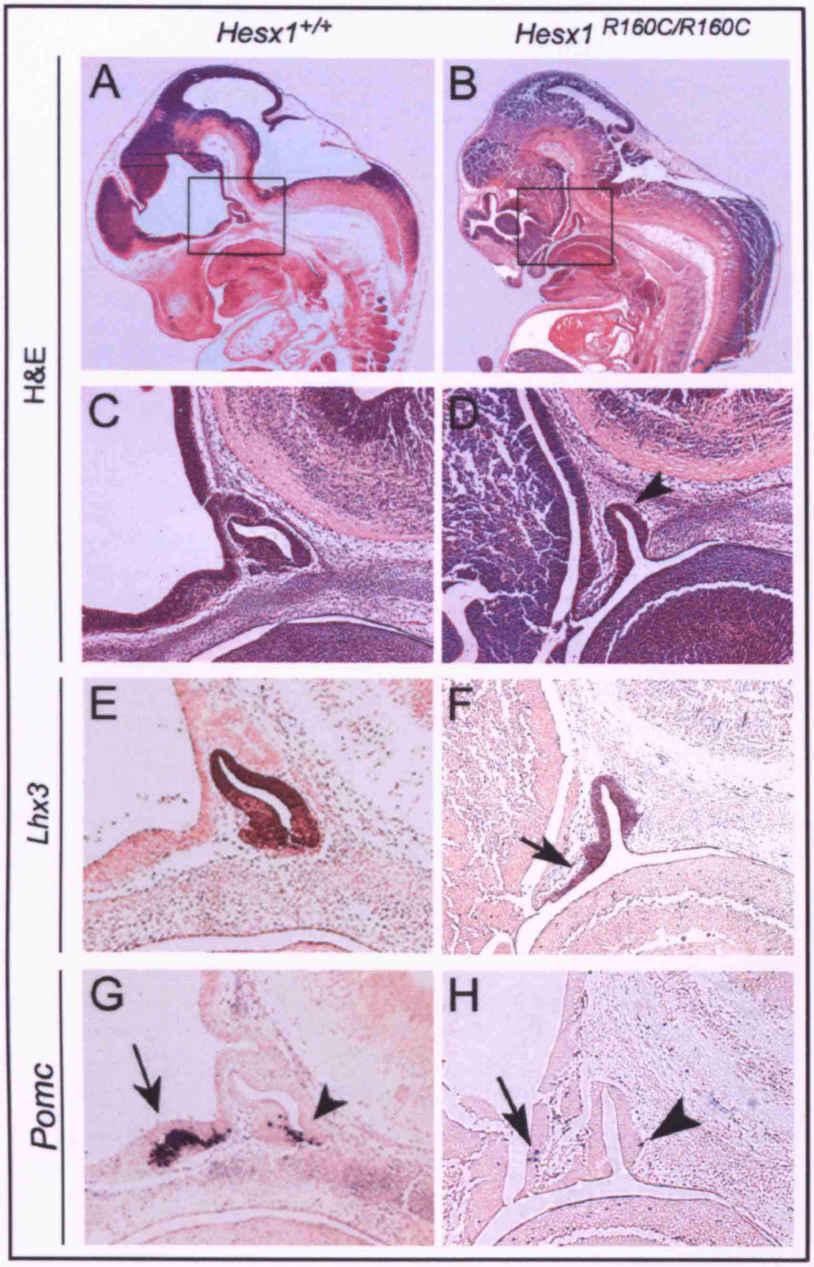

Figure 5.11 – Severe pituitary defects in *Hesx1*$^{R160C/R160C}$ embryos at 12.5 dpc. (A-D) Hematoxylin and eosin staining on sagittal sections of wild-type and *Hesx1*$^{R160C/R160C}$ embryos at 12.5 dpc, with anterior to the left. C and D are the higher magnification images corresponding to the boxed regions in A and B, respectively. Notice that in these severely affected *Hesx1*$^{R160C/R160C}$ embryos, RP development is delayed so that the pouch has not detached from the oral ectoderm (arrowhead in D). (E-H) In-situ hybridisation with *Lhx3*, showing expression in the RP (E). There is a rostral expansion of *Lhx3* expression in these *Hesx1*$^{R160C/R160C}$ embryos (arrow in F). (J-L) In-situ hybridisation with *Pomc*, showing expression in the ventral diencephalon (arrow in G) and the RP (arrowhead in G). *Pomc* is barely detectable in these mutants, except for sporadic cells in both the ventral diencephalon (arrow in H) and the RP (arrowhead in H).

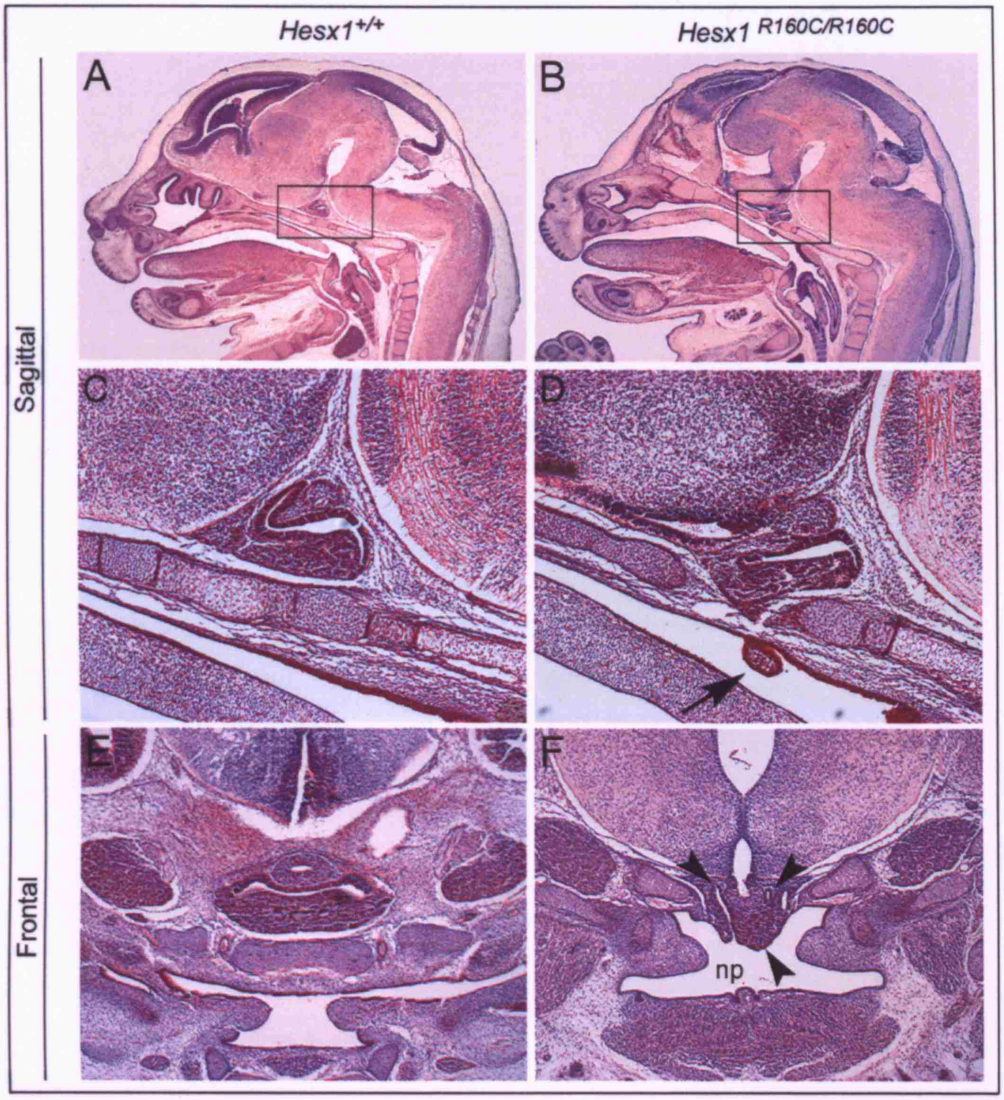

Figure 5.12 – Severe pituitary defects in *Hesx1*$^{R160C/R160C}$ embryos at 15.5 dpc. Hematoxylin and eosin staining on sagittal (A-D) and frontal (E-F) sections, of *Hesx1*$^{R160C/R160C}$ and wild-type embryos at 15.5 dpc. C and D are the higher magnification images, corresponding to the boxed regions in A and B, respectively. Notice the pituitary tissue escaping into the nasopharyngeal cavity of mutant embryos (arrow in D). In the most severely affected *Hesx1*$^{R160C/R160C}$ mutants, the entire pituitary tissue is displaced ventrally into the dorsal wall of the nasopharynx (np), (arrowheads in F).

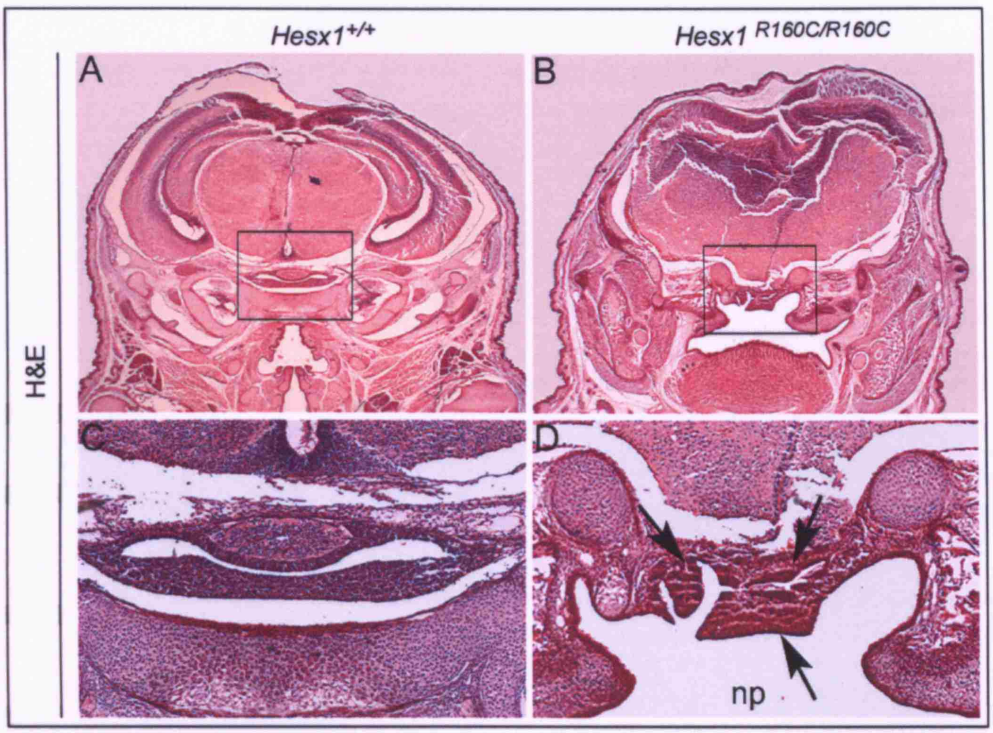

Figure 5.13 – Severe pituitary defects in *Hesx1*$^{R160C/R160C}$ embryos at 17.5 dpc. Hematoxylin and eosin staining on frontal sections of 17.5 dpc *Hesx1*$^{R160C/R160C}$ and wild-type embryos. C and D are the higher magnification images corresponding to the boxed regions in A and B, respectively. Notice that in this class of *Hesx1*$^{R160C/R160C}$ embryos, the telencephalon is severely abnormal (B). The pituitary gland is subsequently pushed ventrally through the basisphenoid bone and lines the dorsal wall of the nasopharynx (arrows in D).

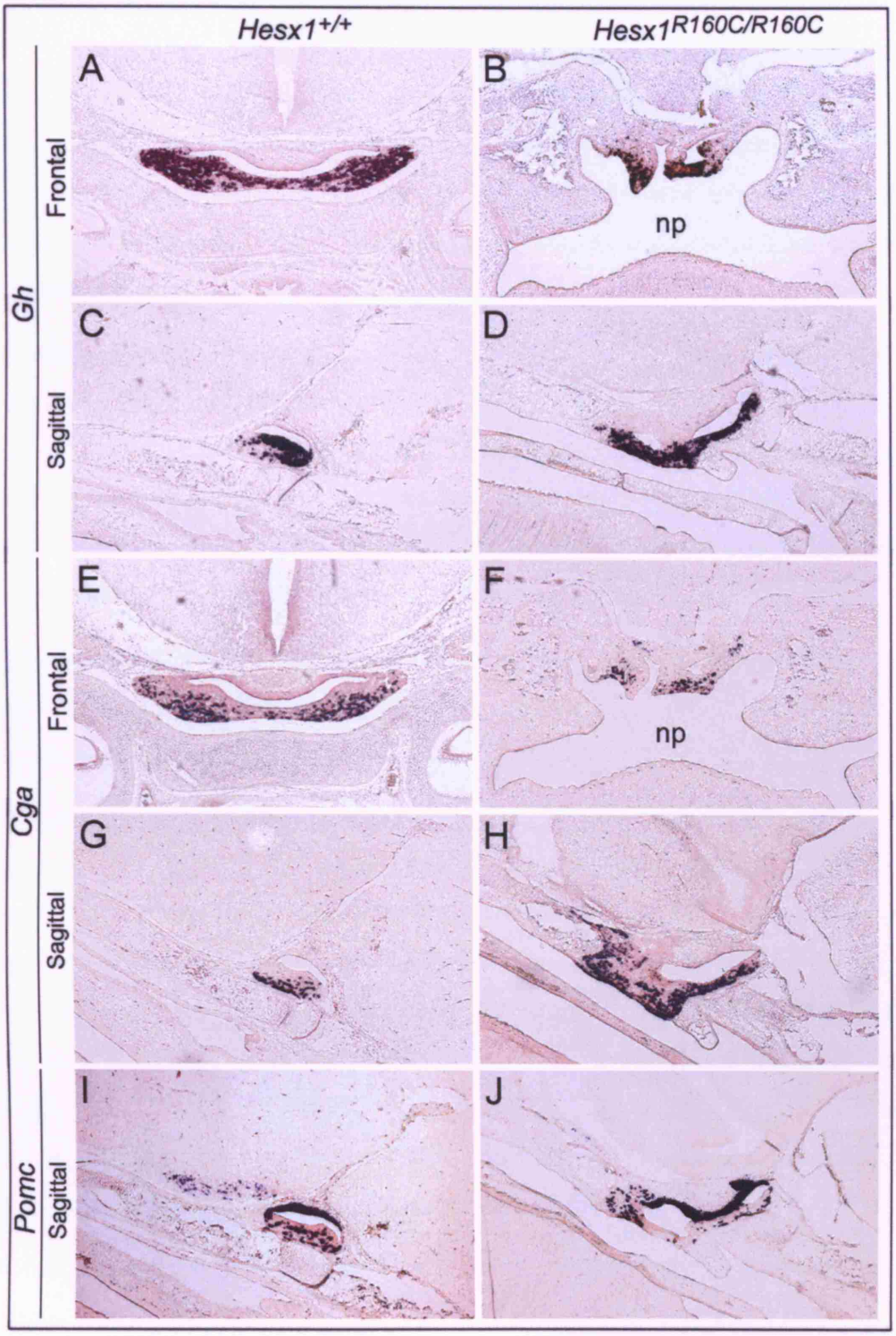

Figure 5.14 – Expression of terminal differentiation markers in the nasopharyngeal pituitary gland at 17.5 dpc. In-situ hybridisation on frontal (A-B and E-F) and sagittal (C-D and G-J) sections of *Hesx1*$^{R160C/R160C}$ and wild-type embryos at 17.5 dpc. The riboprobes used are indicated on the left-hand side of the panels. In this class of severely affected *Hesx1*$^{R160C/R160C}$ mutants, the cells lining the dorsal wall of the nasopharynx (np) express pituitary specific markers such as *Gh* (B) and *Cga* (F). The disorganised and ectopic pituitary gland can be seen in the sagittal views expressing *Gh* (D), *Cga* (H) and *Pomc* (J).

5.2. CONCLUSION

Hesx1$^{R160C/R160C}$ mice show more severe defects compared with *Hesx1*$^{I26T/I26T}$ mutants. This is manifested in fully penetrant eye and pituitary defects in 100%, as well as the occurrence of abnormalities in the telencephalic vesicles and frontonsal mass in ~67% of *Hesx1*$^{R160C/R160C}$ embryos (n=43 for eye and forebrain defects, n=25 for pituitary defects).

Analysis of fore- and midbrain markers, as well as fate mapping revealed that the forebrain is not properly patterned at 8.0 dpc. As shown for *Hesx1*$^{-/-}$ embryos, the early patterning defects in *Hesx1*$^{R160C/R160C}$ embryos are also due to the ongoing posterior transformation of the anterior forebrain. This is shown by the anteriorisation of *Wnt1* and the increased colonisation of *Hesx1* descendants in the posterior forebrain and the 1st bronchial arch in the mutants.

A great majority of homozygous mice die soon after birth. This is partly due to the severe craniofacial defects seen in some of these mice, although this does not account for all of the perinatal lethality.

Both gross morphological and marker analyses of Rathke's pouch (RP) revealed that although, the majority of embryos display comparable pituitary defects to *Hesx1*$^{I26T/I26T}$ embryos, a distinctly more severe phenotype is seen in a small proportion of embryos (~29%, n=21), correlated with severe craniofacial defects. RP development is subsequently, delayed and the pituitary gland is displaced ventrally with only a number of hormone expressing cells lining the dorsal wall of the nasopharynx. In the remaining (and majority) of the homozygous embryos, however, the pituitary is induced normally, but appears expanded by 17.5 dpc, this latter class display defects identical to those seen in *Hesx1*$^{I26T/I26T}$.

Overall, the phenotype in *Hesx1*$^{R160C/R160C}$ mice resembles the one seen in *Hesx1*$^{-/-}$ (Dattani et al., 1998), indicating that *Hesx1-R160C* is effectively a null allele.

6. DISCUSSION

6.1. SUMMARY OF MAIN FINDINGS IN THIS THESIS

Through a yeast two-hybrid screen, five proteins have been identified as interactors of HESX1 (Chapters 2&3; Sajedi et al., 2007). The interaction of HESX1 with DNMT1 is of particular interest as it suggests a novel mechanism of action for HESX1 as a transcriptional repressor (i.e. methylation of DNA). Additionally, analyses of the two mouse models, *Hesx1-R160C* and *Hesx1-I26T*, have revealed that the I26T mutation yields a hypomorphic allele and R160C produces a null allele (Chapters 4&5). Interestingly, the TLE1-mediated repressing activity of HESX1 seems to be primarily required for pituitary development, whilst the eye and telencephalon show a graded sensitivity to impaired HESX1 function.

There are still many unanswered questions, regarding the role of *Hesx1* in forebrain and pituitary development. These points are addressed here according to the existing knowledge of *Hesx1* function and in light of the new findings reported in this thesis, hence providing a good basis for future work.

6.2. FIVE PROTEINS INTERACT DIRECTLY WITH HESX1

Five proteins, selected from a yeast two-hybrid screen, are identified as partners of HESX1. The libraries used in the screen were at stages 9.5-10.5 dpc, corresponding to the time point when *Hesx1* transcripts are expressed both in the ventral forebrain and the Rathke's pouch. The resulting interactions are, therefore, likely to be involved in a broad range of functions carried out by the HESX1 protein.

A brief description of each of these proteins and their functions is provided in section **Error! Reference source not found.**. Three of these proteins (DNMT1, SRFBP1, and SAFB1) are involved in transcriptional repression, whilst the functions of LONP2 and ZFP592 are less known. Binding is demonstrated by the fact that all five interactors were identified several times in the screen and displayed distinct and reproducible interactions with HESX1 sequences in yeast. Additionally, the interactions were shown to be direct,

in GST pull-down assays. Interestingly, results from this assay revealed that different domains of HESX1 interact with different proteins. This is consistent with the previously reported interactions of HESX1 with TLE1 and N-CoR/mSin3/HDAC1/2, which bind different domains of HESX1 (Figure 6.1).

The conserved eh1 and CD2 domains of HESX1 do not selectively interact with any of these proteins, although the interaction with DNMT1 does span this region. The interactions mainly involve the homeodomain and the region adjacent to it. The significance of this is not clear at present, although the homeodomain is known to direct protein-protein interactions in other transcription factors (Stark and Johnson, 1994; Peltenburg and Murre, 1997; Gehring et al., 1994b; Gehring et al., 1994a). Further investigation on the function of each of the HESX1 domains will provide information on the significance of these interactions.

More supporting evidence for these interactions is provided by the localisation of the proteins in mammalian cells as well as the expression pattern of their transcripts in the mouse embryo. HESX1 is primarily a nuclear protein as predicted by its function as a transcription factor. All five proteins co-localise with HESX1 in the nucleus, although LONP2 is also present in the cytoplasm. Furthermore, some of the *HESX1* mutations identified in humans disrupt protein-protein interactions with HESX1 partners (section 6.6).

Given their broad cellular functions, it is not surprising to find that all five interactors are ubiquitously expressed in mouse embryos at 8.5 dpc. This corresponds to the stage when *Hesx1* transcripts are abundant in the ventral forebrain. Thus the transcripts of the five interactors are co-expressed with *Hesx1* in the mouse embryo at this stage. Remarkably, the transcripts of *Dnmt1* and *Safb1* are expressed in the RP at 12.5 dpc, in a pattern that is identical to that of *Hesx1* (high dorsal and low ventral). This opens the possibility that *Dnmt1* and *Safb1* may play more direct roles in the development of the pituitary gland. While there is no direct proof of this either in-vitro or in-vivo, it is interesting to note that the surviving *Safb1*$^{-/-}$ mice display dwarfism, although the pituitary gland has not been analysed (Ivanova et al., 2005).

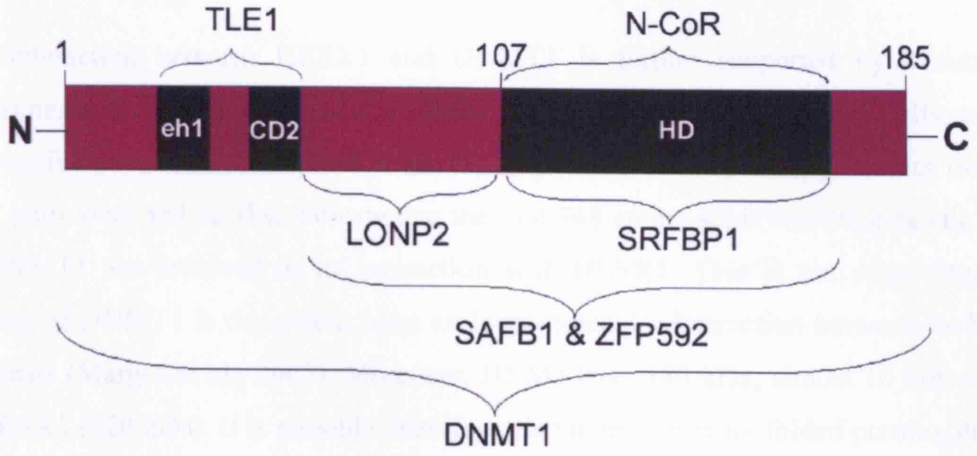

Figure 6.1 – HESX1 regions involved in protein-protein interactions. Schematic representation of the HESX1 protein. The amino (N) and carboxy (C) terminals are indicated. The main domains of the protein are shown in black. LONP2, SRFBP2, SAFB1 and ZFP592 all interact with the C-terminal region of the protein, overlapping with the domain which interacts with N-CoR. TLE1 remains the only identified protein to exclusively interact with the highly conserved consensus eh1/CD2 sequences in the N-terminal. The entire HESX1 protein is involved in its interaction with DNMT1.

6.3. POSSIBLE LINK BETWEEN HESX1 AND DNA METHYLATION

The interaction between HESX1 and DNMT1 is further supported by a number of experiments. Both proteins form complexes with each other in mammalian cells, as shown by positive co-immunoprecipitation (co-IP) experiments. Interestingly, results from both GST pull-down and co-IPs, indicate that the first 748 amino acids and the catalytic domain of DNMT1 are involved in its interaction with HESX1. This is not surprising, as the activity of DNMT1 is dependent upon an intra-molecular interaction between its N and C terminals (Margot et al., 2003). Moreover, DNMT1 is ~180 kDa, almost 10 times the size of HESX1 (~20 kDa). It is possible, therefore, that in the correctly folded protein, the N and C terminals come into contact with each other, forming a pocket into which HESX1 is fitted. This mapping suggests that the whole tertiary structure of both proteins, rather than specific domains, is required for the interaction to take place.

Additionally, the interaction between HESX1 and DNMT1 suggests a novel mechanism for HESX1 repressing activity. DNMT1 is a key epigenetic regulator, involved in transcriptional repression. It is an enzyme responsible for methylation of cytosine at position C5 in CpG dinucleotides. Its activity is controlled in part by its interactions with a number of proteins, including DMAP1, HDAC1/2 and EZH2 among others (Rountree et al., 2000; Robertson et al., 2004; Vire et al., 2006). In fact, the regions which interact with HESX1 are the same ones that mediate its interaction with EZH2 (Vire et al., 2006). EZH2 (Enhancer of Zeste homolog 2) is a Polycomb group histone methyltransferase associated with transcriptional repression (Kuzmichev et al., 2002). It is not inconceivable to hypothesise that HESX1 interacts with DNMT1 in order to repress a set of genes, through DNA methylation.

At present, it is difficult to test this hypothesis due to the lack of existing knowledge on direct targets of HESX1. HESX1 has been shown to bind an artificial sequence (PIII) in-vitro. A recent study has revealed the binding of HESX1 to sites on the *Fshb* promoter, although this is also an in-vitro study (Susa et al., 2007). There are two problems with using these binding sites for methylation and repression studies. Firstly, DNMT1 methylates DNA that is incorporated in chromosomes, but our assays use a plasmid containing the PIII

sequence in transient experiments, thus using "naked" DNA. Secondly, luciferase studies have not been fruitful in the analysis of these interactions, thus the use of an artificial target sequence in these assays (i.e. PIII sequence), may perturb the naturally occurring function of the HESX1/DNMT1 complex.

Nevertheless, it poses a great source for investigation once these targets are elucidated. For example, the presence of methylation target sites as well as their methylation patterns within these promoters, in wild-type and *Hesx1* mutant cells, will shed considerable light on the significance of this interaction. Additionally, it will be possible to clarify whether any of these interactions are implicated in the regulation of HESX1 mediated repression of target genes, HESX1 binding specificity or *Hesx1* regulation.

6.4. ANALYSIS OF *Dnmt1*$^{+/-}$;*Hesx1*$^{+/-}$ MICE

An attempt was made at elucidating the functional significance of this interaction in-vivo, by generating and analysing *Dnmt1*$^{+/-}$;*Hesx1*$^{+/-}$ compound mice and embryos. Unfortunately, no relevant information was obtained from these genetic experiments. Although a proportion of *Dnmt1*$^{+/-}$;*Hesx1*$^{+/-}$ mice (17%, n=59) display microphthalmia or anophthalmia, a similar percentage of *Hesx1*$^{+/-}$ mice also exhibit the same phenotype. Similar results are observed at embryonic stages 12.5-17.5 dpc, when a similar proportion of both *Dnmt1*$^{+/-}$;*Hesx1*$^{+/-}$ (n=20) and *Hesx1*$^{+/-}$ (n=18) embryos display eye defects.

We also find that at earlier stages (10.5 dpc), a low proportion of both *Dnmt1*$^{+/-}$;*Hesx1*$^{+/-}$ (9%, n=20) and *Dnmt1*$^{+/-}$ (8%, n=25) embryos have small telencephalic vesicles. It should be noted that only one *Dnmt1*$^{+/-}$;*Hesx1*$^{+/-}$ embryo displayed a severe developmental delay and abnormal forebrain. However, it is not possible to say with certainty whether it arose as a result of a depleted interaction between HESX1 and DNMT1.

There are two points that remain ambiguous regarding this analysis. Firstly, why a higher proportion of both *Hesx1*$^{+/-}$ and *Dnmt1*$^{+/-}$ embryos, show a phenotype than previously described (Dattani et al., 1998; Li et al., 1992)? This is possibly due to the mixed genetic background created by crossing *Hesx1* and *Dnmt1* mouse lines; these two mouse lines are probably inbred on different backgrounds. Hence, the frequency and severity of phenotype

observed in this work are different compared with previous studies, where the mice are kept on a relatively pure background.

Secondly, why is this phenotype restricted to structures in the forebrain (optic and telencephalic vesicles)? This point is puzzling and cannot be explained on the basis of the current analysis, although interestingly, reduction of *Dnmt1* leads to microcephaly in *Xenopus* embryos (Stancheva and Meehan, 2000).

6.5. INTERACTIONS IN MAMMALIAN CELL LINES

SRFBP1 is also able to immunoprecipitate in a complex with HESX1 in HEK293T cells. However, similar attempts with the other three proteins showed that SAFB1 and LONP2 were not extracted at detectable levels. Alternative lysis conditions and cell lines did not yield optimal levels of either protein for co-immunoprecipitation studies. ZFP592 was not expressed at detectable levels in either HEK293T or CHO cells. Therefore, although these three proteins co-localise with HESX1 in CHO cells, their interactions are yet to be verified in a mammalian cell system.

An attempt was made at detecting interactions in cells using the dual luciferase system. Firstly, a two-hybrid assay was set up using GAL4DBD-HESX1 and VP16AD-interactor. Although the interaction between HESX1 and TLE1 was reproducible in a similar assay, the five interactors identified here were unable to activate reporter activity when co-expressed with GAL4DBD-HESX1. This is very puzzling as the yeast two-hybrid uses a very similar principle. However, the protein and DNA environment of a yeast cell is different from that of a mammalian cell. The presence and/or absence of a number of factors in the mammalian cell lines may impede such studies.

Secondly, a one-hybrid assay was set up in order to investigate the functional significance of these interactions. This assay was only an attempt at elucidating whether the repressing activity of HESX1 could be affected by its interaction(s) with one or all of these proteins. Although the assays were again not fruitful on that account, the possibility cannot be ruled out. This system relies on either Gal4-BS, or the PIII sequence, as potential sites for binding of HESX1. However, they may not mimic the complex environment in which

HESX1 binds its targets, requiring the overlapping and synchronised activities of multiple proteins. Alternatively, the function of some of these interactions may lie in other activities, distinct from repression, such as the regulation of *Hesx1* and/or other genes by recruitment of other, as yet unidentified, factors.

6.6. *HESX1* MUTATIONS DISRUPT SPECIFIC INTERACTIONS

A very informative finding, regarding the interaction of HESX1 and the five named proteins, came from the use of seven human HESX1 proteins with specific mutations, originally identified in human patients. Six of these proteins bear missense mutations resulting in single amino acid substitutions (T181A, V129I, E149K, Q6H, I26T and R160C) and one is the result of the insertion of two nucleotides causing a frameshift mutation (306/307insAG). My results suggest that the binding between HESX1 and some of its interacting proteins is disrupted by specific mutations.

For example, the interaction with SRFBP1 is disrupted by two point mutations, namely I26T and R160C. The interaction between LONP2 is specifically abrogated by the two mutations that cause SOD in humans (R160C and 306/307insAG). It remains to be determined whether the abrogation of the interation of HESX1 with LONP2, is the cause of the more severe phenotype seen in the human patients. Additionally, a pattern is observed where the severity of the phenotype caused by a mutation in humans, is associated with the disruption of a higher number of protein interactions.

Given the roles played by these proteins in a broad range of cell types and their expression during embryogenesis, it is unlikely that mutations in their genes directly result in SOD and hypopituitarism, although the possibility remains open. However, it is probable that these genes act as modifiers involved in the pathogenesis of SOD and hypopituitarism. These human conditions are highly variable and involve mutations in many genes as well as environmental factors. The complexity of these disorders implies the likely involvement of other, as yet unidentified, genes. The identification of these novel HESX1 interactions may facilitate the task of identifying such genes, in the future.

6.7. *HESX1-I26T* CAUSES A MILDER PHENOTYPE IN MICE COMPARED TO *HESX1-R160C*

Hesx1$^{I26T/I26T}$ mice show a milder phenotype compared with either *Hesx1*$^{R160C/R160C}$ or *Hesx1*$^{-/-}$ mice ($p<0.01$ for both severity and penetrance between the two genotypes). *Hesx1*$^{R160C/R160C}$ mice, on the other hand, display a phenotype analogous to that described for *Hesx1*$^{-/-}$ mutants. This is supported by a number of findings. Firstly, phenotypic defects in *Hesx1*$^{I26T/I26T}$ mice and embryos are restricted to the eyes and the pituitary gland. Other forebrain defects are, in general, absent in both embryos and adult mice of this genotype. Hence, in general, homozygous embryos display normal telencephalic vesicles and frontonasal mass and adults display a normal head, nose and intercerebral commissures. Whereas, ~67% of *Hesx1*$^{R160C/R160C}$ mutants (n=43) display some level of truncation in telencephalic and olfactory structures. Intercerebral commissures, such as the corpus callosum and the anterior commissures are also affected in these animals.

Secondly, eye defects (microphthalmia and anophthalmia) are not fully penetrant in *Hesx1*$^{I26T/I26T}$ mutants, as only ~74% of adults (n=50) and ~76% of embryos (n=41), show visible eye abnormalities. Whether the functionality of the eyes is affected in those animals with normal eyes remains to be determined. Conversely, eye abnormalities are fully penetrant in *Hesx1*$^{R160C/R160C}$ embryos.

It should be noted that although there is an occurrence of ~7% perinatal lethality in *Hesx1*$^{I26T/I26T}$ mice, this is not statistically significant (n=271; Table 4.1). Therefore, homozygous mice are, by and large, viable and fertile. On the other hand, *Hesx1*$^{R160C/R160C}$ mice mostly die perinatally, with only 3% of homozygous animals surviving after birth (n=146; Table 5.1). One of the underlying causes of lethality in these mutants is the occurrence of severe craniofacial defects in some of the homozygous neonates. The reason of death is unknown, although these defects may result in breathing problems in the neonates, since the nose is generally affected. Moreover, severe craniofacial defects might impose a restraint on the hypothalamic nuclei, causing defects in the normal control of the hypothalamic-pituitary axis soon after birth.

However, craniofacial defects cannot explain the main reason underlying neonatal death in the homozygous mutants, as this phenotype is only seen in around ~33% of embryos. Since pituitary defects are fully penetrant, it is highly likely that hormone deficiencies also contribute to the cause of death. It is, however, unknown why only a small percentage of *Hesx1*$^{I26T/I26T}$ mice die, when the pituitary defects at embryonic stages are similar to *Hesx1*$^{R160C/R160C}$. Further analysis of the hypothalamus as well as hormone levels in the neonates and surviving adults is required in order to address these issues. For example, ACTH deficiency generally results in death (Brodsky et al., 1997; Turton et al., 2006; Weintrob et al., 2006); therefore, a possibility is that *Hesx1*$^{R160C/R160C}$ mice exhibit low levels of this hormone, whilst *Hesx1*$^{I26T/I26T}$ mice do not.

6.8. HESX1 REPRESSING ACTIVITY IS NECESSARY FOR EARLY FOREBRAIN PATTERNING

What do these results show about the role of HESX1 protein in early forebrain development? As mentioned in chapter 1, *Hesx1* is required in the anterior neural ectoderm for the expansion of forebrain, after its initial induction (Martinez-Barbera et al., 2000). It is thought to achieve this by antagonising members of the Wnt/β-catenin signalling pathway and thereby inhibiting posteriorising signals in the anterior forebrain (Andoniadou et al., 2007).

Evidence from *Hesx1*$^{I26T/I26T}$ mice also supports these ideas, albeit the effect is not as prominent in these animals compared with *Hesx1*$^{-/-}$ and *Hesx1*$^{R160C/R160C}$ mutants. For example, markers expressed in the anterior forebrain such as *Pax6*, *Bf1* and *Fgf8* are reduced in both *Hesx1*$^{I26T/I26T}$ and *Hesx1*$^{R160C/R160C}$ embryos at 8.5 dpc. However, whilst this reduction is observed in the presumptive optic vesicles of *Hesx1*$^{I26T/I26T}$ embryos, in *Hesx1*$^{R160C/R160C}$ mutants both the presumptive optic and the telencephalic vesicles are affected. *Hesx1* itself is clearly only absent from eye precursors of *Hesx1*$^{I26T/I26T}$ embryos at 8.5 dpc, being expressed to the same levels as wild-type in the midline anterior neural plate. In *Hesx1*$^{R160C/R160C}$ embryos, on the other hand, the expression of *Hesx1* in the anterior neural ectoderm is also reduced. The similarity between

Hesx1$^{R160C/R160C}$ and *Hesx1*$^{I26T/I26T}$ is portrayed by the expression of *Wnt1*, which is expanded rostrally in both cases.

We show here, however, that the various forebrain structures affected in *Hesx1*$^{-/-}$ mice display different sensitivities to HESX1 repressing activity. The pituitary gland is the most sensitive followed by the eyes and finally the telencephalon and frontonasal mass. The sensitivity of the eye tissue to HESX1-impaired function, shown by these two mouse models, also supports its role as an anti-Wnt/β-catenin factor. This is further demonstrated in other studies. For example, overexpressing *Hesx1* in the anterior forebrain of *Hesx1*$^{-/-}$ embryos rescues eye defects last, as they require a higher dosage of *Hesx1* (Andoniadou et al., 2007). In frogs and zebrafish, the overactivation of Wnt/β-catenin in the forebrain, affects eye development first, followed by the telencephalon (Fredieu et al., 1997; van de et al., 2001).

6.9. PITUITARY DEVELOPMENT IS DISRUPTED IN BOTH *Hesx1*$^{I26T/I26T}$ AND *Hesx1*$^{R160C/R160C}$ EMBRYOS

As previously mentioned, the pituitary gland is the main tissue affected in *Hesx1*$^{I26T/I26T}$ embryos, being abnormal in every mutant. Similarly, *Hesx1*$^{R160C/R160C}$ embryos display fully penetrant pituitary defects. It is worth noting that ~33% of *Hesx1*$^{R160C/R160C}$ embryos display a more severe phenotype, which is correlated with the more severe forebrain defects.

In *Hesx1*$^{I26T/I26T}$ and ~67% of *Hesx1*$^{R160C/R160C}$ embryos, the Rathke's pouch is induced normally as shown by normal expression of markers such as *Lhx3* (in the RP) and *Fgf8* (in the infundibulum), at 10.5 dpc. The shape of the pouch is also normal at this stage compared with the wild-type counterparts. From 12.5 dpc onwards, however, these homozygous embryos show a morphologically abnormal RP as shown by bifurcations, multiple lumens and an expanded anterior lobe.

An interesting feature of this phenotype is that although the shape of the RP is abnormal from 12.5 dpc, all early and late markers of the pituitary are expressed. Cell lineages are

properly specified as shown by expression of *Lhx3* and *Prop1* at 12.5 dpc and are properly differentiated as *Pit1* and *Cga* are expressed correctly at 15.5 dpc. In fact, the region expressing *Lhx3* is expanded and subsequently the regions expressing *Prop1* and *Pit1* are also expanded. This culminates in an enlarged anterior lobe, shown by a larger area expressing *Gh*, *Tshb*, *Prl* and *Lhb* at 17.5 dpc.

The only difference is in the expression of *Pomc* at 12.5 dpc, which is reduced in the ventral diencephalon of both mutants. This cell lineage is, however, correctly specified by 15.5 dpc and the early reduction is possibly due to abnormalities in the hypothalamus in these mice. Contact between the primordium of the pituitary is important for the formation of the ventral diencephalon and for the differentiation/proliferation of *Pomc* expressing neurons in the rat hypothalamus (Daikoku et al., 1983). So it is possible that the initial reduction of *Pomc* expressing cells in all three *Hesx1* mouse mutants is a secondary phenotype, caused as a result of disruptions in the contact between RP and infundibulum. Once this contact is made later (because of a developmental delay), *Pomc* expression returns to normal.

As mentioned above, a more severe phenotype is observed in a smaller proportion of $Hesx1^{-/-}$ and $Hesx1^{R160C/R160C}$ embryos. In these mutants, pituitary development is delayed, as the RP remains attached to the oral ectoderm at 12.5 dpc, resembling the pouch at 11.0 dpc (Figure 5.11). In the absence of anterior forebrain tissue, head morphogenesis and formation of bone structures cause a ventral displacement of midline structures. This leads to severe craniofacial defects, disruptions in the development of sphenoid cartilage, which are the underlying cause of the displacement of the pituitary gland in the nasopharyngeal cavity. Therefore, although the pituitary gland is not recognisable by 17.5 dpc, dotted expression of pituitary markers (*Gh*, *Cga*, *Tshb* and *Pomc*) in cells lining the dorsal wall of the nasopharynx, confirm its presence there. This does not take place in $Hesx1^{I26T/I26T}$ embryos because the acute forebrain truncations are generally absent in these mutants.

An investigation into the timing of the appearance of each of the pituitary cell types in *Hesx1* mutant embryos, and the conditional inactivation of *Hesx1* in the pituitary gland

and/or telencephalon, will be very informative in establishing the role of *Hesx1* in the development of these structures.

6.10. MOLECULAR MECHANISMS UNDERLYING FOREBRAIN AND PITUITARY DEFECTS IN *Hesx1*$^{I26T/I26T}$ AND *Hesx1*$^{R160C/R160C}$ MUTANTS

Undoubtedly, the repressor activity of HESX1 is very important for the correct development of the pituitary gland, as two copies of a mutant protein with reduced repressing activity (HESX1-I26T) are unable to even partially rescue the defects. One of the reasons underlying the reduced repressing activity of HESX1-I26T, is thought to be its inability to bind TLE1 (Carvalho et al., 2003). This Groucho related protein is a corepressor and presumably aids the repression mediated by HESX1. The HESX1/TLE1 interaction has also been previously shown to be essential for pituitary development (Dasen et al., 2001). The analysis of *Hesx1*$^{I26T/I26T}$ embryos in this thesis, reiterates that this interaction is absolutely required for HESX1 function in the anterior pituitary. In these mice, *Hesx1* is expressed but the mutant HESX1-I26T is unable to recruit TLE1. This is, therefore, a perfect in-vivo model for analysing the function of HESX1, devoid of its interaction with TLE1.

Interestingly, TLE1 has been shown to be important in eye development, through its interaction with SIX3 and SIX6 in this organ (Lopez-Rios et al., 2003). *Six3* displays a similar expression pattern to *Hesx1* during early forebrain development (Oliver et al., 1995). *Six3*$^{-/-}$ mice show forebrain truncations affecting structures such as the telencephalon, eyes and the nose, similar to *Hesx1*$^{-/-}$ mice (Lagutin et al., 2003). *Tle1* and *Six3* are both abundantly expressed in the RP (Dasen et al., 2001; Oliver et al., 1995) and there is also growing evidence that *Hesx1* and *Six3* cooperate in the correct development of the pituitary gland (Gaston-Massuet et al., in press). Additionally, another member of the *tle* gene family, *Aes,* has been shown to be essential for pituitary development (Brinkmeier et al., 2003). *Aes* is also involved in the development of the eye by interacting with *Six3* in this tissue during embryonic development (Lopez-Rios et al., 2003; Zhu et al., 2002). It is,

therefore, likely that members of the *tle* gene family, *Hesx1* and *Six3* have cooperative roles in the development of both the eye and the pituitary gland.

In the forebrain primordium, *Hesx1* acts as a Wnt/β-catenin antagonising factor. It is still unclear whether Wnt/β-catenin signalling is also the target of *Hesx1* action in the pituitary gland. If this is the case, the analysis of *Pitx2* expression in the RP of *Hesx1* mutant embryos might be particularly insightful. This transcription factor is induced by the Wnt/β-catenin pathway. Therefore, if *Hesx1* negatively regulates this pathway in the RP, *Pitx2* expression would be expected to be upregulated in *Hesx1* mutants. *Pitx2,* in cooperation with *Pitx1,* normally promotes cell proliferation by recruiting cofactors necessary for cyclin D2 induction (Kioussi et al., 2002). Therefore, it can be speculated that in the absence of *Hesx1, Pitx2* upregulation leads to increased proliferation in the anterior pituitary. In fact, results from our group have shown that the cellular mechanism underlying the anterior pituitary enlargement in $Hesx1^{-/-}$ mutants is the enhanced proliferation of periluminal progenitors of the RP at 12.5 dpc (Gaston-Massuet et al., in press).

As discussed above, compelling evidence suggests that the interaction of HESX1 and TLE1 is essential in the pituitary gland, but is this interaction also a general requirement for *Hesx1* action in the forebrain? Our data with $Hesx1^{I26T/I26T}$ mice indicates that although this TLE1 mediated repression activity of HESX1 is important in the forebrain, it is not absolutely required. It also highlights the different sensitivity of various forebrain tissues to *Hesx1* but still leaves open the possibility that *Hesx1* may recruit additional factors in the forebrain. For example, as discussed previously (p. 193), two *HESX1* mutations associated with SOD in humans (R160C and 306/307inAG) both result in the loss of interaction with LONP2, suggesting that this interaction may be exclusively required in telencephalic precursors.

6.11. *Hesx1-I26T* IS A HYPOMORPHIC ALLELE, WHILST *Hesx1-R160C* IS A NULL ALLELE

These data increasingly support the idea that I26T is a hypomorphic allele, whilst R160C is a null allele. The above results can be explained in context of the previous in-vitro data, since the HESX1-I26T protein has reduced repressing activity (i.e. its repressing activity is

not completely lost), as well as an intact DNA-binding ability (Carvalho et al., 2003). It, therefore, seems that with two copies of the HESX1-I26T mutant protein, HESX1 targets are still repressed, although to a lesser extent than in the wild-type. Our data supports this, as shown by the dosage effect observed in embryos carrying one copy of *Hesx1-I26T* and one copy of the null allele (*Hesx1*$^{I26T/-}$), versus two copies of *Hesx1-I26T* allele (*Hesx1*$^{I26T/I26T}$). *Hesx1*$^{I26T/-}$ embryos exhibit an increase in both severity and penetrance of the forebrain defects compared to *Hesx1*$^{I26T/I26T}$ embryos.

The HESX1-R160C protein, however, completely lacks a DNA binding ability and in fact abrogates the DNA binding ability of the wild-type HESX1 in-vitro (Dattani et al., 1998; Brickman et al., 2001). This is consistent with the knowledge that R160 is the critical residue located in the third helix of the homeodomain, which makes direct contact with DNA (Chi, 2005). Additionally, the dosage effect seen in *Hesx1*$^{I26T/I26T}$ and *Hesx1*$^{I26T/-}$ embryos is not observed in embryos with two copies of *Hesx1-R160C* allele or one copy of *Hesx1-R160C* and one copy of the null allele (i.e. *Hesx1*$^{R160C/R160C}$ and *Hesx1*$^{R160C/-}$ embryos are similar in severity of phenotype).

Similarly, fate map analysis in *Hesx1*$^{Cre/I26T}$;*R26*$^{cond\text{-}lacZ/+}$ embryos shows that reduced HESX1 repressing activity, results in the same posterior transformation of anterior forebrain as seen in the absence of *Hesx1*. It should be noted, however, that these embryos carry one copy of *Hesx1-I26T* and one copy of *Hesx1-Cre*; they are hence equivalent to *Hesx1*$^{I26T/-}$ embryos. Likewise, fate mapping analysis in *Hesx1*$^{Cre/R160C}$;*R26*$^{cond\text{-}lacZ/+}$ embryos has shown the same posterior transformation of anterior forebrain tissue seen in the absence of *Hesx1*.

We have recently found that although HESX1 and HESX1-I26T are primarily nuclear proteins, this nuclear localisation is disrupted in HESX1-R160C, some of which remain in the cytoplasm (Sajedi et al., in press). These findings demonstrate that HESX1-R160C is a dysfunctional protein that is unable to fully localise to the nucleus, reinforcing the fact that the R160C mutation results in null allele of *Hesx1*. These data may explain why there is no phenotype in *Hesx1*$^{R160C/+}$ humans and mice.

6.12. VARIABILITY OF PHENOTYPE

One common feature in the phenotype caused by the three *Hesx1* alleles (null, I26T and R160C), is the variability in severity. In brief, the range of phenotypic features of mice homozygous for either of these alleles is essentially the same, except that they each affect the forebrain to a different extent. One way of looking at the phenotype portrayed by these mice, is in the form of a spectrum (Figure 6.2). The severity of the allele is hence determined by the frequency of occurrence of each of the phenotypic defects. In this scale, homozygosity for *Hesx1-I26T* is at the mild end of the scale, whilst the *Hesx1* null is at the opposite end. *Hesx1-R160C* is very close to the null allele, although the occurrence of the very severe phenotype is slightly lower in $Hesx1^{R160C/R160C}$, since the genetic background of this line is still relatively mixed compared to $Hesx1^{-/-}$ mice.

Although, the genetic background of the I26T and R160C lines is still not homogeneous, a mixed genetic background may not be the only reason underlying the variable expressivity of phenotype, since a similar phenomenon is observed in $Hesx1^{-/-}$ mutants, which have been kept on a C57BL/6J background for more than 20 generations. In agreement with this, human patients with SOD and hypopituitarism also display highly variable phenotypes (Chapter 1).

One possible explanation is a variation in gene expression caused by epigenetic factors. For example, differential methylation patterns have been shown as an underlying cause of differential gene expression in identical twins (Fraga et al., 2005). It is thought that environmental factors acting on identical genotypes can influence gene expression, which in turn leads to phenotypic differences. Indeed, we show here that HESX1 interacts with DNMT1 (Sajedi et al., 2007). It can be speculated, therefore, that in the absence of HESX1, its targets (posteriorising factors) may be differentially methylated, perhaps as a result of a defective recruitment of DNMT1 to these target sites. This may lead to uneven levels of activation of HESX1 targets in different embryos. Ultimately, the variable methylation of these targets, result in the ectopic activation of posteriorsing factors in the anterior forebrain, causing variable forebrain defects. An analysis on the methylation pattern of HESX1 targets sites will shed considerable light on this issue.

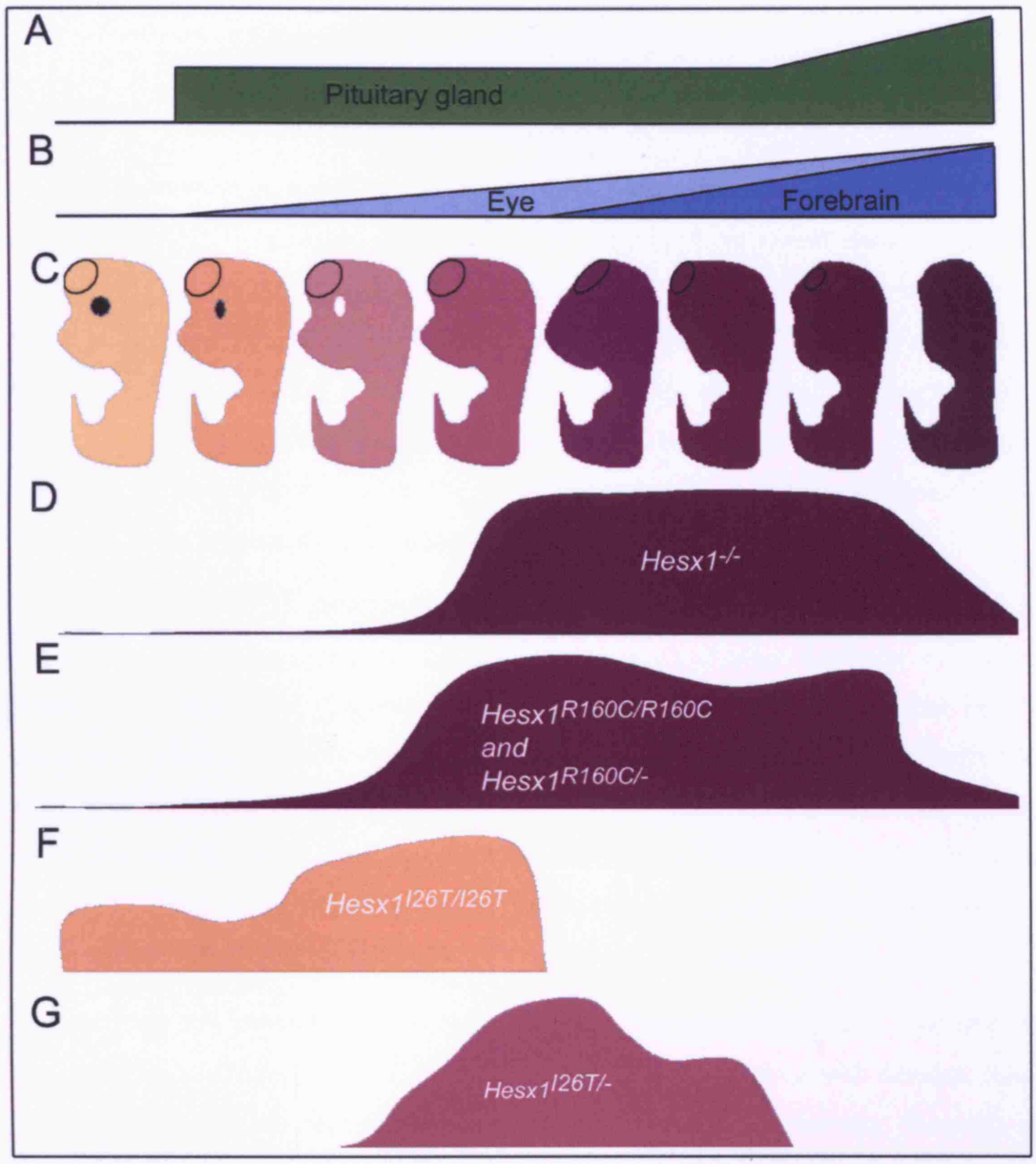

Figure 6.2– Phenotypes associated with *Hesx1* mouse mutants. A) Pituitary defects are similarly severe in all embryos, except in a small proportion of *Hesx1*$^{R160C/R160C}$ and *Hesx1*$^{-/-}$ mutants, which display severe anterior forebrain truncations. This is correlated with a severe nasopharyngeal pituitary phenotype. B) The severity of eye (light blue) and other forebrain defects affecting structures such as the telencephalon and nose (dark blue) is demonstrated in this graph, although these two entities overlap. C) Schematic representation of embryos, displaying the range of defects associated with *Hesx1* mutants. The first embryo on the left is normal; the following three only have eye defects, followed by: small telencephalic vesicles (tv); small nose; small tv and nose; and finally a completely absent anterior forebrain. D) Graph, displaying the relative occurrence of defects observed in *Hesx1*$^{-/-}$ embryos. E) A similar graph for *Hesx1*$^{R160C/R160C}$ and *Hesx1*$^{R160C/-}$ mutants, note that the range of phenotypes is similar to *Hesx1*$^{-/-}$. The minor differences are due to the fact that *Hesx1*$^{R160C/R160C}$ mice are still in a heterogeneous background. F) The graph for *Hesx1*$^{I26T/I26T}$ mice is at the mild end of the scale. G) The phenotype in *Hesx1*$^{I26T/-}$ mice overlaps with the two extremes; note that it is shifted to the right compared with *Hesx1*$^{I26T/I26T}$.

6.13. GENOTYPE-PHENOTYPE RELATIONSHIP

The findings in mice generally correlate with the clinical phenotype of the *HESX1*$^{I26T/I26T}$ and *HESX1*$^{R160C/R160C}$ patients. This is further supported by recent data on *HESX1* expression in human embryos, which is shown to display the same pattern as in mouse (Sajedi et al., in press). *HESX1* transcripts are found in the ventral forebrain at Carnegie stage (CS) 11, and in the RP at CS 11-15 and later disappear. Although, earlier expression in the anterior neural plate has not been assessed in human embryos, the expression in ventral forebrain at CS 11 is indicative of an earlier presence of the transcripts in the precursors of the telencephalon and the eyes.

The human *HESX1*$^{I26T/I26T}$ patient displays a severe pituitary defect, which is manifested in the form of evolving hypopituitarism. However, eye and other forebrain defects are absent in this individual (Carvalho et al., 2003). There are two issues that remain unanswered when comparing the human phenotype with the mouse data. Firstly, the majority of surviving *Hesx1*$^{I26T/I26T}$ mice show eye defects (76%), whilst the human patient does not. Secondly, homozygous mice survive with no indication of an impaired pituitary function, although at embryonic stages they all display pituitary defects. The human patient, on the other hand, suffers from a number of hormone deficiencies.

The first issue can possibly be a species specific phenomenon. The eye field may be more sensitive to a reduction in HESX1 dosage in mice as compared with humans. It has been reported that microphthalmia and anophthalmia are relatively frequent in C57BL/6J mice (mouse genome informatics). On the other hand, eye abnormalities are variable in general, and some 25% of *Hesx1*$^{I26T/I26T}$ mice do not show any eye defects. It is possible, therefore, that this human patient falls within this normal range. This implies that the I26T mutation in humans could be expected to cause eye defects as well as pituitary abnormalities. The analysis of a larger sample of patients with the same point mutation could clarify this issue, but this is not possible given the rarity of this mutation.

Regarding the second issue, pituitary defects are also variable; however, it is evident that in mice, the I26T mutation leads to a fully penetrant pituitary phenotype in homozygous animals. One possibility is that this patient falls within the more severe range of pituitary defects. With respect to this genotype-phenotype correlation therefore, we can conclude

that HESX1-I26T mutation predominantly causes a pituitary phenotype and in some cases eye defects. The overall phenotype is, however, variable and a range in eye and pituitary defects is observed.

The two *HESX1*$^{R160C/R160C}$ homozygous patients show equivalent defects that are more severe than the *HESX1*$^{I26T/I26T}$ patient in terms of forebrain (corpus callosum), eye and pituitary defects. The mouse data mostly correlates with the human phenotype, indicating that this mutation causes defects in forebrain structures, optic nerve and the pituitary. Likewise, both the data from *Hesx1*$^{R160C/R160C}$ mice and the patients indicate variability in phenotype, although it should be noted that the two human patients are clinically similarly affected. Human individuals heterozygous for this mutation are normal and indeed we find that *Hesx1*$^{R160C/+}$ mice are also normal (except for a 1-2% incidence of mild eye defects). These in-vivo findings, however, do not correlate with the in-vitro dominant negative effect of the HESX1-R160C protein (Dattani et al., 1998). The underlying cause of this discrepancy is not known, although the recent finding that the mutant protein does not fully localise to the nucleus may explain this.

Finally, the possible involvement of other genes in modifying this phenotype in the human patients should not be ruled out. In this study we have shown that the interaction between HESX1 and SRFBP1 is lost as a result of the I26T mutation. The R160C mutation also disrupts this interaction as well as abolishing the interaction between HESX1 and LONP2. They both show reduced interaction with DNMT1. These interactions and their selective abrogation by specific mutations may prove to be the underlying cause of the different phenotypes caused by *HESX1* mutations in humans. Furthermore it should not be forgotten that the mouse information is always a more thorough analysis of a phenotype. In humans the most severe mutant embryos are not viable and are hence never analysed. The surviving patients, although a rich source of information about the functionality of HESX1 and its conservation in evolution, only represent a minority, which possibly cover the mild end of the spectrum.

6.14. CONCLUDING REMARKS AND FUTURE DIRECTIONS

The mammalian brain is a vastly complex structure, with a highly intricate organisation that is consequently crucial for its many functions. Thus it is not surprising that although great progress has been made in the discovery of its development, the picture is still not fully clear. It is apparent, however, that the pathways that evolved for the formation of primitive nervous systems, are the same ones involved in the construction of our brains. A vast number of genes have been implicated both in the development of the brain and its functions in the adult.

Homeodomain transcription factors play fundamental roles during embryonic development. A large number of them are expressed throughout the CNS, including the brain (Holland and Takahashi, 2005). *Hesx1* belongs to this class of genes and the studies on *Hesx1*$^{-/-}$ mice, as well as the discovery of human *HESX1* mutations, have highlighted its crucial role in embryonic forebrain and pituitary development.

Although the last two decades have seen an increase in the discovery of function and regulation of numerous transcription factors, it still lags behind those of other proteins, such as secreted factors that are involved in signalling pathways. Thus, the elucidation of the mechanism of action, function and regulation of transcription factors such as *Hesx1* is increasingly crucial for understanding the processes of development. Work presented in this thesis represents an attempt at achieving this.

The discovery of the proteins that interact with HESX1, in this work, has re-iterated the fact that the activity of a transcription factor cannot be considered in isolation. In particular binding of HESX1 to DNMT1 suggests a novel mechanism of action for a homeodomain repressor. Indeed, it is becoming increasingly clear that altering chromatin structure is also an important part of transcriptional regulation. It is, therefore, likely that DNA methylation mediated by DNMT1 is another crucial mechanism of regulation during forebrain patterning.

The other four partners of HESX1 also demand consideration. Although LONP2 and ZFP592 are proteins of unknown function, they may prove significant in the elucidation of HESX1 function. For example, the interaction between LONP2 and HESX1 is completely lost by the R160C mutation, which may implicate this protein in human disease. SRFBP1 is a protein involved in the repression of certain

promoters. The characterisation of these three proteins may, therefore, result in the identification of novel genes involved in forebrain and pituitary development. Finally, SAFB1 is encoded by a gene whose inactivation in mice results in dwarfism. Its possible role in pituitary development requires further investigation.

Much of our progress on the function of transcription factors has come from the analysis of "knock-out" mice. The results from the analysis of *Hesx1*$^{I26T/I26T}$ and *Hesx1*$^{R160C/R160C}$ mice were hence very informative for the characterisation of *Hesx1* function, both during development and in human disease. These two highly conserved amino acid substitutions cause different clinical features in the human patients. The analysis of their mouse models in this work has confirmed that these differences are the direct result of each point mutation within the *HESX1* locus.

These data also indicate that the homeodomain mediated DNA binding ability of HESX1 is absolutely crucial for its function, since the R160C mutation, affecting this property of the protein results in a null allele. This may represent a general feature of homeodomain proteins. Additionally, the TLE1 mediated repression of HESX1 is crucial for its role in pituitary development as the I26T mutation, affecting this interaction predominantly causes pituitary abnormalities. Interestingly, these data also reinforce that HESX1 is potentially an antagonist of posteriosing signals, Wnt/β-catenin in particular, since there is a graded sensitivity to the loss of HESX1 activity within the forebrain. Thus the eye is more sensitive than the telencephalon, as previously reported in lower vertebrates upon ectopic activation of Wnt/β-catenin signalling in the forebrain.

Given that epigenetic changes, such as DNA methylation, are not consistent across the genome and create variable levels of expressivity, the interaction of HESX1 with DNMT1 can also potentially explain the variability in phenotype that is seen in both mice and humans with defective HESX1 function.

Evidently, the identification of genes regulated by HESX1, as well as the proteins that regulate *Hesx1*, will be deeply informative for future studies. Many of the tools used in this work, such as the *Hesx1*$^{I26T/I26T}$ and *Hesx1*$^{R160C/R160C}$ mice, as well as the interactors, can then be applied in order to answer the questions that have been raised throughout the course of this thesis.

7. MATERIALS AND METHODS

7.1. DNA METHODS

7.1.1. Cloning

Approximately 1-3 μg of a vector (high quality DNA), was digested with the appropriate enzyme in a total volume of 50 μl. The vector was then treated with alkaline phosphatase (AP), according to the manufacturer's protocol (Roche). The digested and AP treated vector was purified using a Qiagen PCR purification column.

The insert was either released from a vector, in which case the digested product was run in an agarose gel (usually 1% low melting point agarose) and the insert (single band) was gel purified using a Qiagen gel purification kit; or the insert was amplified by PCR, using primers flanking the region of interest and introducing the restriction enzyme sites on the two ends of the product, which was then column purified. Alternatively, the PCR product was digested with the appropriate enzymes for 4 hrs at 37°C and purified using a Qiagen PCR purification kit.

2 μl of the purified vector and insert were electrophoresed and stained with ethidium bromide. Concentrations were estimated by comparing to a standard marker (hyperladder I, Bioline). Ligation was carried out using T4 ligase (Roche), in a total volume of 15 μl for 3 hrs-o/n, at 16°C. Approximately 50-100 ng of vector was ligated with a 1:1-3:1 molar ratio of insert to vector.

The ligated product was used to transform competent *E. coli* cells by heat shock. Recombinant colonies were picked the next day and DNA was purified from liquid cultures using a Qiagen miniprep kit. The positive clones were identified by restriction enzyme digest analysis. In most cases, positive clones were used to extract larger amounts of DNA using a midi/maxiprep Qiagen kit. The details of inserts, vectors (including plasmid maps) and primers used throughout this work are supplied in section 8 (Appendices).

7.1.2. Preparation of electrocompetent *E. coli* cells

A single, fresh colony of *E. coli* (DH5α) cells was used to inoculate 10 ml LB and grown o/n to stationary phase in a 37°C orbital shaker. Approximately 5 ml of this o/n culture was used to inoculate 500 ml LB, such that the OD_{550nm} was around 0.1.

This was grown further in the 37°C shaker for ~1 hr, or until the OD_{550nm} reached 0.55-0.75, indicating the logarithmic growth phase. The culture was then placed on ice for 20 min and the cells were harvested by centrifuging at 3,000 *g* at 4°C for 15 min. The pellet was resuspended in 10 ml ice-cold 10% glycerol and mixed with a further 390 ml ice-cold 10% glycerol. This was centrifuged as before and the pellet resuspended in ~720 µl 10% glycerol and kept cold. 40 µl aliquots were made in tubes on dry ice and stored at -80°C.

7.1.3. Transformation of bacterial cells by electroporation

~50 ng of plasmid DNA (5 µl of miniprep DNA) was mixed in an eppendorf with 20 µl of electrocompetent DH5α *E. coli* cells (thawed on ice) and placed in a pre-chilled 0.2 mm electrocuvette (Invitrogen). The cells were transformed by electroporation using a Pulser electroporator (Invitrogen). A 2.5 kV, 25 µF, 200 Ω electrical pulse was applied, cells were then immediately diluted with 1 ml chilled SOC medium (see appendix II for details of buffers and solutions) and transferred to a sterile tube. Cells were allowed to recover in a 37°C shaker for 1 hr. The tube was then spun at 5,000 rpm for 3 min, the pellet was resuspended in ~100 µl LB and plated onto an LB agar plate containing the appropriate antibiotic (e.g. ampicillin) and incubated o/n at 37°C.

7.1.4. Preparation of heat-shock competent *E. coli* cells

A single, fresh colony of DH5α or BL21 *E. coli* cells was used to inoculate 5 ml LB (non-selective) and grown o/n to stationary phase in a 37°C orbital shaker. 2 ml of this o/n culture was inoculated into 200 ml medium A (LB, 10mM $MgSO_4$, 0.2% glucose), and grown further in the 37°C orbital shaker until the A_{600nm} reached 0.3-0.5. The culture was chilled on ice for 20 min and the cells were harvested by centrifugation at 1,500 *g* at 4°C for 10 min. The pellet was gently resuspended in 2 ml ice cold medium A. 10 ml of solution B (LB, 36% glycerol, 12% PEG6000, 12mM $MgSO_4$) was added and gently mixed. 100 µl aliquots were prepared in tubes on ice and stored at -80°C.

7.1.5. Transformation of bacterial cells by heat-shock

100 µl of competent cells were thawed on ice, 1-10 µl of DNA solution was added to it and incubated on ice for 20 min. The cells were then heat-shocked at 37°C for 5 min (making sure not to exceeding 5 min), and chilled on ice for a further 2 min. 800 µl LB (non-selective) was then added to the cells and incubated at 37°C for 40-50 min. The cells were then spun at 5,000 rpm for 3 min and the pellet resuspended in the last drop of LB (~100 µl). This was then plated onto a LB agar plate containing the appropriate antibiotic (e.g. ampicillin) and incubated o/n at 37°C.

7.1.6. Isolation and purification of DNA

7.1.6.1. Minipreps

For small scale and low-quality DNA isolation, the Qiagen miniprep kit was used with a microcentrifuge. This technique can yield up to 20 µg DNA. From the 2.5 ml o/n bacterial culture, 1.5 ml was transferred to an eppendorf tube and spun at 13,000 rpm for 1 minute. The pellet was resuspended in 250 µl of cold buffer P1. 250 µl buffer P2 was added, the tube inverted a few times and this was incubated at rt for 3 min. 350 µl of buffer N3 was added and the tube inverted a few times and incubated on ice for 5 min. The sample was then centrifuged at 13,000 rpm for 10-15 min at 4°C. The supernatant was applied to a column and centrifuged at 13,000 rpm for 1 min. The column was washed with 500 µl buffer PB and spun as before. It was then washed with 750 µl buffer PE and spun twice as before. DNA was eluted by applying 50 µl buffer EB, centrifuging as before and collecting the flow-through.

7.1.6.2. Midi/Maxipreps

For larger scale and high quality DNA, the QIAGEN midi/maxi-prep kit was used according to the manufacturer's protocol. Up to 200 µg and 750 µg DNA can be isolated using the midi- and maxiprep kits, respectively. Therefore, a final concentration of ~0.4 µg/µl and ~1.5 µg/µl can be expected from typical midi/maxiprep DNA isolation. From an o/n culture, 100 µl (midi)/200 µl (maxi), was used to inoculate 150 ml (midi)/250 ml (maxi) LB medium, containing the appropriate antibiotic, o/n in a 37°C orbital shaker.

The following day, the entire culture was used to harvest the cells by centrifuging at 1,500 rpm for 30 min at 4°C. The pellet was then resuspended in 6 ml (midi)/10 ml (maxi) cold buffer P1. 6 ml (midi)/10 ml (maxi) buffer P2 was then added and mixed gently by inverting or swirling the tubes. This was incubated at rt for 5 min. 6 ml (midi)/10 ml (maxi) buffer P3 was then added and mixed gently by inverting or swirling the tubes. This lysate was then poured into a cartridge and allowed to settle by incubating at rt for 10 min. 4 ml (midi)/10 ml (maxi) buffer QBT was added to a highspeed tip in order to equilibrate it. The lysate from the previous step was then added to the tips by gently inserting a plunger into the cartridge. The tip was washed with 20 ml (midi)/60 ml (maxi) buffer QC. Finally, DNA was eluted by applying 5 ml (midi)/15 ml (maxi) buffer QF. DNA was precipitated from the eluate by adding 3.5 ml (midi)/10.5 ml (maxi) isopropanol (x 0.7), mixing gently and incubating at rt for 5 min. This was centrifuged at 12,000 rpm for 30 min and the pellet was thoroughly washed with 70% ethanol. This was centrifuged as before and the pellet was air dried. The pellet was resuspended in 500 µl water or buffer TE.

7.1.6.3. Gel purification

The QIAEX II agarose gel extraction kit from Qiagen was used in order to purify DNA fragments from a 1% agarose gel according to the manufacturer's protocol. The desired DNA band was excised from the gel, using a scalpel under UV light. This was then put in an eppendorf tube and its weight determined. 3x the volume of the gel, of solubilisation and binding buffer QX1 (contains high salt conc. at pH <7.5) was added, as well as ~15 µl of QIAEX II (contains silica particles). This was then incubated at 50°C for 10 min, with mixing every 2 min. This was spun at 13,000 rpm for 1 min. The pellet was washed three times with 500 µl buffer PE, spinning as before. After the final wash the pellet was air dried for 15 min until it turned white. The DNA was eluted by resuspending the pellet in 20 µl buffer EB and incubating at 50°C for 5-10 min. This was then centrifuged at 13,000 rpm for 1 min. The supernatant, which contains the DNA was moved to a clean tube.

7.1.6.4. PCR purification

The QIAquick PCR purification kit (Qiagen) was used in order to purify DNA fragments 100bp-10 kb. 5x the volume of DNA sample of buffer PB was added and

applied to a column. This was centrifuged at 13,000 rpm for 1 min and subsequently, washed with 750 µl buffer PE and centrifuged twice as before. The DNA was eluted by applying 40 µl buffer EB to the centre of the column and incubating at rt for 1 min. The column was then centrifuged at 13,000 rpm for 1 min and the flow-through, which contains the DNA, was collected in a clean tube.

7.1.7. Analysis of DNA

7.1.7.1. Electrophoresis of DNA

DNA fragments in the size range 100 bp to 10 kbp were separated by horizontal agarose gel electrophoresis (Gibco horizontal gel tank). Gels consisted of 1-2% agarose dissolved in 1x TAE buffer by microwaving. Once cooled to ~50°C, 0.5 µg/ml ethidium bromide was added and the gel was poured in the appropriate casting tray. The desired comb was placed on the tray before pouring the gel, which was removed before loading the samples. DNA samples were simply prepared before loading by adding 1x loading buffer. A 1 Kb ladder (hyperladder I Bioline) was generally loaded as a molecular marker, for estimating the size of DNA bands. Gels were run in 1x TAE buffer. The voltage and timing varied according to the size of expected bands as well as the resolution required. Generally, gels were run at 80-120 V for 30 min up to 3 hrs. DNA was visualised and photographed under UV light.

7.1.7.2. Restriction enzyme analysis

Digestion of DNA was generally carried out at 37°C for 2 hrs unless it was specified otherwise by the manufacturer. The total volume varied according to the purpose of digest. For cloning, a total volume of up to 100 µl was used, whilst for diagnostic digests the total volume was generally 15-20 µl. The appropriate enzyme buffer was used according to the manufacturer.

If two or more enzymes were required for digestion, which were not compatible, the digests were carried out one at a time. After the first digestion, the first enzyme was heat inactivated (can vary according to the restriction enzyme but generally 10 min at 65°C), followed by treatment with the second enzyme. In this case the volume was increased so that enzymes and buffers did not exceed 10% of the total volume.

7.1.8. Quantification of DNA

The precise method, for quantification of DNA, was to measure the absorbance of the sample at 260nm using a spectrophotometer (one OD_{260nm} unit = 50 µg/ml dsDNA). First, a 1:100 dilution of the DNA sample was prepared in ddH_20 and the OD_{260nm} was measured. The amount of DNA was calculated by considering the dilution factor, as follows:

A_{260} x 50 µg/ml x 100 = amount of DNA in the original sample in µg/ml

The absorbance at 280nm was also measured and the value of A_{260}:A_{280} was determined. This was a measure of the purity of DNA and the value should be in the range ~1.8-2.0, for solutions which are relatively free of proteins.

Additionally, the amount of DNA was estimated by comparing the sample to a molecular marker (hyperladderI, Bioline) in an agarose gel.

7.1.9. Sequencing

Sequence analysis of DNA clones was performed by direct sequencing of the PCR-amplified products, generated with specific primers designed within the region of interest (e.g. within the VP16AD for sequencing the interacting clones after the yeast-two hybrid). Purified PCR products were sequenced using big dye terminator chemistry (Applied Biosystems) and analysed on a MegaBACE 1000 capillary sequencing machine (Amersham). Sequence reads were checked to be in-frame with the VP16AD sequence using Bioedit. BLAST searches were performed using the NCBI web server (http://www.ncbi.nlm.nih.gov/blast).

7.1.10. Polymerase Chain Reaction

DNA to be used for subcloning and expression studies was amplified using *Pfu* DNA polymerase (Strategene), due to its proof-reading activity. For all other applications, DNA was amplified using the standard *Taq* polymerase (Bioline). Reactions were generally made in 50 µl total volume containing 200 µM dNTPs, 1x *Taq*/*Pfu* buffer, 1.5 µM $MgCl_2$, 0.5 µM of each primer, 5 u/µl *Taq*/*Pfu* polymerase and 1-2 µl DNA. This was either scaled down to 25 µl or scaled up to 100 µl total volume according to the application. Generally, a pool containing all the components except DNA was

made and divided between the number of samples. DNA was then separately added to each tube.

Most genotyping was carried out following the "hot-start" protocol in a total volume of 20 µl using the *Taq* pol buffer or in a total volume of 10 µl using JD buffer. In this case, two separate pools were prepared according to Table 8.1. The DNA mix was first added to each tube (11 or 5.5 µl), followed by a drop of oil. 1-2 µl of the template DNA was then added and the tubes were spun briefly. The tubes were placed in the PCR machine with the lids open. After 2 min at 94°C, the machine was paused at the annealing temperature and the enzyme mix was added to each tube (8 or 2.5 µl), closing the lid every time.

Primers were designed and obtained from Operon or Sigma. The stocks were prepared to a concentration of 100 µM and further working stock concentrations of either 25 µM or 10 µM were prepared for use. dNTPs (Roche) were made up to a stock concentration of 25 µM. For every PCR run, a negative control (sample without DNA), and a positive control (sample with known DNA), were also included. The cycling reactions involved an initial step of 94°C for 2 min and 85°C for 1 min. This was followed by 30-35 amplification cycles each consisting of denaturation (94°C for 30 sec.), annealing (50-68°C for 30 sec.) and elongation (72°C for 1 min.). After the final cycle, there was a 72°C step for 5 min. These conditions were varied according to the application for optimal specific amplification; Table 8.10 (Appendices) gives the details of various PCR conditions used for genotyping.

7.2. YEAST METHODS

7.2.1. Buffers, solutions and media

7.2.1.1. Yeast "drop-out" solutions

The amino acids were prepared by adding the correct weight (Appendices, Table 8.4) to 50 ml ddH_2O and mixed until dissolved. They were then filter-sterilised by passing through a 0.2 μm millipore filter (BD), under sterile conditions. They were stored at 4°C for up to six months. The powder amino acids can be stored for longer at rt (see manufacturer's guidelines).

X-α-Gal was prepared by making a 20 mg/ml stock solution in N,N-dimethyl formamide (DMF). 1 ml aliquots were then stored at -20 °C and added to medium at a conc. of 20 mg/L (Table 8.4).

3-aminotriazole (3AT) was made by making a 500 mM stock solution in ddH_2O and storing at -20 °C. Usually a conc. of 3 mM is added to the medium; however we found that for one of the "baits" (Gal4DBD-Hesx1 aa 1-185), a conc. of 4 mM was optimal.

Glucose was made by making a stock conc. of 50% (50 g in 100ml) in ddH_2O (vigorous mixing is needed). The solution was then filter-sterilised by passing through a 0.2 μm millipore filter, under sterile conditions. This stock was added to the autoclaved medium at a final conc. of 2% (Table 8.4).

7.2.1.2. YPAD rich non-selective medium

This medium was used for growth of host yeast strain, either in liquid or solid forms. YPAD (yeast extract, peptone, adenine, dextrose) contains all the essential amino acids, vitamins and nutrients needed for optimal growth of yeast and does not select for transformed yeast. YPAD was prepared by adding bacto-yeast extract (Difco) and bacto-peptone (Difco) to ddH_2O (agar was added for solid YPAD) and autoclaving. Glucose and adenine solutions were added to the autoclaved solution (Table 8.2).

7.2.1.3. SD selective medium

The SD (synthetic defined) medium is the minimal media used to select for the transformed yeast. Bacto yeast nitrogen base without amino acids (Difco) was added to ddH_2O and autoclaved. Bacto agar was added for solid SD medium. Glucose (as above) was added after autoclaving (Table 8.3). To make SD "drop-out" medium, amino acids were prepared according to Table 8.4 and added separately to the autoclaved solution under sterile conditions.

7.2.2. Growth and maintenance of yeast host strain

In all the techniques dealing with yeast, the *S. cerevisiae* strain PJ69-4A (James et al., 1996) was used. When dealing with yeast, it is essential to keep all conditions sterile. Solutions were autoclaved where possible and filter sterilised where stated (e.g for antibiotic solutions and glucose). All procedures were carried out inside a hood, under sterile conditions. Yeast growth is optimal at 30°C; therefore, incubators and shakers set up to this temp and exclusively for yeast work, were used for growth of PJ69-4A.

7.2.2.1. Preparation of yeast competent cells

Yeast strain PJ69-4A was initially streaked onto YPAD plates (this can be from a liquid or solid culture or from a glycerol stock). This was grown in a 30°C incubator for 48-72 hrs, until colonies were noticeable. One colony was picked and grown in 5 ml YPAD liquid medium, shaking o/n at 30°C. The following day, the entire o/n culture was inoculated in 60-100 ml of YPAD liquid medium (or such that the A_{600} is 0.1-0.2) and grown in the orbital shaker at 30°C until OD_{600nm} reached 0.5-0.7 (usually reached after 3-5 hrs). The cells were then harvested by centrifugation at 3,000 *g* (2,500 rpm) for 5 min at 4°C. The pellet was gently washed in 20 ml sterile ddH_2O, centrifuged as before and the pellet was resuspended in 0.3 ml LiAc/TE. This was then divided into 100 µl aliquots and either used immediately for transformation, or stored at 4°C for up to a week.

7.2.2.2. Preparation of glycerol stocks

At the point when the cells have reached exponential growth phase (i.e. when the OD_{600nm} is 0.5-0.7), it is possible to make glycerol stocks. For this purpose, yeast was grown to this stage and 1 ml of this culture was then added to a 2 ml screw cap tube in sterile conditions and 30-50% v/v of glycerol (this should be autoclaved), was added and stored at -80°C.

It is advisable to also keep glycerol stocks of yeast transformed with "bait" and "prey" plasmids. A similar procedure was, therefore, used to make glycerol stocks of PJ69-4A containing Gal4DBD-HESX1 aa1-185 and Gal4DBD-HESX1 aa1-107 (the two bait plasmids) and Gal4DBD-empty. Additionally, glycerol stocks of PJ69-4A containing VP16-empty (empty prey plasmid) as well as VP16-interactors were made and stored at -80°C. Here, however, SD medium lacking the selective amino acid was used to grow the transformed yeast. The interactors correspond to the 10 clones that were isolated after the initial screen, shown in Table 2.1.

7.2.3. Testing for autoactivation in yeast

Yeast was separately transformed with the two baits (i.e. Gal4DBD-HESX1 aa1-185 and Gal4DBD-HESX1 aa1-107) and plated onto SD/glu –ura plates. After incubation for ~3 days at 30°C, 6 colonies of each bait were streaked onto segments of SD/glu –ura plates and incubated a further 3 days at 30°C. Each clone was then re-streaked separately onto SD/glu –ura, - ade and SD/glu –ura, -his, + 3AT. Two different conc. of 3AT (3 and 4 mM) were used. The plates were then incubated at 30°C and checked for autoactivation.

7.2.4. Small scale yeast transformation of yeast

Salmon sperm carrier DNA (Sigma) was denatured at 95°C for 5-10 min and placed on ice. For each transformation, 50 µg of denatured salmon sperm DNA (5 µl of 10 mg/ml stock) and ~100 ng plasmid DNA were added to 100 µl yeast competent cells (prepared as described above). 300 µl freshly prepared LiOAc/TE/PEG was added and mixed thoroughly. After a 30 min incubation shaking at 30°C, 70 µl DMSO was added and the cells were heat shocked by placing in a water bath at 42°C for 5-10 min. Cells were recovered by pulse-spinning in a microcentrifuge, washed with 500

µl sterile ddH_2O, resuspended in 200 µl sterile ddH_2O and plated on selective medium. The plates were incubated for 2-3 days at 30°C.

7.2.5. Large scale library transformation of yeast

For the large-scale library transformation (i.e. the yeast two-hybrid screen), the same protocol as the ones described above, for making yeast competent cells and transformation were scale-up. First, PJ69-4A was transformed separately with the two "bait" vectors (i.e. Gal4DBD-HESX1 aa1-185 and Gal4DBD-HESX1 aa1-107). Several colonies were used to make glycerol stocks and the level of each "bait" protein expression was analysed. The following steps were carried out separately for each "bait" vector.

A positive clone (showing good protein expression and a healthy growth rate), was selected and plated onto SD/glu – ura plates. After 2-3 days, a single colony was used to inoculate 200 ml SD/glu – ura liquid medium shaking at 30°C o/n. The entire culture was used the next day to inoculate 1 litre YPAD medium (this should give an OD_{600nm} of ~0.1). This was gown shaking at 30°C until the OD_{600nm} reached 0.5-0.8 (this generally takes ~4 hrs, although it should be checked regularly). At this point, the cells were harvested by centrifugation at 2,500 rpm for 5 min in sterile containers. The pellet was washed with 500 ml TE x1 and centrifuged as before. The pellet was resuspended in 20 ml TE/LiOAc. Meanwhile, the DNA mix was prepared by denaturing salmon sperm carrier DNA (10 mg/ml) at 95°C for 5 min. 1 ml salmon sperm DNA and 250 µg VP16 E9.5-10.5 mouse library (Hollenberg et al., 1995; provided by Professor P. Scambler, Molecular Medicine Unit, ICH, UCL) were then added to the cells as well as 140 ml TE/LiOAc/PEG. This was incubated shaking at 30°C for 30 min. 17.6 ml DMSO was then added and heat shocked at 42°C for 5-10 min. This was immediately diluted with 400 ml YPAD and pelleted by centrifugation at 2,500 rpm for 5 min. The pellet was washed with 500 ml YPAD by centrifugation as before, resuspended in 1 litre pre-warmed YPAD and incubated shaking at 30°C for 1 hr. The cells were harvested by centrifugation as before and washed with 500 ml SD medium. After centrifugation at 2,500 rpm for 5 min, the pellet was resuspended in 1 litre pre-warmed SD/glu –ura/–leu liquid medium. This was incubated shaking at 30°C o/n (9-10 hrs). The cells were then harvested by centrifugation at 2,500 rpm for 5 min in sterile containers. The pellet was then

washed twice with 500 SD medium and resuspended in 10 ml SD/glu –ura, -leu, -his, + 3AT*. This was plated onto 25 large SD/glu –ura, –leu, –his, + 4mM 3AT plates (400 µl aliquots/plate).

The 25 large plates were incubated at 30°C for up to 3-5 days. Colonies were then streaked onto graded plates with SD/glu –ura, –leu, –his, –ade, + X-α-Gal, + 3AT. The plates were incubated at 30°C for up to 3-5 days. Clones were then re-streaked regularly until the end of analysis.

*Before plating, 10 µl of the 10 ml cell suspension was taken and serial dilutions up to 1:1,000,000 were made. These dilutions were plated onto SD/glu –ura, –leu small plates to determine the transformation efficiency.

7.2.6. Recovering interacting clones and plasmids from yeast

Each potential clone was re-streaked twice onto SD/glu –leu plates. This was used to inoculate 10 ml SD/glu –leu liquid medium shaking o/n at 30°C. Cells were harvested by centrifugation at 2,500 rpm for 5 min. The pellet was resuspended in 50 µl lysis buffer (50 mM Tris-HCl pH 7.5, 1.2 M sorbitol, 10 mM EDTA). 10 mM β-mercaptoethanol and 200 u/7 µl lyticase (30 u/ µl ,Sigma) was then added and incubated at 37°C o/n. Cells were microcentrifuged at 4,000 rpm for 5 min. The Qiagen miniprep kit was used, and DNA was eluted in ddH_2O. This DNA was used to transform electrocompetent DH5α cells using electroporation. Colonies were then picked, inoculated and the DNA was isolated using a Qiagen miniprep kit. Restriction enzyme (NotI) was used to identify positive clones. These were then PCR amplified for subsequent sequence analysis.

7.3. PROTEIN METHODS

7.3.1. Quantification of protein

Protein conc. was determined using the Bradford assay. A standard curve was generated using a series of dilutions of BSA, in a total volume of 100 µl. 1 ml of Bradford reagent (Sigma) was added to the sample and mixed thoroughly. The OD_{595nm} was then measured. The OD_{595nm} of the protein sample was also determined and the protein concentration was calculated from the standard curve.

7.3.2. GST pull-down assay

pGEX-4T plasmids carrying GST–HESX1 and GST–DNMT1 sequences (Table 8.9 – Details of vectors and inserts used in cell culture and in-vitro assays.) were used to transform *E. coli* BL21 cells and plated on ampicillin plates. A fresh colony was used to inoculate 50 ml of LB/amp at 37°C shaking o/n. The o/n culture was inoculated with 450 ml LB/amp and grown until OD_{600nm} reached a value of 0.6 (~1 hr). Induction of protein expression was achieved by an addition of 0.2 mM IPTG and incubation at 37°C for 2-4 hrs. Culture was chilled on ice and 0.1 mM phenylmethane sulphonyl fluoride (PMSF) was added. Bacteria were pelleted by centrifugation at 5,000 *g* at 4°C and resuspended in 10 ml NETN buffer supplemented with protease inhibitor cocktail (Roche). This was incubated on ice for 10 min followed by sonication (3x 15 sec pulses on ice). After sonication, extracts were centrifuged at 12,000 *g* for 30 min at 4°C. 2 ml glutathione–sepharose (GST) beads (Roche) were prepared by washing three times in 20 ml chilled NETN buffer and spinning at 5,000 rpm for 3 min. The beads were then resuspended in 1 ml NETN buffer and 100 µg/ml BSA and incubated at rt for 15 min. This was then washed three times in 500 µl NETN buffer and resuspended as 50% slurry in NETN buffer. GST beads were added to the supernatant from the step before, as well as 200mM KCl and incubated for 2 hrs at 4°C, rotating. This was followed by centrifugation at 3,000 rpm for 5 min at 4°C. After five washes in NETN buffer, GST fusion proteins bound to the beads were resuspended in 300 µl storage buffer and a 5 µl aliquot was used to quantify the amount of protein by performing a Bradford assay (Bradford Reagent, SIGMA). The rest were aliquoted on dry ice and kept at −80 °C.

In-vitro translation was performed using the TNT Quick Couple Transcription/Translation kit (Promega) and ^{35}S-methionine (Amersham) as

recommended by the manufacturer. Around 2 µg of the fusion protein (GST–HESX1, GST-interactor or GST alone) bound to glutathione–sepharose beads was washed three times with 1 ml NETN buffer (without DTT) by centrifuging at 3,000 rpm for 5 min at 4°C. This was resuspended in 500 µl NETN buffer (without DTT) and incubated with 2-20 µl ^{35}S-methionine-labelled protein or ES cell protein extracts for 2 hrs-o/n at 4°C. After three washes in NETN buffer, an equal volume of 2x Laemmli buffer was added and samples were denatured at 100°C for 5 min. Proteins eluted from the beads were subjected to SDS-PAGE, Coomassie stained, dried and exposed to an autoradiographic film.

7.3.3. SDS-PAGE electrophoresis

Plates (0.75mm, 1mm or 1.5mm) were cleaned with detergent and wiped with 70% IMS. They were then set up by sandwiching them together and clamping then along the edge. Resolving gels (7.5-15% acrylamide) were prepared according to Table 8.5. Once TEMED was added, it was poured immediately between the clamed plates until the meniscus reached ~2.5 cm from the top. ddH_2O or isobutanol was layered on top of the poured gel. Once set, the ddH_2O (or isobutanol) layer was removed by decanting. Stacking layer (prepared according to Table 8.5) was poured on top and the comb added without creating bubbles. Once set, the comb was gently removed and the gel was placed in a tank containing running buffer. Samples were prepared for electrophoresis, by adding an equal volume of 2x Leammli buffer, denaturing for 2 min at ~100°C and pulse spinning. These were then carefully loaded in the wells. Gels were run at 180 V and 50 mA for ~1 hr (until the dye front had reached the bottom of the gel). A molecular weight marker (Promega) was loaded in the first lane.

7.3.4. Visualisation of proteins

7.3.4.1. Coomassie staining

Following electrophoresis, the gel was placed in coomassie solution and stained for a minimum of 30 min. The coomassie stain was poured back for re-use and the gel was destained for a few hours in destaining solution at r.t. Destaining can take 1 hr, however, generally done overnight to obtain sufficient visualisation of bands.

7.3.4.2. Autoradiography

For some purposes such as the GST pulldown assay, after coomassie staining, gels were dried in a vacuum drier (Bio-Rad) on a sheet of 3MM paper for 30 min-2 hrs at 65°C. The gel was then exposed overnight or longer to Biomax-MR autoradiography film (Kodak), at rt in the dark.

7.3.4.3. Western blotting

Western blotting was carried out using a semi-dry blotting apparatus (Bio-Rad). Following electrophoresis, the gel was pre-equilibrated for 15 min in transfer buffer. A Hybond-C nitrocellulose membrane (Amersham), was cut to the size of the gel, pre-wetted in methanol for 5 min and pre-equilibrated in transfer buffer. The gel was laid on 4 pieces of 3MM paper on the blotting apparatus, the membrane was laid on top of the gel followed by 4 pieces of 3MM paper on top. Air bubbles were removed by rolling over the stacks with a 10 ml plastic pipette tip. The blotting apparatus was then assembled and run at 20 V and 400 mA for 30 min.

Following transfer, the membrane was placed in blocking solution (10% milk in TBST), rotating at rt for 1 hr. The membrane was then added to a solution containing the primary antibody at the correct concentration and 10% milk in TBST, and rotated at 4°C o/n. The membrane was washed three times in 10% milk and TBST, shaking for 15 min, each wash. It was then exposed to the correct concentration of secondary antibody prepared in 10% milk and TBST, and rotated at rt for 1 hr. This was followed by five washes in TBST shaking at rt for 15 min, each wash. After the final wash, the membrane was exposed to ECL (Sigma) solution for 5 min, which was prepared by mixing solution A: solution B at a ratio of 1:40, in a total volume of 1 ml per membrane.

Once detected with an antibody, it is possible to strip the membrane and expose it to a different antibody. For this, after Western blot detection, the membrane can be stored at -20°C between two sheets of 3MM paper. When needed, it was wetted in methanol and washed with ddH_2O twice for 5 min each wash. The membrane was then washed with 0.2 M NaOH for 10 min, followed by 2 hrs in TBST. The antibody detection was repeated as before. Alternatively, the Restore Western blot stripping buffer (Pierce) was used according to the manufacturer's protocol.

7.4. CELL CULTURE METHODS

7.4.1. Maintenance of cultured cells

All cell lines were grown in a humidified 37°C incubator at 5% CO_2. Medium used was Dulbecco's modified Eagle's medium (Sigma), supplemented with 10% fetal calf serum, 2 mM L-glutamine, 100 u/ml penicillin and 100 µg/ml streptomycin. All cell work was carried out in a tissue culture sterile hood. Equipment and reagents for cell culture use were kept separately, in clean/sterile conditions. All materials were sprayed thoroughly, with 70% IMS, before placing in the hood.

7.4.2. Splitting cells

In order to seed the required amount of cells in a plate, a fully confluent plate was split using trypsin-EDTA. The 10 cm plate (see Table 7.1 for amounts to use for different sized plates) of cells was washed once with 10 ml PBS (x1). 1-1.5 ml trypsin-EDTA (x1) was added to the plate and incubated at 37°C for 5 min. 6 ml (2-3 times the volume) of medium was added and the cells were thoroughly but gently resuspended. This was centrifuged at 1,000 rpm for 5 min. The pellet was then gently but thoroughly resuspended in 10 ml medium and plated. If required, the cells were counted using a haemocytometer and plated accurately. The cells were incubated at 37°C until needed.

Table 7.1 – Relative surface area of tissue culture dishes and flasks.

		Surface area (mm^2)	Growth medium (ml)	x1 Trypsin (ml)	Relative factor
Dishes	35 mm	962	2	1	x4.8
	60 mm	2827	3	1	x14
	100 mm	7854	10	1	x39
	150 mm	17671	20	5	x88
Cluster plates	6-well	962	3	0.45	x5
	12-well	401	1.5	0.25	x2
	24-well	200	1	0.15	x1
	96-well	50	0.2	0.05	x0.2
Flasks	T-25	2500	3	1	x12
	T-75	7500	10	1	x37
	T-160	16000	25	8	x80

7.4.3. Freezing and thawing cells

In order to prepare frozen aliquots of a cell line, a relatively low-passage and healthy sample was grown in a 10 cm or larger plate until the plate was optimally confluent. Medium was changed and the cells were split using trypsin-EDTA as before. However, after centrifugation, the pellet was resuspended in 3 ml freezing medium (90% FCS and 10% DMSO). 1 ml aliquots were transferred into 2 ml cryovials, placed on ice for 15 min and -80°C for a few days. The vials were then placed in a liquid nitrogen tank.

When needed, an aliquot was thawed in a 37°C water bath for ~2 min. Cells were transferred into a tube with 10 ml DMEM and mixed by inverting a few times. Cells were then spun at 1,000 rpm for 5 min. Supernatant was removed and the pellet was gently resuspended in 10 ml DMEM and divided between two 10 cm plates or a T-75 flask. Another 5 ml of DMEM was added to each plate/flask. These were then incubated for a few days until confluent plates were ready for use, if required DMEM was replaced with fresh medium.

7.4.4. Transfection using the calcium phosphate method

1.5 x 10^6 cells were seeded in a 10 cm plate and grown o/n at 37°C until ~40% confluent. 2-3 hrs before transfection, cell medium was replaced with 10 ml fresh DMEM. 50 µl $CaCl_2$ (2.5M) was added to a total of 10 µg DNA (typically added up with 5 µg with herring sperm DNA if one plasmid was used) in 450 µl H_2O at rt. After mixing, this was added drop-wise to 500 µl 2x HEPES, while "bubbling" the HEPES buffer. After 20 min at rt, this was added drop-wise to the cells while swirling the dish for even distribution. Cells were then incubated at 37°C o/n, the medium was changed the following day and the cells were lysed the day after for Co-IP experiments.

7.4.5. Transfection using Lipofectamine

For both immunofluorescence and luciferase experiments, CHO cells were plated on 12-well tissue culture plates by seeding 1.25–1.5 x 10^5 cells per well, the day before transfection. For immunofluorescence, cells were grown on round coverslips in each well. The following day, cells should be 50-80% confluent and evenly distributed;

they are then ready for transfection using Lipofectamine (Invitrogen). 1-2 μg DNA was mixed with 75 μl Opti-MEM (Invitrogen) in a sterile eppendorf tube. At the same time, lipofectamine (3 μl/well) was diluted in Opti-MEM (28 μl/well) in another sterile tube. The lipfectamine/Opti-MEM mix was then added to the DNA mix. This was incubated at rt for 45 min. The cell medium was removed and the cells were washed with 1x PBS. The lipofectamine/DNA/Opti-MEM mix (500 μl/well) was then added to the appropriate well. The cells were incubated for 4 hrs before removing this medium with fresh DMEM medium. The cells were incubated for another 24 hrs, and were then lysed or fixed according to application.

7.4.6. Immunocytochemistry

CHO or 293T cells were grown on cover slips in 12-well plates and transfected with the appropriate plasmid (e.g. HA-tagged HESX1 and/or Flag-tagged interactor). Two days after transfection, cells were gently washed twice with PBS and fixed in 1 ml 4% PFA for 20 min on ice and washed three times for 5 min in PBT (phosphate-buffered saline containing 0.1% Triton X-100). Cells were then incubated with 1 ml 0.5% Triton-X in PBS at rt for 15 min. After blocking in DMEM with 10% fetal calf serum for 1 hr at rt or o/n at 4°C, cells were incubated with either rabbit polyclonal anti-Flag or rat monoclonal anti-HA antibodies at 4°C overnight. Samples were then washed four times for 5 min in PBT and incubated with secondary antibodies for 1 hr at rt. This was followed by a further four washes in PBT as before. Coverslips were then mounted using Vectashield with DAPI (Vector Laboratories). Samples were viewed with a Leica TCS SP Confocal Microscope using an argon–krypton laser and UV10×/0.4 or 40×/0.5 NA dry HC-PLAPO lens (Leica). Images were captured with Leica TCS NTsoftware, composed of 16 sections and four accumulates and processed using ImageJ 1.30v (National Institutes of Health).

7.4.7. Co-immunoprecipitation

For immunoprecipitation experiments, HEK293T cells were co-transfected with 5 μg of each plasmid at 30–40% confluency using the standard calcium phosphate precipitation protocol. Cells were harvested 48 hrs after transfection by washing with 1x PBS and resuspending in lysis buffer (20 mM Tris pH7.5, 150 mM NaCl, 1% Triton X-100). The cells were scraped off the plate in 1 ml lysis buffer and incubated

for 20 min on ice. For SAFB1 and LONP2, five additional lysis conditions were used (see Appendices, Table 8.6). Protein extracts were separated from nuclei by centrifugation at 3000 *g* for 10 min at 4°C and quantified by performing a Bradford assay (Bradford Reagent, SIGMA). Approximately, 0.5–1.0 mg of total protein was incubated with anti-Flag (0.32 µl/IP) and the same amount was incubated with anti-HA (3 µl/IP) antibodies bound to protein G sepharose beads (Roche) for 4 hrs-o/n at 4°C. The next day, protein G beads (50 µl/IP) were washed three times with cold PBS and incubated with the IPs, rotating at 4°C for 3-5 hrs. After three washes in lysis buffer, immunoprecipitates were resolved by SDS-PAGE and transferred to a membrane (Millipore). Membranes were then immunoblotted using HRP conjugated anti-Flag or anti-HA antibodies using standard Western blotting. Immunoreactive proteins were visualised using the ECL Detection Reagent System (Amersham).

7.4.8. Luciferase assay

In all studies, cells were lysed 24 hrs after transfection by washing with 1x PBS and adding 500 µl passive lysis buffer (1x PLB, Promega) and shaking for 20 min at rt. Luciferase assays performed (dual luciferase reporter assay system, Promega), using a FLUOstar Optima fluorescence microplate reader (BMG Labtech, Aylesbury, UK). All data were standardized with *Renilla* expression. Results are shown as the mean +/- SEM of at least three independent experiments, each performed in triplicate. Variable amounts of reporter and effector vectors were used in these experiments, but the total conc. of DNA used for transfections was kept constant at 1.0 µg of DNA per well by adding pBluescript plasmid (Stratagene). For the mammalian two-hybrid assay, cells were transfected with the following plasmids: (1) pRL-SV40 (*Renilla* luciferase); (2) pGL-Gal4BS-Luc (firefly luciferase) or pGL-p3-Luc (firefly luciferase); (3) pM-Gal4DBD-Hesx1; (4) pVP16-interactor. For the mammalian one hybrid assay, cells were transfected with the following plasmids: (1) pRL-SV40 (*Renilla* luciferase); (2) pGL-Gal4BS-Luc/SV40 (firefly luciferase) or pGL-p3-Luc/SV40 (firefly luciferase); (3) p-untagged-Hesx1; (4) p-untagged-interactor.

7.5. ANIMAL METHODS

7.5.1. *Hesx1* null mouse line

The *Hesx1*$^{-/-}$ mouse strain (Dattani et al., 1998), in which the entire coding region has been deleted, has now been backcrossed with C57BL/6J mice for over 20 generations. The C57BL/6J and CD1 inbred strains used in this work were obtained from Harlan.

7.5.2. *Dnmt1* null mouse line

The *Dnmt1*$^{+/-}$ mice were obtained from Dr. En Li (Novartis Institutes for Biomedical Research, Massachusetts). Three heterozygous males were mated with six *Hesx1*$^{+/-}$ females. Several of the *Dnmt1*$^{+/-}$ and *Dnmt1*$^{+/-}$;*Hesx1*$^{+/-}$ offspring were then bred with C57BL/6J mice in order to generate heterozygous and compound heterozygous pups and embryos.

7.5.3. Generation of the *Hesx1-I26T* and *Hesx1-R160C* mouse lines

The *Hesx1-I26T* and *Hesx1-R160C* targeting vectors were generated using homologous regions obtained from plasmids containing the mouse *Hesx1* gene, which have been previously used successfully (Dattani et al., 1998). A *PGK-Neo* cassette flanked by *loxP* sequences was inserted in the EcoRI site located in the first intron of both targeting constructs. In the *Hesx1-I26T* targeting vector, the *PGK-Neo* cassette was cloned in the same orientation of transcription of the *Hesx1* locus (Figure 8.1). Site directed mutagenesis was used to introduce the I26T mutation in the wild-type mouse *Hesx1* DNA sequence. This resulted in the change of the triplet codon ATT at position 26 by ACC and the introduction of a *Bsu36I* restriction site in the mutated allele.

The R160C mutation was introduced in the mouse *Hesx1* locus resulting in the change of the triplet codon CGA at position 160 by TGC and the introduction of a *FspI* restriction site. The initial attempt at generating the *Hesx1-R160C* mouse line was not as straight forward as that of *Hesx1-I26T*. After electroporating this construct in CCE ES cells, however, the cells only formed a countable number of colonies.

This failure of ES cells to form colonies was puzzling. Therefore, other attempts were made at electroporation with different R160C targeting constructs. After making sure the construct was the correct one, it was concluded that *Hesx1-R160C* has a lethal effect in ES cells. This is conceivable since *Hesx1* is normally expressed in undifferentiated ES cells and therefore, upon incorporation HESX1-R160C protein would be translated in these cells. This was interesting as it was previously reported that this mutant protein acts as a dominant negative in-vitro by abrogating the DNA binding ability of wild type HESX1 (Brickman et al., 2001).

A strategy was devised in order to overcome this. First a splicing acceptor (SA) sequence was introduced in the construct. The introduction of this sequence in the *Neo* cassette will result in the premature slicing of *Hesx1-R160C* mRNA and hence the mutant protein will not be produced. However this attempt failed as ES cells did not form colonies.

The next strategy was to place the *PGK-Neo* cassette in an inverted orientation but in the same position in the construct. Placing the *Neo* gene in an opposite orientation to *Hesx1* should interfere with the normal transcription of *Hesx1-R160C* mutant allele. This construct was successfully electroporated in ES cells (Figure 8.1).

The linearised targeting vectors were electroporated in CCE embryonic stem cells (129/SvEv) (kindly provided by E. Robertson) and 500 colonies were picked, expanded and screened by PCR and Southern blot. Two correctly targeted clones for each construct were isolated and injected into blastocysts from C57BL/6J mice. The *PGK-Neo* cassette was excised by mating heterozygous mice with *betaActin-Cre* animals (Meyers et al., 1998).

With the exception of the opposite orientation of the remaining *loxP* sequence after *Cre*-mediated excision of the *PGK-Neo* cassette and the specific point mutation, both *Hesx1-I26T* and *Hesx1-R160C* alleles were identical. This was relevant in order to be able to attribute any differences in phenotype to the effect of the specific mutations, rather than to other effects in transcriptional efficiency or splicing. $Hesx1^{I26T}$ and $Hesx1^{R160C}$ mice, which were viable and fertile, were maintained on the C57BL/6J (Harlan) background. The analysis described here used animals and embryos after 3-4 backcrosses.

Experimental litters containing, *Hesx1*$^{+/+}$, *Hesx1*$^{I26T/+}$, *Hesx1*$^{I26T/I26T}$ embryos were generated by intercrossing *Hesx1*$^{I26T/+}$ mice. Similarly those containing *Hesx1*$^{+/+}$, *Hesx1*$^{R160C/+}$, *Hesx1*$^{R160C/R160C}$ embryos were from *Hesx1*$^{R160C/+}$ intercrosses.

7.5.4. Maintenance of colonies and collection of embryos and brain tissues

Animal studies were carried out under regulations of the Animals (Scientific Procedures) Act 1986 of the UK Government, and according to guidance issued by the Medical Research Council, UK in "Responsibility in the use of animals for medical research". Mice were kept on a 12 hr light, 12 hr dark cycle, with the dark period centred on 1 a.m. Experimental litters (both embryos and pups) were generated by timed matings in which male and female mice were paired overnight and females checked for copulation plugs the following morning. The day of finding a vaginal plug was designated embryonic day (E) 0.5 or 0.5 days post coitum (dpc). Pregnant females were culled by cervical dislocation and embryos were dissected in Dulbecco's Modified Eagle's Medium (Invitrogen), containing 10% fetal calf serum (Sigma) under a dissecting microscope (ZEISS, Semi SV6). Deciduas were freed from the uterine wall and the conceptus was then removed from each decidua. The yolk sac and Reichert's membrane were also separated from the embryo.

Embryos were washed in phosphate buffered saline (1x PBS) and either immediately frozen prior to RNA or protein isolation or fixed in 4% paraformaldehyde (PFA) in 1x PBS at 4°C o/n for in-situ hybridisation, other histological analysis and general storage (adult mouse brains were dissected out from the skull and placed in cold 4% PFA and fixed at 4°C for two days). The following day, embryos (or adult brains) were dehydrated in graded ethanol series and stored at 4°C (1x PBS washes twice, 30% ethanol, 50% ethanol and 70% ethanol twice) for paraffin sections; or in graded methanol series and stored at -20°C (1x PBS washes twice, 25% methanol, 50% methanol, 75% methanol, 100% methanol twice) for whole mount in-situ hybridisation. The timing varied according to the size of tissue and hence determined by the developmental stage but a general guideline is: 7.5-8.5 dpc 10min washes, 9.5-10.5 dpc 25min washes, 11.5-13.5 dpc 45 min washes, 14.5-16.5 1 hr washes, 17.5 dpc and above 1.30 hrs washes.

7.5.5. Genotyping mice and embryos

Genomic DNA from mice was prepared from tail extraction and ear biopsies taken at the time of weaning. Each tail tip was digested by proteinase K (500 µg/ml) in a total volume of 200 µl lysis buffer containing 5 mM EDTA, 100 mM NaCl, 50 mM Tris, 1% SDS, at 55°C o/n. The DNA was extracted by adding 0.2x volume (80 µl) of saturated salt solution (NaCl), followed by incubation on ice for 30 min. The protein precipitate was removed by centrifugation at 13,000 rpm at 4°C for 10 min. The supernatant (containing DNA) was removed and 2x volume of ice cold 100% ethanol was added to it, the tube inverted a few times until DNA precipitate was visible. The DNA was pelleted by spinning at 13,000 rpm for 5 min. The pellets were washed with 70% ethanol (500 µl), pulse-spun and air dried. The pellet was resuspended in 200-500 µl ddH_2O.

Embryos were genotyped from DNA samples prepared from a piece or the whole embryo. The total volume varied according the size of tissue taken to genotype but the embryo piece was generally digested with PK in 20-100 µl of RNA-free ddH_2O. Genotyping analysis was carried out by PCR; table contains a list of the primers and PCR conditions used for the genotype analyses.

7.5.6. Paraffin embedding and sectioning of embryos and adult brains

Embryos and adult brains (stored in 70% ethanol), were prepared for paraffin wax embedding by first dehydrating them up to 100% ethanol (80% ethanol, 95% ethanol and 100% ethanol twice). They were then cleared by two washes of Histoclear (National Diagnostics) at rt. The timing varied according to the developmental stage (15-20 min for 10.5 dpc, up to 1 hr for 17.5 dpc and older). For embryos older than 16.5 dpc the skin was removed to allow good penetration of liquid and wax. After Histoclear washes, embryos were placed in Histoclear:wax (1:1) at 60°C for 30 min (up to an hr for 17.5 dpc and above). This was followed by three warm wax washes at 60°C (1 hr each). Finally in the fourth wax wash, the embryos were placed in plastic or glass molds with warm wax and oriented using a heated needle and a microscope. They were then left to set o/n at rt and stored at 4°C until needed for sectioning.

Sagittal, coronal/frontal and transverse sections (6-8 µm) were cut using a rotary microtome (Davydoo's microtome HM 325) and serial sections were prepared in 6 series for up to 12.5 dpc embryos and 8 series for older embryos. Sections were floated

on distilled water on superfrost slides (BHD) and placed on a heated plate to flatten the tissue. The excess water was removed and the samples were left to dry at 37°C o/n. The dry samples were stored at 4°C until needed for further analysis.

7.5.7. X-Gal staining

Embryos were fixed in 0.2% gluteraldehyde (prepared in 1x PBS) for 30-45 min at 4°C for embryos up to 10.5dpc (or in 0.1% gluteraldehyde and 0.1% Tween 20 if not needed for histological analysis). They were then washed three times in 1x PBS for 5 min each wash, shaking at rt. They were stained in X-Gal solution (staining solution plus 1 mg/ml X-Gal) at 37°C overnight. After staining the following day they were washed three times in 1x PBS and post-fixed in 4% PFA overnight at 4°C. They were washed with 1x PBS three times and stored in 0.1% PFA.

7.5.8. Haematoxylin and eosin staining

Paraffin sections were de-waxed and re-hydrated in ethanol series (Histoclear washes twice, 100% ethanol twice, 90% ethanol, 70% ethanol, 50% ethanol, 30% ethanol, ddH_2O twice). They were stained in haematoxylin (Sigma) for 1-5 min and left in running water for a few minutes. Once the desired staining was achieved they were stained with eosin (Sigma) for 5-10 min and left in running water until the desired staining was achieved. At this point they were dehydrated in separate ethanol series (30%, 50%, 70% and 100% ethanol twice) and mounted in DPX (BDH).

7.5.9. Microscopy and imaging

Wholemount embryo images were obtained using a microscope fitted with a digital camera (Leica MZFL III) and Image Manager Software (IM Leica1000 V1.20). Images from sections were generated with a Zeiss Axiophot 2 microscope, fitted with a digital camera (Kontron Electronik) using Adobe Photoshop 6.0. Openlab 3.11 software was used for cell images after immunofluorescence experiments.

All images presented in this thesis were processed using the Adobe Photoshop 6.0 software.

7.6. RNA METHODS

7.6.1. Riboprobe synthesis and preparation

General laboratory practice when working with RNA was to wear gloves at all times and clean (RNA-free) equipment and reagents were used. All reagents and tubes were kept on ice. Autoclavable solutions and water were treated with DEPC (0.05% v/v), left o/n in the fumehood and autoclaved the next day. Solutions which could not be autoclaved such as Tris, EDTA and SDS were made using DEPC treated water. The working area was cleaned and all metal and glassware were rinsed with ddH2O and baked (180°C for 6 hrs).

Antisense RNA probes were transcribed in-vitro either from existing plasmids (usually purified by either midi- or maxiprep) or directly from PCR products which had incorporated a suitable RNA polymerase promoter during the amplification process (e.g. T3 RNA pol) and cloned into the appropriate vector (Table 8.11), plasmid DNA from positive clones were then purified by midi- or maxiprep.

10-20µg of vector was digested in a volume of 100 µl with the appropriate enzyme. The linearised plasmid was then treated with PK by adding the following to the tube (1 µl of 0.5M EDTA, 5 µl of 20% SDS and 1 µl of 20 mg/ml PK) and incubated at 55°C for 30 min. The DNA was then purified using phenol chloroform extraction by adding an equal volume (100 µl) of the phenol:choloform:isoamylalcohol (25:24:1) mix. Mixed by vigorous shaking/vortexing until a homogeneous solution was formed. The tubes were centrifuged at 13,000 rpm for 20-45 min at rt. The aqueous phase (top layer), which contains the DNA, was collected and precipitated by adding 1/10 3M NaAc and 2x 100% ethanol and storing at -80°C for 30 minutes or alternatively at -20°C o/n. This was centrifuged at 13,000 rpm for 20-45 min at 4°C. The pellet was washed by adding 70% ethanol, vortexing and centrifuging at 13,000 rpm at rt for 5 min. The pellet was air dried and dissolved in 40 µl RNA-free ddH_2O.

The probe was then transcribed in-vitro with the appropriate polymerase: T3; T7 or SP6 (Roche) and labelled with either digoxigenin (Roche) or fluorescein (Roche) by incubating the reaction mixture: 1 µg linearised DNA; 2 µl DNA labelling mix (containing either DIG or fluorescein); 0.5 µl RNAse inhibitor (Roche); 2 µl transcription buffer; 2 µl RNA polymerase (T3, T7 or SP6) in a total volume of 20 µl, at the correct temp (37°C for T3 and T7, 40°C for SP6) for 2 hrs.

The reaction was stopped by adding 1 µl of EDTA and storing on ice. This was then cleaned using Chroma Spin-100 columns (Clontech) as described by the manufacturer's manual. 2 µl of the cleaned probe was run on an agarose gel to check the amount of probe and that no degradation had occurred. Table contains a list of probes used in this work.

7.6.2. Wholemount in-situ hybridisation

Before hybridisation, embryos were re-hydrated in a graded methanol series for 5 min each wash followed by two washes in PBT (1x PBS and 0.1 % Tween-20). They were then bleached in 6% hydrogen peroxide for 1 hr at rt followed by three PBT washes. This was followed by 10 µg/ml proteinase K in PBT treatment for 5-15 min (timing varied according to developmental stage 6.0-8.5 dpc). They were then rinsed in 2 mg/ml glycine in PBT for 5 min followed by two quick PBT washes. Fixation was for 20 min in 0.2% gluteraldehyde/4% paraformaldehyde in PBT followed by three 5 min PBT washes. After this, the embryos were prehybridised in hybridisation buffer (50% formamide; 5xSSC; 0.1% Tween-20; 50µg/ml heparin) for 1 hr at 70°C. Afterwards the hybridisation buffer was replaced by fresh hybridisation buffer containing 50 µg/ml tRNA and 50 µg/ml denatured salmon/herring sperm DNA. The digoxigenin labelled RNA probe was also added at 150-200 ng/ml final concentration and incubated overnight at 70°C.

After hybridisation (the next day), embryos were washed at 70°C shaking for 30 min each wash with solution I (50% formamide, 4xSSC, 1% SDS). This was followed by three 5 min washes at room temperature in solution II (0.5M NaCl, 0.01M Tris pH7.5, 0.1% Tween-20) and two 30 min washes at 65°C with solution III (50% formamide, 2 xSSC pH4.5). The embryos were washed four times at room temperature with TBST (1x TBS: 40 g NaCl, 1 g KCl, 0.25 M Tris pH7.5 plus 0.1 % Tween-20 in 500ml water). The embryos were blocked at room temperature shaking for 1 hr in 10% heat inactivated sheep serum (HISS) in TBST. They were incubated in fresh TBST with 1% HISS and 1:2000 anti-DIG FAB antibody at 4°C overnight. The embryos were subsequently washed three times in NTMT (100 mM NaCl, 100 mM Tris pH 9.5, 50 mM $MgCl_2$, 0.1% Tween-20) at rt and stained using the NBT/BCIP system (Roche) by adding 4.5 µl/ml NBT and 3.5 µl/ml BCIP in NTMT until an optimal signal was obtained (check after 20 min). The staining reaction was

stopped by three 5 min washes in NTMT and PBT. They were then post-fixed in 4% PFA and stored at 4°C in 0.1% PFA/PBT.

7.6.3. Section in-situ hybridisation

Sections were de-waxed (Histoclear washes twice 10min each wash), re-hydrated (100% ethanol twice, 70% ethanol, 50% ethanol, 25% ethanol, 1x PBS twice 2 min each wash) and fixed in 4% PFA (20 min). After proteinase K (20 µg/ml in 1x PBS) treatment (8 min at rt) and fixation (4% PFA, 5 min), they were treated with 0.1M triethanolamine plus 0.25% acetic anhydride (10 min stirring at rt). The slides were then de-hydrated and hybridised on the same day. Hybridisation was carried out o/n at 55-65°C in 50% formamide, 0.3 M sodium chloride, 20 mM Tris HCl, 5 mM EDTA, 10% Dextran sulphate, 1x Denhardt's reagent (SIGMA) supplemented with tRNA (SIGMA), RNAase inhibitor (Roche) and the relevant digoxigenin-labelled riboprobe (1 µl per slide). Stringency washes consisting of 2x SSC (twice, 30 min), formamide: 2x SSC at 1:1 ratio (twice, 30 min), 2x SSC (twice, 30 min), were carried out the following day at 65°C. Slides were then blocked for one hour in 10% fetal calf serum (FCS) prepared in buffer 1 (0.1M Tris pH 7.6 and 0.15M sodium chloride) and placed in a humid chamber in buffer 1 plus anti-digoxigenin antibody conjugated with alkaline phosphatase (1:1000 from Roche) and 2% FCS. The following day the slides were washed with buffer 1 (three times 5min each wash) and washed twice with buffer 2 (0.1M Tris pH 9.5, 0.1M NaCl and 0.05M $MgCl_2$). Staining was carried out the following day using the NBT/BCIP system (Roche) in 2x buffer 2 : 10% PVA at 1:1 ratio. Reaction was stopped by a 10 min wash in water and placing the slides at 50°C for 15-30 min. They were then dehydrated in a separate alcohol series and two Histoclear washes. Finally sections were mounted in Vector Mount (Vector Laboratories) and photographed with a Leica microscope.

7.6.4. RT-PCR

Total RNA was isolated from the anterior region of the neural plate of 8.5 dpc embryos and the developing Rathke's pouch of 12.5 dpc wild-type mouse embryos using the RNeasy Micro Kit (Qiagen). First strand cDNA synthesis was performed using the Omniscript RT Kit (Qiagen) according to manufacturer's protocol.

8. APPENDICES

8.1. APPENDIX I – GENERATION OF *Hesx1-I26T* AND *Hesx1-R160C* TARGETED ALLELES

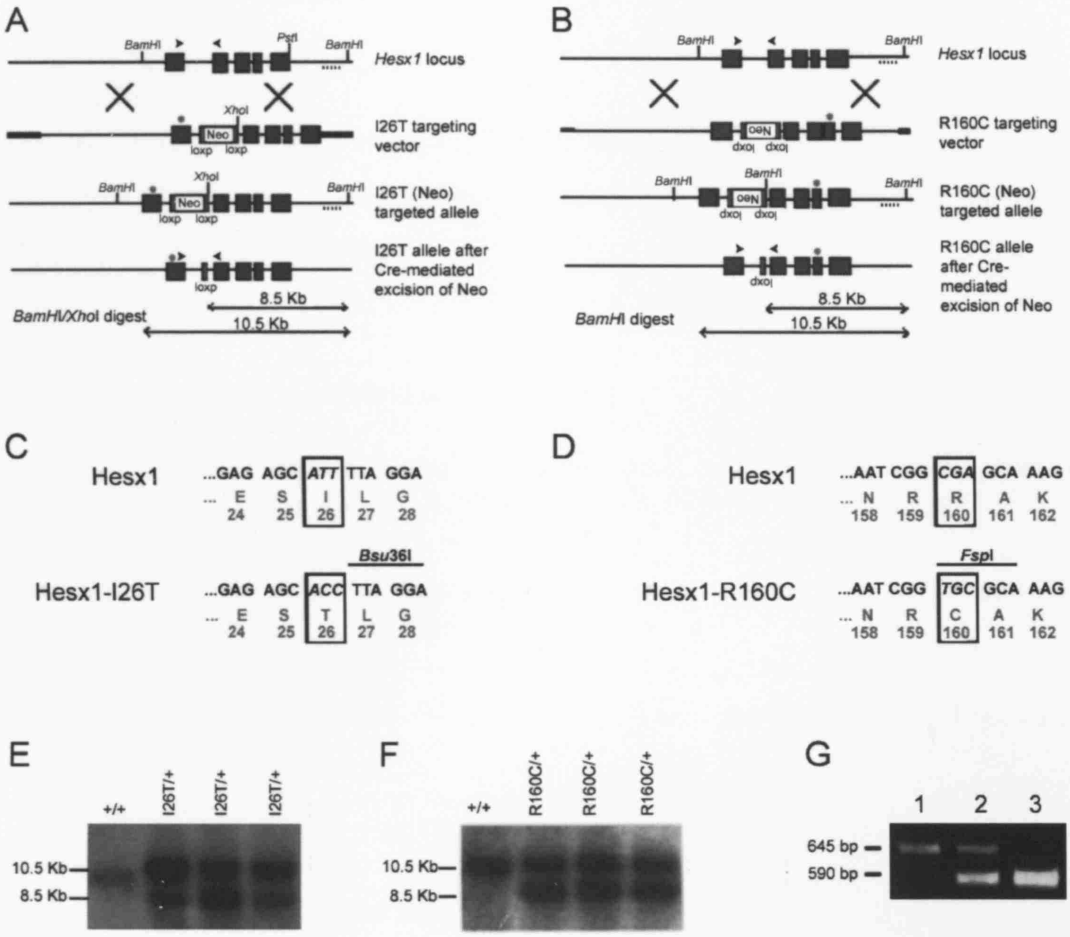

Figure 8.1 – Generation of the *Hesx1-I26T* and *Hesx1-R160C* targeted alleles. (A,B) Top to bottom: structure of the murine *Hesx1* locus; *Hesx1-I26T* (A) and *Hesx1-R160C* (B) targeting vectors; targeted alleles prior to and after Cre-mediated excision of the *Neo* cassette; expected bands for the targeted and wild-type alleles after Southern blot analysis of DNA samples digested with the indicated restriction enzymes and hybridised with and external probe (dotted line). The position of the mutation is indicated with an asterisk on exons one (I26T) and four (R160C) of the targeting vectors and targeted alleles. Note that the orientation of the *loxP* and *Neo* cassette has been inverted in the *Hesx1-R160C* targeting vector. (C) The triplet ATT encoding isoleucine at position 26 was replaced by ACC, which encodes the amino acid threonine. This mutation introduces a novel *Bsu36I* restriction site on the mutated allele. (D) The triplet encoding arginine at position 160 was replaced by TGC, which encodes the amino acid cysteine. This mutation introduces a novel *FspI* restriction site in the mutated allele. (E,F) Southern blot analysis of DNA samples from wild-type (+/+), $Hesx1^{I26T/+}$ (E) and $Hesx1^{R160C/+}$ (F) ES cell clones digested with either *BamHI/XhoI* (E) or *BamHI* (F) and hybridised with an external probe (dotted line in A,B). (G) Representative example of PCR genotyping of DNA samples from either $Hesx1^{I26T/I26T}$ or $Hesx1^{R160C/R160C}$ homozygous (1), $Hesx1^{I26T/+}$ or $Hesx1^{R160C/+}$ heterozygous (2) or $Hesx1^{+/+}$ (3) wild-type embryos. Note that the primers used for genotyping both targeted alleles are the same (black arrowheads in A and B).

8.2. APPENDIX II – BUFFERS AND SOLUTIONS

8.2.1. DNA Methods

8.2.1.1. Media

SOC medium: 20g/l bacto-tryptone, 5g/l yeast extract, 10mM NaCl, 2.5 mM KCl. Autoclave, then add filter sterilised 20mM Mg2+ (1M MgCl2.6H2O, 1M MgSO4.7H2O) and 20mM glucose.

8.2.1.2. Antibiotics

Ampicillin: stock conc. 50 mg/ml, filter sterilised, working conc. 100 μg/ml in agar/50 μg/ml in liquid LB.

Kanamycin: stock conc. 10 mg/ml, filter sterilised, working conc. 50 μg/ml in agar/10 μg/ml in liquid LB.

Chloramphenicol: stock conc. 34 mg/ml in ethanol, working conc. 170 μg/ml in agar/34 μg/ml in liquid LB.

8.2.1.3. Qiagen kits

Solution P1: 50 mM Tris-HCl pH 8.0, 10 mM EDTA, 100 μg/ml RNase I.

Solution P2: 200 mM NaOH, 1% SDS.

Solution P3: 3 M KOAc, adjusted to pH 5.5 with 2M glacial acetic acid.

Solution PB: 7.6 M NaSCN, 10% ethanol, 5% Tween-20, 60 mM glycine.

Solution PE: contains 80% ethanol (possibly in 10 mM Tris-HCl pH8.5).

Solution EB: 10 mM Tris-HCl pH 8.5.

Solution QBT: 750 mM NaCl, 50 mM MOPS pH 7.0, 15% v/v isopropanol, 0.15% v/v Triton X-100.

Solution QC: 1 M NaCl, 50 mM MOPS pH 7.0, 15% v/v isopropanol.

Solution QF: 1.25 M NaCl, 50 mM Tris-HCl pH 8.5, 15% v/v isopropanol.

Solution TE: 10 mM Tris-HCl pH 8.0, 1 mM EDTA.

8.2.1.4. Agarose gel electrophoresis

1x TAE buffer: 40mM Tris-acetate, 1mM EDTA pH 8.0.

10x loading buffer (blue): 0.5% bromophenol blue, 0.5% xylene cyanol, 50% Ficoll 400 .

5x loading buffe (orange): 0.1% Orange G, 50% TE (x1), 50% glycerol.

8.2.1.5. Polymerase Chain Reaction

Table 8.1 – PCR reaction mix.

Component	DNA mix (µl)		Enzyme mix (µl)	
	Taq buffer	JD buffer	*Taq* buffer	JD buffer
H2O	7.08	1.7	6.4	1.55
Taq Pol buffer (x10)	1.2	-	0.8	-
MgCl2 (25 mM)	0.72	-	0.48	-
JD buffer (x3)	-	2.5	-	0.83
Primer 1	1 (of 25 µM)	0.5 (of 10 µM)	-	-
Primer 2	1 (of 25 µM)	0.5 (of 10 µM)	-	-
dNTP (25 mM)	-	0.3	0.16	-
Taq Pol (5 u/µl)	-	-	0.16	0.12

3x JD buffer: 60 mM K-glutamate, 24 mM Hepes, 90 mM Tris, 15 mM $MgCl_2$, 6 mM DTT, 180 mM NH_4Ac, 3% DMSO, 24% glycerol.

8.2.2. RNA Methods

8.2.2.1. Whole mount in-situ hybridisation

PBT: 1x PBS, 0.1% Tween-20.

Hybridisation buffer: 50% formamide; 5xSSC; 0.1% Tween-20; 50µg/ml heparin.

Solution I: 50% formamide, 4xSSC, 1% SDS.

Solution II: 0.5M NaCl, 0.01M Tris pH7.5, 0.1% Tween-20.

Solution III: 50% formamide, 2 xSSC pH4.5.

NTMT: 100 mM NaCl, 100 mM Tris pH 9.5, 50 mM $MgC1_2$, 0.1% Tween-20.

8.2.2.2. Section in-situ hybridisation

Hybridisation mix: 50% formamide, 0.3 M sodium chloride, 20 mM Tris HCl, 5 mM EDTA, 10% Dextran sulphate, 1x Denhardt's reagent.

Buffer 1: 0.1M Tris pH 7.6 and 0.15M sodium chloride.

Buffer 2: 0.1M Tris pH 9.5, 0.1M NaCl and 0.05M $MgCl_2$.

8.2.3. Yeast Methods

8.2.3.1. Media

Table 8.2 – Components of YPAD medium.

Constituent	Concentration (%)	Amount	Company
Bacto yeast extract	1	10 g	Difco
Bacto peptone	2	20 g	Difco
Glucose	2	40 ml of 50% solution	Sigma
Adenine sulfate	0.004	10 ml of 0.2% solution	Sigma
Bacto agar	2	20 g	Difco
Distilled water	~93	Up to 1000 ml	-

Table 8.3 – Components of SD selective medium.

Constituent	Concentration (%)	Amount	Company
Bacto yeast nitrogen base w/o amino acids	0.67	6.7 g	Difco
Bacto agar	2	30 g	Difco
Glucose	2	40 ml of 50% solution	Sigma
Distilled water	~95	Up to 1000 ml	-

Table 8.4 – Amino acid concentrations used in SD "drop-out" media.

Constituent	Stock conc.	Volume of stock for 500 ml	Final conc.	Supplier
Adenine sulfate	2 mg/ml	5 ml	20 mg/ L	Sigma
Uracil	2 mg/ml	5 ml	20 mg/ L	Sigma
L-Triptophan	10 mg/ml	1 ml	20 mg/ L	Sigma
L-Histidine	10 mg/ml	1 ml	20 mg/ L	Fluka
L-Methionine	10 mg/ml	1 ml	20 mg/ L	Sigma
L-Leucine	10 mg/ml	3 ml	60 mg/ L	Fluka
L-Lysine	10 mg/ml	1.5 ml	30 mg/ L	Fluka
X-α-Gal	20 mg/ml	0.5 ml	20 mg/ L	BD Biosciences
3-AT	500 mM	4 ml	4 mM	Sigma

8.2.3.2. Buffers

10x TE: 0.1M Tris pH 7.5 (50ml of 1M stock) is added to 0.01M EDAT (10ml of 0.5M stock) in 500ml of distilled water and autoclaved.

10x LiOAc: 51g of lithium acetate is dissolved in 500ml of distilled water and autoclaved (1M).

50% PEG-4000: 250g of polyethylene glycol-4000 is dissolved in 500ml distilled water and autoclaved.

TE/LiOAc: 1x TE and 0.1M LiOAc: 1 part 10x TE is added to 1 part 10x LiOAc and 8 parts distilled autoclaved water.

TE/LiOAc/PEG: 1x TE, 0.1M LiOAc and 10% PEG: 1 part 10x TE is added to 1 part 10x LiOAc and 8 parts 50% PEG-4000.

Yeast lysis buffer: 50 mM Tris-HCl pH 7.5, 1.2 M sorbitol, 10 mM EDTA, 10 mM β-mercaptoethanol (added fresh) plus 200 u lyticase enzyme (Sigma).

8.2.4. Protein Methods

8.2.4.1. Buffers

NETN buffer: 20 mM Tris–HCl pH 7.5, 200 mM NaCl, 1mM DTT, 1 mM EDTA, 0.5% NP-40 and protease inhibitor cocktail added fresh (Roche).

Storage buffer: 10 mM Hepes pH 7.6, 100 mM NaCl, 1mM EDTA, 25% glycerol, 1mM DTT and protease inhibitor.

10x SDS-PAGE running buffer: 30.2 g Tris base, 144g glycine, 10g SDS up to 1 litre with ddH_2O.

5x Leammli loading buffer: 25 mM Tris-HCl (pH 6.8), 2% SDS, 25% glycerol, 0.1% bromophenol blue, 5% β-mercaptoethanol (added fresh).

Coomassie staining solution: 50% methanol, 10% acetic acid, 0.25% Coomassie Blue R-250.

Destaining solution: 25% methanol, 7% acetic acid in water.

TBST: 40 g NaCl, 1 g KCl, 0.25 M Tris pH7.5 in 500ml water plus 0.1 % Tween-20.

Blocking solution: 10% milk in TBST.

Transfer/blotting buffer x10: 58.2 g Tris base, 3.75 g SDS, 2.94 glycine, 20% methanol up to 1 litre with ddH_2O.

Table 8.5 – Composition of SDS-PAGE resolving and stacking gels.

Component	Resolving gel				Stacking gel
	15%	12.5%	10%	7.5%	~5%
30% acrylamide	5.0 ml	4.2 ml	3.3 ml	2.5 ml	0.88 ml
H2O	2.8 ml	3.7 ml	4.5 ml	5.3 ml	3.6 ml
Tris-HCl buffer*	2 ml	2 ml	2 ml	2 ml	0.3 ml
10% SDS	100 µl	100 µl	100 µl	100 µl	50 µl
10% APS	50 µl	50 µl	50 µl	50 µl	40 µl
TEMED	10 µl	10 µl	10 µl	10 µl	7 µl

*: 1.5 M Tris, pH 8.8 is used for resolving gels; 1 M Tris, pH 6.8 is used for stacking gels.

8.2.5. Cell culture Methods

8.2.5.1. Lysis buffers

Table 8.6 – Conditions used for cell lysis following transfection.

Condition*	Lysis buffer	Incubation
Standard	20 mM Tris pH7.5 150 mM NaCl 1% Triton X-100	Ice, 20 min
1	20 mM Tris 100 mM NaCl 0.5% NP40 1 mM EDTA	Sonication (3-4 x 10 sec pulses)
2	20 mM Tris 200 mM NaCl 0.5% NP40 1 mM EDTA	Sonication (3-4x 10 sec pulses)
3	20 mM Tris 300 mM NaCl 0.5% NP40 1 mM EDTA	Sonication (3-4x 10 sec pulses)
4	50 mM Tris 150 mM NaCl 1% NP40 0.5% Deoxycholic Acid	Ice, 20 min
5	20 mM Tris 150 mM NaCl 1% TritonX-100 1 mM EDTA	Sonication (3-4x 10 sec pulses)

*: Conditions 1-5 were used for co-immunoprecipitation experiments using HA-HESX1 and Flag-SAFB1 or Flag-LONP2 (see Figure 3.7).

8.2.5.2. Antibodies

Table 8.7 – Details of primary and secondary antibodies.

Antibody	Host Species	Dilution	Company
Anti-Flag M2 monoclonal	Mouse	1 µg/IP	Sigma
Anti-Flag M2 peroxidase conjugate	Mouse	1:1000	Sigma
Anti-Flag polyclonal	Rabbit	1:250	Sigma
Anti-HA high affinity monoclonal	Rat	1:250/0.5 µg/µl	Roche
Polyclonal rabbit anti-mouse HRP	Mouse	1:2000	DakoCytomation
Alexa Fluor 594	Rabbit	1:350	Invitrogen
Alexa Fluor 488	Mouse	1:350	Invitrogen

8.2.6. Animal Methods

8.2.6.1. X-Gal staining

Buffer L (x1): 2 mM $MgCl_2$, 0.2% NP40, 20 mM Tris-HCl pH 7.5, 0.1% Na-Deoxycholate made in 1x PBS.

LacZ solution: x1 Buffer L plus 10 mM $K_3Fe(CN)_6$ and 10 mM $K_4Fe(CN)_6.3H_2O$.

X-Gal solution: LacZ solution plus 1 mg/ml X-Gal (50mg/ml stock dissolved in DMF).

8.2.6.2. Genotyping

Tail lysis buffer: 5 mM EDTA, 100 mM NaCl, 50 mM Tris, 1% SDS plus 500 μg/ml proteinase K added fresh.

8.3. APPENDIX III - VECTORS AND PRIMERS

Table 8.8 – Details of vectors and inserts used in the yeast two-hybrid screen.

Vector	Insert	RE cloning sites	Primer
pGBDU-C3	Hesx1 aa 1-185	EcoRI/BamHI	cggaattcatgtctcccagccttcg cgggatcctactatttcagaagatctgg
pGBDU-C3	Hesx1 aa 1-107	EcoRI/BamHI	cggaattcatgtctcccagccttcg cgggatcctactatcggtaccaactcaattc
pGBDU-C3 pVP16-AD	Hesx1 mutants* Mouse cDNA library 9.5 and 10.5 dpc	- NotI	- tcgagtttgagcagatgtttaccg gttgtaaaacgacggccagt

* The plasmids carrying the HESX1 mutant sequences were provided by Prof. Dattani's laboratory (Clinical and Molecular Genetics Unit, ICH). The pGBDU-C3 vector essentially contained the cDNA sequences for each of the mutant HESX1 in frame with the Gal4DBD sequence.

Table 8.9 – Details of vectors and inserts used in cell culture and in-vitro assays.

Vector	Insert	RE cloning sites	Primer
pM	*Hesx1*	EcoRI/BamHI	-
pVP16	*Dnmt1*	XhoI/XbaI	-
	Lonp2	EcoRI/XbaI	-
	Srfbp1	EcoRI/XbaI	-
	Zfp592	SalI/XbaI	-
pGEX-4T	*Hesx1*[1]	EcoRI/SalI	-
	Dnmt1[2]	-	-
pCMV/svflag	*Dnmt1*	XhoI/XbaI	ggcctcgagccaccatgccagcgcgaacagct ctagcatctcctcatcgatg
	Lonp2	EcoRI/XbaI	gcgaattcaccatgtcctccgtgagccccatc gctctagactatagtttgctgtcaatgag
	Srfbp1	EcoRI/XbaI	gcgaattcaccatggcggctgaccctcttcct gctctagaccaaaatcaatcatcaaatgtaa
	Safb1	BamHI/XbaI	gcggatccaccatggcggagactctgtcgggtt gctctagagctcaatagcggcgggtgaagc
	Zfp592	SalI/NotI	ggccgtcgacaaaccatgtccaagcactctgacagttat
pcDNA-3	*Safb1*[3]	-	-
	Hesx1	EcoRI/XhoI	-

[1]: *Hesx1* full-length sequences, as well as sequences encoding 7 different fragments of the protein (section 3.2.1) were all cloned into the pGEX-4T vector in-frame with GST.
[2]: *Dnmt1* full-length sequences, as well as sequences encoding 7 different fragments of the protein (section 3.2.7.1.1) were all cloned into the pGEX-4T vector in frame with GST. The 7 fragments were obtained from Dr. P.J. Hurd (Gurdon Institute, University of Cambridge).
[3]: *Safb1* full-length sequences cloned into pcDNA-3 was obtained from Prof. S. Oesterreich (Baylor College of Medicine, Houston, Texas).

Table 8.10 – Details of primers and PCR condtions used for genotyping.

Allele	PCR condition	Primer sequence (5'-3')	Product sizes
Hesx1-I26T	94°C - 30 sec		WT: 590 bp
and	58°C - 30 sec	OL40: tgaagtctcactgggaagatctgg	Mutant: 650 bp
Hesx1-R160C	72°C - 60 sec	OL41: acagacacctgcggtaactcag	
	30 cycles		
Hesx1	94°C - 30 sec	OL1A: cccagatcttcccagtgagacttc	WT: 500 bp
	58°C - 30 sec	OL2A: gattctgtcttcctctaagtttagc	Mutant: 300 bp
	72°C - 45 sec	3'KO: cacctgtgaaggtttcaaaga	
	35 cycles	PGK2: accaaattaagggccagctc	
Cre	94°C - 30 sec		Single band:
	63°C - 30 sec	Cre A: gatgcaacgagtgatgaggttcgc	~500 bp
	72°C - 45 sec	Cre B: accctgatcctggcaatttcggc	
	30 cycles		
Beta-actin cre	94°C - 30 sec		Single band of
	60°C - 30 sec	βActin 1: cgaccagtgtttgccttttatgg	450 bp
	72°C - 45 sec	βActin 2: attcaacttgcaccatgcc	
	30 cycles		
Neo	94°C - 30 sec		Single band:
	60°C - 30 sec	Neo 5'-1: ctgggcacaacagacaatcggct	~500 bp
	72°C - 45 sec	Neo 3'-1: tattcggcaagcaggcatcgcca	
	33 cycles		
Smc	94°C - 60 sec		♂: 2 bands
(Sex specific)	58°C - 60 sec	Smcx: ccgctgccaaattctttgg	♀: 1 band
	72°C - 60 sec	Smcy: tgaagcttttggctttgag	
	34 cycles		
Dnmt1	94°C - 30 sec	ex32F: agtggcatgaaccgcttcaac	WT: ~1.5 kb
	58°C - 30 sec	ex34R: tgcagccaagatgatggccct	Mutant: ~1.4 kb
	72°C - 90 sec	Neo/a: attcgcagcgcatcgccttcta	
	30 cycles		

Table 8.11– Details of probes used for in-situ hybridisation.

Probe	Vector (if available)	Enzyme for linearisation	RNA Polymerase	Primer (if available)
Hesx1	-	BamHI	T3	JP Martinez-Barbera Lab, UCL-ICH
Fgf8	-	NotI	T7	JP Martinez-Barbera Lab, UCL-ICH
Pax6	-	NotI	T3	JP Martinez-Barbera Lab, UCL-ICH
Wnt1	-	HindIII	T7	JP Martinez-Barbera Lab, UCL-ICH
Bf1	-	BamHI	T7	JP Martinez-Barbera Lab, UCL-ICH
Dnmt1	pCMV/sv-Flag1	NotI	Sp6	-
Lonp2	pCMV/sv-Flag1	EcoRI	Sp6	-
Zfp592	pCMV/sv-Flag1	SalI	Sp6	-
Srfbp1	pCMV/sv-Flag1	EcoRI	Sp6	-
Safb1	pVP16	-	T3	pVP16(F): tcgagtttgagcagatgtttaccg pVP16(RT3): aattaaccctcactaaagggttgtaaaacgacggccagt
Lhx3	pCRII	XhoI	Sp6	I. Robinson Lab, UCL-NIMR
Pomc	pCRII	BamHI	T7	I. Robinson Lab, UCL-NIMR
Pit1	pBS/SKII (+/-) in NotI/SalI	NotI	T7	mPit(F): gggcggccgcatgagttgccaatctttcacctcg mPit(R): gcgtcgacccagccttatctgcactctagatg
Prop1	-	EcoRI	T7	MG Rosenfeld Lab, HHMI, California
Cga	pBS/SKII (+/-) in EcoRI/SacI	EcoRI	T3	mGSU(F): cggaattcgcagaagagctatggattactac mGSU(R): cgagctccgcgcccagaagctacgacttgtg
Tshb	pCR4-Topo in NotI/AccI	NotI	T3	IMAGE Consortium, MRC, Cambridge
Gh	pBS/SKII (+/-) in EcoRI/SacI	EcoRI	T3	mGh(F): cgaattcatggctacagactctcggacctcc mGh(R): cgagctcctagaaggcacagctgctttccac
Lhb	-	XbaI	T3	MG Rosenfeld Lab, MRC, Cambridge
Prl	pBS/SKII (+/-) in NotI/SalI	NotI	T7	mPrl(F): gcgcggccgcatgaccatgaacagccaggg mPrl(R): gcgtcgacggactgaatgtgggtttagcag

8.3.1. RT-PCR

Amplification of *Hesx1*, *Dnmt1*, *Safb1*, *Lonp2*, *Zfp592*, *Srfbp1* and *Gapdh* (endogenous control) was performed using specific primers:

Hesx1s: cccagatcttcccagtgagacttc and Hesx1as: gattctgtcttcctctaagtttagc

Dnmt1s: agttccgtggctacgaggag and Dnmt1as: gtctccgtttggcagctggat

Safb1s: tgcaggagatggaagaggcatc and Safb1as: gccgtgctactctgttcaactg

Lonp2s: atgtcctccgtgagccccatc and Lonp2as: aactgcagggacggacatatc

Zfp592s: aagtcctcagcacagagacg and Zfp592as: aagtggcaaggctggaattacag

Srfbp1s: atggcggctgaccctcttcct and Srfbp1as: cccctggtgttcagtgttaacc

Gapdhs: ttccagtatgactccactcacg and Gapdhas: ggatgcagggatgatgttct

8.3.2. Sequencing

Primers used to amplify the cDNA clones from the pVP16 plasmid, after the yeast two-hybrid screen:

pVP16 (F): atggccgacttcgagtttgag

pVP16 (R): gttgtaaaacgacggccagt

8.4. APPENDIX IV - PLASMID MAPS

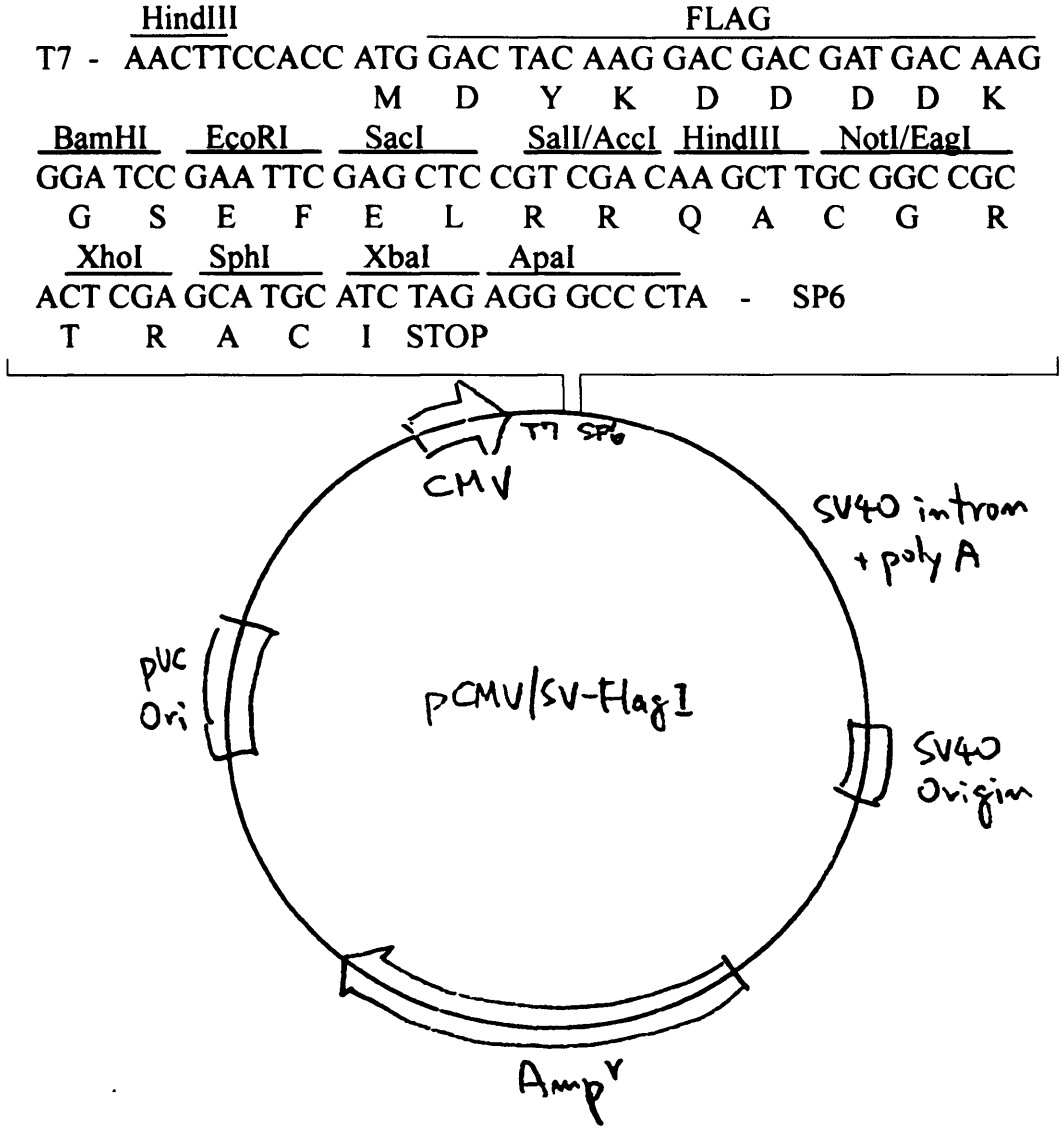

Figure 8.2 – pCMV/SV-Flag1 for the contruction of Flag-tagged proteins.

f1 (+) origin 138–444
β-galactosidase α-fragment 463–816
multiple cloning site 653–760
lac promoter 817–938
pUC origin 1158–1825
ampicillin resistance (*bla*) ORF 1976–2833

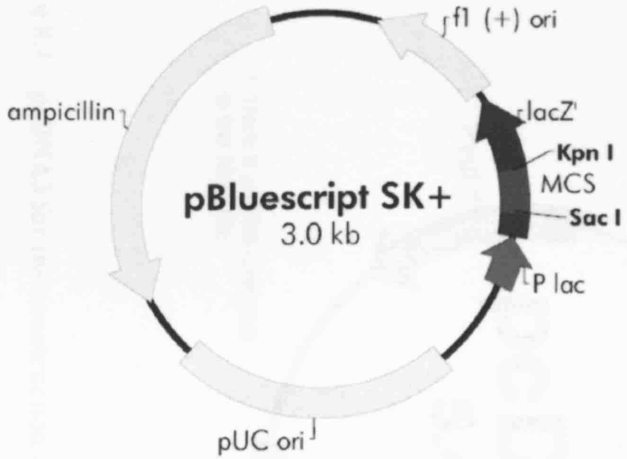

pBluescript SK (+/–) Multiple Cloning Site Region
(sequence shown 601–826)

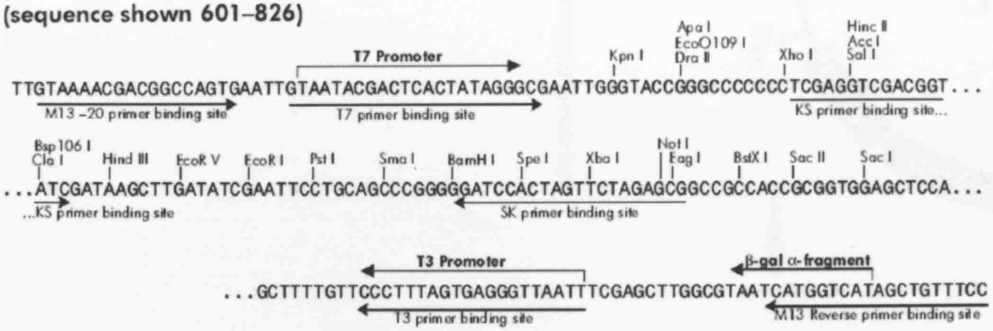

Figure 8.3 – pBluescript SK+/-.

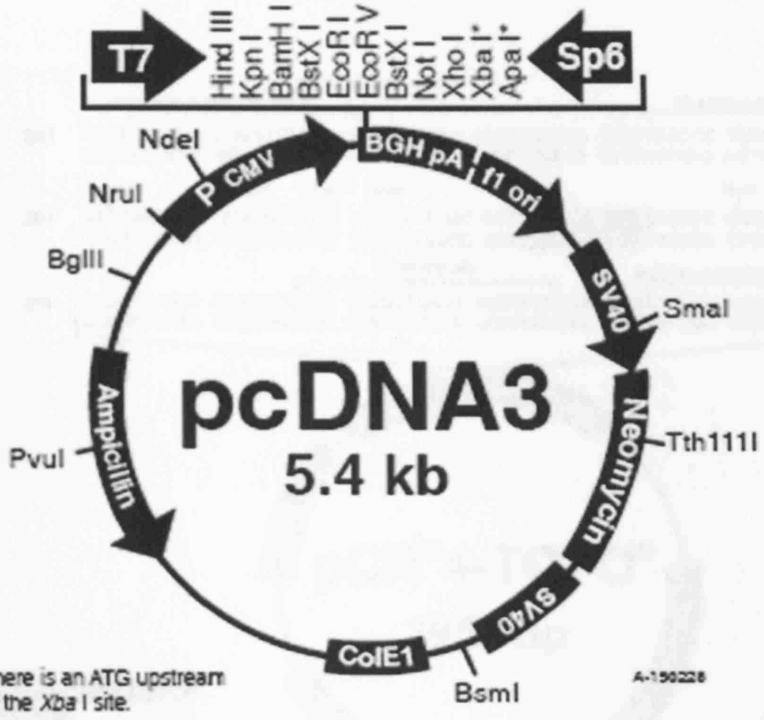

Figure 8.4 – pcDNA3 for the construction of HA-tagged proteins.

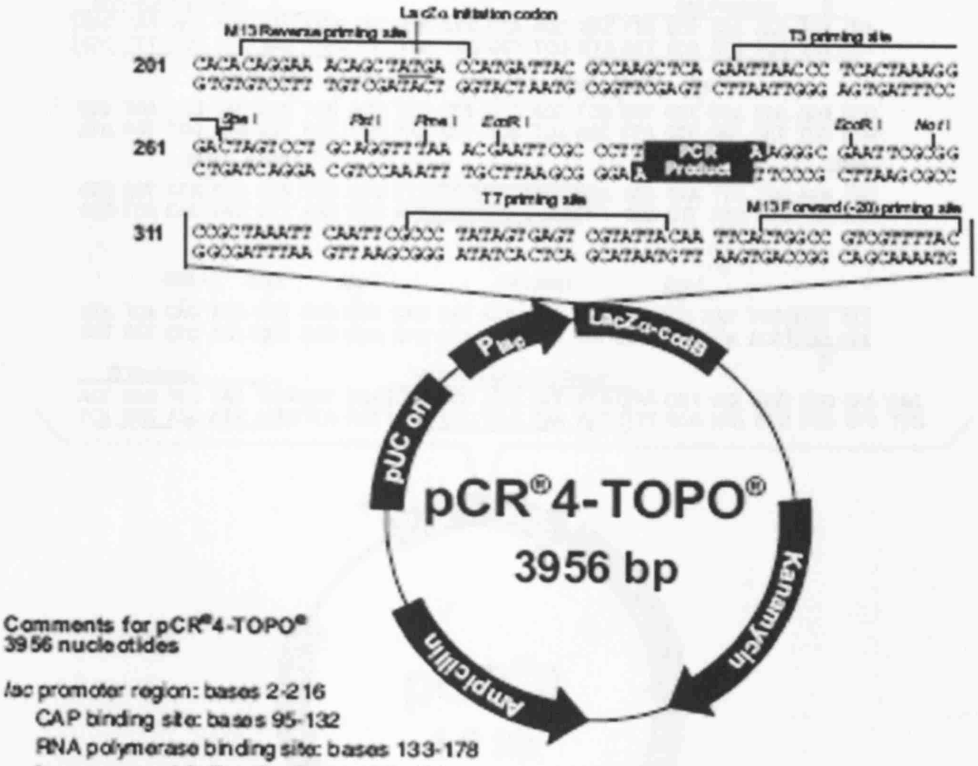

Comments for pCR®4-TOPO®
3956 nucleotides

lac promoter region: bases 2-216
CAP binding site: bases 95-132
RNA polymerase binding site: bases 133-178
Lac repressor binding site: bases 179-199
Start of transcription: base 179
M13 Reverse priming site: bases 205-221
LacZα-*ccdB* gene fusion: bases 217-810
LacZα portion of fusion: bases 217-497
ccdB portion of fusion: bases 508-810
T3 priming site: bases 243-262
TOPO® Cloning site: bases 294-295
T7 priming site: bases 328-347
M13 Forward (-20) priming site: bases 355-370
Kanamycin promoter: bases 1021-1070
Kanamycin resistance gene: bases 1159-1953
Ampicillin (*bla*) resistance gene: bases 2203-3063 (c)
Ampicillin (*bla*) promoter: bases 3064-3160 (c)
pUC origin: bases 3161-3834
(c) = complementary strand

Figure 8.5 – pCR4-TOPO for the synthesis of probes.

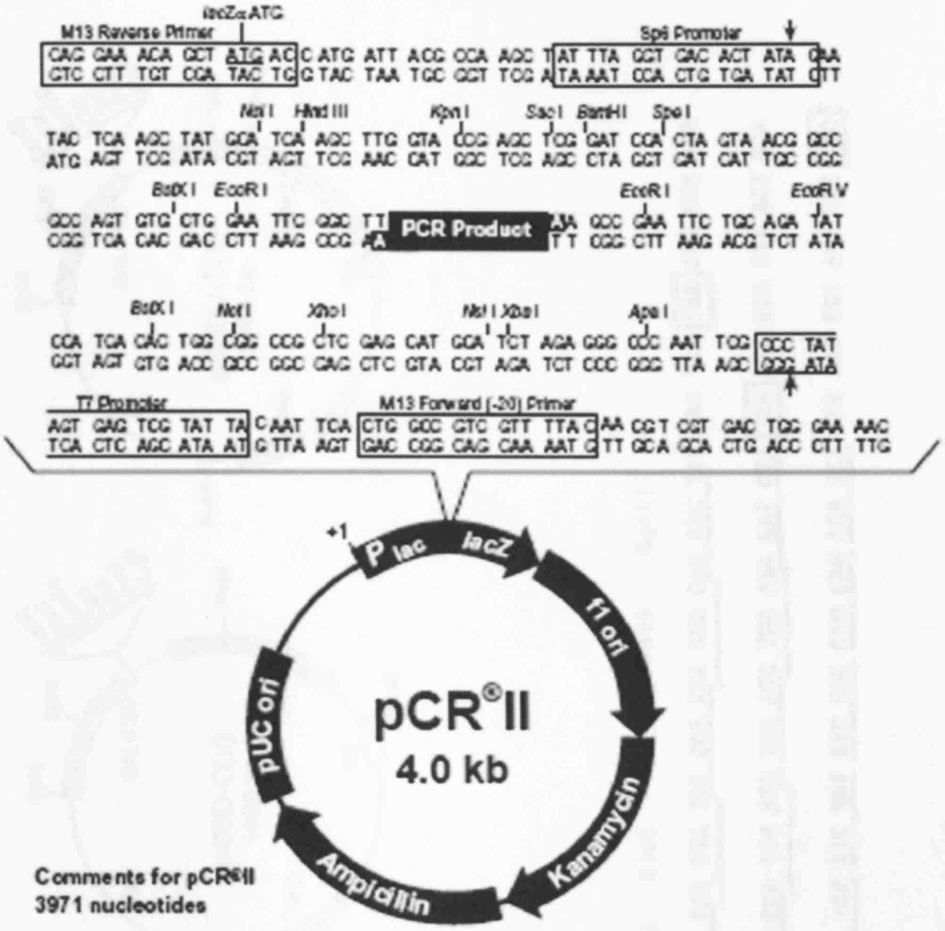

Comments for pCR®II
3971 nucleotides

LacZα gene: bases 1-587
M13 Reverse priming site: bases 205-221
Sp6 promoter: bases 239-256
T7 promoter: bases 404-423
M13 (-20) Forward priming site: bases 431-446
f1 origin: bases 588-1025
Kanamycin resistance ORF: bases 1359-2153
Ampicillin resistance ORF: bases 2171-3031
pUC origin: bases 3176-3849

Figure 8.6 – pCR-II for the synthesis of probes.

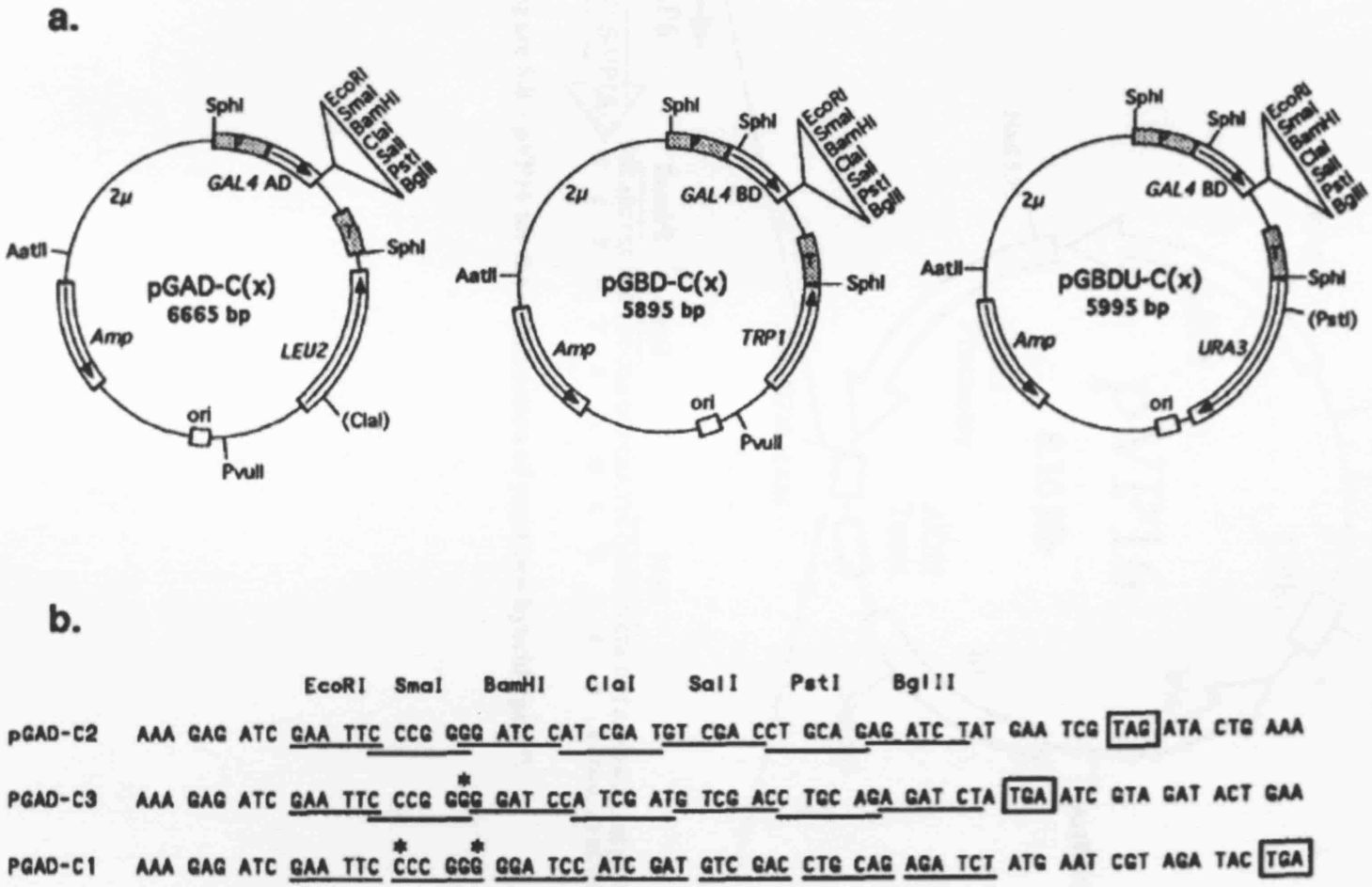

Figure 8.7 – pGBDUC3 for the construction of yeast two-hybrid "bait".

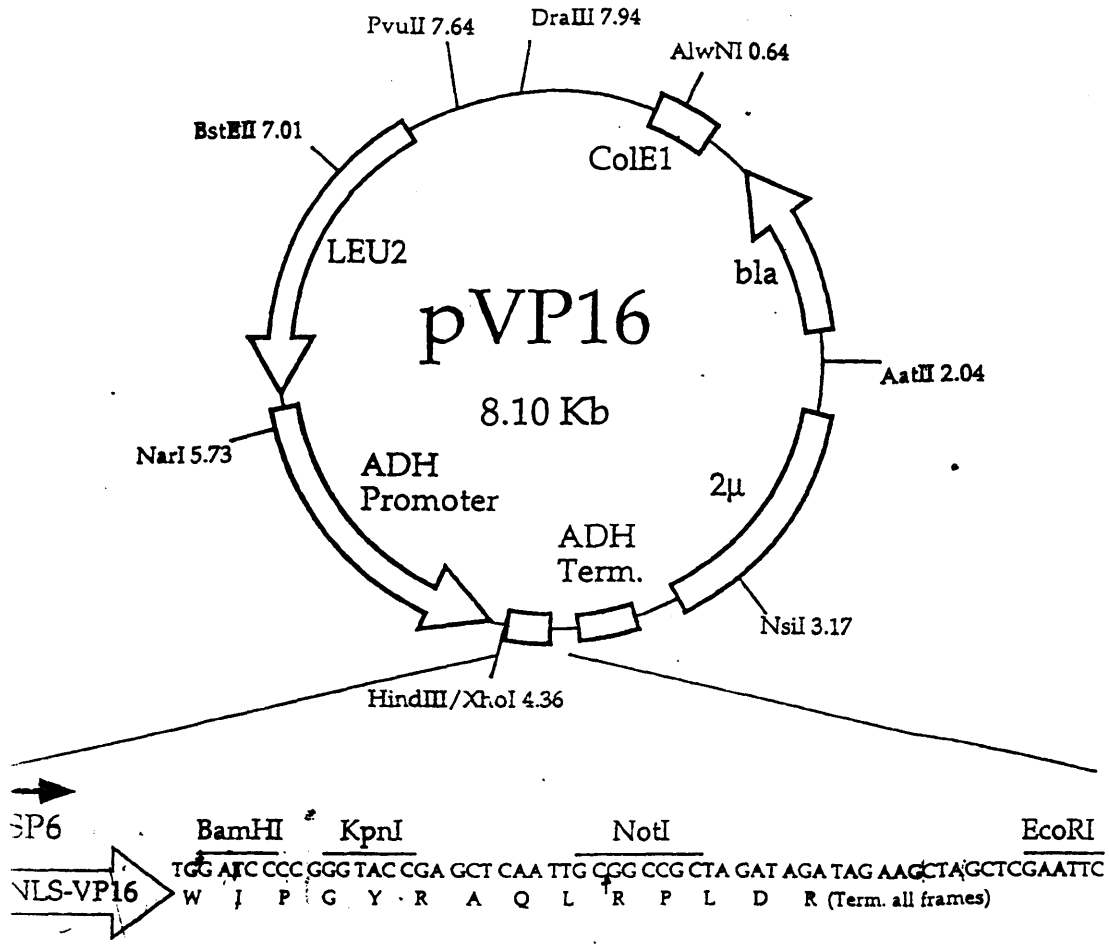

Figure 8.8 – pVP16 for the construction of yeast two hybrid "prey".

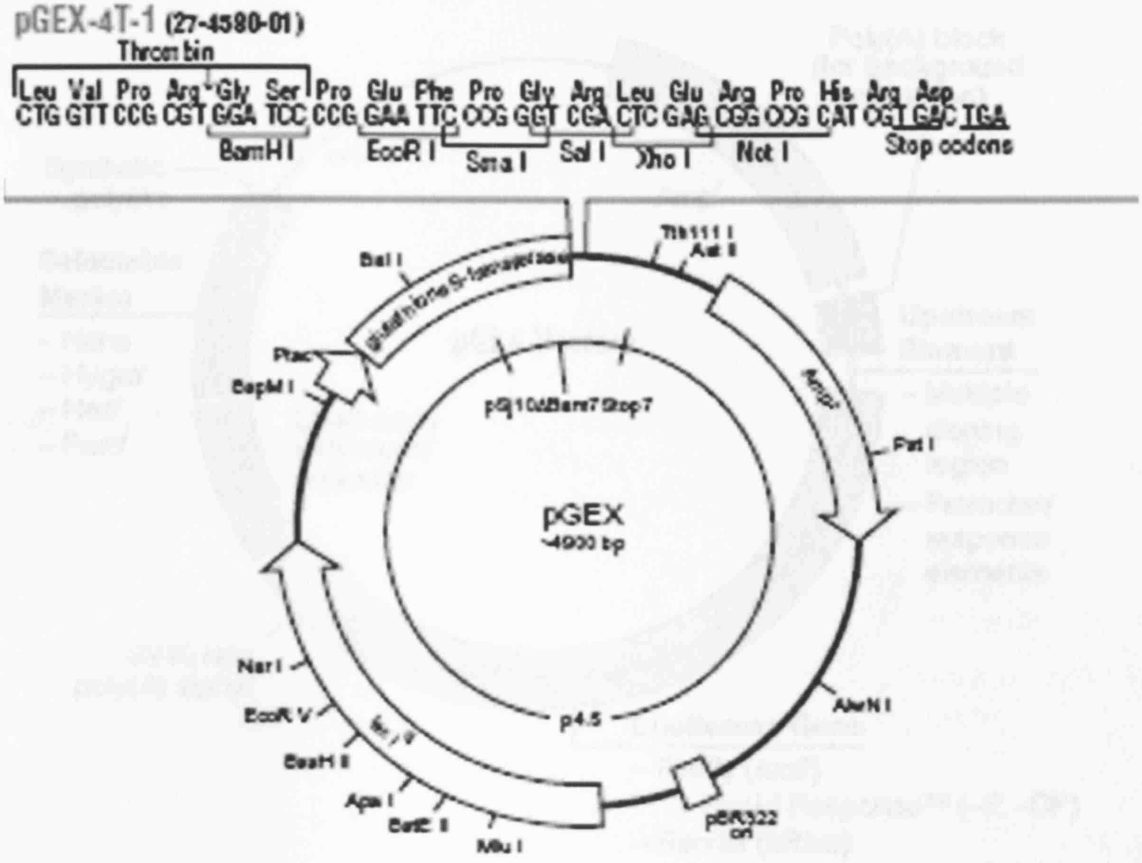

Figure 8.9 – pGEX-4T for the construction of GST-tagged proteins.

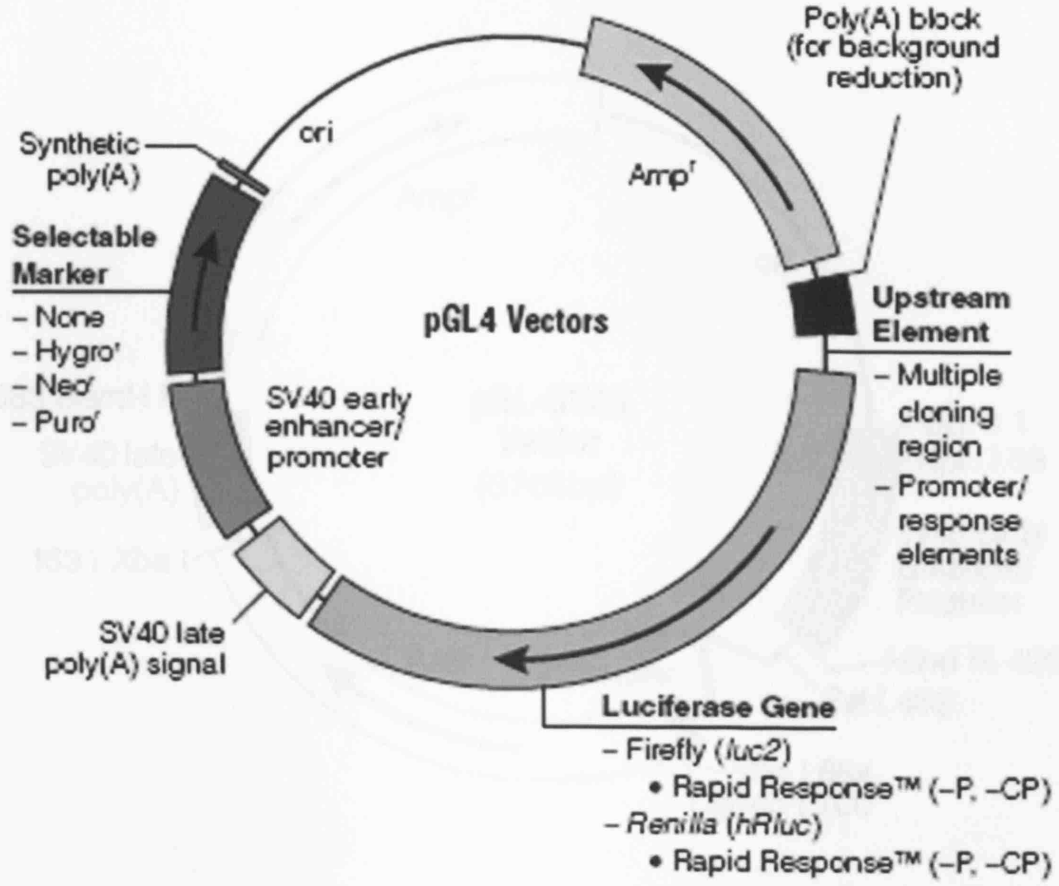

Figure 8.10 – pGL4, firefly luciferase vector for luciferase assays.

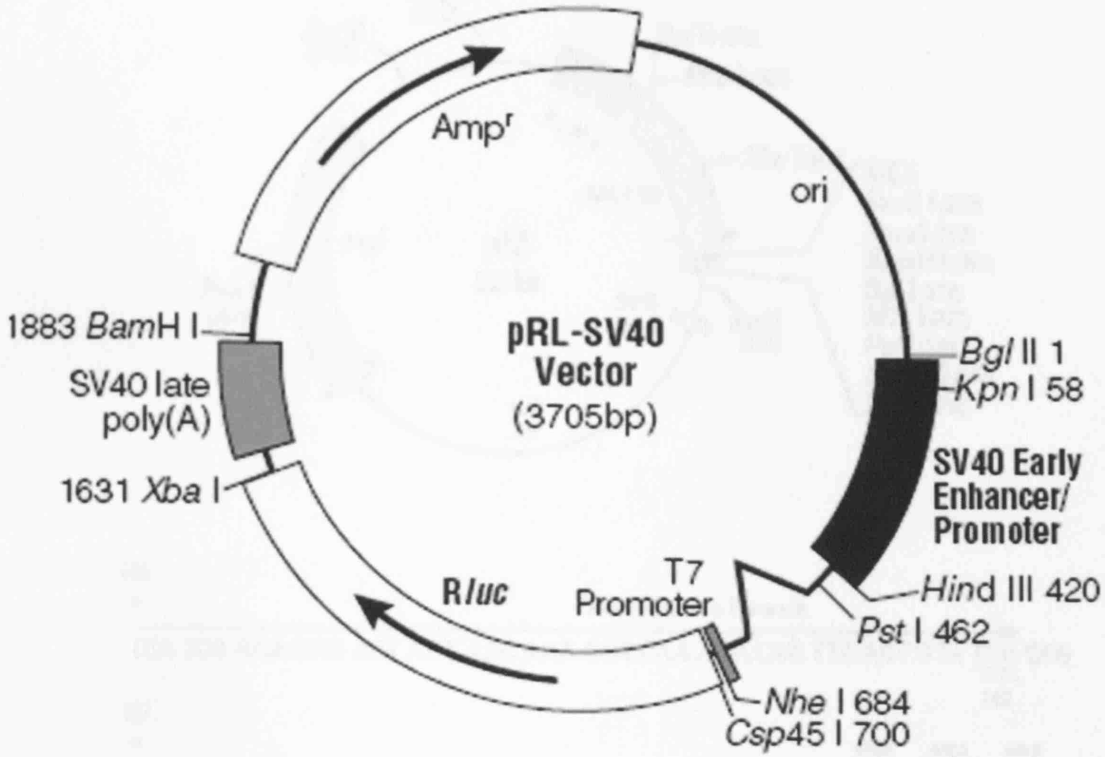

Figure 8.11 – pRL-SV40, *renilla* luciferase vector for luciferase assays.

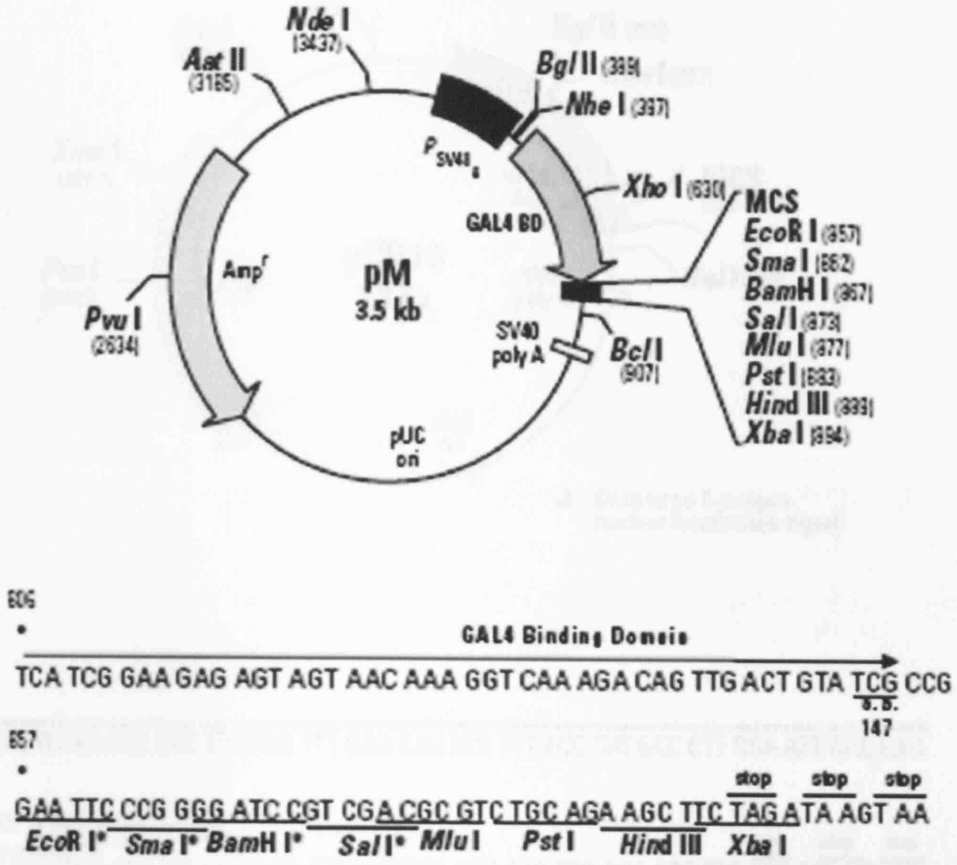

Figure 8.12 – pM for the construction of GAL4DBD-tagged proteins in mammalian two-hybrid assays.

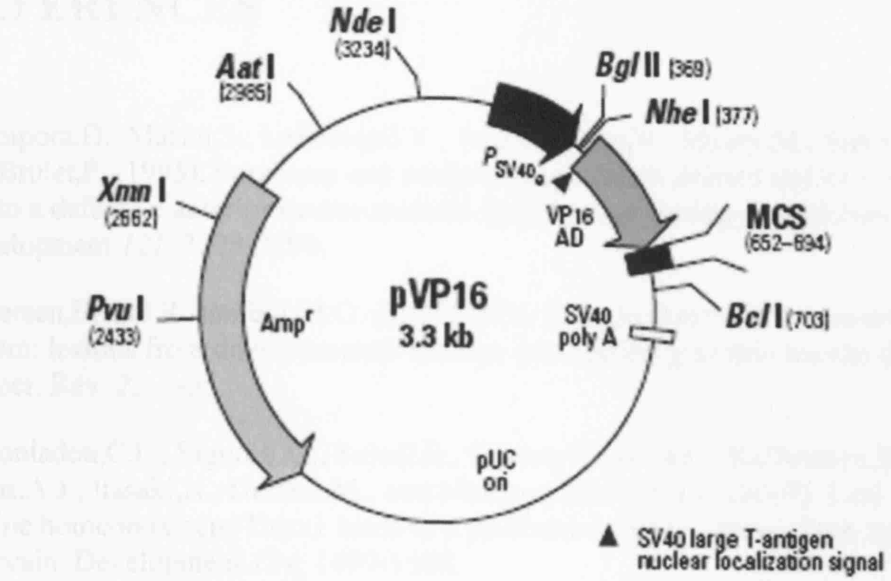

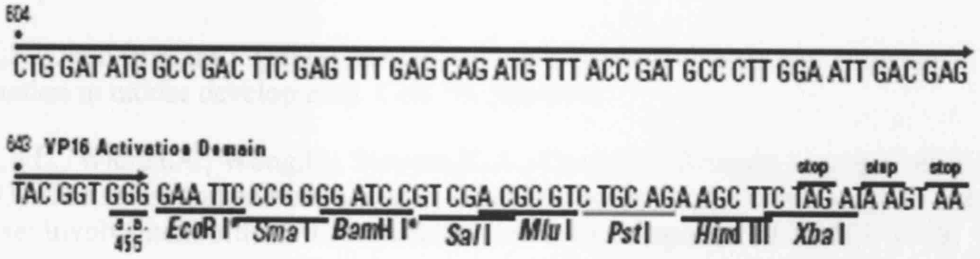

Figure 8.13 – pVP16 for the construction of VP16AD-tagged proteins in mammalian two-hybrid assays.

REFERENCES

Acampora,D., Mazan,S., Lallemand,Y., Avantaggiato,V., Maury,M., Simeone,A., and Brulet,P. (1995). Forebrain and midbrain regions are deleted in Otx2-/- mutants due to a defective anterior neuroectoderm specification during gastrulation. Development *121*, 3279-3290.

Andersen,B. and Rosenfeld,M.G. (2001). POU domain factors in the neuroendocrine system: lessons from developmental biology provide insights into human disease. Endocr. Rev. *22*, 2-35.

Andoniadou,C.L., Signore,M., Sajedi,E., Gaston-Massuet,C., Kelberman,D., Burns,A.J., Itasaki,N., Dattani,M., and Martinez-Barbera,J.P. (2007). Lack of the murine homeobox gene Hesx1 leads to a posterior transformation of the anterior forebrain. Development *134*, 1499-1508.

Ang,S.L., Conlon,R.A., Jin,O., and Rossant,J. (1994). Positive and negative signals from mesoderm regulate the expression of mouse Otx2 in ectoderm explants. Development *120*, 2979-2989.

Ang,S.L. and Rossant,J. (1994). HNF-3 beta is essential for node and notochord formation in mouse development. Cell *78*, 561-574.

Ang,S.L., Wierda,A., Wong,D., Stevens,K.A., Cascio,S., Rossant,J., and Zaret,K.S. (1993). The formation and maintenance of the definitive endoderm lineage in the mouse: involvement of HNF3/forkhead proteins. Development *119*, 1301-1315.

Arao,Y., Kuriyama,R., Kayama,F., and Kato,S. (2000). A nuclear matrix-associated factor, SAF-B, interacts with specific isoforms of AUF1/hnRNP D. Arch. Biochem. Biophys. *380*, 228-236.

Arkell,R. and Beddington,R.S. (1997). BMP-7 influences pattern and growth of the developing hindbrain of mouse embryos. Development *124*, 1-12.

Aubin,J., Davy,A., and Soriano,P. (2004). In vivo convergence of BMP and MAPK signaling pathways: impact of differential Smad1 phosphorylation on development and homeostasis. Genes Dev. *18*, 1482-1494.

Avilion,A.A., Nicolis,S.K., Pevny,L.H., Perez,L., Vivian,N., and Lovell-Badge,R. (2003). Multipotent cell lineages in early mouse development depend on SOX2 function. Genes Dev. *17*, 126-140.

Bachiller,D., Klingensmith,J., Kemp,C., Belo,J.A., Anderson,R.M., May,S.R., McMahon,J.A., McMahon,A.P., Harland,R.M., Rossant,J., and De Robertis,E.M. (2000). The organizer factors Chordin and Noggin are required for mouse forebrain development. Nature *403*, 658-661.

Bachiller,D., Klingensmith,J., Shneyder,N., Tran,U., Anderson,R., Rossant,J., and De Robertis,E.M. (2003). The role of chordin/Bmp signals in mammalian pharyngeal development and DiGeorge syndrome. Development *130*, 3567-3578.

Baker,C.V. and Bronner-Fraser,M. (2001). Vertebrate cranial placodes I. Embryonic induction. Dev. Biol. *232*, 1-61.

Beddington,R.S. (1994). Induction of a second neural axis by the mouse node. Development *120*, 613-620.

Beddington,R.S. and Robertson,E.J. (1998). Anterior patterning in mouse. Trends Genet. *14*, 277-284.

Beddington,R.S. and Robertson,E.J. (1999). Axis development and early asymmetry in mammals. Cell *96*, 195-209.

Belo,J.A., Bachiller,D., Agius,E., Kemp,C., Borges,A.C., Marques,S., Piccolo,S., and De Robertis,E.M. (2000). Cerberus-like is a secreted BMP and nodal antagonist not essential for mouse development. Genesis. *26*, 265-270.

Belo,J.A., Bouwmeester,T., Leyns,L., Kertesz,N., Gallo,M., Follettie,M., and De Robertis,E.M. (1997). Cerberus-like is a secreted factor with neutralizing activity expressed in the anterior primitive endoderm of the mouse gastrula. Mech. Dev. *68*, 45-57.

Bestor,T.H. (2000). The DNA methyltransferases of mammals. Hum. Mol. Genet. *9*, 2395-2402.

Blumberg,B., Wright,C.V., De Robertis,E.M., and Cho,K.W. (1991). Organizer-specific homeobox genes in Xenopus laevis embryos. Science *253*, 194-196.

Bouillet,P., Oulad-Abdelghani,M., Ward,S.J., Bronner,S., Chambon,P., and Dolle,P. (1996). A new mouse member of the Wnt gene family, mWnt-8, is expressed during early embryogenesis and is ectopically induced by retinoic acid. Mech. Dev. *58*, 141-152.

Bouwmeester,T., Kim,S., Sasai,Y., Lu,B., and De Robertis,E.M. (1996). Cerberus is a head-inducing secreted factor expressed in the anterior endoderm of Spemann's organizer. Nature *382*, 595-601.

Bradley,L., Sun,B., Collins-Racie,L., LaVallie,E., McCoy,J., and Sive,H. (2000). Different activities of the frizzled-related proteins frzb2 and sizzled2 during Xenopus anteroposterior patterning. Dev. Biol. *227*, 118-132.

Brennan,J., Lu,C.C., Norris,D.P., Rodriguez,T.A., Beddington,R.S., and Robertson,E.J. (2001). Nodal signalling in the epiblast patterns the early mouse embryo. Nature *411*, 965-969.

Brent,R. and Finley,R.L., Jr. (1997). Understanding gene and allele function with two-hybrid methods. Annu. Rev. Genet. *31*, 663-704.

Brent,R. and Ptashne,M. (1984). A bacterial repressor protein or a yeast transcriptional terminator can block upstream activation of a yeast gene. Nature *312*, 612-615.

Brent,R. and Ptashne,M. (1985). A eukaryotic transcriptional activator bearing the DNA specificity of a prokaryotic repressor. Cell *43*, 729-736.

Brickman,J.M., Clements,M., Tyrell,R., McNay,D., Woods,K., Warner,J., Stewart,A., Beddington,R.S., and Dattani,M. (2001). Molecular effects of novel mutations in Hesx1/HESX1 associated with human pituitary disorders. Development *128*, 5189-5199.

Brinkmeier,M.L., Potok,M.A., Cha,K.B., Gridley,T., Stifani,S., Meeldijk,J., Clevers,H., and Camper,S.A. (2003). TCF and Groucho-related genes influence pituitary growth and development. Mol. Endocrinol. *17*, 2152-2161.

Brodsky,M.C., Conte,F.A., Taylor,D., Hoyt,C.S., and Mrak,R.E. (1997). Sudden death in septo-optic dysplasia. Report of 5 cases. Arch. Ophthalmol. *115*, 66-70.

Brown,C.O., Chi,X., Garcia-Gras,E., Shirai,M., Feng,X.H., and Schwartz,R.J. (2004). The cardiac determination factor, Nkx2-5, is activated by mutual cofactors GATA-4 and Smad1/4 via a novel upstream enhancer. J. Biol. Chem. *279*, 10659-10669.

Burdge,G.C., Hanson,M.A., Slater-Jefferies,J.L., and Lillycrop,K.A. (2007). Epigenetic regulation of transcription: a mechanism for inducing variations in phenotype (fetal programming) by differences in nutrition during early life? Br. J. Nutr. *97*, 1036-1046.

Camus,A., Perea-Gomez,A., Moreau,A., and Collignon,J. (2006). Absence of Nodal signaling promotes precocious neural differentiation in the mouse embryo. Dev. Biol. *295*, 743-755.

Carvalho,L.R., Woods,K.S., Mendonca,B.B., Marcal,N., Zamparini,A.L., Stifani,S., Brickman,J.M., Arnhold,I.J., and Dattani,M.T. (2003). A homozygous mutation in HESX1 is associated with evolving hypopituitarism due to impaired repressor-corepressor interaction. J. Clin. Invest *112*, 1192-1201.

Cha,K.B., Douglas,K.R., Potok,M.A., Liang,H., Jones,S.N., and Camper,S.A. (2004). WNT5A signaling affects pituitary gland shape. Mech. Dev. *121*, 183-194.

Charles,M.A., Suh,H., Hjalt,T.A., Drouin,J., Camper,S.A., and Gage,P.J. (2005). PITX genes are required for cell survival and Lhx3 activation. Mol. Endocrinol. *19*, 1893-1903.

Chea,H.K., Wright,C.V., and Swalla,B.J. (2005). Nodal signaling and the evolution of deuterostome gastrulation. Dev. Dyn. *234*, 269-278.

Chi,Y.I. (2005). Homeodomain revisited: a lesson from disease-causing mutations. Hum. Genet. *116*, 433-444.

Chiang,C., Litingtung,Y., Lee,E., Young,K.E., Corden,J.L., Westphal,H., and Beachy,P.A. (1996). Cyclopia and defective axial patterning in mice lacking Sonic hedgehog gene function. Nature *383*, 407-413.

Chien,C.T., Bartel,P.L., Sternglanz,R., and Fields,S. (1991). The two-hybrid system: a method to identify and clone genes for proteins that interact with a protein of interest. Proc. Natl. Acad. Sci. U. S. A *88*, 9578-9582.

Cho,K.W., Morita,E.A., Wright,C.V., and De Robertis,E.M. (1991). Overexpression of a homeodomain protein confers axis-forming activity to uncommitted Xenopus embryonic cells. Cell *65*, 55-64.

Chou,S.J., Hermesz,E., Hatta,T., Feltner,D., El Hodiri,H.M., Jamrich,M., and Mahon,K. (2006). Conserved regulatory elements establish the dynamic expression of Rpx/Hesxl in early vertebrate development. Dev. Biol. *292*, 533-545.

Christian,J.L., Olson,D.J., and Moon,R.T. (1992). Xwnt-8 modifies the character of mesoderm induced by bFGF in isolated Xenopus ectoderm. EMBO J. *11*, 33-41.

Cohen,L.E. and Radovick,S. (2002a). Molecular basis of combined pituitary hormone deficiencies. Endocr. Rev. *23*, 431-442.

Cohen,L.E. and Radovick,S. (2002b). Other transcription factors and hypopituitarism. Rev. Endocr. Metab Disord. *3*, 301-311.

Cohen,R.N., Cohen,L.E., Botero,D., Yu,C., Sagar,A., Jurkiewicz,M., and Radovick,S. (2003). Enhanced repression by HESX1 as a cause of hypopituitarism and septooptic dysplasia. J. Clin. Endocrinol. Metab *88*, 4832-4839.

Conlon,F.L., Lyons,K.M., Takaesu,N., Barth,K.S., Kispert,A., Herrmann,B., and Robertson,E.J. (1994). A primary requirement for nodal in the formation and maintenance of the primitive streak in the mouse. Development *120*, 1919-1928.

Cooney,C.A., Dave,A.A., and Wolff,G.L. (2002). Maternal methyl supplements in mice affect epigenetic variation and DNA methylation of offspring. J. Nutr. *132*, 2393S-2400S.

Cox,W.G. and Hemmati-Brivanlou,A. (1995). Caudalization of neural fate by tissue recombination and bFGF. Development *121*, 4349-4358.

Coya,R., Vela,A., Perez,d.N., Rica,I., Castano,L., Busturia,M.A., and Martul,P. (2007). Panhypopituitarism: genetic versus acquired etiological factors. J. Pediatr. Endocrinol. Metab *20*, 27-36.

Crossley,P.H. and Martin,G.R. (1995). The mouse Fgf8 gene encodes a family of polypeptides and is expressed in regions that direct outgrowth and patterning in the developing embryo. Development *121*, 439-451.

Cushman,L.J., Showalter,A.D., and Rhodes,S.J. (2002). Genetic defects in the development and function of the anterior pituitary gland. Ann. Med. *34*, 179-191.

Cushman,L.J., Watkins-Chow,D.E., Brinkmeier,M.L., Raetzman,L.T., Radak,A.L., Lloyd,R.V., and Camper,S.A. (2001). Persistent Prop1 expression delays gonadotrope differentiation and enhances pituitary tumor susceptibility. Hum. Mol. Genet. *10*, 1141-1153.

Daikoku,S., Chikamori,M., Adachi,T., Okamura,Y., Nishiyama,T., and Tsuruo,Y. (1983). Ontogenesis of hypothalamic immunoreactive ACTH cells in vivo and in vitro: role of Rathke's pouch. Dev. Biol. *97*, 81-88.

Dale,J.K., Vesque,C., Lints,T.J., Sampath,T.K., Furley,A., Dodd,J., and Placzek,M. (1997). Cooperation of BMP7 and SHH in the induction of forebrain ventral midline cells by prechordal mesoderm. Cell *90*, 257-269.

Dale,K., Sattar,N., Heemskerk,J., Clarke,J.D., Placzek,M., and Dodd,J. (1999). Differential patterning of ventral midline cells by axial mesoderm is regulated by BMP7 and chordin. Development *126*, 397-408.

Dalton,S. and Treisman,R. (1992). Characterization of SAP-1, a protein recruited by serum response factor to the c-fos serum response element. Cell *68*, 597-612.

Dasen,J.S., Barbera,J.P., Herman,T.S., Connell,S.O., Olson,L., Ju,B., Tollkuhn,J., Baek,S.H., Rose,D.W., and Rosenfeld,M.G. (2001). Temporal regulation of a paired-like homeodomain repressor/TLE corepressor complex and a related activator is required for pituitary organogenesis. Genes Dev. *15*, 3193-3207.

Dasen,J.S. and Rosenfeld,M.G. (2001). Signaling and transcriptional mechanisms in pituitary development. Annu. Rev. Neurosci. *24*, 327-355.

Dattani,M.L., Martinez-Barbera,J., Thomas,P.Q., Brickman,J.M., Gupta,R., Wales,J.K., Hindmarsh,P.C., Beddington,R.S., and Robinson,I.C. (2000). Molecular genetics of septo-optic dysplasia. Horm. Res. *53 Suppl 1*, 26-33.

Dattani,M.T. (2004). Novel insights into the aetiology and pathogenesis of hypopituitarism. Horm. Res. *62 Suppl 3*, 1-13.

Dattani,M.T. (2005). Growth hormone deficiency and combined pituitary hormone deficiency: does the genotype matter? Clin. Endocrinol. (Oxf) *63*, 121-130.

Dattani,M.T., Martinez-Barbera,J.P., Thomas,P.Q., Brickman,J.M., Gupta,R., Martensson,I.L., Toresson,H., Fox,M., Wales,J.K., Hindmarsh,P.C., Krauss,S., Beddington,R.S., and Robinson,I.C. (1998). Mutations in the homeobox gene HESX1/Hesx1 associated with septo-optic dysplasia in human and mouse. Nat. Genet. *19*, 125-133.

Dattani,M.T. and Robinson,I.C. (2002). HESX1 and Septo-Optic Dysplasia. Rev. Endocr. Metab Disord. *3*, 289-300.

Davidson,B.P., Kinder,S.J., Steiner,K., Schoenwolf,G.C., and Tam,P.P. (1999). Impact of node ablation on the morphogenesis of the body axis and the lateral asymmetry of the mouse embryo during early organogenesis. Dev. Biol. *211*, 11-26.

De Moerlooze,L., Spencer-Dene,B., Revest,J., Hajihosseini,M., Rosewell,I., and Dickson,C. (2000). An important role for the IIIb isoform of fibroblast growth factor receptor 2 (FGFR2) in mesenchymal-epithelial signalling during mouse organogenesis. Development *127*, 483-492.

De Robertis,E.M. and Kuroda,H. (2004). Dorsal-ventral patterning and neural induction in Xenopus embryos. Annu. Rev. Cell Dev. Biol. *20*, 285-308.

De Robertis,E.M., Larrain,J., Oelgeschlager,M., and Wessely,O. (2000). The establishment of Spemann's organizer and patterning of the vertebrate embryo. Nat. Rev. Genet. *1*, 171-181.

Delaune,E., Lemaire,P., and Kodjabachian,L. (2005). Neural induction in Xenopus requires early FGF signalling in addition to BMP inhibition. Development *132*, 299-310.

Di Gregorio,A., Sancho,M., Stuckey,D.W., Crompton,L.A., Godwin,J., Mishina,Y., and Rodriguez,T.A. (2007). BMP signalling inhibits premature neural differentiation in the mouse embryo. Development *134*, 3359-3369.

Ding,J., Yang,L., Yan,Y.T., Chen,A., Desai,N., Wynshaw-Boris,A., and Shen,M.M. (1998). Cripto is required for correct orientation of the anterior-posterior axis in the mouse embryo. Nature *395*, 702-707.

Dirksen,M.L. and Jamrich,M. (1992). A novel, activin-inducible, blastopore lip-specific gene of Xenopus laevis contains a fork head DNA-binding domain. Genes Dev. *6*, 599-608.

Dudley,A.T., Lyons,K.M., and Robertson,E.J. (1995). A requirement for bone morphogenetic protein-7 during development of the mammalian kidney and eye. Genes Dev. *9*, 2795-2807.

Dufort,D., Schwartz,L., Harpal,K., and Rossant,J. (1998). The transcription factor HNF3beta is required in visceral endoderm for normal primitive streak morphogenesis. Development *125*, 3015-3025.

Ericson,J., Muhr,J., Placzek,M., Lints,T., Jessell,T.M., and Edlund,T. (1995). Sonic hedgehog induces the differentiation of ventral forebrain neurons: a common signal for ventral patterning within the neural tube. Cell *81*, 747-756.

Ericson,J., Norlin,S., Jessell,T.M., and Edlund,T. (1998). Integrated FGF and BMP signaling controls the progression of progenitor cell differentiation and the emergence of pattern in the embryonic anterior pituitary. Development *125*, 1005-1015.

Ermakova,G.V., Alexandrova,E.M., Kazanskaya,O.V., Vasiliev,O.L., Smith,M.W., and Zaraisky,A.G. (1999). The homeobox gene, Xanf-1, can control both neural differentiation and patterning in the presumptive anterior neurectoderm of the Xenopus laevis embryo. Development *126*, 4513-4523.

Ermakova,G.V., Solovieva,E.A., Martynova,N.Y., and Zaraisky,A.G. (2007). The homeodomain factor Xanf represses expression of genes in the presumptive rostral forebrain that specify more caudal brain regions. Dev. Biol. *307*, 483-497.

Eroshkin,F., Kazanskaya,O., Martynova,N., and Zaraisky,A. (2002). Characterization of cis-regulatory elements of the homeobox gene Xanf-1. Gene *285*, 279-286.

Fainsod,A., Steinbeisser,H., and De Robertis,E.M. (1994). On the function of BMP-4 in patterning the marginal zone of the Xenopus embryo. EMBO J. *13*, 5015-5025.

Fekany,K., Yamanaka,Y., Leung,T., Sirotkin,H.I., Topczewski,J., Gates,M.A., Hibi,M., Renucci,A., Stemple,D., Radbill,A., Schier,A.F., Driever,W., Hirano,T., Talbot,W.S., and Solnica-Krezel,L. (1999). The zebrafish bozozok locus encodes Dharma, a homeodomain protein essential for induction of gastrula organizer and dorsoanterior embryonic structures. Development *126*, 1427-1438.

Fekany-Lee,K., Gonzalez,E., Miller-Bertoglio,V., and Solnica-Krezel,L. (2000). The homeobox gene bozozok promotes anterior neuroectoderm formation in zebrafish through negative regulation of BMP2/4 and Wnt pathways. Development *127*, 2333-2345.

Fields,S. and Song,O. (1989). A novel genetic system to detect protein-protein interactions. Nature *340*, 245-246.

Filosa,S., Rivera-Perez,J.A., Gomez,A.P., Gansmuller,A., Sasaki,H., Behringer,R.R., and Ang,S.L. (1997). Goosecoid and HNF-3beta genetically interact to regulate neural tube patterning during mouse embryogenesis. Development *124*, 2843-2854.

Foley,A.C. and Stern,C.D. (2001). Evolution of vertebrate forebrain development: how many different mechanisms? J. Anat. *199*, 35-52.

Fraga,M.F., Ballestar,E., Paz,M.F., Ropero,S., Setien,F., Ballestar,M.L., Heine-Suner,D., Cigudosa,J.C., Urioste,M., Benitez,J., Boix-Chornet,M., Sanchez-Aguilera,A., Ling,C., Carlsson,E., Poulsen,P., Vaag,A., Stephan,Z., Spector,T.D., Wu,Y.Z., Plass,C., and Esteller,M. (2005). Epigenetic differences arise during the lifetime of monozygotic twins. Proc. Natl. Acad. Sci. U. S. A *102*, 10604-10609.

Fredieu,J.R., Cui,Y., Maier,D., Danilchik,M.V., and Christian,J.L. (1997). Xwnt-8 and lithium can act upon either dorsal mesodermal or neurectodermal cells to cause a loss of forebrain in Xenopus embryos. Dev. Biol. *186*, 100-114.

Fu,G.K. and Markovitz,D.M. (1998). The human LON protease binds to mitochondrial promoters in a single-stranded, site-specific, strand-specific manner. Biochemistry *37*, 1905-1909.

Fuentealba,L.C., Eivers,E., Ikeda,A., Hurtado,C., Kuroda,H., Pera,E.M., and De Robertis,E.M. (2007). Integrating Patterning Signals: Wnt/GSK3 Regulates the Duration of the BMP/Smad1 Signal. Cell *131*, 980-993.

Gage,P.J., Suh,H., and Camper,S.A. (1999). The bicoid-related Pitx gene family in development. Mamm. Genome *10*, 197-200.

Galceran,J., Farinas,I., Depew,M.J., Clevers,H., and Grosschedl,R. (1999). Wnt3a-/--like phenotype and limb deficiency in Lef1(-/-)Tcf1(-/-) mice. Genes Dev. *13*, 709-717.

Gehring,W.J., Affolter,M., and Burglin,T. (1994a). Homeodomain proteins. Annu. Rev. Biochem. *63*, 487-526.

Gehring,W.J., Qian,Y.Q., Billeter,M., Furukubo-Tokunaga,K., Schier,A.F., Resendez-Perez,D., Affolter,M., Otting,G., and Wuthrich,K. (1994b). Homeodomain-DNA recognition. Cell *78*, 211-223.

Gilbert,S.F. (2006). Developmental biology. (Sunderland, Mass: Sinauer Associates).

Gleiberman,A.S., Fedtsova,N.G., and Rosenfeld,M.G. (1999). Tissue interactions in the induction of anterior pituitary: role of the ventral diencephalon, mesenchyme, and notochord. Dev. Biol. *213*, 340-353.

Glinka,A., Wu,W., Delius,H., Monaghan,A.P., Blumenstock,C., and Niehrs,C. (1998). Dickkopf-1 is a member of a new family of secreted proteins and functions in head induction. Nature *391*, 357-362.

Glinka,A., Wu,W., Onichtchouk,D., Blumenstock,C., and Niehrs,C. (1997). Head induction by simultaneous repression of Bmp and Wnt signalling in Xenopus. Nature *389*, 517-519.

Godsave,S.F. and Slack,J.M. (1989). Clonal analysis of mesoderm induction in Xenopus laevis. Dev. Biol. *134*, 486-490.

Greco,T.L., Takada,S., Newhouse,M.M., McMahon,J.A., McMahon,A.P., and Camper,S.A. (1996). Analysis of the vestigial tail mutation demonstrates that Wnt-3a gene dosage regulates mouse axial development. Genes Dev. *10*, 313-324.

Gritsman,K., Zhang,J., Cheng,S., Heckscher,E., Talbot,W.S., and Schier,A.F. (1999). The EGF-CFC protein one-eyed pinhead is essential for nodal signaling. Cell *97*, 121-132.

Grunz,H. and Tacke,L. (1989). Neural differentiation of Xenopus laevis ectoderm takes place after disaggregation and delayed reaggregation without inducer. Cell Differ. Dev. *28*, 211-217.

Haegel,H., Larue,L., Ohsugi,M., Fedorov,L., Herrenknecht,K., and Kemler,R. (1995). Lack of beta-catenin affects mouse development at gastrulation. Development *121*, 3529-3537.

Hamilton,F.S., Wheeler,G.N., and Hoppler,S. (2001). Difference in XTcf-3 dependency accounts for change in response to beta-catenin-mediated Wnt signalling in Xenopus blastula. Development *128*, 2063-2073.

Harland,R. (2000). Neural induction. Curr. Opin. Genet. Dev. *10*, 357-362.

Hawley,S.H., Wunnenberg-Stapleton,K., Hashimoto,C., Laurent,M.N., Watabe,T., Blumberg,B.W., and Cho,K.W. (1995). Disruption of BMP signals in embryonic Xenopus ectoderm leads to direct neural induction. Genes Dev. *9*, 2923-2935.

Heisenberg,C.P., Houart,C., Take-Uchi,M., Rauch,G.J., Young,N., Coutinho,P., Masai,I., Caneparo,L., Concha,M.L., Geisler,R., Dale,T.C., Wilson,S.W., and Stemple,D.L. (2001). A mutation in the Gsk3-binding domain of zebrafish Masterblind/Axin1 leads to a fate transformation of telencephalon and eyes to diencephalon. Genes Dev. *15*, 1427-1434.

Hemmati-Brivanlou,A., Kelly,O.G., and Melton,D.A. (1994). Follistatin, an antagonist of activin, is expressed in the Spemann organizer and displays direct neuralizing activity. Cell *77*, 283-295.

Hemmati-Brivanlou,A. and Melton,D.A. (1992). A truncated activin receptor inhibits mesoderm induction and formation of axial structures in Xenopus embryos. Nature *359*, 609-614.

Hemmati-Brivanlou,A. and Melton,D.A. (1994). Inhibition of activin receptor signaling promotes neuralization in Xenopus. Cell *77*, 273-281.

Hermann,A., Gowher,H., and Jeltsch,A. (2004). Biochemistry and biology of mammalian DNA methyltransferases. Cell Mol. Life Sci. *61*, 2571-2587.

Hermesz,E., Mackem,S., and Mahon,K.A. (1996). Rpx: a novel anterior-restricted homeobox gene progressively activated in the prechordal plate, anterior neural plate and Rathke's pouch of the mouse embryo. Development *122*, 41-52.

Hermesz,E., Williams-Simons,L., and Mahon,K.A. (2003). A novel inducible element, activated by contact with Rathke's pouch, is present in the regulatory region of the Rpx/Hesx1 homeobox gene. Dev. Biol. *260*, 68-78.

Hoang,B.H., Thomas,J.T., Abdul-Karim,F.W., Correia,K.M., Conlon,R.A., Luyten,F.P., and Ballock,R.T. (1998). Expression pattern of two Frizzled-related genes, Frzb-1 and Sfrp-1, during mouse embryogenesis suggests a role for modulating action of Wnt family members. Dev. Dyn. *212*, 364-372.

Holland,P.W. and Takahashi,T. (2005). The evolution of homeobox genes: Implications for the study of brain development. Brain Res. Bull. *66*, 484-490.

Hollenberg,S.M., Sternglanz,R., Cheng,P.F., and Weintraub,H. (1995). Identification of a new family of tissue-specific basic helix-loop-helix proteins with a two-hybrid system. Mol. Cell Biol. *15*, 3813-3822.

Houart,C., Caneparo,L., Heisenberg,C., Barth,K., Take-Uchi,M., and Wilson,S. (2002). Establishment of the telencephalon during gastrulation by local antagonism of Wnt signaling. Neuron *35*, 255-265.

Houart,C., Westerfield,M., and Wilson,S.W. (1998). A small population of anterior cells patterns the forebrain during zebrafish gastrulation. Nature *391*, 788-792.

Huelsken,J., Vogel,R., Brinkmann,V., Erdmann,B., Birchmeier,C., and Birchmeier,W. (2000). Requirement for beta-catenin in anterior-posterior axis formation in mice. J. Cell Biol. *148*, 567-578.

Ingham,P.W. and Placzek,M. (2006). Orchestrating ontogenesis: variations on a theme by sonic hedgehog. Nat. Rev. Genet. *7*, 841-850.

Inoue,T., Nakamura,S., and Osumi,N. (2000). Fate mapping of the mouse prosencephalic neural plate. Dev. Biol. *219*, 373-383.

Ishikawa,T.O., Tamai,Y., Li,Q., Oshima,M., and Taketo,M.M. (2003). Requirement for tumor suppressor Apc in the morphogenesis of anterior and ventral mouse embryo. Dev. Biol. *253*, 230-246.

Itasaki,N., Sharpe,J., Morrison,A., and Krumlauf,R. (1996). Reprogramming Hox expression in the vertebrate hindbrain: influence of paraxial mesoderm and rhombomere transposition. Neuron *16*, 487-500.

Ivanova,M., Dobrzycka,K.M., Jiang,S., Michaelis,K., Meyer,R., Kang,K., Adkins,B., Barski,O.A., Zubairy,S., Divisova,J., Lee,A.V., and Oesterreich,S. (2005). Scaffold attachment factor B1 functions in development, growth, and reproduction. Mol. Cell Biol. *25*, 2995-3006.

James,P., Halladay,J., and Craig,E.A. (1996). Genomic libraries and a host strain designed for highly efficient two-hybrid selection in yeast. Genetics *144*, 1425-1436.

Jean,D., Bernier,G., and Gruss,P. (1999). Six6 (Optx2) is a novel murine Six3-related homeobox gene that demarcates the presumptive pituitary/hypothalamic axis and the ventral optic stalk. Mech. Dev. *84*, 31-40.

Jimenez-Sanchez,G., Childs,B., and Valle,D. (2001). Human disease genes. Nature *409*, 853-855.

Kaufman,M.H. (1992). The atlas of mouse development.

Kawamura,K. and Kikuyama,S. (1998). Morphogenesis of the hypothalamus and hypophysis: their association, dissociation and reassociation before and after "Rathke". Arch. Histol. Cytol. *61*, 189-198.

Kawamura,K., Kouki,T., Kawahara,G., and Kikuyama,S. (2002). Hypophyseal development in vertebrates from amphibians to mammals. Gen. Comp Endocrinol. *126*, 130-135.

Kazanskaya,O.V., Severtzova,E.A., Barth,K.A., Ermakova,G.V., Lukyanov,S.A., Benyumov,A.O., Pannese,M., Boncinelli,E., Wilson,S.W., and Zaraisky,A.G. (1997). Anf: a novel class of vertebrate homeobox genes expressed at the anterior end of the main embryonic axis. Gene *200*, 25-34.

Kelberman,D. and Dattani,M.T. (2007a). Genetics of septo-optic dysplasia. Pituitary.

Kelberman,D. and Dattani,M.T. (2007b). Hypothalamic and pituitary development: novel insights into the aetiology. Eur. J. Endocrinol. *157 Suppl 1*, S3-14.

Kelberman,D., Rizzoti,K., Avilion,A., Bitner-Glindzicz,M., Cianfarani,S., Collins,J., Chong,W.K., Kirk,J.M., Achermann,J.C., Ross,R., Carmignac,D., Lovell-Badge,R., Robinson,I.C., and Dattani,M.T. (2006). Mutations within Sox2/SOX2 are associated with abnormalities in the hypothalamo-pituitary-gonadal axis in mice and humans. J. Clin. Invest *116*, 2442-2455.

Kelly,G.M., Erezyilmaz,D.F., and Moon,R.T. (1995). Induction of a secondary embryonic axis in zebrafish occurs following the overexpression of beta-catenin. Mech. Dev. *53*, 261-273.

Kemler,R., Hierholzer,A., Kanzler,B., Kuppig,S., Hansen,K., Taketo,M.M., de Vries,W.N., Knowles,B.B., and Solter,D. (2004). Stabilization of beta-catenin in the mouse zygote leads to premature epithelial-mesenchymal transition in the epiblast. Development *131*, 5817-5824.

Kim,C.H., Oda,T., Itoh,M., Jiang,D., Artinger,K.B., Chandrasekharappa,S.C., Driever,W., and Chitnis,A.B. (2000). Repressor activity of Headless/Tcf3 is essential for vertebrate head formation. Nature *407*, 913-916.

Kimura,S., Hara,Y., Pineau,T., Fernandez-Salguero,P., Fox,C.H., Ward,J.M., and Gonzalez,F.J. (1996). The T/ebp null mouse: thyroid-specific enhancer-binding protein is essential for the organogenesis of the thyroid, lung, ventral forebrain, and pituitary. Genes Dev. *10*, 60-69.

Kioussi,C., Briata,P., Baek,S.H., Rose,D.W., Hamblet,N.S., Herman,T., Ohgi,K.A., Lin,C., Gleiberman,A., Wang,J., Brault,V., Ruiz-Lozano,P., Nguyen,H.D., Kemler,R., Glass,C.K., Wynshaw-Boris,A., and Rosenfeld,M.G. (2002). Identification of a Wnt/Dvl/beta-Catenin --> Pitx2 pathway mediating cell-type-specific proliferation during development. Cell *111*, 673-685.

Kispert,A., Vainio,S., Shen,L., Rowitch,D.H., and McMahon,A.P. (1996). Proteoglycans are required for maintenance of Wnt-11 expression in the ureter tips. Development *122*, 3627-3637.

Klingensmith,J., Ang,S.L., Bachiller,D., and Rossant,J. (1999). Neural induction and patterning in the mouse in the absence of the node and its derivatives. Dev. Biol. *216*, 535-549.

Knoetgen,H., Viebahn,C., and Kessel,M. (1999). Head induction in the chick by primitive endoderm of mammalian, but not avian origin. Development *126*, 815-825.

Koshida,S., Shinya,M., Mizuno,T., Kuroiwa,A., and Takeda,H. (1998). Initial anteroposterior pattern of the zebrafish central nervous system is determined by differential competence of the epiblast. Development *125*, 1957-1966.

Kuroda,H., Wessely,O., and De Robertis,E.M. (2004). Neural induction in Xenopus: requirement for ectodermal and endomesodermal signals via Chordin, Noggin, beta-Catenin, and Cerberus. PLoS. Biol. *2*, E92.

Kuzmichev,A., Nishioka,K., Erdjument-Bromage,H., Tempst,P., and Reinberg,D. (2002). Histone methyltransferase activity associated with a human multiprotein complex containing the Enhancer of Zeste protein. Genes Dev. *16*, 2893-2905.

LaBonne,C. and Whitman,M. (1997). Localization of MAP kinase activity in early Xenopus embryos: implications for endogenous FGF signaling. Dev. Biol. *183*, 9-20.

Laclef,C., Hamard,G., Demignon,J., Souil,E., Houbron,C., and Maire,P. (2003a). Altered myogenesis in Six1-deficient mice. Development *130*, 2239-2252.

Laclef,C., Souil,E., Demignon,J., and Maire,P. (2003b). Thymus, kidney and craniofacial abnormalities in Six 1 deficient mice. Mech. Dev. *120*, 669-679.

Lagutin,O.V., Zhu,C.C., Kobayashi,D., Topczewski,J., Shimamura,K., Puelles,L., Russell,H.R., McKinnon,P.J., Solnica-Krezel,L., and Oliver,G. (2003). Six3 repression of Wnt signaling in the anterior neuroectoderm is essential for vertebrate forebrain development. Genes Dev. *17*, 368-379.

Lamonerie,T., Tremblay,J.J., Lanctot,C., Therrien,M., Gauthier,Y., and Drouin,J. (1996). Ptx1, a bicoid-related homeo box transcription factor involved in transcription of the pro-opiomelanocortin gene. Genes Dev. *10*, 1284-1295.

Larabell,C.A., Torres,M., Rowning,B.A., Yost,C., Miller,J.R., Wu,M., Kimelman,D., and Moon,R.T. (1997). Establishment of the dorso-ventral axis in Xenopus embryos is presaged by early asymmetries in beta-catenin that are modulated by the Wnt signaling pathway. J. Cell Biol. *136*, 1123-1136.

Launay,C., Fromentoux,V., Shi,D.L., and Boucaut,J.C. (1996). A truncated FGF receptor blocks neural induction by endogenous Xenopus inducers. Development *122*, 869-880.

Leonhardt,H., Page,A.W., Weier,H.U., and Bestor,T.H. (1992). A targeting sequence directs DNA methyltransferase to sites of DNA replication in mammalian nuclei. Cell *71*, 865-873.

Leyns,L., Bouwmeester,T., Kim,S.H., Piccolo,S., and De Robertis,E.M. (1997). Frzb-1 is a secreted antagonist of Wnt signaling expressed in the Spemann organizer. Cell *88*, 747-756.

Li,E., Bestor,T.H., and Jaenisch,R. (1992). Targeted mutation of the DNA methyltransferase gene results in embryonic lethality. Cell *69*, 915-926.

Li,S., Crenshaw,E.B., III, Rawson,E.J., Simmons,D.M., Swanson,L.W., and Rosenfeld,M.G. (1990). Dwarf locus mutants lacking three pituitary cell types result from mutations in the POU-domain gene pit-1. Nature *347*, 528-533.

Li,X., Perissi,V., Liu,F., Rose,D.W., and Rosenfeld,M.G. (2002). Tissue-specific regulation of retinal and pituitary precursor cell proliferation. Science *297*, 1180-1183.

Linker,C. and Stern,C.D. (2004). Neural induction requires BMP inhibition only as a late step, and involves signals other than FGF and Wnt antagonists. Development *131*, 5671-5681.

Liu,A., Losos,K., and Joyner,A.L. (1999a). FGF8 can activate Gbx2 and transform regions of the rostral mouse brain into a hindbrain fate. Development *126*, 4827-4838.

Liu,P., Wakamiya,M., Shea,M.J., Albrecht,U., Behringer,R.R., and Bradley,A. (1999b). Requirement for Wnt3 in vertebrate axis formation. Nat. Genet. *22*, 361-365.

Lopez-Rios,J., Tessmar,K., Loosli,F., Wittbrodt,J., and Bovolenta,P. (2003). Six3 and Six6 activity is modulated by members of the groucho family. Development *130*, 185-195.

Lumsden,A. and Krumlauf,R. (1996). Patterning the vertebrate neuraxis. Science *274*, 1109-1115.

Magnaghi,P., Roberts,C., Lorain,S., Lipinski,M., and Scambler,P.J. (1998). HIRA, a mammalian homologue of Saccharomyces cerevisiae transcriptional co-repressors, interacts with Pax3. Nat. Genet. *20*, 74-77.

Margot,J.B., Ehrenhofer-Murray,A.E., and Leonhardt,H. (2003). Interactions within the mammalian DNA methyltransferase family. BMC. Mol. Biol. *4*, 7.

Marikawa,Y. (2006). Wnt/beta-catenin signaling and body plan formation in mouse embryos. Semin. Cell Dev. Biol. *17*, 175-184.

Martinez-Barbera,J.P. and Beddington,R.S. (2001). Getting your head around Hex and Hesx1: forebrain formation in mouse. Int. J. Dev. Biol. *45*, 327-336.

Martinez-Barbera,J.P., Rodriguez,T.A., and Beddington,R.S. (2000). The homeobox gene Hesx1 is required in the anterior neural ectoderm for normal forebrain formation. Dev. Biol. *223*, 422-430.

Martinez-Barbera,J.P., Signore,M., Boyl,P.P., Puelles,E., Acampora,D., Gogoi,R., Schubert,F., Lumsden,A., and Simeone,A. (2001). Regionalisation of anterior neuroectoderm and its competence in responding to forebrain and midbrain inducing activities depend on mutual antagonism between OTX2 and GBX2. Development *128*, 4789-4800.

Martynova,N., Eroshkin,F., Ermakova,G., Bayramov,A., Gray,J., Grainger,R., and Zaraisky,A. (2004). Patterning the forebrain: FoxA4a/Pintallavis and Xvent2 determine the posterior limit of Xanf1 expression in the neural plate. Development *131*, 2329-2338.

Matsuo,I., Kuratani,S., Kimura,C., Takeda,N., and Aizawa,S. (1995). Mouse Otx2 functions in the formation and patterning of rostral head. Genes Dev. *9*, 2646-2658.

McMahon,J.A., Takada,S., Zimmerman,L.B., Fan,C.M., Harland,R.M., and McMahon,A.P. (1998). Noggin-mediated antagonism of BMP signaling is required for growth and patterning of the neural tube and somite. Genes Dev. *12*, 1438-1452.

McNay,D.E., Turton,J.P., Kelberman,D., Woods,K.S., Brauner,R., Papadimitriou,A., Keller,E., Keller,A., Haufs,N., Krude,H., Shalet,S.M., and Dattani,M.T. (2007). HESX1 mutations are an uncommon cause of septooptic dysplasia and hypopituitarism. J. Clin. Endocrinol. Metab *92*, 691-697.

Meehan,R.R. (2003). DNA methylation in animal development. Semin. Cell Dev. Biol. *14*, 53-65.

Meno,C., Ito,Y., Saijoh,Y., Matsuda,Y., Tashiro,K., Kuhara,S., and Hamada,H. (1997). Two closely-related left-right asymmetrically expressed genes, lefty-1 and lefty-2: their distinct expression domains, chromosomal linkage and direct neuralizing activity in Xenopus embryos. Genes Cells *2*, 513-524.

Meno,C., Saijoh,Y., Fujii,H., Ikeda,M., Yokoyama,T., Yokoyama,M., Toyoda,Y., and Hamada,H. (1996). Left-right asymmetric expression of the TGF beta-family member lefty in mouse embryos. Nature *381*, 151-155.

Merrill,B.J., Pasolli,H.A., Polak,L., Rendl,M., Garcia-Garcia,M.J., Anderson,K.V., and Fuchs,E. (2004). Tcf3: a transcriptional regulator of axis induction in the early embryo. Development *131*, 263-274.

Meyers,E.N., Lewandoski,M., and Martin,G.R. (1998). An Fgf8 mutant allelic series generated by Cre- and Flp-mediated recombination. Nat. Genet. *18*, 136-141.

Muhr,J., Graziano,E., Wilson,S., Jessell,T.M., and Edlund,T. (1999). Convergent inductive signals specify midbrain, hindbrain, and spinal cord identity in gastrula stage chick embryos. Neuron *23*, 689-702.

Mukhopadhyay,M., Shtrom,S., Rodriguez-Esteban,C., Chen,L., Tsukui,T., Gomer,L., Dorward,D.W., Glinka,A., Grinberg,A., Huang,S.P., Niehrs,C., Belmonte,J.C., and Westphal,H. (2001). Dickkopf1 is required for embryonic head induction and limb morphogenesis in the mouse. Dev. Cell *1*, 423-434.

Munoz-Sanjuan,I. and Brivanlou,A.H. (2002). Neural induction, the default model and embryonic stem cells. Nat. Rev. Neurosci. *3*, 271-280.

Muromoto,R., Sugiyama,K., Takachi,A., Imoto,S., Sato,N., Yamamoto,T., Oritani,K., Shimoda,K., and Matsuda,T. (2004). Physical and functional interactions between Daxx and DNA methyltransferase 1-associated protein, DMAP1. J. Immunol. *172*, 2985-2993.

Nakamura,M., Runko,A.P., and Sagerstrom,C.G. (2004). A novel subfamily of zinc finger genes involved in embryonic development. J. Cell Biochem. *93*, 887-895.

Nakano,T., Murata,T., Matsuo,I., and Aizawa,S. (2000). OTX2 directly interacts with LIM1 and HNF-3beta. Biochem. Biophys. Res. Commun. *267*, 64-70.

Nayler,O., Stratling,W., Bourquin,J.P., Stagljar,I., Lindemann,L., Jasper,H., Hartmann,A.M., Fackelmayer,F.O., Ullrich,A., and Stamm,S. (1998). SAF-B protein couples transcription and pre-mRNA splicing to SAR/MAR elements. Nucleic Acids Res. *26*, 3542-3549.

Niehrs,C. (1999). Head in the WNT: the molecular nature of Spemann's head organizer. Trends Genet. *15*, 314-319.

Niehrs,C. (2004). Wnt signals and antagonists. In The vertebrate organizer, H.Grunz, ed., pp. 127-143.

Niehrs,C., Keller,R., Cho,K.W., and De Robertis,E.M. (1993). The homeobox gene goosecoid controls cell migration in Xenopus embryos. Cell *72*, 491-503.

Nomura,M. and Li,E. (1998). Smad2 role in mesoderm formation, left-right patterning and craniofacial development. Nature *393*, 786-790.

Nordstrom,U., Jessell,T.M., and Edlund,T. (2002). Progressive induction of caudal neural character by graded Wnt signaling. Nat. Neurosci. *5*, 525-532.

Norlin,S., Nordstrom,U., and Edlund,T. (2000). Fibroblast growth factor signaling is required for the proliferation and patterning of progenitor cells in the developing anterior pituitary. Mech. Dev. *96*, 175-182.

Oelgeschlager,M., Kuroda,H., Reversade,B., and De Robertis,E.M. (2003). Chordin is required for the Spemann organizer transplantation phenomenon in Xenopus embryos. Dev. Cell *4*, 219-230.

Ohuchi,H., Hori,Y., Yamasaki,M., Harada,H., Sekine,K., Kato,S., and Itoh,N. (2000). FGF10 acts as a major ligand for FGF receptor 2 IIIb in mouse multi-organ development. Biochem. Biophys. Res. Commun. *277*, 643-649.

Oliver,G., Mailhos,A., Wehr,R., Copeland,N.G., Jenkins,N.A., and Gruss,P. (1995). Six3, a murine homologue of the sine oculis gene, demarcates the most anterior border of the developing neural plate and is expressed during eye development. Development *121*, 4045-4055.

Olson,L.E., Tollkuhn,J., Scafoglio,C., Krones,A., Zhang,J., Ohgi,K.A., Wu,W., Taketo,M.M., Kemler,R., Grosschedl,R., Rose,D., Li,X., and Rosenfeld,M.G. (2006). Homeodomain-mediated beta-catenin-dependent switching events dictate cell-lineage determination. Cell *125*, 593-605.

Oosterwegel,M., van de,W.M., Timmerman,J., Kruisbeek,A., Destree,O., Meijlink,F., and Clevers,H. (1993). Differential expression of the HMG box factors TCF-1 and LEF-1 during murine embryogenesis. Development *118*, 439-448.

Oulad-Abdelghani,M., Chazaud,C., Bouillet,P., Mattei,M.G., Dolle,P., and Chambon,P. (1998). Stra3/lefty, a retinoic acid-inducible novel member of the transforming growth factor-beta superfamily. Int. J. Dev. Biol. *42*, 23-32.

Ozaki,H., Watanabe,Y., Takahashi,K., Kitamura,K., Tanaka,A., Urase,K., Momoi,T., Sudo,K., Sakagami,J., Asano,M., Iwakura,Y., and Kawakami,K. (2001). Six4, a putative myogenin gene regulator, is not essential for mouse embryonal development. Mol. Cell Biol. *21*, 3343-3350.

Park,H.L., Bai,C., Platt,K.A., Matise,M.P., Beeghly,A., Hui,C.C., Nakashima,M., and Joyner,A.L. (2000). Mouse Gli1 mutants are viable but have defects in SHH signaling in combination with a Gli2 mutation. Development *127*, 1593-1605.

Peltenburg,L.T. and Murre,C. (1997). Specific residues in the Pbx homeodomain differentially modulate the DNA-binding activity of Hox and Engrailed proteins. Development *124*, 1089-1098.

Pera,E.M. and De Robertis,E.M. (2000). A direct screen for secreted proteins in Xenopus embryos identifies distinct activities for the Wnt antagonists Crescent and Frzb-1. Mech. Dev. *96*, 183-195.

Perea-Gomez,A., Shawlot,W., Sasaki,H., Behringer,R.R., and Ang,S. (1999). HNF3beta and Lim1 interact in the visceral endoderm to regulate primitive streak

formation and anterior-posterior polarity in the mouse embryo. Development *126*, 4499-4511.

Perea-Gomez,A., Vella,F.D., Shawlot,W., Oulad-Abdelghani,M., Chazaud,C., Meno,C., Pfister,V., Chen,L., Robertson,E., Hamada,H., Behringer,R.R., and Ang,S.L. (2002). Nodal antagonists in the anterior visceral endoderm prevent the formation of multiple primitive streaks. Dev. Cell *3*, 745-756.

Pevny,L. and Placzek,M. (2005). SOX genes and neural progenitor identity. Curr. Opin. Neurobiol. *15*, 7-13.

Pevny,L.H. and Lovell-Badge,R. (1997). Sox genes find their feet. Curr. Opin. Genet. Dev. *7*, 338-344.

Pevny,L.H., Sockanathan,S., Placzek,M., and Lovell-Badge,R. (1998). A role for SOX1 in neural determination. Development *125*, 1967-1978.

Piccolo,S., Agius,E., Leyns,L., Bhattacharyya,S., Grunz,H., Bouwmeester,T., and De Robertis,E.M. (1999). The head inducer Cerberus is a multifunctional antagonist of Nodal, BMP and Wnt signals. Nature *397*, 707-710.

Placzek,M. (1995). The role of the notochord and floor plate in inductive interactions. Curr. Opin. Genet. Dev. *5*, 499-506.

Placzek,M. and Briscoe,J. (2005). The floor plate: multiple cells, multiple signals. Nat. Rev. Neurosci. *6*, 230-240.

Placzek,M., Jessell,T.M., and Dodd,J. (1993). Induction of floor plate differentiation by contact-dependent, homeogenetic signals. Development *117*, 205-218.

Popperl,H., Schmidt,C., Wilson,V., Hume,C.R., Dodd,J., Krumlauf,R., and Beddington,R.S. (1997). Misexpression of Cwnt8C in the mouse induces an ectopic embryonic axis and causes a truncation of the anterior neuroectoderm. Development *124*, 2997-3005.

Pownall,M.E., Welm,B.E., Freeman,K.W., Spencer,D.M., Rosen,J.M., and Isaacs,H.V. (2003). An inducible system for the study of FGF signalling in early amphibian development. Dev. Biol. *256*, 89-99.

Raetzman,L.T., Ross,S.A., Cook,S., Dunwoodie,S.L., Camper,S.A., and Thomas,P.Q. (2004). Developmental regulation of Notch signaling genes in the embryonic pituitary: Prop1 deficiency affects Notch2 expression. Dev. Biol. *265*, 329-340.

Reim,G. and Brand,M. (2002). Spiel-ohne-grenzen/pou2 mediates regional competence to respond to Fgf8 during zebrafish early neural development. Development *129*, 917-933.

Reversade,B. and De Robertis,E.M. (2005). Regulation of ADMP and BMP2/4/7 at opposite embryonic poles generates a self-regulating morphogenetic field. Cell *123*, 1147-1160.

Reversade,B., Kuroda,H., Lee,H., Mays,A., and De Robertis,E.M. (2005). Depletion of Bmp2, Bmp4, Bmp7 and Spemann organizer signals induces massive brain formation in Xenopus embryos. Development *132*, 3381-3392.

Rhinn,M., Dierich,A., Shawlot,W., Behringer,R.R., Le Meur,M., and Ang,S.L. (1998). Sequential roles for Otx2 in visceral endoderm and neuroectoderm for forebrain and midbrain induction and specification. Development *125*, 845-856.

Rhinn,M., Picker,A., and Brand,M. (2006). Global and local mechanisms of forebrain and midbrain patterning. Curr. Opin. Neurobiol. *16*, 5-12.

Rhodes,S.J., Chen,R., DiMattia,G.E., Scully,K.M., Kalla,K.A., Lin,S.C., Yu,V.C., and Rosenfeld,M.G. (1993). A tissue-specific enhancer confers Pit-1-dependent morphogen inducibility and autoregulation on the pit-1 gene. Genes Dev. *7*, 913-932.

Rizzoti,K., Brunelli,S., Carmignac,D., Thomas,P.Q., Robinson,I.C., and Lovell-Badge,R. (2004). SOX3 is required during the formation of the hypothalamo-pituitary axis. Nat. Genet. *36*, 247-255.

Rizzoti,K. and Lovell-Badge,R. (2005). Early development of the pituitary gland: induction and shaping of Rathke's pouch. Rev. Endocr. Metab Disord. *6*, 161-172.

Robertson,A.K., Geiman,T.M., Sankpal,U.T., Hager,G.L., and Robertson,K.D. (2004). Effects of chromatin structure on the enzymatic and DNA binding functions of DNA methyltransferases DNMT1 and Dnmt3a in vitro. Biochem. Biophys. Res. Commun. *322*, 110-118.

Robertson,K.D., Ait-Si-Ali,S., Yokochi,T., Wade,P.A., Jones,P.L., and Wolffe,A.P. (2000). DNMT1 forms a complex with Rb, E2F1 and HDAC1 and represses transcription from E2F-responsive promoters. Nat. Genet. *25*, 338-342.

Rodriguez,T.A., Srinivas,S., Clements,M.P., Smith,J.C., and Beddington,R.S. (2005). Induction and migration of the anterior visceral endoderm is regulated by the extra-embryonic ectoderm. Development *132*, 2513-2520.

Roeser,T., Stein,S., and Kessel,M. (1999). Nuclear beta-catenin and the development of bilateral symmetry in normal and LiCl-exposed chick embryos. Development *126*, 2955-2965.

Rosenfeld,M.G., Lunyak,V.V., and Glass,C.K. (2006). Sensors and signals: a coactivator/corepressor/epigenetic code for integrating signal-dependent programs of transcriptional response. Genes Dev. *20*, 1405-1428.

Rountree,M.R., Bachman,K.E., and Baylin,S.B. (2000). DNMT1 binds HDAC2 and a new co-repressor, DMAP1, to form a complex at replication foci. Nat. Genet. *25*, 269-277.

Rual,J.F., Venkatesan,K., Hao,T., Hirozane-Kishikawa,T., Dricot,A., Li,N., Berriz,G.F., Gibbons,F.D., Dreze,M., Ayivi-Guedehoussou,N., Klitgord,N., Simon,C., Boxem,M., Milstein,S., Rosenberg,J., Goldberg,D.S., Zhang,L.V., Wong,S.L., Franklin,G., Li,S., Albala,J.S., Lim,J., Fraughton,C., Llamosas,E., Cevik,S., Bex,C., Lamesch,P., Sikorski,R.S., Vandenhaute,J., Zoghbi,H.Y.,

Smolyar,A., Bosak,S., Sequerra,R., Doucette-Stamm,L., Cusick,M.E., Hill,D.E., Roth,F.P., and Vidal,M. (2005). Towards a proteome-scale map of the human protein-protein interaction network. Nature *437*, 1173-1178.

Rubenstein,J.L., Shimamura,K., Martinez,S., and Puelles,L. (1998). Regionalization of the prosencephalic neural plate. Annu. Rev. Neurosci. *21*, 445-477.

Sajedi,E., Gaston-Massuet,C., Andoniadou,C.L., Signore,M., Hurd,P.J., Dattani,M., and Martinez-Barbera,J.P. (2007). DNMT1 interacts with the developmental transcriptional repressor HESX1. Biochim. Biophys. Acta.

Sajedi,E, Gaston-Massuet,C., Signore,M., Andoniadou,C.L., Kelberman,D., Castro,S., Etchevers,H.C., Gerrelli, D., Dattani,M., and Martinez-Barbera,J.P. Analysis of the mouse models carrying the I26T and R160C substitutions in the transcriptional repressor HESX1as models for septo-optic dysplasia and hypopituitarism. Hum. Mol. Gen. *in press*.

Sasai,Y., Lu,B., Piccolo,S., and De Robertis,E.M. (1996). Endoderm induction by the organizer-secreted factors chordin and noggin in Xenopus animal caps. EMBO J. *15*, 4547-4555.

Sasai,Y., Lu,B., Steinbeisser,H., Geissert,D., Gont,L.K., and De Robertis,E.M. (1994). Xenopus chordin: a novel dorsalizing factor activated by organizer-specific homeobox genes. Cell *79*, 779-790.

Sater,A.K. and Jacobson,A.G. (1990). The role of the dorsal lip in the induction of heart mesoderm in Xenopus laevis. Development *108*, 461-470.

Schier,A.F. and Shen,M.M. (2000). Nodal signalling in vertebrate development. Nature *403*, 385-389.

Schulte-Merker,S., Lee,K.J., McMahon,A.P., and Hammerschmidt,M. (1997). The zebrafish organizer requires chordino. Nature *387*, 862-863.

Semina,E.V., Datson,N.A., Leysens,N.J., Zabel,B.U., Carey,J.C., Bell,G.I., Bitoun,P., Lindgren,C., Stevenson,T., Frants,R.R., van Ommen,G., and Murray,J.C. (1996a). Exclusion of epidermal growth factor and high-resolution physical mapping across the Rieger syndrome locus. Am. J. Hum. Genet. *59*, 1288-1296.

Semina,E.V., Reiter,R., Leysens,N.J., Alward,W.L., Small,K.W., Datson,N.A., Siegel-Bartelt,J., Bierke-Nelson,D., Bitoun,P., Zabel,B.U., Carey,J.C., and Murray,J.C. (1996b). Cloning and characterization of a novel bicoid-related homeobox transcription factor gene, RIEG, involved in Rieger syndrome. Nat. Genet. *14*, 392-399.

Shawlot,W. and Behringer,R.R. (1995). Requirement for Lim1 in head-organizer function. Nature *374*, 425-430.

Shawlot,W., Deng,J.M., and Behringer,R.R. (1998). Expression of the mouse cerberus-related gene, Cerr1, suggests a role in anterior neural induction and somitogenesis. Proc. Natl. Acad. Sci. U. S. A *95*, 6198-6203.

Sheng,H.Z., Moriyama,K., Yamashita,T., Li,H., Potter,S.S., Mahon,K.A., and Westphal,H. (1997). Multistep control of pituitary organogenesis. Science *278*, 1809-1812.

Sheng,H.Z., Zhadanov,A.B., Mosinger,B., Jr., Fujii,T., Bertuzzi,S., Grinberg,A., Lee,E.J., Huang,S.P., Mahon,K.A., and Westphal,H. (1996). Specification of pituitary cell lineages by the LIM homeobox gene Lhx3. Science *272*, 1004-1007.

Shih,J. and Fraser,S.E. (1996). Characterizing the zebrafish organizer: microsurgical analysis at the early-shield stage. Development *122*, 1313-1322.

Shimamura,K. and Rubenstein,J.L. (1997). Inductive interactions direct early regionalization of the mouse forebrain. Development *124*, 2709-2718.

Smith,W.C. and Harland,R.M. (1992). Expression cloning of noggin, a new dorsalizing factor localized to the Spemann organizer in Xenopus embryos. Cell *70*, 829-840.

Smith,W.C., McKendry,R., Ribisi S Jr, and Harland,R.M. (1995). A nodal-related gene defines a physical and functional domain within the Spemann organizer. Cell *82*, 37-46.

Sobrier,M.L., Maghnie,M., Vie-Luton,M.P., Secco,A., di Iorgi,N., Lorini,R., and Amselem,S. (2006). Novel HESX1 mutations associated with a life-threatening neonatal phenotype, pituitary aplasia, but normally located posterior pituitary and no optic nerve abnormalities. J. Clin. Endocrinol. Metab *91*, 4528-4536.

Sobrier,M.L., Netchine,I., Heinrichs,C., Thibaud,N., Vie-Luton,M.P., Van Vliet,G., and Amselem,S. (2005). Alu-element insertion in the homeodomain of HESX1 and aplasia of the anterior pituitary. Hum. Mutat. *25*, 503.

Sokol,S., Christian,J.L., Moon,R.T., and Melton,D.A. (1991). Injected Wnt RNA induces a complete body axis in Xenopus embryos. Cell *67*, 741-752.

Soriano,P. (1999). Generalized lacZ expression with the ROSA26 Cre reporter strain. Nat. Genet. *21*, 70-71.

Sornson,M.W., Wu,W., Dasen,J.S., Flynn,S.E., Norman,D.J., O'Connell,S.M., Gukovsky,I., Carriere,C., Ryan,A.K., Miller,A.P., Zuo,L., Gleiberman,A.S., Andersen,B., Beamer,W.G., and Rosenfeld,M.G. (1996). Pituitary lineage determination by the Prophet of Pit-1 homeodomain factor defective in Ames dwarfism. Nature *384*, 327-333.

Spemann,H. and Mangold,H. (1924). Induction of embryonic primordia by implantation of organizers from a different species (Reprinted from Archiv Mikroskopische Anatomie Entwicklungsmechanik, vol 100, pg 599-638, 1924). International Journal of Developmental Biology *45*, 13-38.

Spieler,D., Baumer,N., Stebler,J., Koprunner,M., Reichman-Fried,M., Teichmann,U., Raz,E., Kessel,M., and Wittler,L. (2004). Involvement of Pax6 and Otx2 in the forebrain-specific regulation of the vertebrate homeobox gene ANF/Hesx1. Dev. Biol. *269*, 567-579.

Srinivas,S., Rodriguez,T., Clements,M., Smith,J.C., and Beddington,R.S. (2004). Active cell migration drives the unilateral movements of the anterior visceral endoderm. Development *131*, 1157-1164.

Stancheva,I. and Meehan,R.R. (2000). Transient depletion of xDnmt1 leads to premature gene activation in Xenopus embryos. Genes Dev. *14*, 313-327.

Stark,M.R. and Johnson,A.D. (1994). Interaction between two homeodomain proteins is specified by a short C-terminal tail. Nature *371*, 429-432.

Stern,C.D. (2001). Initial patterning of the central nervous system: how many organizers? Nat. Rev. Neurosci. *2*, 92-98.

Stern,C.D. (2005). Neural induction: old problem, new findings, yet more questions. Development *132*, 2007-2021.

Stern,C.D. (2006). Neural induction: 10 years on since the 'default model'. Curr. Opin. Cell Biol. *18*, 692-697.

Stern,S., Tanaka,M., and Herr,W. (1989). The Oct-1 homoeodomain directs formation of a multiprotein-DNA complex with the HSV transactivator VP16. Nature *341*, 624-630.

Sun,X., Meyers,E.N., Lewandoski,M., and Martin,G.R. (1999). Targeted disruption of Fgf8 causes failure of cell migration in the gastrulating mouse embryo. Genes Dev. *13*, 1834-1846.

Susa,T., Nakayama,M., Kitahara,K., Kimoto,F., Kato,T., and Kato,Y. (2007). Homeodomain transcription factor Hesx1/Rpx occupies Prop-1 activation sites in porcine follicle stimulating hormone (FSH) beta subunit promoter. Biochem. Biophys. Res. Commun. *357*, 712-717.

Szeto,D.P., Ryan,A.K., O'Connell,S.M., and Rosenfeld,M.G. (1996). P-OTX: a PIT-1-interacting homeodomain factor expressed during anterior pituitary gland development. Proc. Natl. Acad. Sci. U. S. A *93*, 7706-7710.

Taira,M., Jamrich,M., Good,P.J., and Dawid,I.B. (1992). The LIM domain-containing homeo box gene Xlim-1 is expressed specifically in the organizer region of Xenopus gastrula embryos. Genes Dev. *6*, 356-366.

Tajima,T., Hattorri,T., Nakajima,T., Okuhara,K., Sato,K., Abe,S., Nakae,J., and Fujieda,K. (2003). Sporadic heterozygous frameshift mutation of HESX1 causing pituitary and optic nerve hypoplasia and combined pituitary hormone deficiency in a Japanese patient. J. Clin. Endocrinol. Metab *88*, 45-50.

Takada,S., Stark,K.L., Shea,M.J., Vassileva,G., McMahon,J.A., and McMahon,A.P. (1994). Wnt-3a regulates somite and tailbud formation in the mouse embryo. Genes Dev. *8*, 174-189.

Takemoto,T., Uchikawa,M., Kamachi,Y., and Kondoh,H. (2006). Convergence of Wnt and FGF signals in the genesis of posterior neural plate through activation of the Sox2 enhancer N-1. Development *133*, 297-306.

Takuma,N., Sheng,H.Z., Furuta,Y., Ward,J.M., Sharma,K., Hogan,B.L., Pfaff,S.L., Westphal,H., Kimura,S., and Mahon,K.A. (1998). Formation of Rathke's pouch requires dual induction from the diencephalon. Development *125*, 4835-4840.

Tam,P.P. and Steiner,K.A. (1999). Anterior patterning by synergistic activity of the early gastrula organizer and the anterior germ layer tissues of the mouse embryo. Development *126*, 5171-5179.

Tam,P.P., Steiner,K.A., Zhou,S.X., and Quinlan,G.A. (1997). Lineage and functional analyses of the mouse organizer. Cold Spring Harb. Symp. Quant. Biol. *62*, 135-144.

Tam,P.P.L. and Gad,J.M. (2004). Gastrulation in the mouse embryo. In Gastrulation : from cells to embryo, C.D.Stern, ed., pp. 233-262.

Tan,K., Shlomi,T., Feizi,H., Ideker,T., and Sharan,R. (2007). Transcriptional regulation of protein complexes within and across species. Proc. Natl. Acad. Sci. U. S. A *104*, 1283-1288.

Tanabe,Y. and Jessell,T.M. (1996). Diversity and pattern in the developing spinal cord. Science *274*, 1115-1123.

Thomas,P. and Beddington,R. (1996). Anterior primitive endoderm may be responsible for patterning the anterior neural plate in the mouse embryo. Curr. Biol. *6*, 1487-1496.

Thomas,P.Q., Brown,A., and Beddington,R.S. (1998). Hex: a homeobox gene revealing peri-implantation asymmetry in the mouse embryo and an early transient marker of endothelial cell precursors. Development *125*, 85-94.

Thomas,P.Q., Dattani,M.T., Brickman,J.M., McNay,D., Warne,G., Zacharin,M., Cameron,F., Hurst,J., Woods,K., Dunger,D., Stanhope,R., Forrest,S., Robinson,I.C., and Beddington,R.S. (2001). Heterozygous HESX1 mutations associated with isolated congenital pituitary hypoplasia and septo-optic dysplasia. Hum. Mol. Genet. *10*, 39-45.

Thomas,P.Q. and Rathjen,P.D. (1992). HES-1, a novel homeobox gene expressed by murine embryonic stem cells, identifies a new class of homeobox genes. Nucleic Acids Res. *20*, 5840.

Tian,T. and Meng,A.M. (2006). Nodal signals pattern vertebrate embryos. Cell Mol. Life Sci. *63*, 672-685.

Townson,S.M., Kang,K., Lee,A.V., and Oesterreich,S. (2004). Structure-function analysis of the estrogen receptor alpha corepressor scaffold attachment factor-B1: identification of a potent transcriptional repression domain. J. Biol. Chem. *279*, 26074-26081.

Treier,M., Gleiberman,A.S., O'Connell,S.M., Szeto,D.P., McMahon,J.A., McMahon,A.P., and Rosenfeld,M.G. (1998). Multistep signaling requirements for pituitary organogenesis in vivo. Genes Dev. *12*, 1691-1704.

Treier,M., O'Connell,S., Gleiberman,A., Price,J., Szeto,D.P., Burgess,R., Chuang,P.T., McMahon,A.P., and Rosenfeld,M.G. (2001). Hedgehog signaling is required for pituitary gland development. Development *128*, 377-386.

Tremblay,J.J., Goodyer,C.G., and Drouin,J. (2000). Transcriptional properties of Ptx1 and Ptx2 isoforms. Neuroendocrinology *71*, 277-286.

Triezenberg,S.J., Kingsbury,R.C., and McKnight,S.L. (1988a). Functional dissection of VP16, the trans-activator of herpes simplex virus immediate early gene expression. Genes Dev. *2*, 718-729.

Triezenberg,S.J., LaMarco,K.L., and McKnight,S.L. (1988b). Evidence of DNA: protein interactions that mediate HSV-1 immediate early gene activation by VP16. Genes Dev. *2*, 730-742.

Turton,J.P., Buchanan,C.R., Robinson,I.C., Aylwin,S.J., and Dattani,M.T. (2006). Evolution of gonadotropin deficiency in a patient with type II autosomal dominant GH deficiency. Eur. J. Endocrinol. *155*, 793-799.

Uchikawa,M., Ishida,Y., Takemoto,T., Kamachi,Y., and Kondoh,H. (2003). Functional analysis of chicken Sox2 enhancers highlights an array of diverse regulatory elements that are conserved in mammals. Dev. Cell *4*, 509-519.

Van Criekinge,W. and Beyaert,R. (1999). Yeast Two-Hybrid: State of the Art. Biol. Proced. Online. *2*, 1-38.

van de,W.S., van de,W.M., Joore,J., Esseling,J., Bink,R., Clevers,H., and Zivkovic,D. (2001). Ectopic Wnt signal determines the eyeless phenotype of zebrafish masterblind mutant. Development *128*, 3877-3888.

van Genderen,C., Okamura,R.M., Farinas,I., Quo,R.G., Parslow,T.G., Bruhn,L., and Grosschedl,R. (1994). Development of several organs that require inductive epithelial-mesenchymal interactions is impaired in LEF-1-deficient mice. Genes Dev. *8*, 2691-2703.

Varlet,I., Collignon,J., Norris,D.P., and Robertson,E.J. (1997a). Nodal signaling and axis formation in the mouse. Cold Spring Harb. Symp. Quant. Biol. *62*, 105-113.

Varlet,I., Collignon,J., and Robertson,E.J. (1997b). nodal expression in the primitive endoderm is required for specification of the anterior axis during mouse gastrulation. Development *124*, 1033-1044.

Vesque,C., Ellis,S., Lee,A., Szabo,M., Thomas,P., Beddington,R., and Placzek,M. (2000). Development of chick axial mesoderm: specification of prechordal mesoderm by anterior endoderm-derived TGFbeta family signalling. Development *127*, 2795-2809.

Vire,E., Brenner,C., Deplus,R., Blanchon,L., Fraga,M., Didelot,C., Morey,L., Van Eynde,A., Bernard,D., Vanderwinden,J.M., Bollen,M., Esteller,M., Di Croce,L., de Launoit,Y., and Fuks,F. (2006). The Polycomb group protein EZH2 directly controls DNA methylation. Nature *439*, 871-874.

Vojtek,A.B., Hollenberg,S.M., and Cooper,J.A. (1993). Mammalian Ras interacts directly with the serine/threonine kinase Raf. Cell *74*, 205-214.

Waldrip,W.R., Bikoff,E.K., Hoodless,P.A., Wrana,J.L., and Robertson,E.J. (1998). Smad2 signaling in extraembryonic tissues determines anterior-posterior polarity of the early mouse embryo. Cell *92*, 797-808.

Wales,J.K. and Quarrell,O.W. (1996). Evidence for possible Mendelian inheritance of septo-optic dysplasia. Acta Paediatr. *85*, 391-392.

Wallis,D.E., Roessler,E., Hehr,U., Nanni,L., Wiltshire,T., Richieri-Costa,A., Gillessen-Kaesbach,G., Zackai,E.H., Rommens,J., and Muenke,M. (1999). Mutations in the homeodomain of the human SIX3 gene cause holoprosencephaly. Nat. Genet. *22*, 196-198.

Webb,G.C., Thomas,P.Q., Ford,J.H., and Rathjen,P.D. (1993). Hesx1, a homeobox gene expressed by murine embryonic stem cells, maps to mouse chromosome 14, bands A3-B. Genomics *18*, 464-466.

Weintrob,N., Drouin,J., Vallette-Kasic,S., Taub,E., Marom,D., Lebenthal,Y., Klinger,G., Bron-Harlev,E., and Shohat,M. (2006). Low estriol levels in the maternal triple-marker screen as a predictor of isolated adrenocorticotropic hormone deficiency caused by a new mutation in the TPIT gene. Pediatrics *117*, e322-e327.

Wilkinson,D.G., Bhatt,S., and Herrmann,B.G. (1990). Expression pattern of the mouse T gene and its role in mesoderm formation. Nature *343*, 657-659.

Wilson,D., Sheng,G., Lecuit,T., Dostatni,N., and Desplan,C. (1993). Cooperative dimerization of paired class homeo domains on DNA. Genes Dev. *7*, 2120-2134.

Wilson,P.A. and Hemmati-Brivanlou,A. (1995). Induction of epidermis and inhibition of neural fate by Bmp-4. Nature *376*, 331-333.

Wilson,S.I. and Edlund,T. (2001). Neural induction: toward a unifying mechanism. Nat. Neurosci. *4 Suppl*, 1161-1168.

Wilson,S.I., Rydstrom,A., Trimborn,T., Willert,K., Nusse,R., Jessell,T.M., and Edlund,T. (2001). The status of Wnt signalling regulates neural and epidermal fates in the chick embryo. Nature *411*, 325-330.

Wilson,S.W. and Houart,C. (2004). Early steps in the development of the forebrain. Dev. Cell *6*, 167-181.

Wilson,S.W. and Rubenstein,J.L. (2000). Induction and dorsoventral patterning of the telencephalon. Neuron *28*, 641-651.

Wilson,V., Manson,L., Skarnes,W.C., and Beddington,R.S. (1995). The T gene is necessary for normal mesodermal morphogenetic cell movements during gastrulation. Development *121*, 877-886.

Winnier,G., Blessing,M., Labosky,P.A., and Hogan,B.L. (1995). Bone morphogenetic protein-4 is required for mesoderm formation and patterning in the mouse. Genes Dev. *9*, 2105-2116.

Withington,S., Beddington,R., and Cooke,J. (2001). Foregut endoderm is required at head process stages for anteriormost neural patterning in chick. Development *128*, 309-320.

Wolberger,C. (1996). Homeodomain interactions. Curr. Opin. Struct. Biol. *6*, 62-68.

Wolff,G.L., Kodell,R.L., Moore,S.R., and Cooney,C.A. (1998). Maternal epigenetics and methyl supplements affect agouti gene expression in Avy/a mice. FASEB J. *12*, 949-957.

Wood,H.B. and Episkopou,V. (1999). Comparative expression of the mouse Sox1, Sox2 and Sox3 genes from pre-gastrulation to early somite stages. Mech. Dev. *86*, 197-201.

Xu,L., Lavinsky,R.M., Dasen,J.S., Flynn,S.E., McInerney,E.M., Mullen,T.M., Heinzel,T., Szeto,D., Korzus,E., Kurokawa,R., Aggarwal,A.K., Rose,D.W., Glass,C.K., and Rosenfeld,M.G. (1998a). Signal-specific co-activator domain requirements for Pit-1 activation. Nature *395*, 301-306.

Xu,Q., D'Amore,P.A., and Sokol,S.Y. (1998b). Functional and biochemical interactions of Wnts with FrzA, a secreted Wnt antagonist. Development *125*, 4767-4776.

Yamaguchi,T.P., Bradley,A., McMahon,A.P., and Jones,S. (1999). A Wnt5a pathway underlies outgrowth of multiple structures in the vertebrate embryo. Development *126*, 1211-1223.

Ying,Q.L., Stavridis,M., Griffiths,D., Li,M., and Smith,A. (2003). Conversion of embryonic stem cells into neuroectodermal precursors in adherent monoculture. Nat. Biotechnol. *21*, 183-186.

Zaraisky,A.G., Lukyanov,S.A., Vasiliev,O.L., Smirnov,Y.V., Belyavsky,A.V., and Kazanskaya,O.V. (1992). A novel homeobox gene expressed in the anterior neural plate of the Xenopus embryo. Dev. Biol. *152*, 373-382.

Zeng,L., Fagotto,F., Zhang,T., Hsu,W., Vasicek,T.J., Perry,W.L., III, Lee,J.J., Tilghman,S.M., Gumbiner,B.M., and Costantini,F. (1997). The mouse Fused locus encodes Axin, an inhibitor of the Wnt signaling pathway that regulates embryonic axis formation. Cell *90*, 181-192.

Zhang,H. and Bradley,A. (1996). Mice deficient for BMP2 are nonviable and have defects in amnion/chorion and cardiac development. Development *122*, 2977-2986.

Zhang,X., Azhar,G., Zhong,Y., and Wei,J.Y. (2004). Identification of a novel serum response factor cofactor in cardiac gene regulation. J. Biol. Chem. *279*, 55626-55632.

Zhu,C.C., Dyer,M.A., Uchikawa,M., Kondoh,H., Lagutin,O.V., and Oliver,G. (2002). Six3-mediated auto repression and eye development requires its interaction with members of the Groucho-related family of co-repressors. Development *129*, 2835-2849.

Zhu,X., Gleiberman,A.S., and Rosenfeld,M.G. (2007). Molecular physiology of pituitary development: signaling and transcriptional networks. Physiol Rev. *87*, 933-963.

Zhu,X., Zhang,J., Tollkuhn,J., Ohsawa,R., Bresnick,E.H., Guillemot,F., Kageyama,R., and Rosenfeld,M.G. (2006). Sustained Notch signaling in progenitors is required for sequential emergence of distinct cell lineages during organogenesis. Genes Dev. *20*, 2739-2753.

PUBLICATIONS